Studies in density stratified flows. April 1970.

Author:
Wilkinson, D. L.

Publication details:
Report No. UNSW Water Research Laboratory Report No. 118
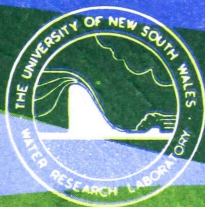
Publication Date:
1970

DOI:
https://doi.org/10.4225/53/579eb0326c4ea

License:
https://creativecommons.org/licenses/by-nc-nd/3.0/au/
Link to license to see what you are allowed to do with this resource.

The quality of this digital copy is an accurate reproduction of the original print copy

STUDIES IN
DENSITY STRATIFIED FLOWS

by

D. L. Wilkinson

University of New South Wales

School of Civil Engineering.

Studies   in   Density   Stratified   Flows.

by

D. L. Wilkinson.

- - - - - - - - - - - - - - - - - - - -

Preface.

The work reported herein was part of the program of research carried out at the Water Research Laboratory, funds for which were provided by the School of Civil Engineering as distinct from external sponsorship. Printing and publication is by permission of the author through service facilities provided by the Water Research Laboratory.

R. T. Hattersley,
Assoc. Professor of Civil Engineering,
Officer-in-Charge.

Summary

This thesis examines the rapidly varied flow phenomenon in a two layer density stratified system. Only one layer flows, the other being stationary. The flow regime changes from supercritical to subcritical across the region of rapidly varied flow. The analagous phenomenon in open channel hydraulics is the hydraulic jump. In stratified flows it will be referred to as a density jump because it is generally accompanied by a change in the density of the flowing layer.

It is shown there is a fundamental difference between the hydraulic and the density jump in that the conjugate conditions on either side of a density jump are not uniquely related as they are with the hydraulic jump. There are a range of possible states which may be attained downstream of a density jump for a given upstream state. It is shown that the rate of entrainment of ambient fluid into a density jump and therefore the conditions downstream of the jump are a function of the downstream control. The limiting cases of maximum and minimum entrainment and the control mechanism within the jump are examined. Several forms of control are investigated among these being the broad-crested weir, a free overfall and channel friction.

An entrainment function is derived, relating a local entrainment parameter to a local Froude number within the entraining zone of a density jump.

Some features of unsteady density flows are examined and it is shown that all the properties of starting flow or nose are controlled by the following layer, which in turn, is generally controlled by boundary friction.

An approximate expression is derived for the fall in momentum flux across a density jump and this is compared with experimental data.

Finally, experimental velocity and density distributions downstream of density jumps are presented, and are shown to be functions of the Froude number of the flow upstream of the density jump, and the rate of entrainment within the jump.

The significant result arising from this work is that conditions downstream of density jump, which will occur, for example, at power station cooling pond outfalls and some ocean sewage outfalls, can be predicted. A design example, showing how power station cooling pond efficiencies can be optimised, by the control of mixing at the outfall, is included in the appendices.

Table of Contents

Table of Contents (cont'd.)

List of Appendices

List of Figures.

Chapter 1 - General Introduction

The term 'density current' is used to describe the motion of a fluid within another fluid of slightly differing density. The difference in specific weight of the two fluids provides the driving force for the motion. The density difference may be due to dissolved salts or temperature variation. The name gravity current is probably a more exact description of the motion; nevertheless the term 'density current' is firmly entrenched in the literature and will be used. The term 'turbidity current' is used when a suspension of solids cause the density difference.

Many density flows occur in nature. These are generally large scale phenomena such as atmospheric cold fronts or geostropic ocean currents. All these density flows are of concern to man; they affect either his environment, his comfort, or his pocket, and he therefore wishes to gain some understanding of their behaviour.

Interest in density flows, at this laboratory, originated when advice was sought by the Electricity Commission of New South Wales, on outfall design for power station cooling ponds.

Power stations require huge volumes of cooling water to condense steam which has passed through the turbines, used to drive the generators. The efficiency of the generation cycles is in part dependent on the temperature of the cooling water; the lower the temperature, the

greater the efficiency.   The cooling water is sometimes drawn from a nearby reservoir constructed for that purpose.   Hence, the cooling water, like the steam, recirculates.   When the cooling water is discharged back into the reservoir it is warmer than the surrounding pond water.   The difference in density of the inflowing and ambient fluids causes the hot water to spread and form a layer at the surface of the reservoir.   Density stratification of this type is desirable in cooling ponds, since it promotes maximum heat transfer from the heated water to the atmosphere before the cooling water is re-used.

Evaporation and radiation are the dominant mechanisms of heat exchange in the pond, and these are optimised when the surface layer is as hot and as thin as possible.   This is achieved by minimising mixing of the inflowing and ambient fluids at the outfall.

The laboratory was asked to investigate the outfall requirements necessary to achieve these optimal conditions.   The investigation described in this report arose out of earlier studies into the outfall problem (Wood, 1967).

The problem of outfall design is not specifically geographic in nature but is more a question of basic fluid mechanics.   It is necessary to gain an understanding of the physical mechanisms operating at a cooling pond outfall.   Only then, can an attempt be made at predicting the extent of mixing, and layer thickness at an outfall.

Before proceeding with this problem, some basic general features of density flow are reviewed.

The same laws govern the motion of density currents as govern free surface flow, and in the appropriate places many of the approximations made in deriving the open channel flow equations may be applied to density current flow.

For a density current consisting of a single flowing layer and provided the streamline curvature is small, the gradually varied flow assumption leads to subcritical and supercritical flow regimes.

Two major differences exist between the flow described above and free surface flows.

(i) Firstly, since differences in density of the fluids are generally small the resulting forces, causing the motions, will also be small. However, the fluid inertia remains unchanged, so that accelerations in the density current will be orders less than in analagous free surface flow. Hence, density currents move with a characteristic slow motion. It is this slowness of movement which makes density currents so interesting to observe, especially if the flow is unsteady. Starting flows such as occur in the "dam-break" problem are quite beautiful to watch in the exaggerated time scale associated with density flows.

(ii) The second major difference between density and free surface flows arise from the fact that density flows are generally miscible with the

surrounding fluid. If there is sufficient turbulence at the interface of the density current and the ambient fluid, the two will mix.

Density gradients in a fluid tend to suppress turbulence normal to that gradient, so that in certain cases, density currents can flow for appreciable distances and only mix very slightly with the surrounding fluid (Lofquist 1960). It is this feature of density flows that is desirable to promote in power station cooling ponds.

It was stated previously that density flows, like open channel flows, have supercritical and subcritical regimes. An hydraulic jump is the mechanism by which an open channel flow changes from the former to the latter regime. Such a transition can occur in density flows, and will almost always form at a power station cooling pond outfall. Although the Froude number of the flow in the outfall channel may be subcritical, the flow, when considered as a density current, will almost always be supercritical.

It is shown later that supercritical density flows are unstable at an outfall, and a transition to subcritical flow will occur. Such a transition is analagous to the open channel hydraulic jump and is similar to it in many ways. There is, however, a significant difference between the two phenomena. The density of a density current generally changes at a transition from supercritical to subcritical flow. For this reason, the transition will be referred to as a density jump. The reason for this

change in density at a density jump, is that part of the upstream energy

is dissipated entraining ambient fluid. If the two fluids are miscible,

the fluid entrained at the jump will change the density of the downstream

flow. Some interesting cases of naturally occurring density jump have

been reported in the literature.   Density jumps have been observed in

Föhn winds and the katabatic flows in Antarctica (Schweitzer, 1953, and

Ball, 1956, 57, 59). Lied (1961) gives a particularly vivid account of

meteorological measurements taken through a jump in katabatic flow.

The depth of flow on the supercritical side of the jump was typically 60

to 100 feet and on the subcritical side 100 to 300 feet, varying with

different jumps. Pressure drops of up to 20 m.b. were measured across

the jump, in one instance, over a distance of only 60 yards. Lied's account

of his walking through a jump is worth recounting.

"The experience of actually walking through a standing katabatic

jump is somewhat unusual. Invariably the following sequence of events

took place:-

(i)   The observer walked upslope in calm conditions, or with light and

variable winds.

(ii)   Taking measurements of pressure, temperature, and wind-speed

and direction downhill from the jump while still in the calm air, the ob-

server had the odd sensation of approaching a strongly roaring wall of

drift snow, which was neither retreating nor advancing, and towering up

to 300 feet above him.

(iii) Series of measurements were taken immediately outside the edge of the jump, whereafter the observer stepped into a totally different world, like walking through a door opening out into a full blizzard. At the very edge of the jump violently rotating swirls of wind and snow, with strong updrafts and downdrafts alternately forced snow up into his nostrils and eyes and at the next moment blew it down his neck. A severe buffeting was experienced.

(iv) At this point further measurements were taken. These showed a sudden drop in pressure, an immediate rise in temperature, and just inside the very turbulent edge of the jump, a violent increase in wind speed, blowing downslope with strong gusts, and accompanied by moderate to dense drift snow.

(v) To make sure of his measurements the observer passed in and out of the jump a number of times repeating his observations on either side of it. He then walked upslope into the wind to obtain measurements well behind the turbulent edge of the jump.

(vi) Upslope the wind was usually stronger than near the edge, with denser drift, and the differences in pressure and temperature from the values obtained in the calm air also increased upslope.

(vii) Walking downslope with the wind behind him the observer could determine the standing edge of the jump by the sudden increase in turbulence. On leaving the jump, the transition from highly turbulent to calm, or light

and variable conditions usually occurred over a distance of only about 5 yards."

It has been shown experimentally, and was anticipated from analysis, that a density jump with upstream conditions fixed, can entrain varying amounts of ambient fluid, depending upon the tailwater control. The mechanism by which a jump varies its entrained flow is worth examining in some detail. Figure (1) shows a typical density jump. A jet of dense fluid, say salt water, issues from the inlet slot which extends the full width of the test tank. The tank is filled with less dense fluid, say fresh water. When the flow is started, a vortex forms which moves away from the slot, followed by a layer of diluted, salt water. The starting vortex is subsequently called a nose and moves initially with a velocity which is solely a function of the flux of density difference.

Figure (1) shows the form of the density current a short time after commencement of flow. At this stage, the jump closely resembles a neutral jet except for the downstream region where the density difference acts to suppress turbulence, and mixing finally decreases to a negligible amount. The interfacial slope of this type of density jump is noticeably less than the slope of an open channel jump. The surface roller observed in open channel jumps is absent in this density jump.

The mean velocity in the layer behind the nose is very nearly equal to the velocity of the nose. This will be shown in Cahpter 5 which deals with unsteady density currents. The starting vortex or nose acts as the

tailwater control and it will be shown that this is a possible conjugate

state for the jump.

Unlike the open channel jump the conjugate conditions for a density

jump are not unique. The reason for this is that a density jump can en-

train, within limits, varying amounts of ambient fluid, to satisfy a range

of conjugate depths. The mechanism by which this happens is now ex-

amined.

Consider an open channel jump controlled downstream by an over-

shot gate, which has been adjusted so that the jump forms next to the

slot as shown in Figure 2. If the gate is raised abruptly by a small

amount, a wave will travel upstream causing the jump to partially flood

so that the outlet becomes submerged (Figure 2b). The unique conjugate

conditions which enable a jump to form are no longer satisfied. If the

same experiment is performed on a density jump, again a wave moves

upstream, but instead of submerging the inlet as happened above, a roller

will be observed to form on the downstream end of the existing jump as

shown in Figure 3. The interfacial slope of this roller is noticeably

steeper than the original jump, which itself remains unchanged. The

roller which forms at the interface in this type of density jump, is sim-

ilar in form to the roller observed in open channel hydraulic jumps. This

roller, when present in a density jump, causes a marked reduction in in-

terfacial shear, resulting in reduced entrainment. The steeper slope of
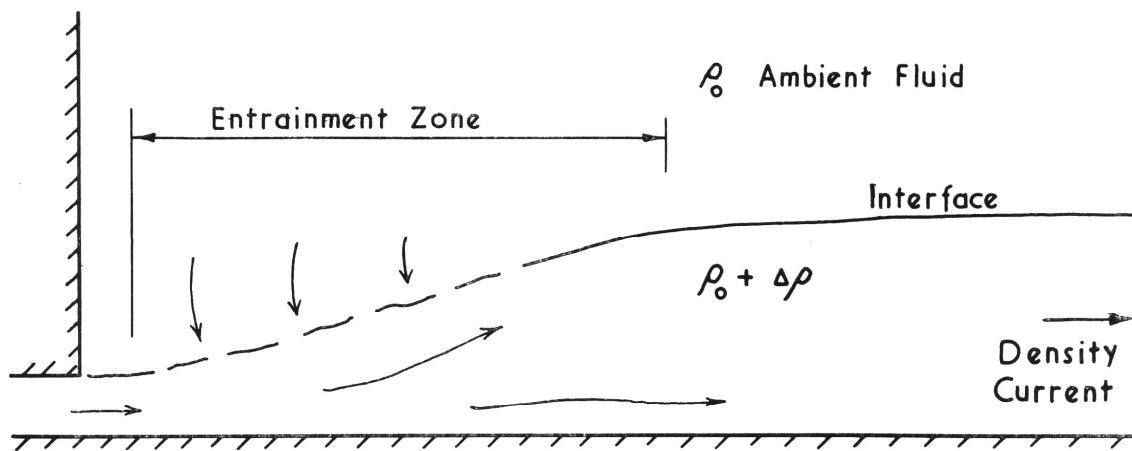
THE ENTRAINING DENSITY JUMP
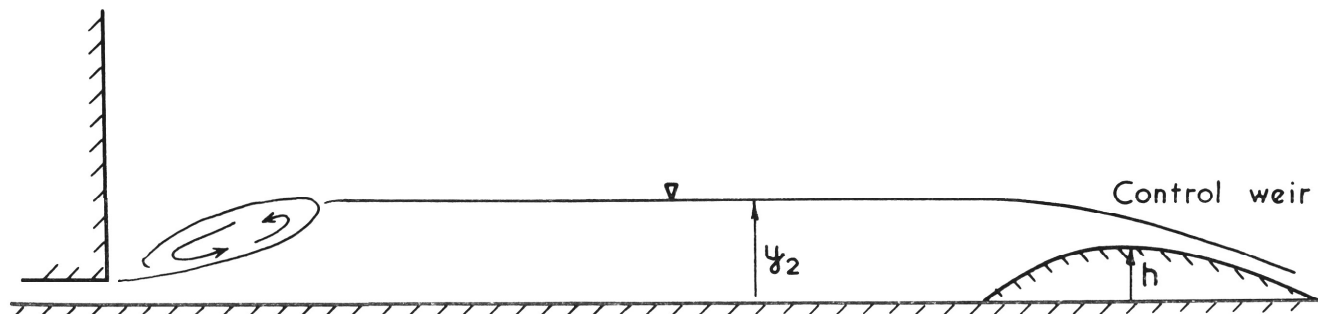
FIGURE 1.

FIG. 2a.

THE HYDRAULIC JUMP
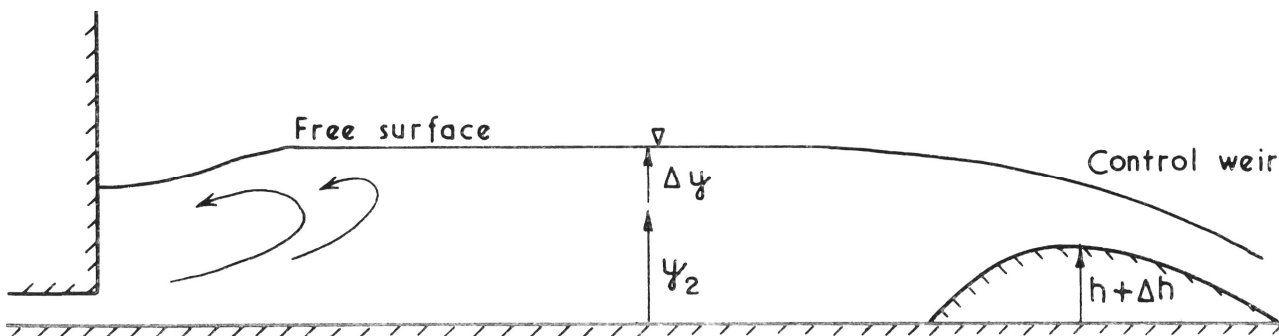
FIG. 2b.

Weir raised causing level to rise by Δy

THE FLOODED HYDRAULIC JUMP

FIGURE 2.

Entrainment Zone

Roller Region

ρ_0 Ambient Fluid

$\rho_0 + \Delta\rho$

Density Current
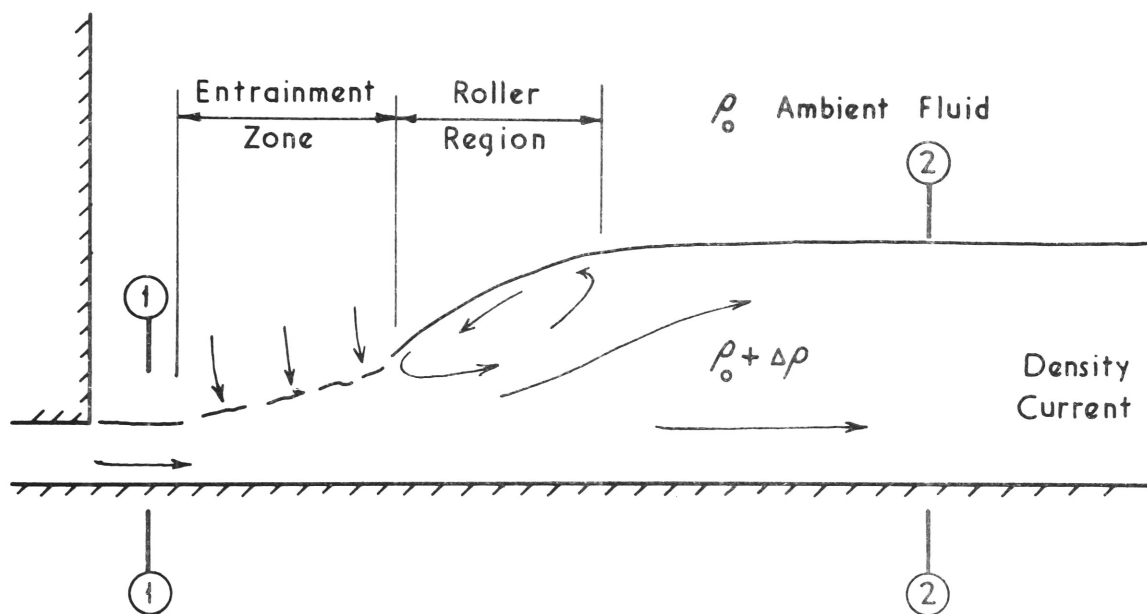
THE PARTIALLY ENTRAINING DENSITY JUMP

FIGURE 3.

the roller region results in a shortening of the transition zone. The mixing remains unchanged in the initial section of the jump, which will be referred to as the entrainment zone. If the gate controlling the tail-water depth is raised further, the roller advances further upstream, reducing the entrained flow until the limit is reached where the entrainment zone is entirely replaced by the roller region. This density jump is non-entraining and is exactly similar in appearance to the free surface hydraulic jump. If the tailwater level is increased further, the outlet and the upstream end of both the hydraulic and density jumps becomes submerged as shown in Figure 2b. Jumps in this state will in future be referred to as flooded jumps. The non-entraining jump represents one limiting case of the density jump.

Summary - The Characteristics of a Density Jump

Briefly, the distinguishing features of a density jump are as follows:-

(1) The density jump generally consists of two zones although at the limits either zone could only be present. There is an entrainment zone followed by a roller region over which there is very little entrainment. The roller region is similar in appearance to the open channel hydraulic jump.

(2) The relative length of these zones is controlled by the tailwater conditions.

(3) Non-entraining and flooded jumps are exactly analagous in appearance and behaviour to the free surface hydraulic jump.

The following chapters examine the various conjugate states attainable by a density jump, and compare these with experimental data. Several forms of tailwater control are then analysed, and the feed back phenomenon between control and jump is examined in the light of experimental results.

Finally the form of the entrainment function is examined, together with the unsteady density current or nose.

Chapter 2 - The Force Flow Equation

2.1 Introduction

In this chapter it is proposed to examine the conditions under which a density jump can form. The conjugate states either side of a density jump are not necessarily unique. Ambient fluid may be entrained into the density jump, thereby increasing discharge and lowering the density difference downstream. The flow is approximately uniform on either side of the jump. A density current issuing from a slot does not become unstable immediately, as can be seen from the photograph in Fig. 4. There is a short region over which the flow is uniform and hence the pressure is hydrostatic. Downstream of the density jump, the turbulence has been suppressed and the flow is again nearly uniform.

2.2 Analysis - The Continuity Equation

The equation of conservation of mass, for a steady incompressible two dimensional flow, is given by:-

$$\frac{\partial}{\partial x}(\rho u) + \frac{\partial}{\partial y}(\rho v) = 0 \qquad (1)$$

where ρ is the fluid density and u and v are the velocity components in the x and y directions respectively as shown in Figure 5. Molecular diffusion, in the flows considered here, is of a lower order than the terms in equation 1 and has therefore been neglected (Koh, 1964)

The density of the ambient fluid (ρ_o) is uniform throughout. Let the density of the flowing layer be $\rho_o + \Delta\rho$ where $\Delta\rho$ is a function of

depth (y). It is assumed the section under examination is sufficiently far

upstream or downstream of the jump for conditions to be uniform in the

x direction.

When equation (1) is integrated across a section normal to the velocity

vector, as in Figure 5, one has

$$\int_0^D (\rho_o + \Delta\rho) \, u \, dy = C_1 = \text{a constant,}$$ where D is the distance to the

upper fluid boundary (the free surface in this case). However, since the

flow is incompressible and steady $\int_0^D u \, dy = C_2 = \text{a constant,}$ hence

$$\int_0^D \frac{\Delta\rho}{\rho_o} u \, dy = \frac{C_1}{\rho_o} - C_2 = \emptyset$$ where $\emptyset$ is also a constant. The

equation

$$\int_0^D \frac{\Delta\rho}{\rho_o} u \, dy = \emptyset \tag{2}$$

will be referred to as the equation of continuity of density difference.

$\emptyset$ is termed the flux of density difference.

2.2 The Boussinesq Assumption

The following analysis is much simplified if the Boussinesq assumption

is made (Batchelor 1953), (Rouse, Yih and Humphries 1952). Differences

in density of the moving and ambient fluids are assumed small, so that

variation in inertial forces can be ignored. Mathematically this may be

expressed as

$$\rho_o \approx \rho = \rho_o + \Delta\rho$$

The change in density is only considered important when associated with

gravity and acts as a buoyancy force. The error introduced by making

this assumption was less than 0.5 per cent for the thermal density

Fig. 4: The uniform flow region upstream of a
density jump.

currents used in experiments.

2.3 The Equation of Motion

The equation of motion for the steady flow shown in Figure 5 is given by

$$\rho_0\left(u\frac{\partial u}{\partial x} + v\frac{\partial u}{\partial y}\right) = -\frac{\partial h}{\partial x} + \frac{\partial \tau}{\partial y} \tag{3}$$

This may be rearranged to give:-

$$\rho_0\left(\frac{d(u^2)}{dx} + \frac{d(uv)}{dy}\right) = -\frac{\partial h}{\partial x} + \frac{\partial \tau}{\partial y} \tag{4}$$

If equation (4) is integrated across a section of the tank with the limits y = 0 at the lower boundary, and y = D at the free surface, the convective terms reduce to

$$\rho_0\left(\frac{d}{dx}\int_0^D u^2\,dy + \left[uv\right]_0^D\right)$$

where $\left[u\,v\right]_0^D = 0$
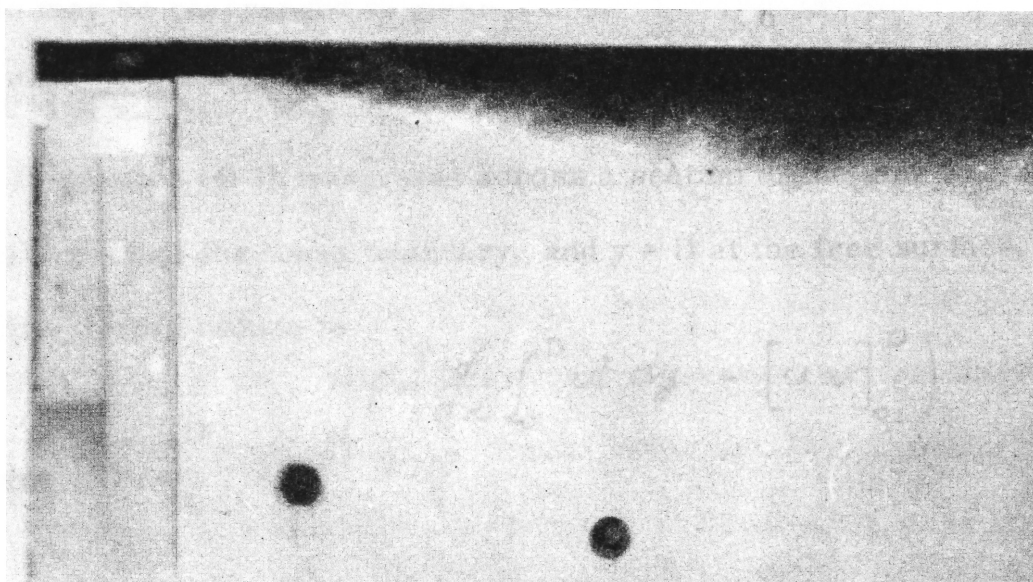
The streamlines are not curved. Therefore pressures are hydrostatic.

Hence

$$h = \int_y^D \rho g\,dy = \int_y^D (\rho_0 + \Delta\rho)\,g\,dy$$

and on integrating across the section one obtains

$$-\int_0^D \frac{\partial h}{\partial x}\,dy = -\int_0^D \frac{\partial}{\partial x}\int_y^D (\rho_0 + \Delta\rho)g\,dy\,dy$$

However, upstream, and far downstream of the jump, $\Delta\rho$ is independent of x, so that the partial differential with respect to x may be taken outside the integral. The right hand side of the above equation reduces to:-

$$\frac{\partial}{\partial x}\int_0^D\int_y^D \Delta\rho\,g\,dy\,dy$$

Integration of the shear force across the section yileds:- $\left[\tau\right]_{o}^{D} = -\tau_{w}$

where τ_w is the bottom shear stress, since shear at the free surface

is negligible. The equation of motion, for the case under examination can

be written as:-

$$\frac{\partial}{\partial x}\left(\rho_o \int_c^D u^2\,dy + \int_o^D \int_y^D \Delta\rho\,dy\,dy\right) = -\tau_w \tag{5}$$

It is convenient to define new parameters dealing with the mean flow.

Equation 5 may then be expressed in terms of mean flow parameters.

A characteristic depth of the density current (y') is defined as the dis-

tance between the fixed boundary, against which the density current flows,

and the mean position of the visual interface. It was found that the

characteristic depth generally coincided with the depth to maximum vel-

ocity and density gradients. This was fortunate since the latter depth

has been used as the characteristic depth by other investigators (Ellison

and Turner 1959). The writer defined the characteristic depth to the

visual interface because the latter could be rapidly and simply detected

by dyeing the moving layer. The position of the visual interface was

found to be independent of the concentration of dye in the layer, and co-

incided with the region of steepest density gradient. This was verified

experimentally, for numerous layers, with varying dye concentrations

and density gradients. The interface in most laboratory experiments was

laminar, so the interfacial depth could be measured accurately. Hence-

∇ Free surface

D

Ambient Fluid

ρ_o

Interface

$\rho_o + \Delta\rho$

y'

u'

u

Density Current

y

x
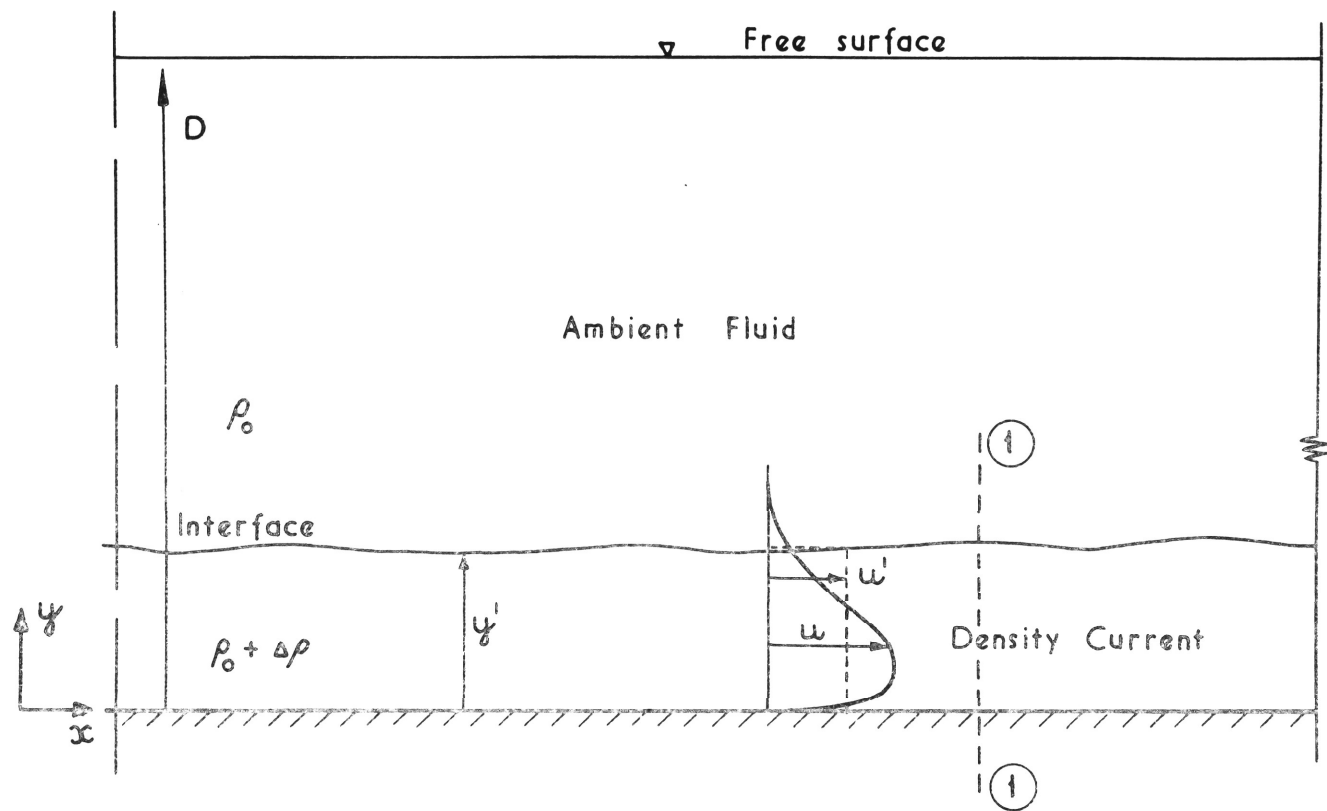
DEFINITION SKETCH OF A UNIFORM DENSITY FLOW

FIGURE 5.

forth the characteristic depth shall be simply referred to as the depth of a density current.

The velocity and density distributions downstream of a jump are generally non-uniform across the section. Hence a characteristic velocity (u') is defined as:

$$u' \equiv \frac{1}{y'} \int_0^D u \, dy \tag{6}$$

Similarly a characteristic density difference (Δ) is defined by:

$$\Delta \equiv \frac{\phi}{u'y'} = \frac{1}{u'y'} \int_0^D u \frac{\Delta\rho}{\rho_0} g \, dy \tag{7}$$

If the density distribution is uniform across the section and the density discontinuity coincides with the visual interface, the characteristic density is given by:

$$\Delta = \frac{\Delta\rho}{\rho_0} g$$

The latter is independent of the velocity distribution. However, if as is generally the case, the density is non-uniform across the section, the characteristic density is dependent on the velocity distribution.

It is convenient to define a momentum distribution correction factor as:

$$S_m \equiv \frac{1}{u'^2 y'} \int_0^D u^2 \, dy \tag{8}$$

S_m is unity if the velocity is uniform from $y = 0$ to $y = y'$ and zero elsewhere. Experimental values of S_m were found to lie in the range 1.05 to 1.32.

Secondly a hydrostatic force correction factor is defined as:

$$S_H \equiv \frac{2}{\Delta y'^2} \int_0^D \int_y^D \frac{\Delta\rho}{\rho_0} \, dy \, dy \tag{9}$$

S_H is unity if the density is uniform from $y = 0$ to $y = y'$ and

is zero thereafter. S_H was found to be less than one and lay in the range

0.59 to 1.0.

Equation (5) may be written in terms of the new parameters as:-

$$\frac{\partial}{\partial x}\left(\frac{S_m (u' y')^2}{y'} + \frac{S_H \Delta y'^2}{2}\right) = -\frac{\tau_w}{\rho_o}$$

the density flow Q, is defined as

$$Q = \int_0^D u \, dy = u'y'$$

and from equation (7)

$$\Delta = \frac{\phi}{Q} \tag{10}$$

On substituting for u'y' and Δ , the equation of motion reduces to

$$\frac{\partial}{\partial x}\left(\frac{S_m Q^2}{y'} + \frac{S_H y'^2}{2Q}\phi\right) = -\frac{\tau_w}{\rho_o} \tag{11}$$

Integration of the above with respect to x gives

$$\frac{S_m Q^2}{y'} + \frac{S_H y'^2}{2Q}\phi = M$$

$$and \; M = M_1 - \int_{x_1}^{x_2}\frac{\tau_w}{\rho_o}\, dx \tag{12}$$

The variable M is equal to the sum of the horizontal momentum flux

and pressure force per unit span, at a cross section of the flow.

M_1 is the magnitude of M at some reference section (1 in Figure 5).

The integral term, in equation 12, is the total boundary shear force

acting on the flow between the reference section and the section of interest.

Boundary shear forces are usually neglected in the hydraulic jump

analysis because of their small magnitude. However, since the Reynolds

numbers associated with density flows are generally low, the shear forces

are proportionately larger. The ratio of upstream force flow to the

boundary shear between Sections 1 and 2 was found to be fifteen to

thirty per cent. It was therefore necessary to account for boundary

shear in the analysis of the density jump.

It is convenient to non-dimensionalise Equation 12. This may be

accomplished by dividing equation 12 by $\dfrac{y^2_{1c}}{Q_1}$. The variable y_{1c} is

the critical depth of the upstream density flow; defined by

$$y_{1c} \equiv \left(\frac{Q_1{}^2}{\Delta_1} \right)^{1/3} \tag{13}$$

The subscripts 1 and 2 refer to sections upstream and downstream of

the jump respectively.

Equations (10) and (13) can be combined to give $\phi = \left(\dfrac{Q_1}{y_{1c}} \right)^3$

Hence

$$\frac{y_{1c}}{Q_1{}^2} = \frac{Q_1}{y_{1c}{}^2 \phi}$$

It is convenient to define two dimensionless parameters K and Y.

K is defined as the ratio of flows upstream and downstream of the density

jump, so that

$$K \equiv \frac{Q_2}{Q_1} = \frac{\Delta_1}{\Delta_2} \tag{14}$$

The flow upstream of the jump will have a K value of one. That

downstream of the jump must be equal to, or greater than one, depending

on the quantity of ambient fluid entrained.

The second dimensionless parameter Y is defined as the ratio of

the characteristic depth of flow, at the section of interest, to the critical
upstream depth y_{1c}, hence

$$Y = \frac{y'}{y_{1c}} \qquad (15)$$

Upstream of a jump Y must be less than one, as the flow is super-
critical. It will be shown, that if the upstream depth is equal to, or
greater than critical depth, no jump will occur. This result might be ex-
pected from knowledge of hydraulic jump behaviour. Downstream of the
jump Y is greater than one.

The non-dimensional equation of motion is given below.

$$\frac{M y_{1c}}{\rho_c Q^2} = \frac{S_m K^2}{Y} + \frac{S_H Y^2}{2K} \qquad (16)$$

Equation (16) will be referred to as the force flow equation where the

quantity $\dfrac{M y_{1c}}{\rho_c Q_1^2}$ is termed the force flow (Benjamin 1962).

2.4 The Force Flow Diagram

The force flow equation is plotted in Figure 6 with the force flow and Y
as the abscissa and ordinate axes respectively. The flow ratio (K) is used
as the plotting parameter, and it can be seen that a family of curves exists
bounded by an envelope(DF in Figure 6) and the force flow axis. Only force
flow curves with K values of one or greater are of practical interest.
Values of K less than one are physically unattainable.

The momentum and hydrostatic force correction factors (S_m and S_H)
have been taken as unity when plotting the diagram. Since its purpose is
illustrative, and is not intended to be quantitative, the selection of S_m and
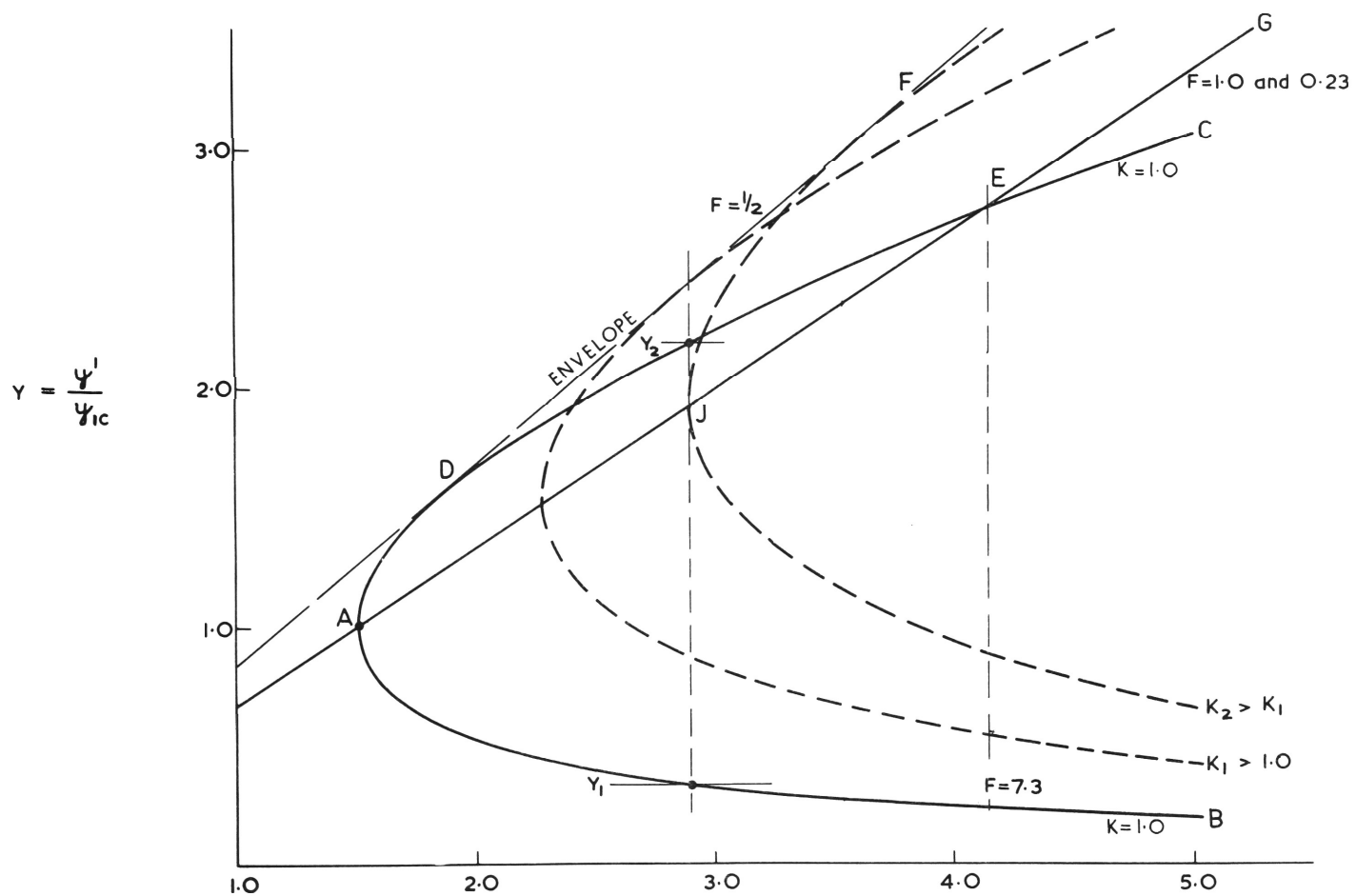
$$\frac{M\psi_{IC}}{\rho Q_1{}^2} = \frac{Sm K^2}{Y} + \frac{Sh Y^2}{2K} \qquad \text{for } Sm = S_H = 1.0$$

THE FORCE FLOW DIAGRAM

FIGURE. 6.

S_H values is not important.

Any supercritical upstream flow may be represented by a point on the lower arm of the K = 1.0 curve (AB in Figure 6). If a density jump occurs without entrainment, the conjugate state is found directly above on the upper arm of the K = 1.0 curve. The conjugate ratios of the non-entraining density jump, are identical to those of the open channel, hydraulic jump, for which K is always unity.

An an example, consider the depth Y_1 in Figure 6. The conjugate state for a non-entraining jump with zero boundary friction, is given by moving vertically up to the point Y_2, on the K = 1.0 curve. The ratio $\dfrac{Y_2}{Y_1}$ is the conjugate depth ratio.

The K = 1.0 curve has a minimum value of force flow at the point A (Y = 1.0 and $\dfrac{M_{y1c}}{\rho_o Q_1{}^2}$ = 1.5). The depth at this point is critical and the Froude number defined as

$$F \equiv \left(\frac{Q^2}{\Delta \cdot y'^3}\right)^{\frac{1}{2}} \tag{17}$$

is equal to unity. As one moves away from the minima on the lower arm of the K = 1.0 curve, the upstream Froude number increases in value, while on the upper arm the downstream Froude number decreases.

Equation (16) is a cubic in K. Hence there are three values of K, which will satisfy the force flow equation, at any point below the envelope (DF) of the force flow diagram (Figure 6). One K value is

always negative and is of no interest; the other two solutions are real and positive. Both values of K are physically possible in certain regions of the force flow diagram; in others, only one or no solution has meaning. At any point in the zone between the envelope and the abscissa axis, the upper value of K shall be denoted by K_u and the lower value by K_L.

All possible states upstream of a density jump lie on the line AB in Figure 6.

It is evident from the above, that only certain regions of the force flow diagram represent physically attainable, downstream states, for a density jump.

Dimensional analysis shows if frictional forces are neglected, a density current flowing as shown in Figure 5 is fully defined by its Froude number (F) where $F = \left(\dfrac{Q^2}{\Delta y^3}\right)^{\frac{1}{2}}$ provided D is much larger than y'.

It is shown in Chapter 6, that for the flow geometry being examined, flows with Froude numbers greater than unity are unstable and can entrain ambient fluid until the Froude reduces to unity. The unity limit on the Froude number applies only if the velocity and density distributions are uniform. It will be shown the general limit is given when $F = (S_H / S_m)^{\frac{1}{2}}$.

Meaningful solutions for the force flow equation must have sub-critical flow downstream of a density jump. Therefore, the Froude number in this region must be unity or less.

Before proceeding further with examination of the zones of the force

flow diagram it is advisable to familiarise oneself as to how the Froude

number plots on the force flow diagram.

It will now be shown that a curve of constant Froude number is a

straight line passing through the origin of the force flow diagram and lies

on, or below the envelope. The Froude number is defined by

$$F = \left(\frac{Q^2}{\Delta y^3}\right)^{\frac{1}{2}}$$

but when $y'_1 = y_{1c}$, then

$$F_{1c} = \left(\frac{Q_1^2}{\Delta_1 y_{1c}^3}\right)^{\frac{1}{2}} = 1.0$$

Equations (14) and (15) may be combined with the above to show

$$F = \left(\frac{K}{Y}\right)^{3/2} \tag{18}$$

The force flow equation can be rearranged into

$$\frac{M y_{1c}}{\rho_0 Q_1^2} = \frac{S_H}{2} \frac{Y}{K} \left(2 \frac{S_m K^3}{S_H Y^3} + 1\right) Y$$

$$= \frac{S_H}{2} \left(\frac{2 \frac{S_m}{S_H} F^2 + 1}{F^{2/3}}\right) Y \tag{19}$$

Hence for a constant Froude Number

$$\frac{M y_{1c}}{\rho_0 Q_1^2} = \gamma Y$$

where

$$\gamma = \frac{S_H}{2} \frac{2 \frac{S_m}{S_H} F^2 + 1}{F^{2/3}}$$

S_m and S_H are both taken as unity on the force flow diagram. Therefore

the plot of equation (19) is a straight line passing through the origin. Its

slope (γ) is a function of the Froude number.

F is double valued for any γ except at the maxima, where

$$\frac{\partial \gamma}{\partial F} = \frac{4 F^2 + 1}{3 F^{5/3}} = 0$$

and $F = \frac{1}{2}$. A plot of γ versus F is shown in Figure 7, where it can

be seen γ is a maximum when $F = \frac{1}{2}$. It follows from equation (18)

that $\frac{\partial F}{\partial K}$ is positive, hence for a given value of Y, K_u will be assoc-

iated with the larger value of Froude number and K_L with a lower value.

F is only single valued at the stationary point. Hence K also is single

valued at this point. Therefore the line $F = \frac{1}{2}$ is the envelope of the force

flow diagram.

2.41 Zones of the Force Flow Diagram

The force flow diagram can be divided into zones as shown in Figure 9.

No solutions exist in the region above the envelope ODF. All points

below this envelope represent mathematical solutions to the force flow

equations. For these solutions to represent a physical state downstream

of a density jump two further conditions must be satisfied:-

(i) K must be equal to or greater than one and

(ii) F must be equal to or less than one.

K curves having force flow minima to the left of the K = 1.0 curve minima

(A), in Figures 6 and 8, have K values of less than one and therefore do

not represent physically attainable solutions. Hence it can be shown that

all K_L points lying below the K = 1.0 curve (ADEC) do not represent

physical solutions. Curves of constant Froude number lying below the

$$\gamma = \frac{2F^2 + 1}{2F^{2/3}}$$
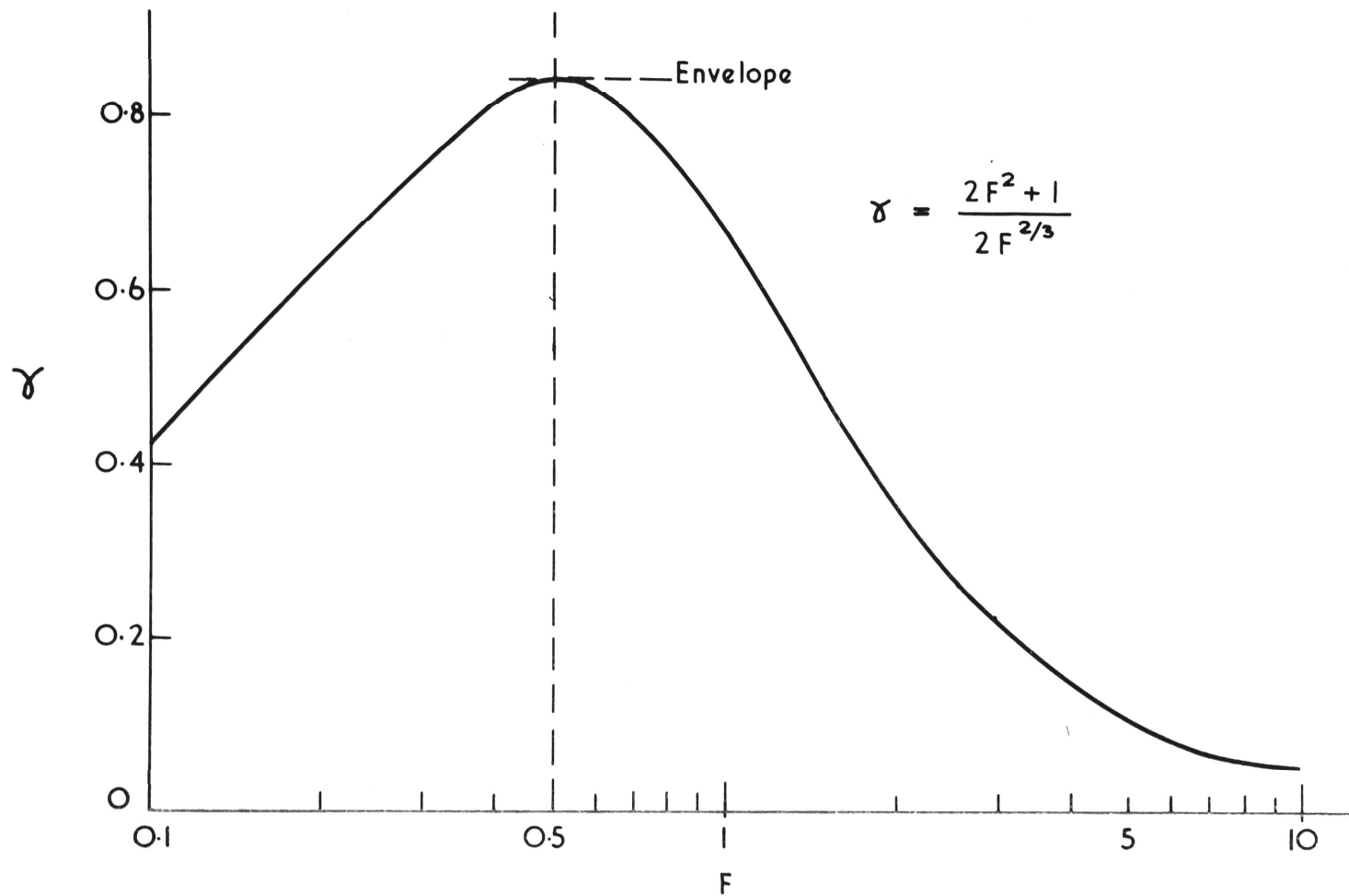
SLOPE OF CONSTANT FROUDE No.
LINES ON THE FORCE FLOW DIAGRAM

FIGURE 7.
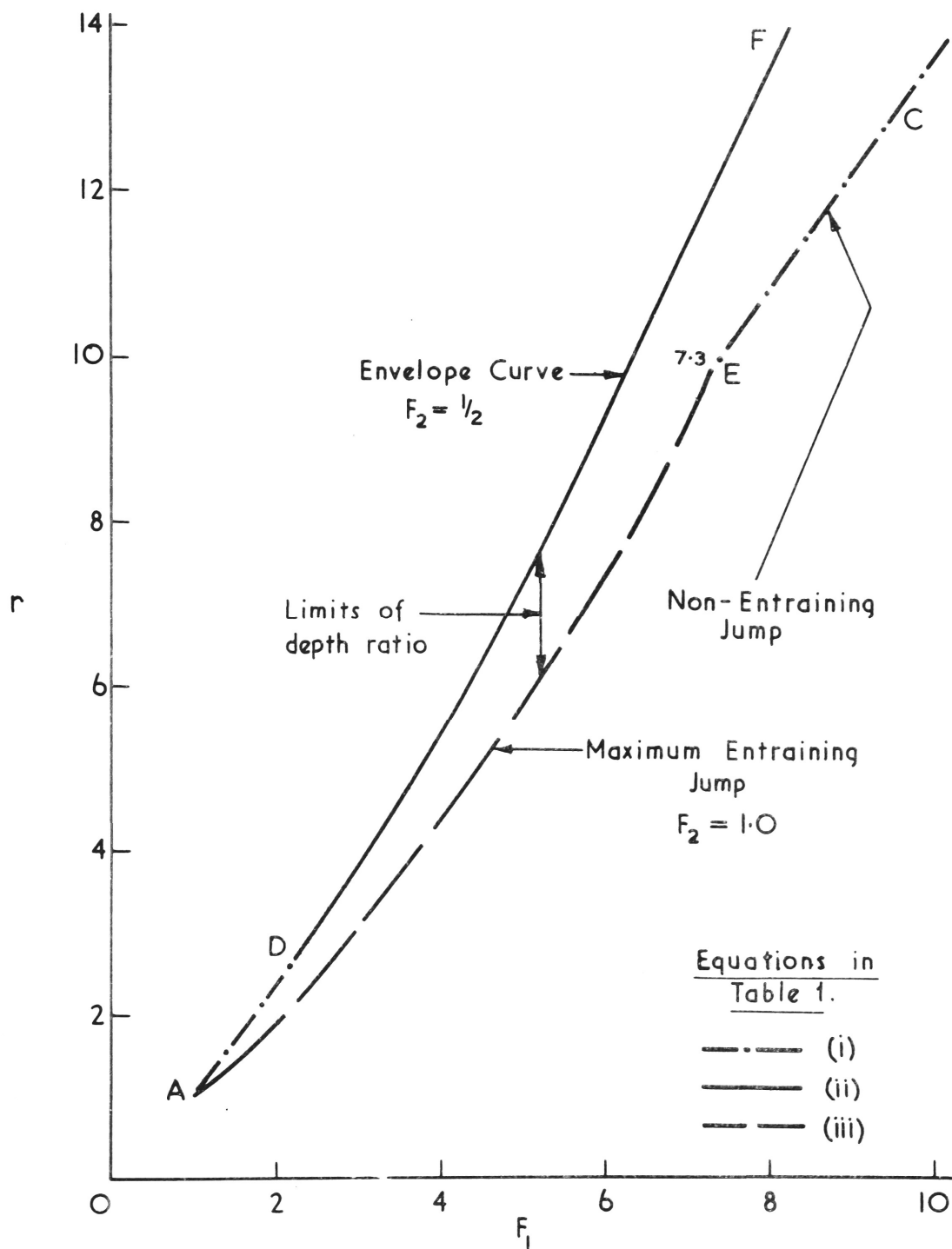
CONJUGATE DEPTH RATIO VERSUS FROUDE No.

FIGURE 8.
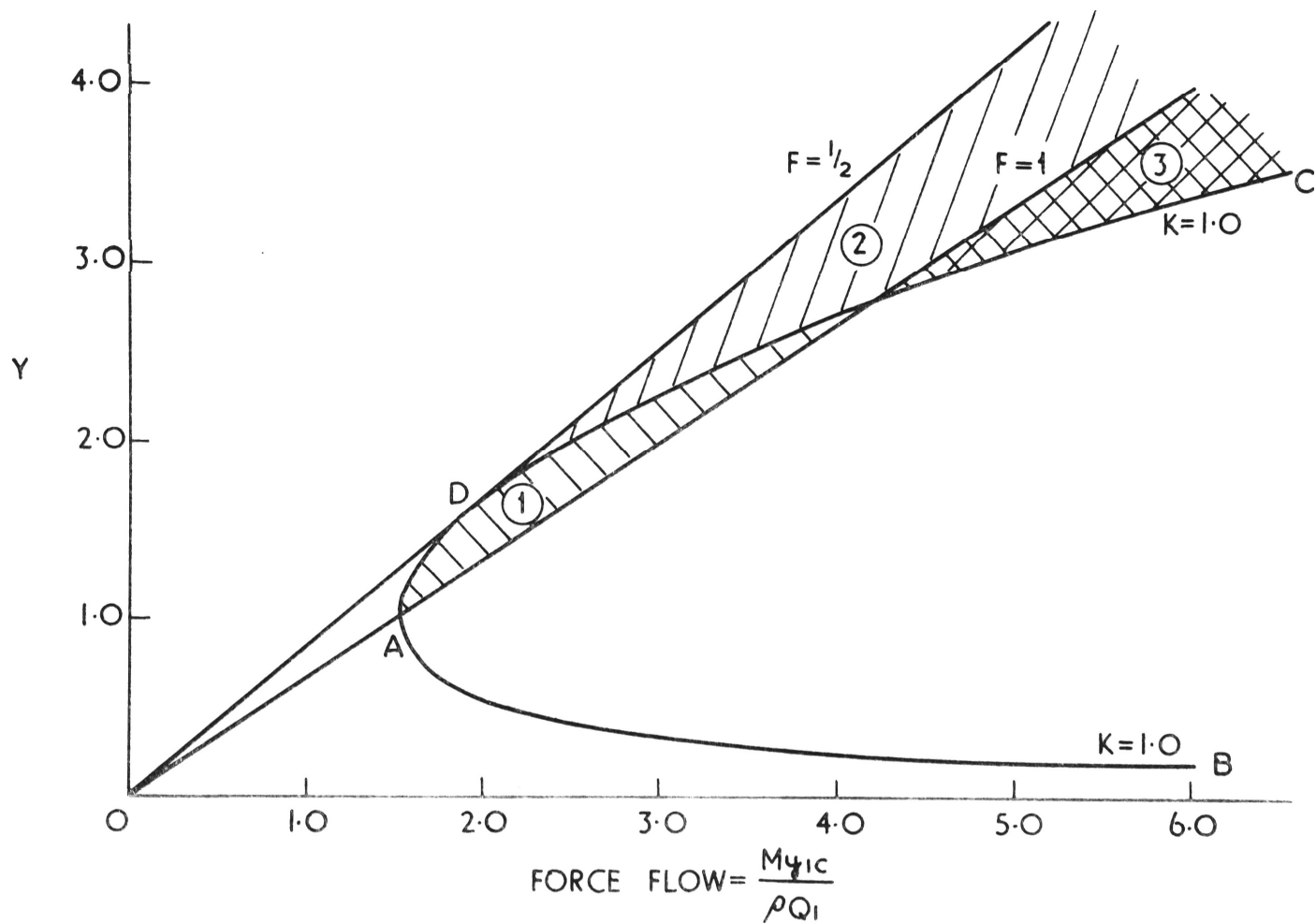
THE ZONAL FORCE FLOW DIAGRAM

FIGURE 9.

F = 1.0 curve (AEG) and associated with a K_u value have Froude

numbers greater than one. These also do not represent physically attain-

able downstream states.

The three zones where downstream solutions do exist are:-

Zone 1 ADEA is bounded by the K = 1.0 (ADE) curve and the F = 1.0

line (AE) only the upper K value has meaning since the lower value is less

than one.

Zone 2 GEDF is bounded by the F = $\frac{1}{2}$ line (DF), the F = 1.0 line (EG)

and the K = 1.0 (DE) curve. Both K values can be attained in this zone.

Zone 3 (CEG) is bounded by the F = 1.0 line (EG) and the K = 1.0

curve (EC). The K_u values yield Froude numbers greater than one in this

zone; therefore only the K_L values can represent a tailwater condition.

It is apparent from the above that, unlike an open channel hydraulic

jump, depths and densities downstream of a density jump cannot be pre-

dicted from upstream conditions alone. Limits to the conjugate state can

be established, but within those limits, entrainment and depths down-

stream are dependent on the tailwater control.

2.5 <u>Further Deductions from the Force Flow Diagram</u>

Minimum depth is given by conjugate states lying along the curve

AEC. Along the AE of this curve entrainment is a maximum and along

EC there is no entrainment. The point E is the transition point for these

two minimum depth regimes. The point E has a force flow of 4.15 and

the upstream Froude number associated with this value of force flow

is 7. 3, as shown in Figure 6.

Maximum depth is given by conjugate states lying along the curve

ADF. It can be seen in Figure 6 that conjugate states having force flows

less than 1. 88, and therefore upstream Froude numbers less than $\mathbb{F}_1 = 2.25$

lie to the left of D. In this case conjugate depth is a maximum when there

is no entrainment at the density jump. Conjugate states of density jumps

with force flows greater than 1. 88 lie to the right of D, and have maximum

conjugate depths when the conjugate state lies on the envelope DF. It has

been shown previously that along the envelope the Froude number is single

valued and equal to one-half.

The conjugate depth ratio (r) is defined as the ratio of depths upstream

and downstream of a density jump. Hence

$$r = \frac{y_2{}'}{y_1{}'}$$

The equations of the limits to the conjugate depth ratio as stated above

are tabulated below. These limiting equations are plotted in Figure 8.

Maximum Entrainment

It can be seen from the force flow diagram that maximum entrainment

occurs when the conjugate state lies on the minima of a K curve, the point

J in Fig. 6. At this point $\quad \frac{\partial}{\partial Y}\left(\frac{M y_{1c}}{\rho_c Q_1^2}\right) = \frac{S_H - S_m F^2}{F^{2/3}} = 0$

so the Froude number is equal to $\left(\frac{S_H}{S_m}\right)^{1/2}$.

As S_H and S_m are taken as unity on the force flow diagram, the downstream Froude number is equal to one when entrainment is a maximum.

The $F = 1.0$ line (AEG) in Figure 6 is therefore one limit to the entrainment (a maximum). No entrainment (ADEC) in Figure 6 is the second limiting condition.

3. Limits on the Downstream Depths

Maximum Depth Ratios

Range				Conjugate depth ratio	Section in Fig. 9	No.
Force Flow		Froude No.				
min.	max.	min.	max.			
1.50	1.88	1.00	2.25	$\frac{1}{2}\left[\left(1+8F_1^2\right)^{1/2}-1\right]$	AD	i
1.88	∞	2.25	∞	$\dfrac{2(2F_1^2+1)}{3(2F_1)^{2/3}}$	DF	ii

Minimum Depth Ratios

1.50	4.10	1.0	7.3	$\dfrac{2F_1^2+1}{3\,F_1^{2/3}}$	AE	iii
4.10	∞	7.3	∞	$\frac{1}{2}\left[\left(1+8F_1\right)^{1/2}-1\right]$	EC	i

Unlike the open channel hydraulic jump, the density jump problems cannot be solved using the force flow equation alone. Characteristics of the control downstream of the density jump must also be known. The downstream control determines the degree of entrainment into a density jump and hence its form. Before proceeding further with the mathematical analysis of the density jump, the physical aspects of the phenomena are examined. This is done in the following chapter.

Chapter 3 - The Mechanics of the
Density Jump.

It is necessary to examine the mechanism of a density jump in some further detail, before the interaction between a density jump and its control can be fully appreciated.   Therefore, the characteristics of the density jump itself are now discussed.

3.1 The Zones of a Density Jump

The density jump, in general, can be divided into two distinct zones, an entrainment zone followed by a roller region. Nearly all the entrainment which occurs at the jump takes place in the entrainment zone.

The roller region is characterised by a flow in the reverse direction to the main flow, close to the interface. This roller is similar in appearance to the roller observed in open channel jumps. The roller region may be regarded as surge, which under steady flow conditions remains stationary, and covers the downstream end of the entrainment zone. The presence of the roller causes the interfacial shear to fall to a low level as shown in Figure 10. The change in profile of the jump, before and after raising a controlling weir, is also shown. The roller region is quite distinct in the exaggerated scale used for plotting. The change of profile is less easily detected in experiments. Dye probes were used to find the region of reverse flow and so determine the boundary of the roller region and the entrainment zone. The roller region can be forced upstream by a control, so as to cover the entire entrainment zone. The
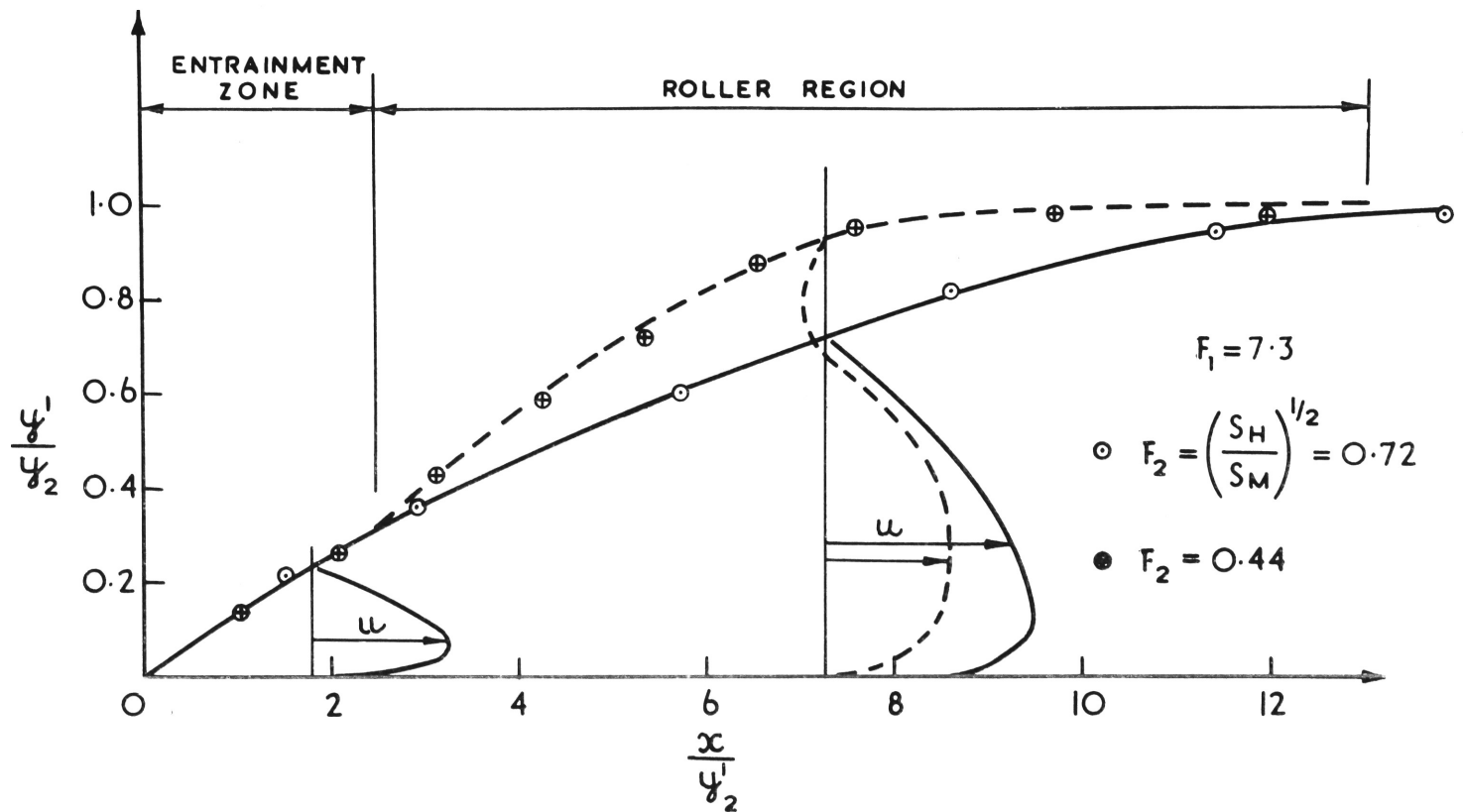
THE EFFECT OF DOWNSTREAM CONTROL ON THE PROFILE AND
VELOCITY DISTRIBUTION IN A DENSITY JUMP

FIGURE 10.

roller region then extends the full length of the jump which becomes non-entraining. The control can also be adjusted so as to cause the roller region to retreat so that in the limit the jump is of the maximum entraining type with no roller region.

3.2 The Control Mechanism

The control downstream of a density jump acts directly on the roller region of that jump. Adjustment of the downstream control will cause the roller region to migrate. The migration will be upstream if the adjustment has caused a temporary increase in the downstream force flow. Conversely the migration will be downstream if the adjustment results in a temporary fall in the downstream force flow.

The direction of migration is important as it will affect the equilibrium of the jump. Consider as an example a density jump controlled by a weir downstream (Figure 11). If the weir height is raised by a small amount, the force flow at the weir will be temporarily increased. A positive surge will move upstream causing the roller region to migrate further upstream and entrainment at the jump will be reduced. Now provided the reduction in entrainment causes a drop in the downstream force flow, which can compensate for the initial increment, a new equilibrium will be obtained. The new equilibrium will result in new values of depth and discharge downstream of the jump.

However, if the reduction in entrainment had lead to an increase in the

downstream force flow, then a new equilibrium could not be obtained and the jump would become unstable. The imbalance of force flow upstream and downstream of the jump would cause the roller region to move further into the entraining zone so that eventually the jump would flood.

Under certain conditions density jumps do become unstable as will be seen in the following chapter.

3.3 Effect of Roller Region Migration on the Downstream State of a Density Jump

The downstream state of a density jump can be expressed in terms of two factors; firstly the upstream flow state, as defined by the upstream Froude number and secondly, by the amount of entrainment at the jump. The downstream control only affects entrainment by determining the length of the entraining zone. The entrainment mechanism is entirely independent of the downstream control.

Therefore in order to understand how roller region migration affects the downstream state of a jump it is necessary to examine how the roller region affects entrainment.

If one considers a highly supercritical density current, the fluid momentum is the dominant component of the force flow, and the hydrostatic pressure force is small. In the limiting case, where the momentum component completely dominates, it could be expected that the density current would behave in a similar manner to a neutrally buoyant jet.

Time t_1

Time $t_2 > t_1$
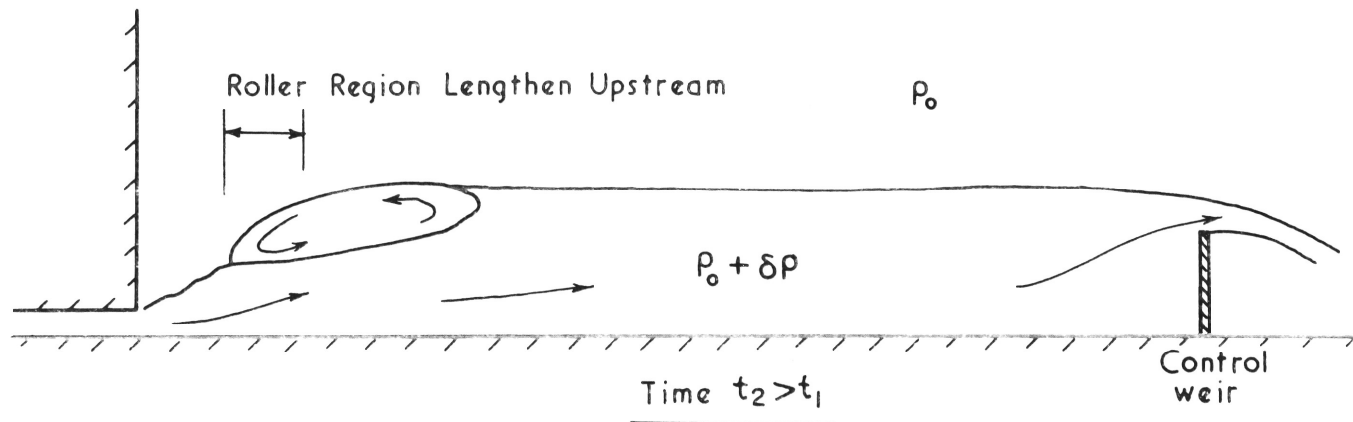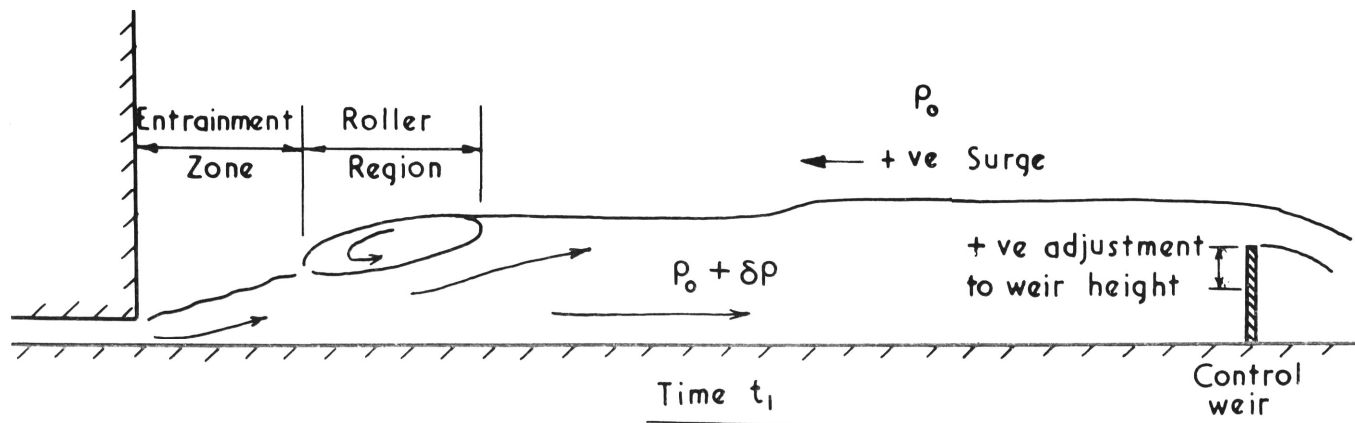
CONTROL OF THE ROLLER REGION OF A DENSITY JUMP BY
THE DOWNSTREAM CONTROL

FIGURE 11.

When a neutral jet issues from a slot as shown in Figure 12, the severe velocity gradient between the moving fluid and the ambient fluid gives rise to high local shear. Eddies are generated in this zone of maximum instability and the ambient fluid is entrained into the jet.

A supercritical density current is unstable in the same way under similar boundary conditions.

It can be seen from the force flow equation (19), that as the density current spreads the local Froude F number reduces in value. A continuous range of local Froude numbers will exist along the length of the entrainment zone, ranging from $F = F_1$ to a possible minimum of $\left(\dfrac{S_H}{S_m}\right)^{1/2}$ or unity in the idealised case.

As there is negligible entrainment in the roller region of a density jump, the roller region can be modelled mathematically, as a non-entraining hydraulic jump, and represents a discontinuity in depth but not in discharge nor density. The local Froude number at the end of the entrainment zone or the commencement of the roller region, is therefore related to the Froude number downstream of the jump by the same equation used to relate conjugate Froude Numbers in hydraulic jumps.

3.4 Summary

A density jump can generally be divided into two zones; an entrainment zone and a roller region. The entrainment zone, which is perhaps more exactly described as a negatively buoyant jet, occupies the upstream

end of the jump. The roller region, characterised by an interfacial roller, occupies the downstream end of the jump. Nearly all entrainment into the density jump occurs in the entrainment zone.

The limits of form of a density jump occur when only one of either of the zones is present. A continuous range of forms between these limits is available. The roller region can be regarded as a non-entraining jump whose position is determined by the downstream control. If the roller region is forced further into the entrainment zone, the Froude number at the upstream end of the roller region is increased and the Froude number downstream of the jump is correspondingly reduced.
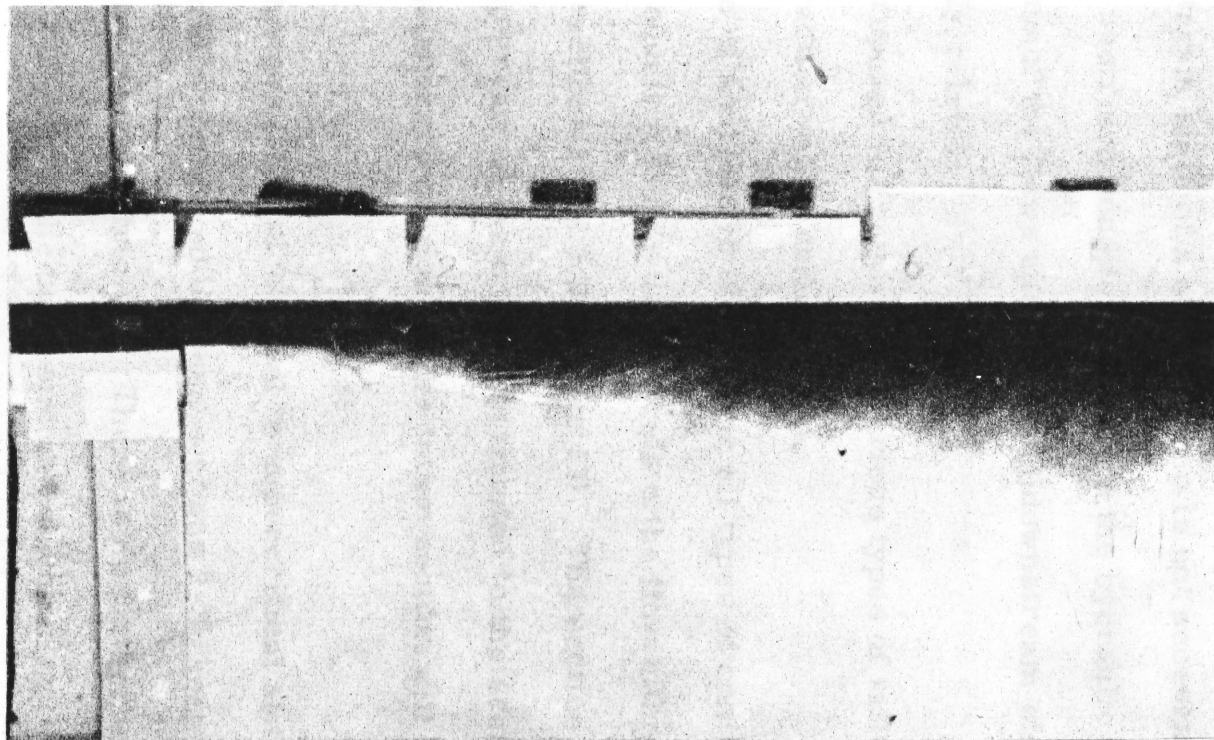
Fig. 12: A jet of neutral density.

Note the region of uniform flow near the inlet.

Chapter 4.   Control of a Density Jump

4. 1 Introduction

The downstream state of a density jump is not necessarily a direct function of the upstream conditions.   Unlike the hydraulic jump, the Froude numbers of the flows upstream and downstream of a density jump are not uniquely related.

It is now proposed to examine the various types of tailwater control and their interaction with a density jump.

The method of analysis is similar for all types of control.   Firstly the force flow equation (16) is used to relate the flow either side of the density jump (sections 1 and 2 in Figure 13).   The section downstream of the jump and upstream of the control is equated to the section at the control by means of the energy equation.   This latter section will be denoted by the subscript 3.

The flow changes from subcritical to supercritical at the control, and energy is generally conserved between sections 2-3 except for minor losses caused by boundary friction.   There is no further entrainment between sections 2-3 so that the upstream and downstream discharges are the same.

The density jump analysis is similar for all forms of control; therefore general equations relating between sections (1) and (2) will be derived first.   The later analysis will examine individual controls in

some detail. The theoretical derivations will be compared with the experimental results.

4.2 Analysis - Conjugate Equations at the Jump

The critical depth of the flow downstream of the jump, y_{2c}, is a useful reference parameter by which to relate sections 2 and 3. As there is no entrainment between these sections, critical depth at either will be the same, hence

$$y_{2c} = y_{3c}$$

The force flows, upstream and downstream of the jump, may be equated using equation (19), so that

$$\frac{}{} = \frac{Y_2}{Y_1} = \quad \cdots \quad \cdots$$

where θ, the force flow ratio across the density jump is defined by

$$\theta = \frac{M_2}{M_1} = \frac{1 - \int \dfrac{\tau_w}{\rho_o}\, dx}{M_1}$$

But $y_{1c} = y_1' F_1^{2/3}$ and $y_{2c} = y_2' F_2^{2/3}$ and on substitution into the above equation one finds

$$\cdots \qquad\qquad (20)$$

The energy equations between sections 2 and 3 may be used to express the variable y_{2c} in terms of a control parameter, say a weir height, or a channel contraction ratio, depending on the individual control.

To avoid confusion, the density difference will be assumed to be an
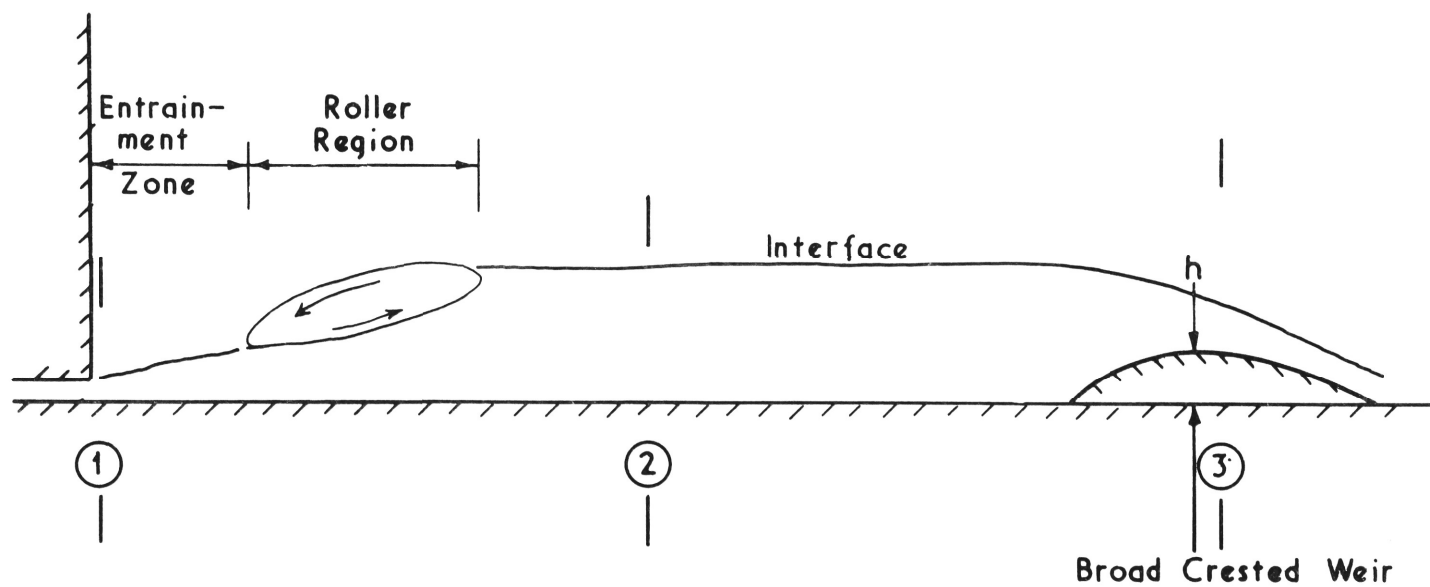
DENSITY JUMP CONTROLLED BY A BROAD CRESTED WEIR

FIGURE 13.

excess; so that density currents will flow along the bottom of a channel. Up and down have their usual directions. Later when density currents with density deficits are discussed, it will be convenient to have the directions of up and down reversed. By definition then, down is understood to be in the direction of the body, or apparent gravity force.

Boundary friction except where it itself acts as a control, has been ignored in the following analysis. It was convenient to do this so that explicit solutions could be obtained. Numerical solutions or backwater calculations which included boundary friction could have been determined, but this was not the writer's aim. It was desired that the effect of individual controls could be examined independently. The inclusion of friction in the analysis would have masked individual behaviour. Friction as a control of a density jump was examined separately.

4.3 The Broad Crested Weir

4.31 Introduction

The mechanism by which a density jump can vary its entrainment to comply with a downstream control has already been described, so that only a brief review will be repeated.

A free overfall is a limiting state of a broad-crested weir where the weir height (h) is zero.

In this limiting case, as will be shown in Section 4.4, the density jump will be of the maximum entraining type. A control which could establish a back water and roller region in the jump does not exist.

As a result, the density jump entrains along the length of the establishment zone.

Under these conditions the Froude number of the flow downstream of the jump is given by $F_2 = (\frac{S_H}{S_m})^{\frac{1}{2}}$ and the ratio $\frac{h}{y_2}$ is zero. When the weir is raised a surge moves upstream to form a roller region or standing surge at the downstream end of the density jump.

Further raising of the weir causes the length of the roller region to increase and the entrained flow is reduced. It would appear that if this process is continued, the roller region would eventually cover the entire entrainment zone and entrainment at the jump would cease. Further raising of the gate would cause the jump to flood.

Although the above picture satisfactorily describes the phenomena at upstream Froude numbers less than 13.2, it will be shown in the following analysis, that at Froude numbers greater than 13.2, the jump floods before the stage of zero entrainment is reached. The reason for this lies in the form of the energy equation, which relates the downstream Froude number to the weir height. Two values of downstream Froude number satisfy the energy equations for any weir height below a critical maximum height.

When the Froude number upstream of the jump is greater than 13.2, it will be shown both downstream Froude numbers are possible solutions, but that only the upper value is a stable solution. Therefore, the minimum

stable Froude number downstream of a jump controlled by a broad

crested weir is 0.17, the Froude number at which the critical weir height

is reached. The minimum conjugate Froude number to this value is that

for a non-entraining density jump and is equal to 13.2.

4.32 Analysis

The energy equation is used to equate flows upstream and at the control

point of a broad-crested weir (see Figure 3). If one makes the Boussinesq

assumption the total energy flow in a steady density current is given by:-

$$\mathcal{E} = \frac{\rho_o}{2} \int_0^{y'} u^3 dy + \int_0^{y'} u \int_y^{y'} \Delta \rho g \, dy \, dy + \int_0^{y'} u y \Delta \rho g \, dy \tag{21}$$

where $\mathcal{E}$ is the energy flow. The first term is the kinetic energy,

the second is the pressure energy and the third is the potential energy of

the density current.

If correction factors S_K and S_P are defined as

$$S_K = \frac{Q^3}{y'^2} \int_0^{y'} u^3 dy$$

$$S_P = \frac{Q}{\Delta y'} \left[\int_0^{y'} u \int_y^{y'} \frac{\Delta \rho}{\rho_o} g \, dy \, dy + \int_0^{y'} u y \frac{\Delta \rho}{\rho_o} g \, dy \right]$$

then the energy equation can be written in the form

$$\mathcal{E} = Q \left(\frac{S_K Q^2}{2 y'^2} + S_P \Delta y' \right)$$

If S_E is defined as $S_E = \dfrac{S_K}{S_P}$

the above equation reduces to

$$\mathcal{E} = Q S_P \left(\frac{S_E Q^2}{2 y'^2} + \Delta y' \right) \tag{22}$$

form $\quad \dot{\epsilon} = S_p \dot{\epsilon} \left(\dfrac{S_E \dot{c}^{\epsilon}}{2 \dot{v}^{\prime\prime}} + \dot{\epsilon} \, y^{\prime} \right)$ $\qquad\qquad$ 22

Further discussion on the above equation is included in section 4.44

of this chapter.

If equation 22 is differentiated with respect to x and it is assumed

that

(a) energy is conserved

(b) the velocity distribution is self preserving

(c) there is no entrainment between Sections 2 and 3, then

$$\left(- \dfrac{S_E \, Q^2}{\dot{y}^{\,\dot{}}} + \dot{\Delta} \right) \dfrac{\dot{j}\,\dot{y}^{\prime}}{\dot{j}\,x} = \dot{0} \qquad\qquad (23)$$

At critical depth there is a transition from subcritical to supercritical

flow hence $\quad \dfrac{d_y{}^{\prime}}{dx}\quad$ is negative and non-zero.

It follows then at the point of control

$$\dfrac{\dot{E} \, \dot{\cdot}}{\dot{\cdot} \, \dot{\cdot}} = 1 \qquad\qquad (24)$$

Since there is no further entrainment downstream of the density jump

$$y^{\prime}_3 = y_{2c}$$

$$K_3 = K$$

and $\quad \dot{\Delta}_3 = \Delta_2$

Equating energy flows at the control and upstream one finds

$$\dfrac{\dot{\epsilon} \, \dot{\cdot} \, \dot{\cdot}}{\dot{\cdot} \, \dot{v}_{-}} + \Delta_2 \left(y_{2c} + \dot{\cdot}_{\cdot} \right) = \dfrac{\dot{\cdot}_E \, (\dot{\cdot} \, Q)^2}{\dot{\cdot} \, \dot{y}_{-}} + \Delta_2 \, y^{\prime}_2$$

and on substituting equation 24 into the above one obtains

$$\frac{y_2'}{y_{2c}} = \frac{3 + 2\frac{h}{y_{2c}}}{S_{E2}F_2^2 + 2} \tag{25}$$

Equation (24) and continuity may be combined to give

$$\frac{y_2'}{y_{2c}} = \frac{S_{E3}^{-1/3}}{F^{2/3}} \tag{26}$$

Substituting for $\dfrac{y_2'}{y_{2c}}$ in equation 25 and rearranging one obtains

$$\frac{h}{y_{2c}} = \frac{S_{E3}^{-1/3}\left(S_{E2}F^2 + 2\right) - 3F_2^{2/3}}{2F_2^{2/3}} \tag{27}$$

Equation 27 gives the weir height in terms of the downstream reference depth, as a function of the downstream Froude number. Equation 27 is not in a useful form because y_{2c} is also a function of downstream conditions. y_{2c} may be eliminated by use of the force flow equation 20 derived earlier. This equation relates the conjugate states either side of the density jump in terms of the reference depth y_{2c}. Hence one can show

$$\frac{h}{y_{1c}}f = \frac{\left[S_{E3}^{-1/3}\left(S_{E2}F^2 + 2\right) - 3F_2^{2/3}\right]F_2^{2/3}\,\theta}{2S_{m2}F_2^2 + S_{H2}} \tag{28}$$

where

$$f = \frac{2F_1^{4/3}}{2S_{m1}F^2 + 1} \tag{29}$$

Equation (28) relates the weir height to the downstream Froude number and plotted in Figure 14.

Several significant points arise from examination of this figure.

(a) Firstly when the weir height is zero, and in the absence of friction

or any other downstream control, the density jump will be of the max-

imum entraining type and the downstream Froude number will be equal

to $\left(\dfrac{S_H}{S_m}\right)^{\frac{1}{2}}$. This limiting case is examined in more detail in Section

4.4 later in this chapter.

(b) Secondly it can be seen the density jump is initially very sensitive to

weir height. Raising of the weir to only 5-6 pc. of its potential height

for flooding, at Froude numbers greater than 13.2 causes the downstream

Froude number to drop from 1.0 to 0.8.

(c) There is a maximum value of $\dfrac{h}{y_{1c}}$ f for which a solution is possible.

If a weir is raised above this maximum the jump must flood, since the

force flow downstream has been increased above that attainable upstream.

Consider a density jump having a high upstream Froude number. As

the weir is raised, the downstream state moves up the curve from the

starting point at $\dfrac{h}{y_{1c}}$ f = 0 and F_2 = 1.0 in Figure 14.

The Froude number downstream of the jump will continually decrease

in value as the weir height increases, and the roller region lengthens,

covering more and more of the entrainment zone. The process continues

until the maximum weir height for which a solution is possible is reached

at F_2 = 0.17 and $\dfrac{h}{y_{1c}}$ f = 0.322. At this stage the density jump would

appear as shown in Figure 15. The jump is still entraining ambient fluid.

Further increase in the weir height results in an increase in the

force flow downstream, which can no longer be balanced by any change

$$\frac{h}{\psi_{1c}} f = \frac{\left[(S_{E3})^{-1/3} (S_{E2} F_2^2 + 2) - 3 F_2^{2/3}\right]}{(2\; S_{m2} F_2^2 + S_{H2})} \cdot F_2^{2/3} \theta$$

where
$$f = \frac{2 F_1^{4/3}}{2 S_{M1} F_1^2 + 1}$$

plotted for

$S_E,\; S_M,\; S_H\; \&\; \theta = 1$
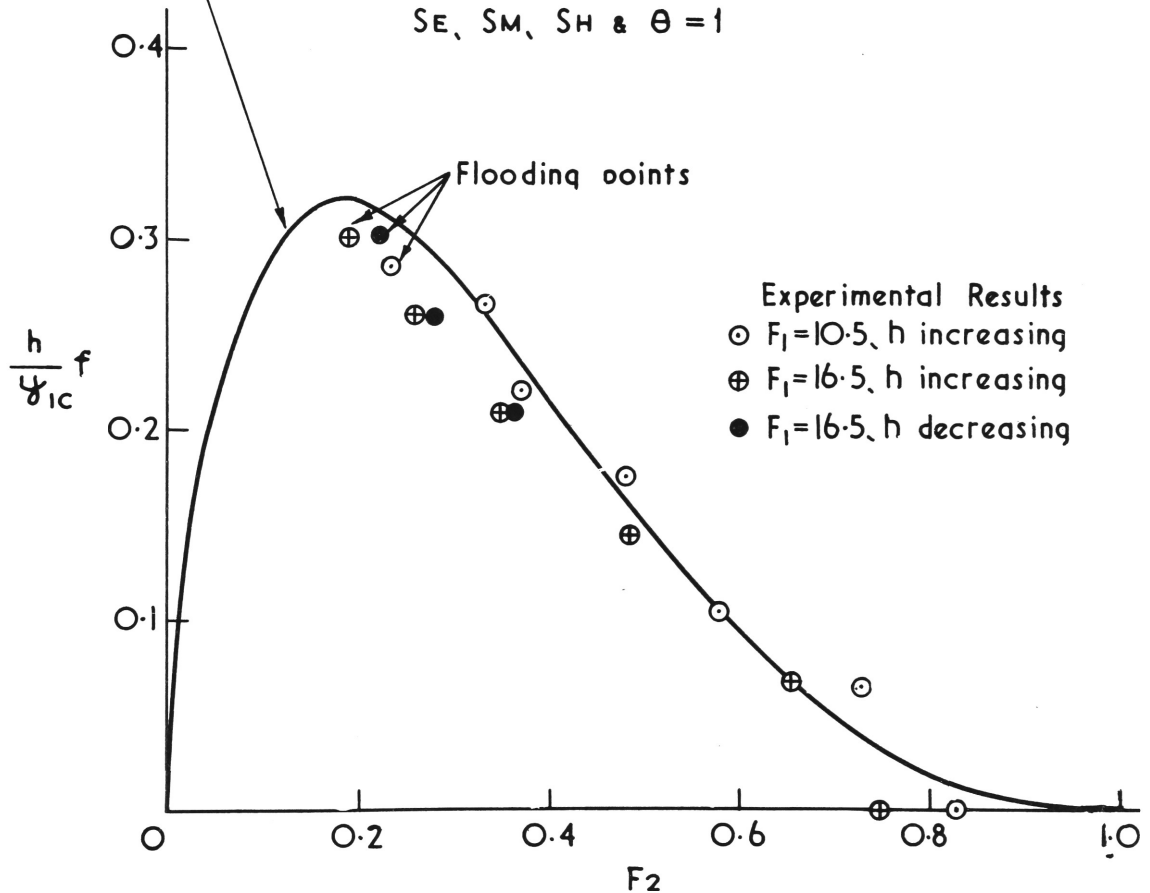
Flooding points

Experimental Results
$\odot$ $F_1 = 10.5$, h increasing
$\oplus$ $F_1 = 16.5$, h increasing
$\bullet$ $F_1 = 16.5$, h decreasing

$\frac{h}{\psi_{1c}} f$ (vertical axis)

F_2 (horizontal axis)

WEIR HEIGHT VERSUS DOWNSTREAM FROUDE No.
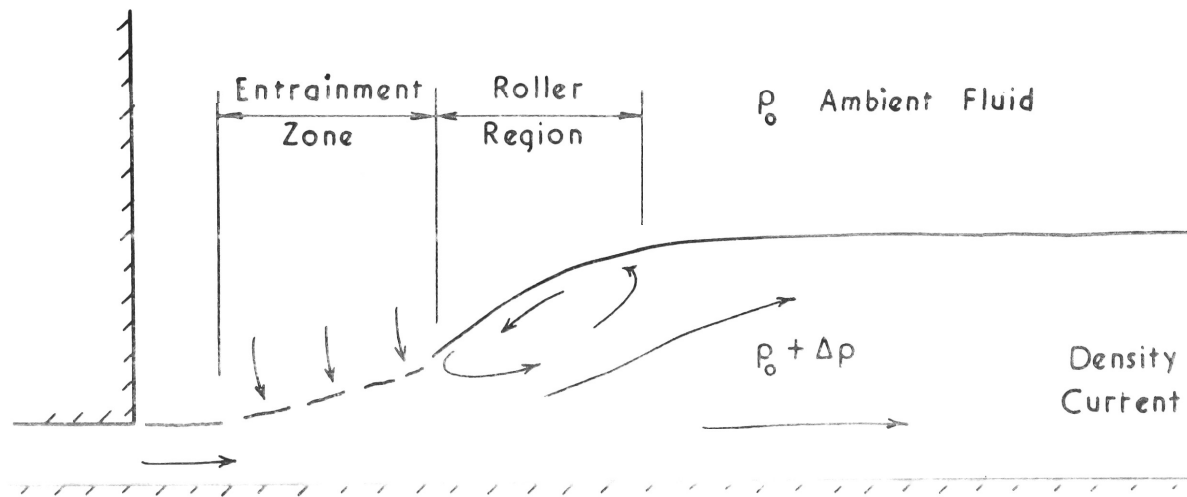
FIGURE 14.

THE PARTIALLY ENTRAINING DENSITY JUMP

FIGURE 15.

in entrainment at the jump. The roller region is seen to move up-stream as a surge which rapidly covers the entire entrainment zone. Flooding of the density jump continues until the hydrostatic pressure at the flooded upstream end of the jump balances the downstream force flow. When equilibrium of force flows upstream and downstream of the flooded jump is attained, the jump appears as shown in Figure 16. Figures 17 and 18 show photographs of the jump just before and after flooding has taken place.

From Figure 14 it can be seen two values of F_2 satisfy equation 28 for any weir height less than the maximum at $F_2 = 0.17$.

It should be noted that downstream Froude numbers less than 0.17 are only potentially accessible to density jumps with upstream Froude numbers greater than 13.2 since this is the minimum value of F_1 con-jugate to $F_2 = 0.17$. Density jumps with F_1 less than 13.2 will flood before F_2 reaches 0.17. Once a jump has flooded entrainment ceases, and its equilibrium conditions are no longer given by Equation 28. Analysis of the flooded density jump is given in Appendix A.

It will now be shown that downstream Froude numbers of less than 0.17 are unattainable by all entraining density jumps, irrespective of their upstream Froude number.

The reasons for this can be best understood by tracing a cycle of weir raising and lowering on a plot of $\dfrac{h}{y_{1c}}$ f vs F_2.

The locus of a weir raising-lowering cycle is shown in Figure 19 for a density jump with an upstream Froude number of 50. Commencing at point A with a weir of zero height and a maximum entraining density jump, as the weir height is increased the downstream Froude number decreases. This mechanism has been described in the previous chapter. The process continues until the point B is reached. At this stage the density jump is still entraining ambient fluid. An increase in weir height will cause the jump to flood to point C. The downstream flow rate abruptly decreases as entrainment ceases and it can be shown that the flooded state of the jump can be represented by the line PCD (Appendix A).

Lowering of the weir will not cause the jump to revert to its entraining state. The small positive perturbation in h at the point B caused a dramatic irreversible change in the jump form. Therefore as the weir is lowered the jump remains flooded and follows the curve for a flooded density jump PCD. This curve is derived in Appendix A. As the weir is lowered the depth of dense fluid lying above the inlet decreases finally reducing to zero at D. The density jump becomes a non-entraining jump and the roller region extends the length of the establishment zone.

It was shown in Section 3.4 that the non-entraining roller region of a density jump is analgous to the open channel hydraulic jump. Hence lowering of a weir downstream of a density jump results in a downstream migration of the roller region, until a new equilibrium is established.

Interface

P_o

$\Delta h \approx \Delta \mathcal{y}_2 \approx \Delta \mathcal{y}_1$

Control weir

$\Delta \mathcal{y}_2$

$\Delta \mathcal{y}_1$

$\mathcal{y}_2'$ $P_o + \delta p$

$h + \Delta h$
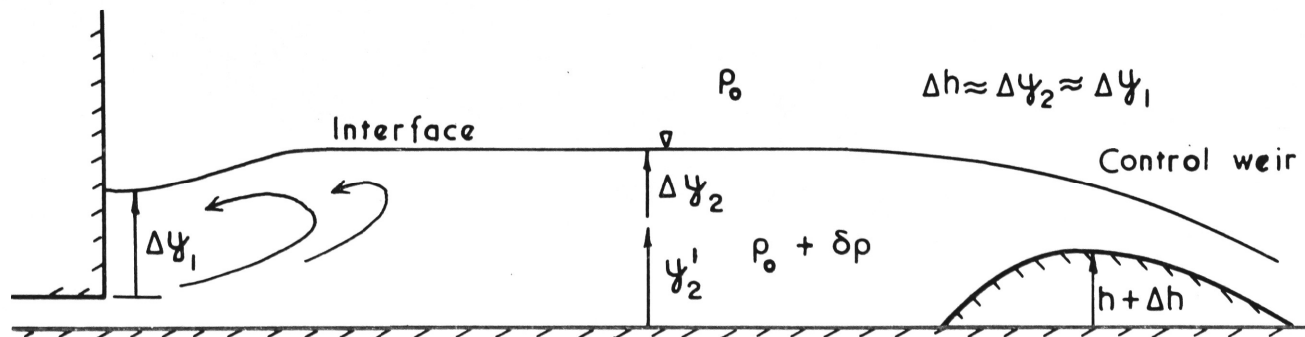
Weir raised causing level to rise by $\Delta \mathcal{y}$

THE FLOODED DENSITY JUMP
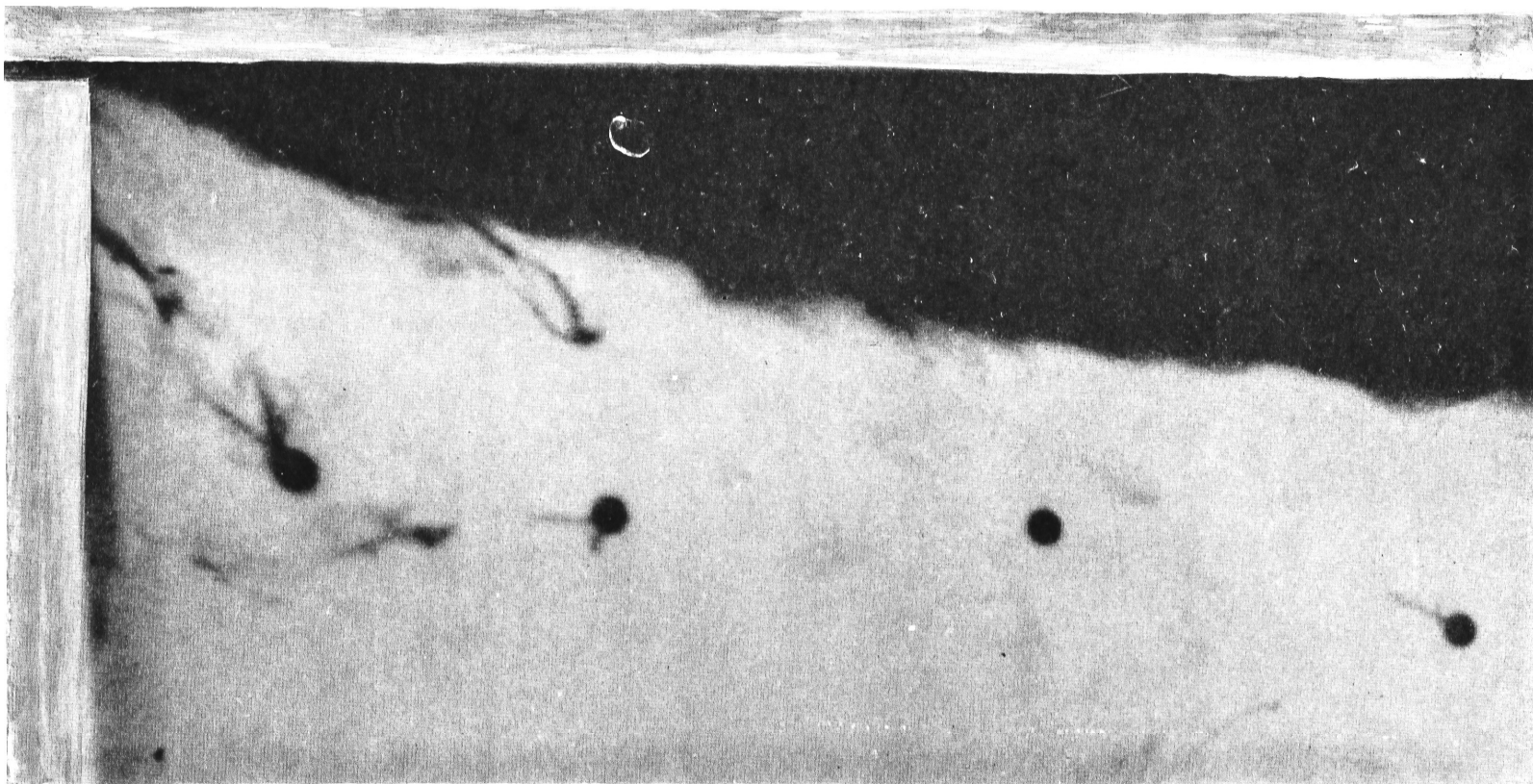
FIGURE 16.

Fig. No. 17: A density jump immediately before flooding - a non-entraining density jump.
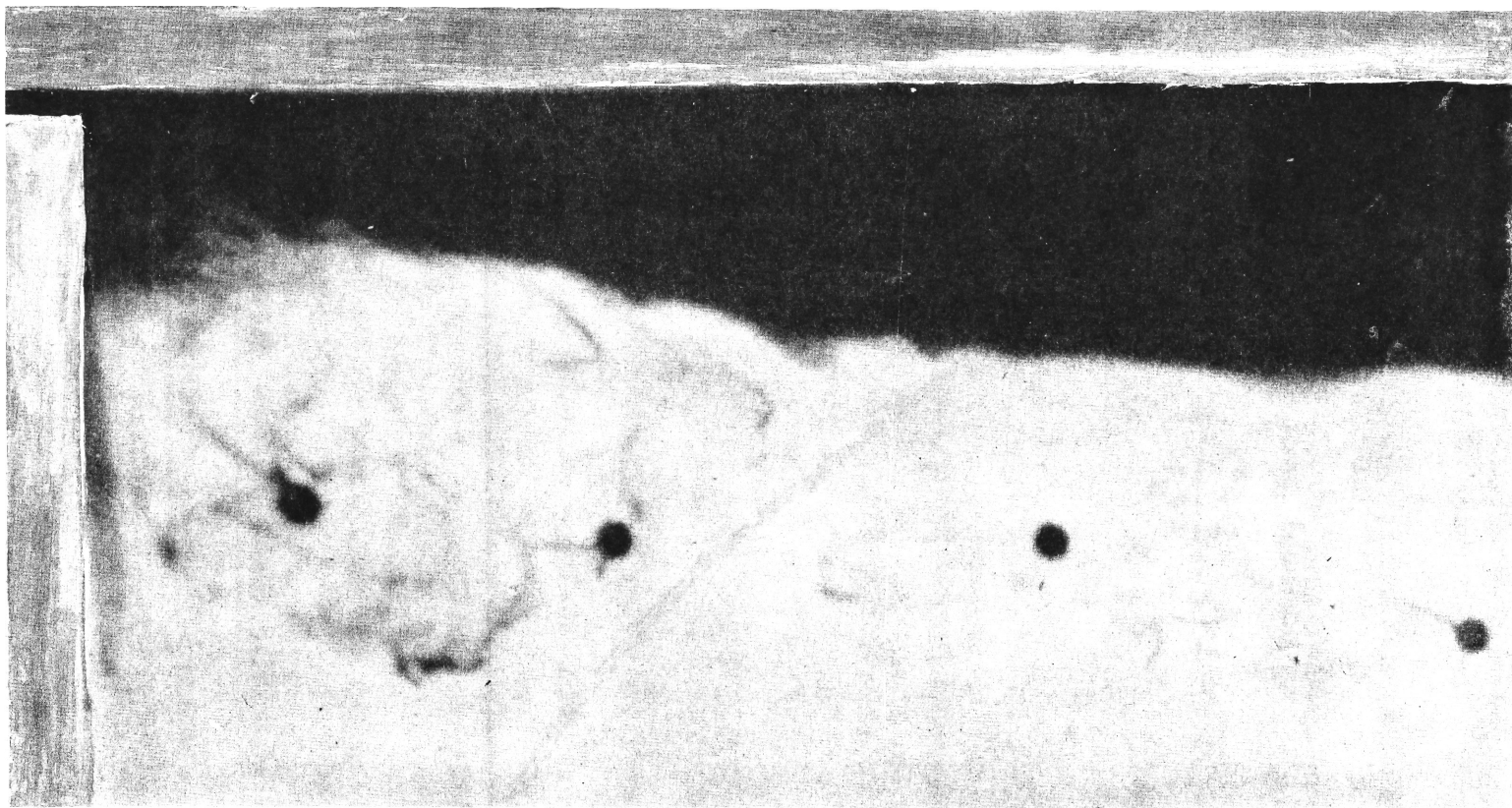
Fig. No. 18:   A flooded density jump.

Flooded Jump Equation

$$\frac{h}{y_{1c}} f = \frac{1}{2}\left(\frac{F_2^2 + 2}{F_2^{2/3}} - 3\right) f$$
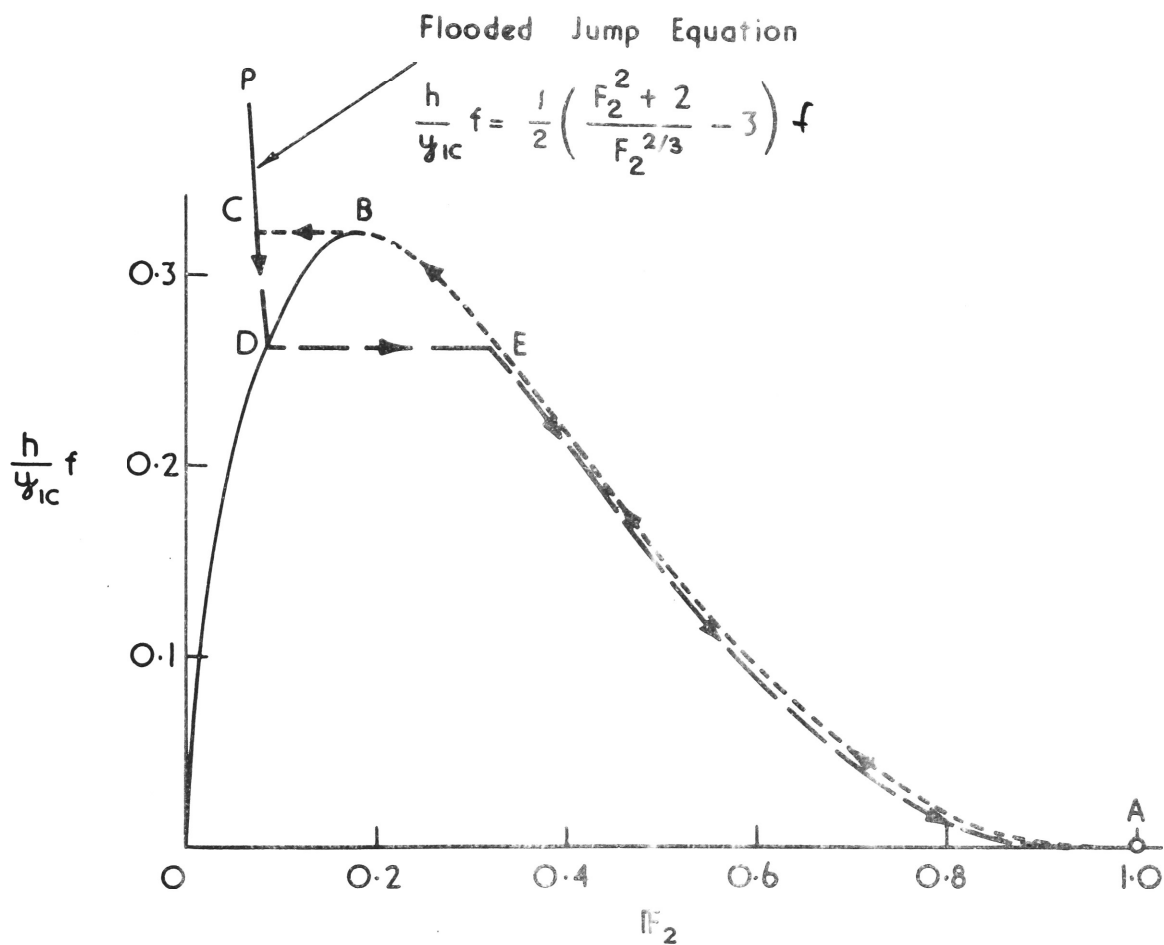
EFFECT OF A WEIR RAISING AND LOWERING CYCLE

ON A DENSITY JUMP

FIGURE 19.

When the roller region moves downstream, a greater length of entrain-ment zone is exposed, so that total entrainment at the jump increases. The flow downstream of the density jump therefore increases until the interfacial slope is equal to the bottom slope and equilibrium is restored.

If the weir is raised, then by the same mechanism, the roller region migrates upstream and entrainment is reduced.

It is now shown that downstream migration of the roller region will result in an increase in the Froude number (F_2) downstream of a density jump. If F_t denotes the local Froude number at the transition of the roller region and the entrainment zone, a whole range of values for F_t are available between the limits $F_t = F_1$ and $F_t = \left(\dfrac{S_H}{S_m}\right)^{1/2}$. If the roller region moves downstream, F_t must decrease in value. Now the down-stream Froude number (F_2) is related to F_t by the same equation that re-lates conjugate Froude numbers in hydraulic jumps (Bakmettef 1932)

$$F_2 = \frac{F_t}{\left\{ \tfrac{1}{2} \left(\left[8F_t^2 + 1 \right]^{1/2} - 1 \right) \right\}^{3/2}}$$

It can be seen from the above equation that as F_t decreases in value F_2 must increase in value. Hence one can conclude that if a control downstream of a density jump is perturbed as to cause a fall in the inter-facial slope, the downstream Froude number will increase in value.

Consider now a density jump whose state is described by the point D

in Figure 20a. It has been shown this state can be reached by lower-ing a weir downstream of a flooded density jump having a sufficiently high upstream Froude number. At D the density jump is at the limit of flood-ing and is therefore non-entraining. If the weir height is now dropped by a small amount (δ h), the interfacial slope will become negative, the roller region will move downstream and the jump will commence to en-train. Its downstream Froude number will increase in value. It can be seen in Figure 20a that if the Froude number is to increase in value, equilibrium cannot be attained until the point E is reached. A density jump whose state is given by points to the left of B in Figure 20a are unstable for negative perturbations in h, the weir height. The perturb-ation will cause a dramatic change in the flow rate and depth downstream of the jump, as the form of the density jump itself is changed.

It is also necessary to examine the effects of a positive perturbation in weir height for a density jump at D (Figure 20b). This time a positive surge will travel upstream from the weir. The roller region will be forced further upstream and flooding of the jump will ensue. Further raising of the weir would cause the jump to move back along the curve for a flooded jump DCP.

It can be seen that density jumps given by points to the left of B in Figure 19 are unstable for negative perburbations in h. Perburbations in the controlling weir will cause the jump to either flood if the perturb-ation is positive, or the roller region shorten and the downstream Froude
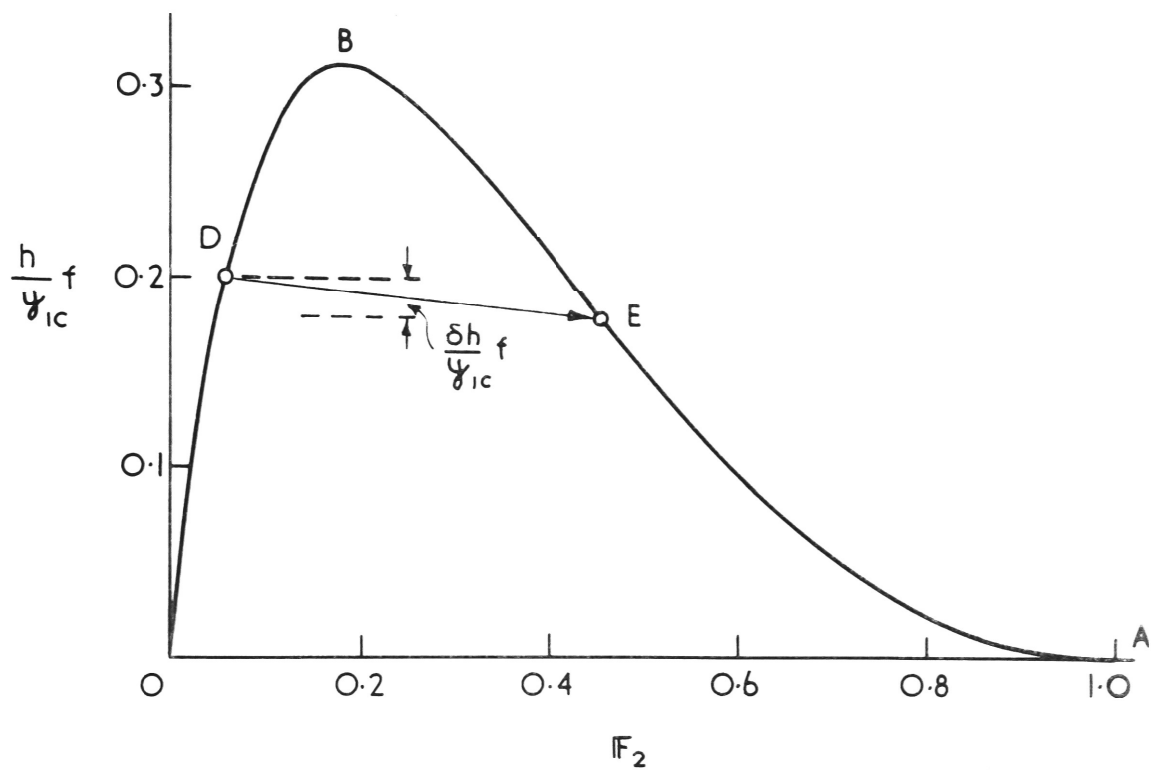
EFFECT OF A NEGATIVE PERTURBATION IN h.

FIGURE 20a.

Flooded Jump Equation

$$\frac{h}{y_{1c}} f = \frac{1}{2} \left(\frac{F_2^2 + 2}{F_2^{2/3}} - 3 \right) f$$
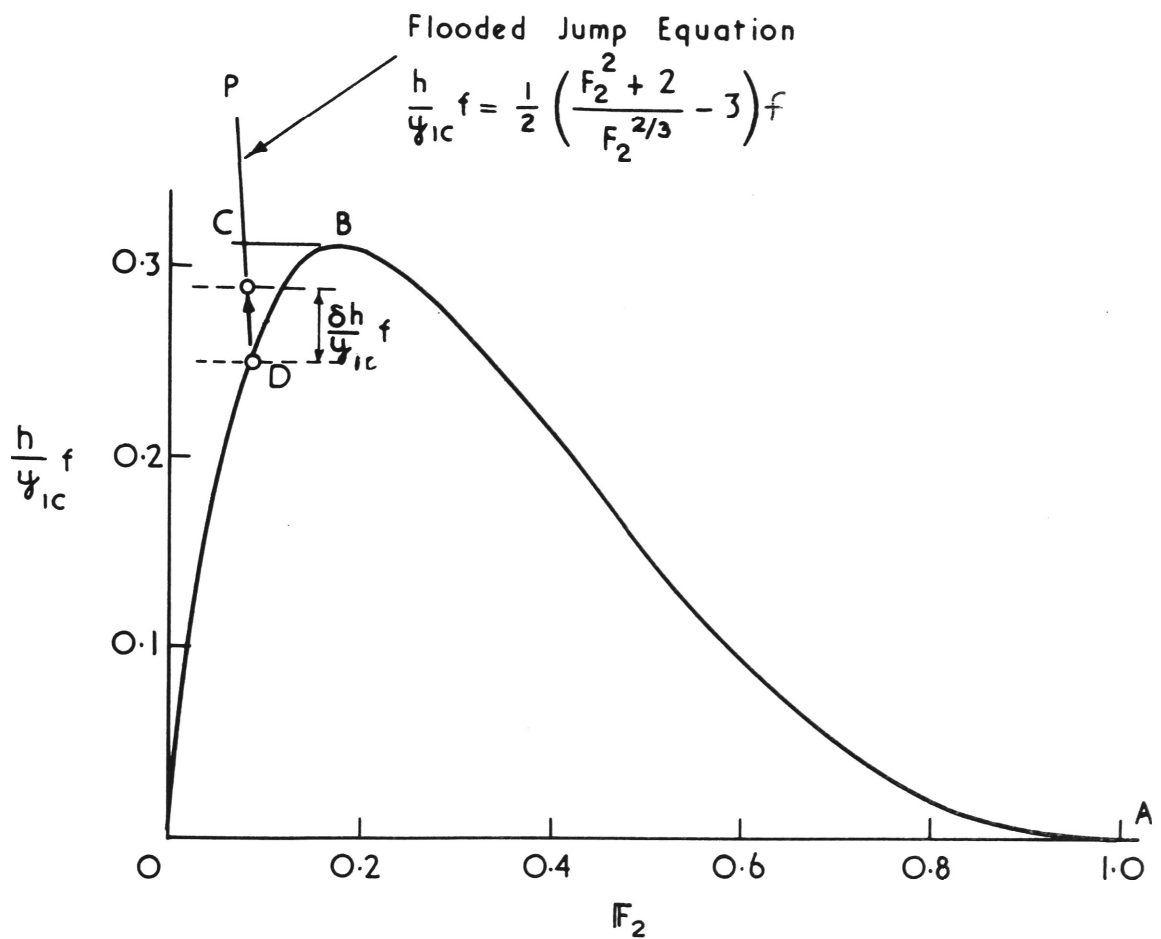
EFFECT OF A POSITIVE PERTURBATION IN h.

FIGURE 20b.

number to increase rapidly, if the perturbation is negative.

Mathematically the stability of a density jump to negative perturbations in a controlling weir downstream are given by -

$$\frac{\partial h}{\partial F_2} \quad - \quad ve \qquad \text{stable}$$

$$\frac{\partial h}{\partial F_2} \quad + \quad ve \qquad \text{unstable}$$

$$\frac{\partial h}{\partial F_2} \quad = \quad 0 \qquad \text{limit of stability}$$

It can be seen in Figure 20 that the limit of stability is given by the point B where $F_2 = 0.17$. Regions of the curve to the right of B are stable (AEB) and regions to the left are unstable (BDO).

4.33 Experimental Results

Equation 28 has been plotted in Figure 14 together with experimental data. It can be seen agreement between theory and experiment is close. It should be noted, however, that the theoretical curve was plotted for S_E, S_m, S_H and θ values of one. The closeness of the curve and the data indicates that the various correction factors are self compensatory. This is indeed fortunate since the correction parameters are not simple functions of F_2 so that no general curve could have been plotted relating weir height and downstream Froude number.

In Figure 14 the flooding points of experimental density jumps have been indicated for jumps with upstream Froude numbers of 10.5 and 16.5.

Unfortunately, with the experimental apparatus available, Froude numbers greater than 16.5 could not be attained. It was not possible therefore to experimentally verify with any certainty, the stability arguments.

Flooding of the density jump with F_1 = 16.5 at a downstream Froude number of 0.19 was earlier than its non-entraining value. However, experimental accuracy was not sufficient to observe any hysteris effect which itself would have been small for this value of upstream Froude number.

A further intriguing relationship exists between weir height and depth downstream of the jump.

It has already been shown that the depth downstream of a jump can be expressed as a function of the upstream and downstream Froude numbers. From the force flow equation (19) one has

$$\frac{\rho_2 \, q^2}{M_1 \, y_2} \quad \frac{y_2}{y_2} \; = \; \frac{2 \, F_2^{2/3}}{2F_2^2 + 1} \qquad \theta \; = \; \frac{y_2'}{y_1'} \quad \frac{2\,F_1^{2/3}}{2F_1^2 + 1}$$

It follows from continuity that

$$\frac{y_1}{y_2} \; = \; F_1^{-2/3}$$

and f has already been defined in equation 29

$$f = \frac{2F_1^{4/3}}{2F_1^2 + 1}$$

so that

$$\frac{\rho_c Q_1^2}{M_1 y_{1c}} = f \qquad (30)$$

Hence ·

$$\frac{y_2' f}{y_{1c}} = \frac{2 F_2^{2/3}}{2 F_2^2 + 1} \theta \qquad (31)$$

The above equation is plotted in Figure 21.

The downstream Froude number-depth equation (31) can be solved with the weir height-Froude number equation (28) to obtain downstream depth in terms of the weir height. Unfortunately, this is not an explicit relationship and so a graphical solution is given in Figure 22.

The feature of interest, illustrated in this plot is a decrease in depth downstream of the jump, with increase in the weir height for downstream Froude numbers less than one half.

Although this result could be anticipated from the downstream Froude number-depth relationship the result is quite novel; an increase in weir height causing a drop in level, upstream of the weir.

4.35 Note on the Validity of the Energy Equation Used

The energy equation (22) used in deriving the rating relationships is not strictly valid unless the density distribution in the moving layer is uniform.

However, use of the energy equation in the present form is justified, provided the differences in density within the moving layer are small compared with the density difference between the layer and the ambient

fluid. When this is not the case, density stratification within the layer can lead to blockage effects and selective withdrawal of only part of the layer (Wood 1968). However, for selective withdrawal to occur it is necessary that (a) the density gradient within the layer be steep and (b) the Froude number of the layer be low.

These conditions are never satisfied simultaneously downstream of a density jump.

Density jumps having low downstream Froude numbers will always have fairly uniform downstream densities. Firstly, because there is little entrainment at the jump. Secondly, the fluid which is entrained, is thoroughly mixed with incoming flow in the roller region. It would appear then, that blocking is most unlikely to occur, and hence there is reasonable justification in using the energy equation in the present form. Experimental results tend to confirm this.

4.4 The Maximum Entraining Density Jump

Maximum entrainment represents one limit on the form a density jump may take. A maximum entraining density jump forms when (a) there is a weir of zero height downstream, i.e. effectively a free overfall, or (b) the jump is friction controlled and the slope is such that the uniform flow depth is critical depth. In the ideal case, where the downstream density and velocity distributions are uniform, the Froude number downstream of a maximum entraining density jump will

$$\frac{y_2'}{y_{1C}} f = \frac{F_2^{2/3}}{2F_2^2 + 1}$$

where

$$f = \frac{2F_1^{4/3}}{2F_1^2 + 1}$$

Broad Crested Weir
Controlling
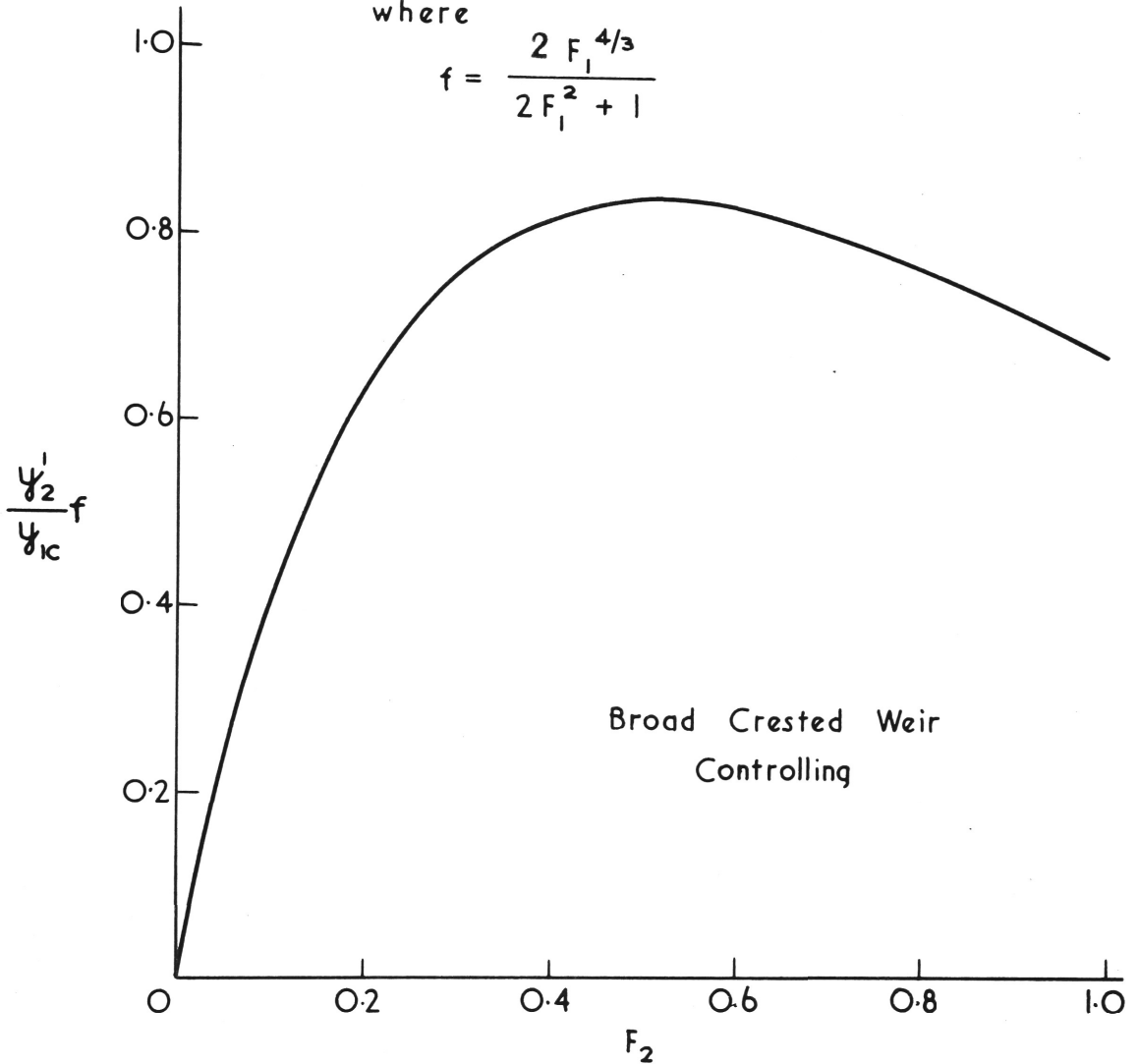
DOWNSTREAM DEPTH FUNCTION VERSUS
THE DOWNSTREAM FROUDE No.

FIGURE 21.

UNSTABLE STABLE

$F_2 = 0.17$

$\dfrac{h}{y_{1c}} f$

Obtained from
simultaneous solution
of Equations 31 & 28
See text

$F_2 = 0.5$

$F_2 = 0$

$F_2 = 1.0$

$\dfrac{y_2'}{y_{1c}} f$
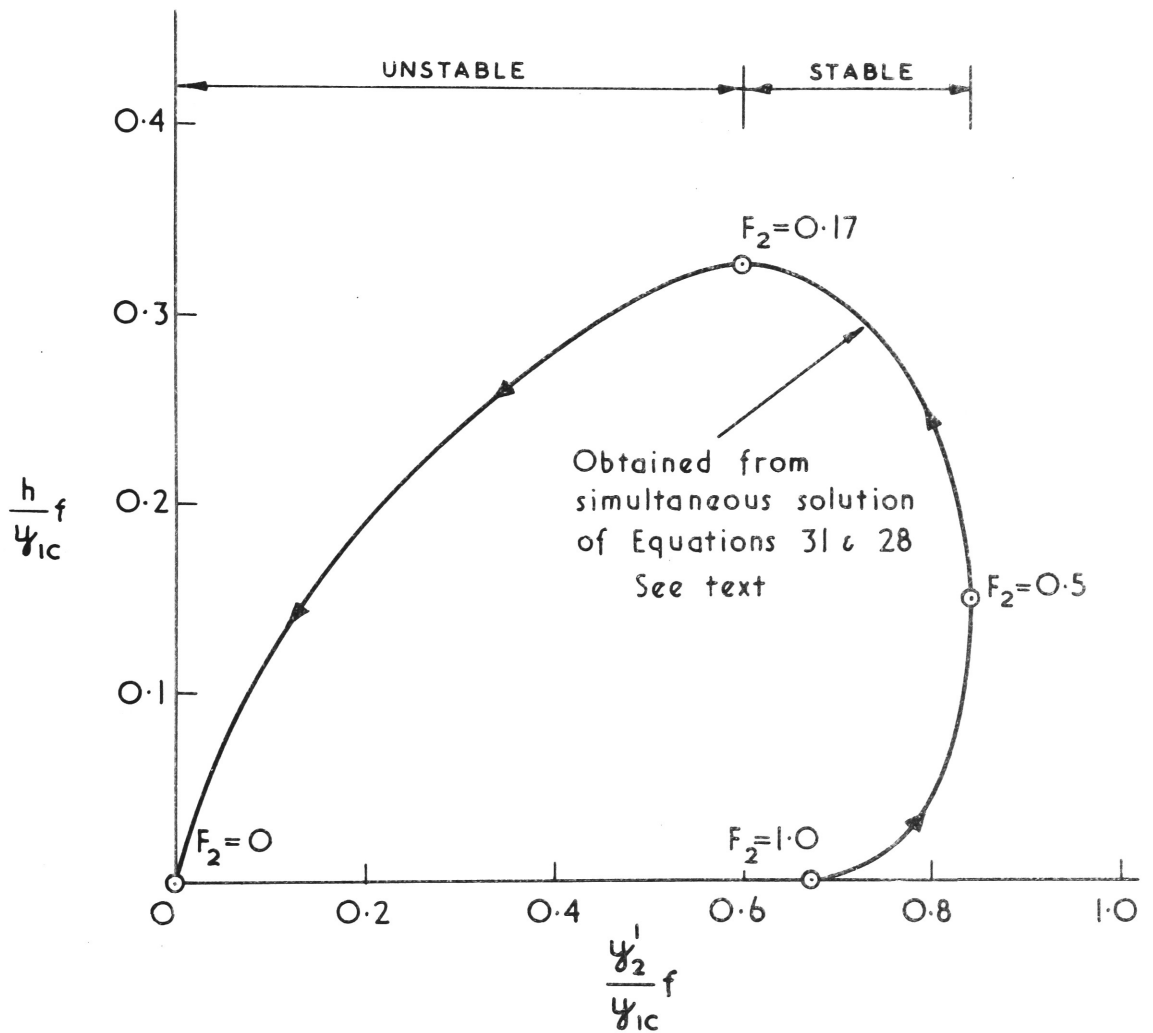
WEIR HEIGHT VERSUS DOWNSTREAM DEPTH

FIGURE 22.

will be one. However, this is generally not so; the velocity and density distributions are non-uniform as can be seen in Figures 23 and 24. As a result of this the downstream Froude number at which entrainment ceases and uniform downstream conditions are attained, is less than one. It will be shown in Chapter 6 where the mechanism of entrainment is examined in some detail, that the maximum Froude number attainable downstream of a density jump is equal to $\left(\dfrac{S_H}{S_m}\right)^{\frac{1}{2}}$. This is found to be less than one as shown in Figure 25.

Ambient fluid is entrained along the length of the establishment zone in this type of jump (Figure 26). There is no downstream control in the accepted sense. A control is not necessary for the formation of the entraining zone of a density jump. The entrainment zone results from an instability of the supercritical density flow under the boundary conditions of the experiment. A neutral wall jet is unstable in an exactly similar way.

When a control is present it must act such that its upstream flow is at critical depth if the density jump is to be of the maximum entraining type. Two forms of control where this is possible are (a) a free overfall and (b) friction on a sloping channel.

The case of a density jump with a free overfall as control or equivalently a weir of zero height will be examined in more detail. The latter case (b) of a friction controlled jump is discussed in Section 4.5.

4.41 The Density Jump with a Free Overfall Downstream

4.411 Introduction

In open channel flows, a free overfall will only act as a control if the upstream flow is already subcritical. The subcritical flow is generally friction controlled and the free overfall will only control depths in its immediate vicinity. It is not correct, therefore, to regard a free overfall as a control in the same way a weir is a control. Admittedly there is a change in flow regime from subcritical upstream to supercritical downstream of a free overfall, but unless there is some other controlling influence, such as friction acting on the upstream flow, the free overfall cannot generate a subcritical backwater. All that can be said of a free overfall in open channel flows is that it provides a useful metering or reference point. Simple one dimensional analysis indicates the depth of flow at the brink if a free overfall is critical. However, flow in the vicinity of the brink is highly curvilinear, and far removed from the approximations of one dimensional theory. As a result, critical depth occurs a distance approximately five times the brink depth, upstream of the overfall. Experiments performed by Rouse (1936) and others have shown the depth at the brink (yb) is 0.712 times critical depth. Depths of density flows in the vicinity of a brink are examined in Appendix B.

The free overfall by itself cannot act as a control of an open channel
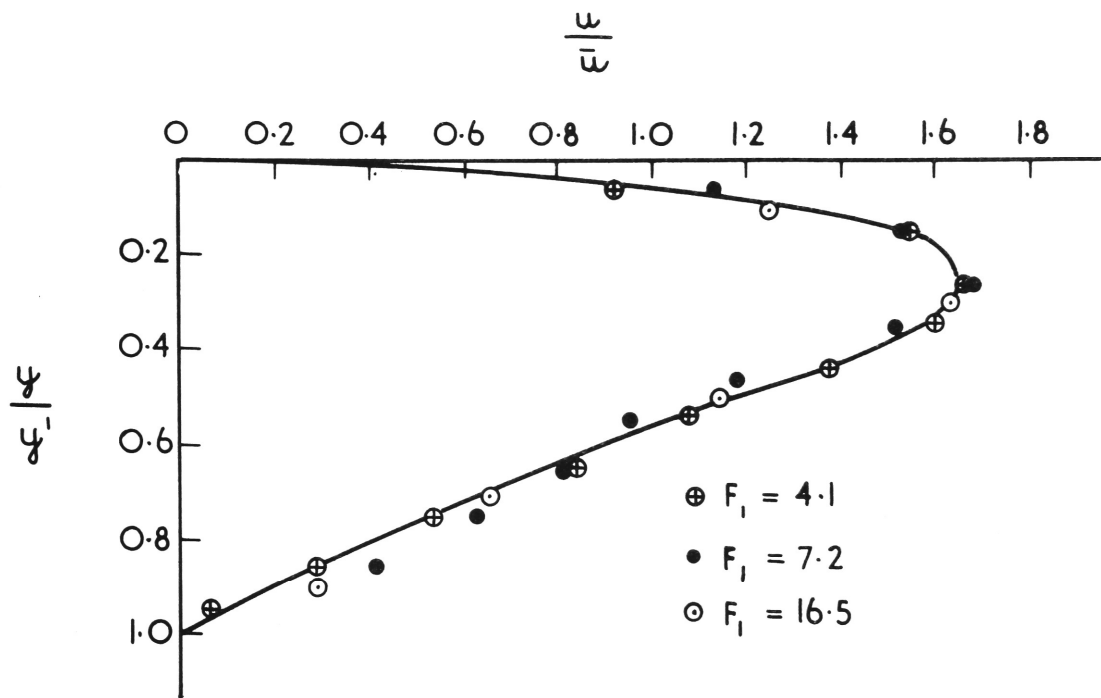
TYPICAL DOWNSTREAM VELOCITY DISTRIBUTIONS

FOR A MAXIMUM ENTRAINING JUMP

i.e $\left(\frac{S_M}{S_H}\right)^{1/2}$ $F_2 = 1 \cdot 0$

FIGURE 23.
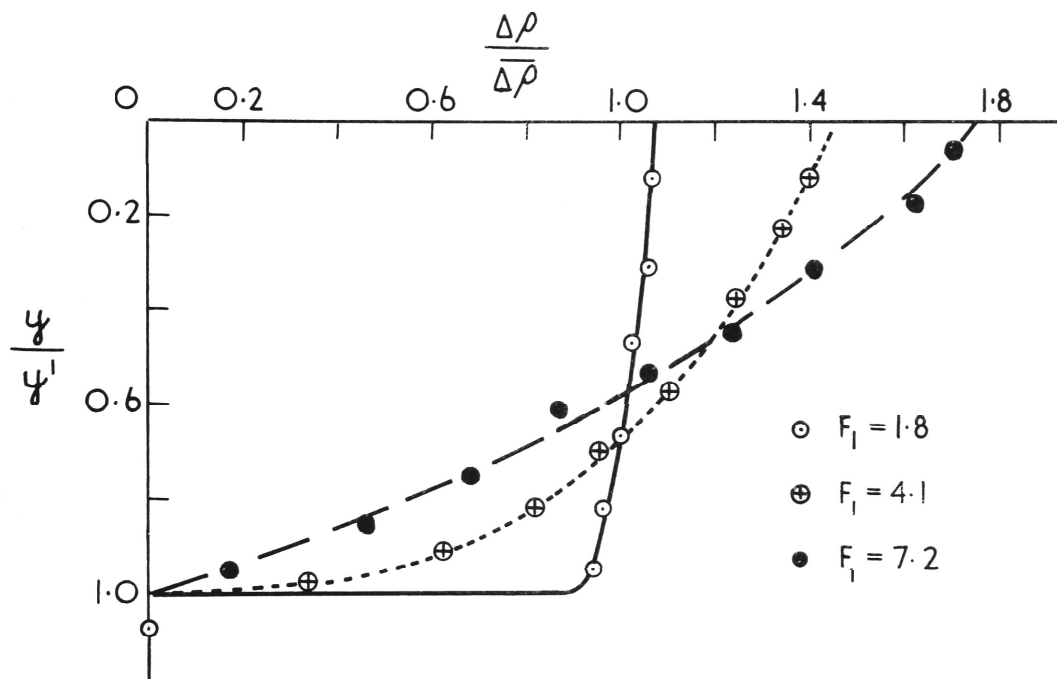
DENSITY DISTRIBUTIONS DOWNSTREAM OF A
MAXIMUM ENTRAINING DENSITY JUMP

FIGURE 24.

$\left(\dfrac{S_H}{S_M}\right)^{1/2}$ Versus F_1

⊙ Experimental values
of F_2

Curve obtained from
meaned data of S_M &
S_H versus F_1 for
maximum entraining jumps

F_2
and

$\sqrt{\dfrac{S_H}{S_M}}$

F_1
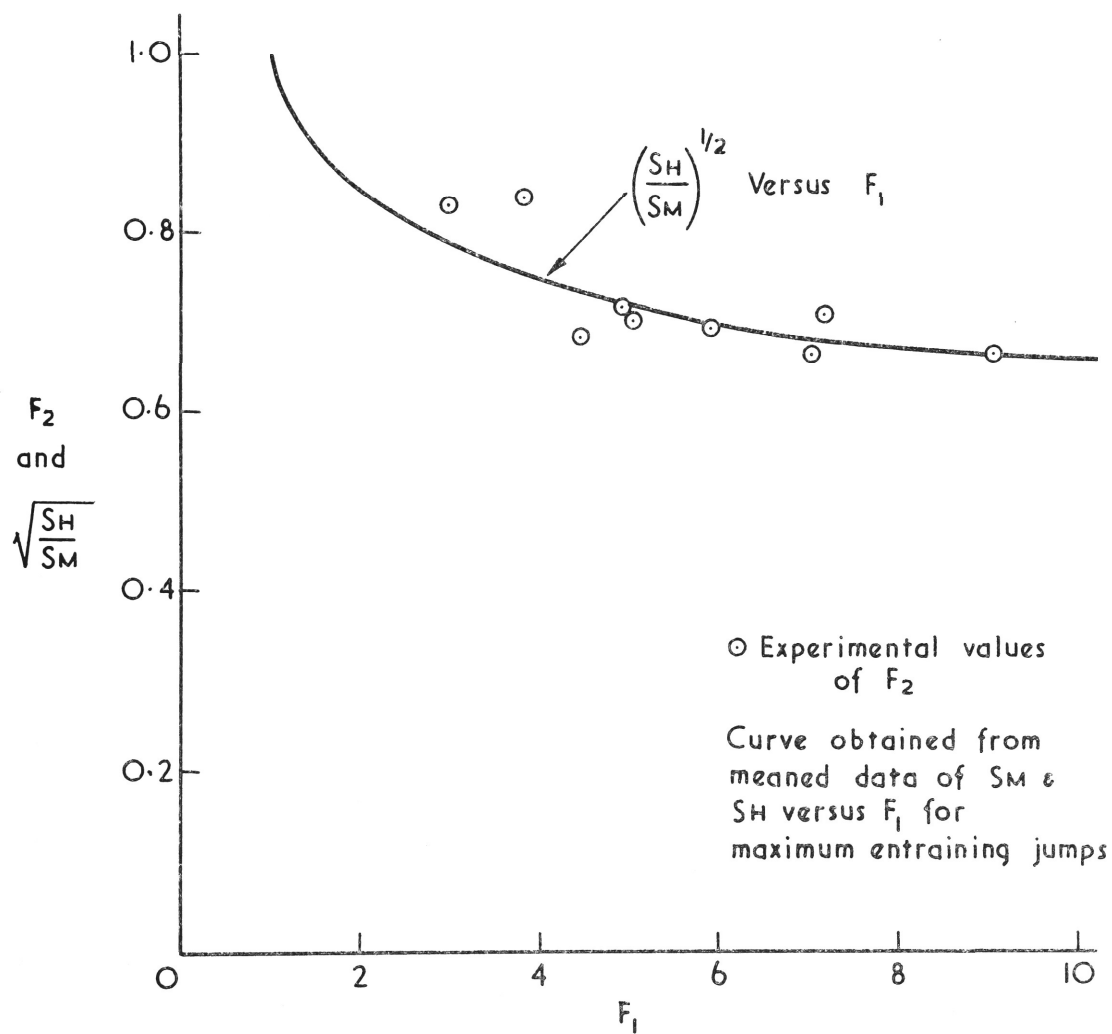
FROUDE Nos. DOWNSTREAM OF MAXIMUM

ENTRAINING JUMPS

FIGURE 25.

Entrainment Zone

P_0 Ambient Fluid

Interface

$P_0 + \Delta \rho$

Density Current
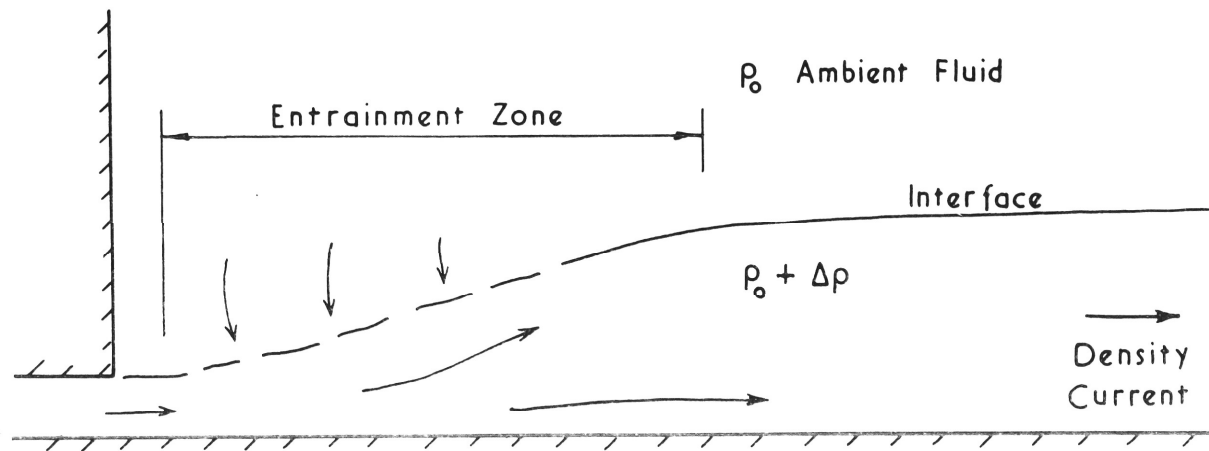
THE MAXIMUM ENTRAINING DENSITY JUMP

FIGURE 26.

hydraulic jump. However, a density jump will form upstream of a free overfall, not because the density jump is controlled by the free overfall, but because the density jump is self forming and is due to the instability of the supercritical upstream flow. The free overfall creates no backwater, so that no roller region forms. The density jump is therefore of the maximum entraining type.

4.412 Analysis

It was stated earlier and is shown in Chapter 6 that entrainment into a density jump is a maximum when the downstream Froude number is equal to $(\frac{S_H}{S_m})^{\frac{1}{2}}$, or unity in the idealised case. Knowing the value of the Froude number downstream of a density jump, one can obtain the conjugate depth ratio and the flow ratio in terms of the Froude number of the flow upstream of the density jump. The conjugate depth ratio of a maximum entraining jump is obtained by equating force flows, upstream and downstream of the jump and substituting $(S_{H2}/S_{m2})^{\frac{1}{2}}$ for F_2. From Equation (19) one finds

$$S_{m2}^{1/3} \, S_{H2}^{2/3} \, r = \frac{2 \, S_{m1} F_1^2 + 1}{3 \, F_1^{2/3}} \, \theta \tag{32}$$

where θ is the force flow ratio. The entrainment ratio K can be determined from equation (32) by means of equation (18)

$$F = \left(\frac{K}{Y}\right)^{3/2} \tag{33}$$

it follows

$$F_1 = \left(\frac{1}{Y_1}\right)^{3/2}$$

and $F_2 = \left(\frac{K}{Y_2}\right)^{3/2} = \left(\frac{S_{H2}}{S_{m2}}\right)^{1/2}$

so that

$$K = \left(\frac{S_{H2}}{S_{m2}}\right)^{1/3} \frac{Y_2}{Y_1} \frac{1}{F_2^{2/3}} = \left(\frac{S_{H2}}{S_{m2}}\right)^{1/3} \frac{r}{F_2^{2/3}} \qquad (34)$$

hence

$$S_{m2}^{2/3} S_{H2}^{1/3} K = \frac{2 S_{m1} F_1^2 + 1}{3 F_1^{4/3}} \theta \qquad (35)$$

4.413 Experimental Results

The conjugate depth ratio and the entrainment ratio are plotted as functions of the upstream Froude number, in Figures 28 and 29 respectively. It can be seen the experimental data, in both cases, lies below the theoretical curves for which the force flow ratio is assumed to be unity and the upstream velocity distribution is assumed uniform.

The effect of friction on the experimental density jump is far greater than that experienced in tests on open channel hydraulic jumps. Measured velocity distributions indicated that the boundary layer in the density jumps was laminar, so that relatively high boundary shears are to be expected. Reynolds numbers based on u' and y' of the density flows investigated were in the range 500 to 3000.

Force flow losses calculated using boundary layer theory in Chapter 7 agree with measured falls in force flow.
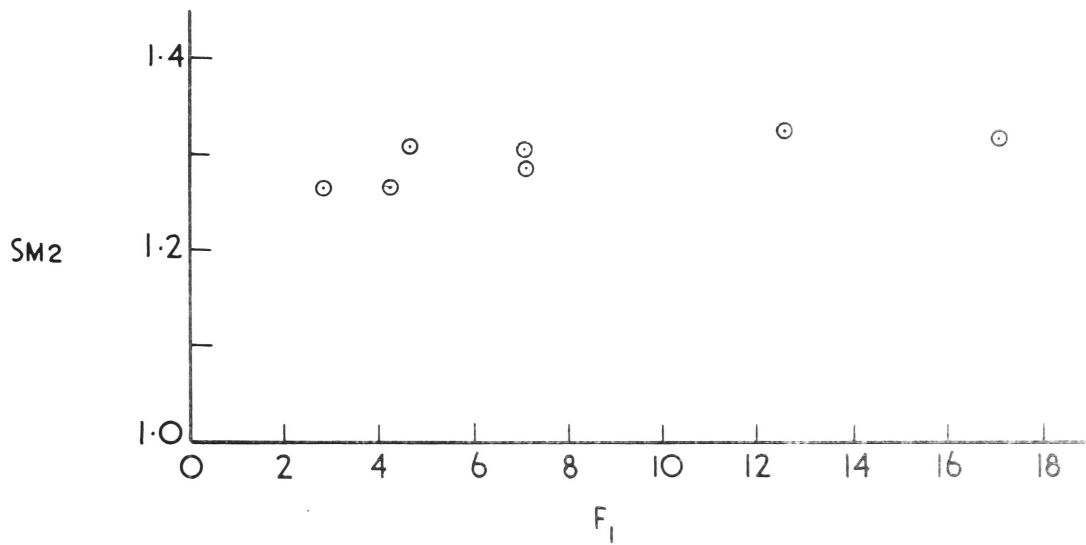
DOWNSTREAM FORCE FLOW CORRECTION
FACTOR VERSUS UPSTREAM FROUDE No.
FOR A MAXIMUM ENTRAINING JUMP

FIGURE 27.

$$SM_2^{1/3} SH_2^{2/3} \Upsilon = \frac{2 SM_1 F_1^2 + 1}{3 F_1^{2/3}} \cdot \theta$$

for

$$S_{M1} = 1 \cdot 0$$

$$\theta = 1 \cdot 0$$

Depth Ratio corrected for θ and S_{M1}
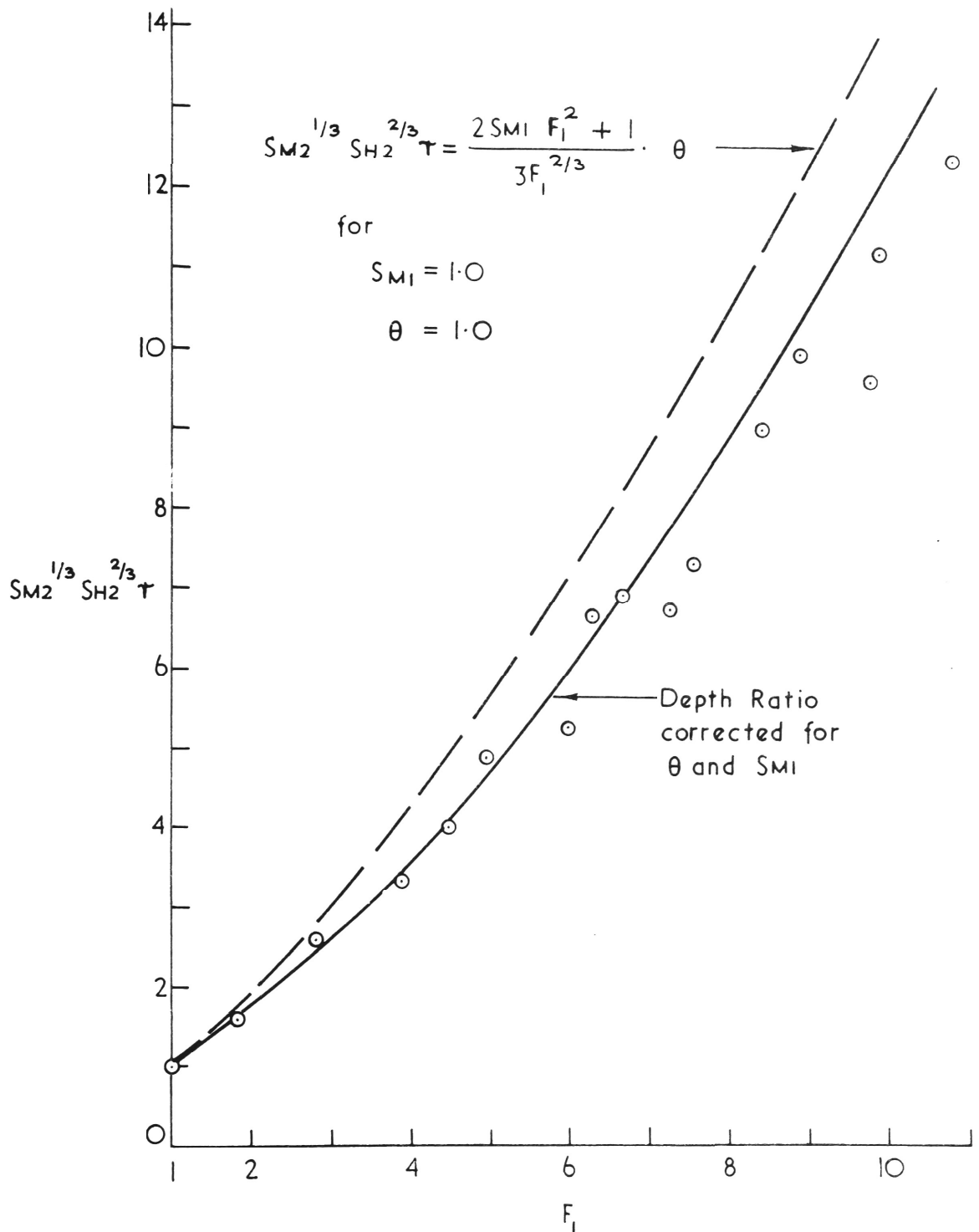
CONJUGATE DEPTH RATIO VERSUS FROUDE No.

For Max. Entraining Jump with free overfall as control

FIGURE 28.

$$SM2^{2/3}\, SH2\, K = \frac{2\, SM1\, F_1^2 + 1}{3\, F_1^{4/3}} \cdot \theta$$

for

$$\theta = 1\cdot O$$

$$SM1 = 1\cdot O$$

$SM1 = 1\cdot O$

Entrainment Ratio corrected for $SM1$ and θ

$SM2^{2/3}\, SH2^{1/3}\, K$

F_1
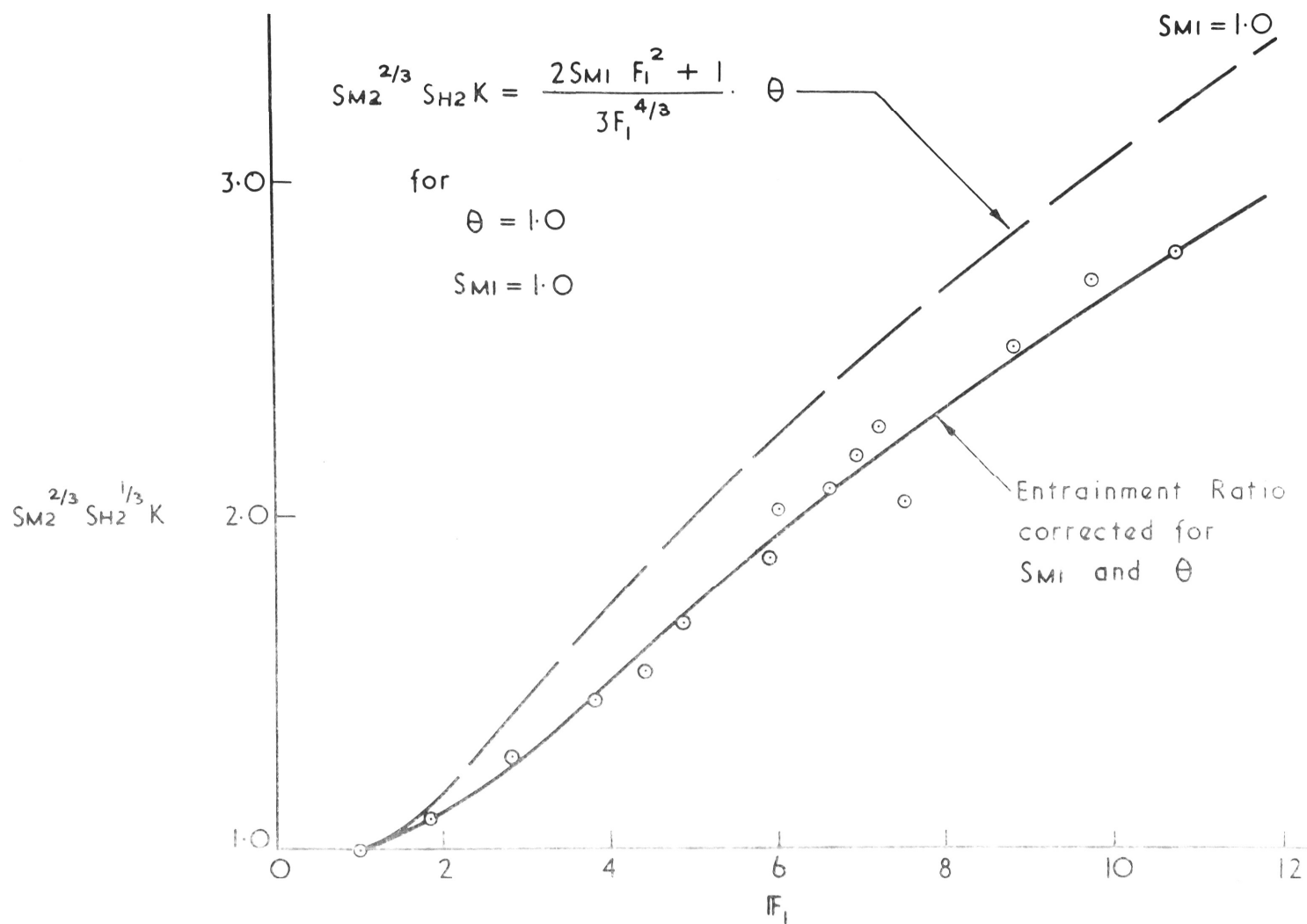
ENTRAINMENT FUNCTION VERSUS FROUDE No.

For a Max. Entraining Jump with free overfall as control

FIGURE 29.

When the theoretical depth and entrainment functions are corrected

for the loss in force flow agreement between experiment and theory is

satisfactory, as may be seen in Figures 28 and 29.

4.414 Effect of Non-Uniform Density and Velocity Distributions

The entrainment and depth downstream of a density jump are insep-

arably tied in with the downstream density and velocity distributions.

Dimensional analysis gives two parameters, the upstream and downstream

Froude numbers, which fully describe any density jump. However, in the

case under analysis where the downstream Froude number is always a

maximum, it itself is a function of the upstream Froude number. There-

fore a maximum entraining density jump can be fully defined in terms of

one variable, the upstream Froude number. The velocity and density

distributions determine the force flow and hydrostatic force correction

terms which are now examined.

(a) The force flow correction factor was found to remain constant in

value, for upstream Froude numbers greater than three (Figure 27).

Experiments indicated that velocity distributions in the entraining zone

of a density jump are self preserving. It follows, therefore, that max-

imum entraining density jumps with upstream Froude numbers greater

than three will have similar downstream velocity distributions. This

similarity of the downstream velocity distribution can be seen in Figure

23 where a number of velocity distributions downstream of maximum

entraining density jumps are plotted for a range of upstream Froude numbers.

(b) The density distribution is far more dependent on the upstream Froude number than is the velocity distribution. Relatively more fluid will be entrained into a maximum entraining jump with a high up-stream Froude number than would be entrained into a maximum entrain-ing jump of low upstream Froude number. It is to be expected then, that the downstream density distributions of the above jumps will differ. Typical density distributions for maximum entraining density jumps, at high and low upstream Froude numbers, are shown in Figure 24. The difference in form is notable. For the limiting case under examin-ation, the hydrostatic pressure correction factor is fully defined by the upstream Froude number and a graph of the relationship is shown in Figure 30.

4.5 Friction as a Control of a Density Jump

4.51 Introduction

So far, the effects of boundary friction as a controlling influence downstream of a density jump, has been ignored. Bed slopes and friction slopes have been taken as zero and, in experiments, the various controls were situated close to the downstream end of the jump so as to minimise frictional influence. The bed slope was horizontal in these experiments.

The effect of friction was examined experimentally using a long sloping channel downstream of the jump, and adjusting an overshot weir
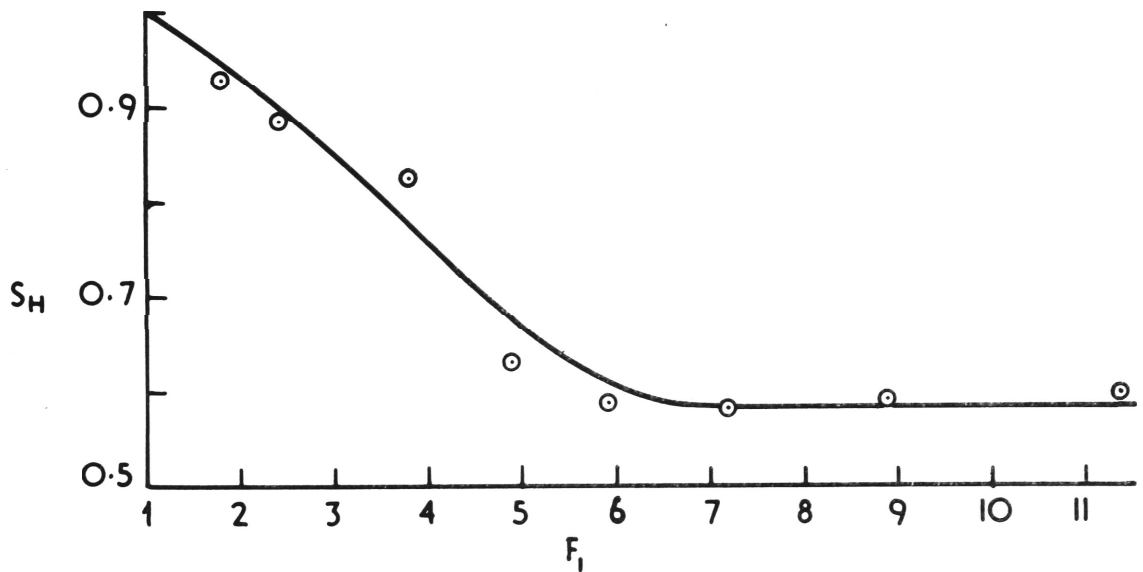
HYDROSTATIC PRESSURE CORRECTION FACTORS FOR
MAXIMUM ENTRAINING DENSITY JUMP
FIGURE 30.

at the end of the channel, until uniform conditions were obtained in

in the x direction. The friction slopes were very high by open channel

standards and subcritical flow was maintained at a slope of 1 pc. The

low Reynold numbers associated with the density flows are the cause of

the relatively high frictional forces. Reynolds numbers of the boundary

layer, based on boundary layer thickness and mean layer velocity, were

in the range 100-600. Measured velocity distributions showed that the

main flow was turbulent with laminar boundary layers at the interface

and the solid boundary.

In the following analysis the shear forces acting on the moving layer

are calculated in terms of the velocity and velocity distribution of the flow.

It is shown that the interfacial shear of flows downstream of a density

jump is small compared with the boundary shear. The equation of motion

for uniform flow of a density layer down an incline is expressed in terms

of the Froude number and Reynolds number of the flow. The uniform flow

equation is then related to the force flow equation at the density jump.

Finally, the Froude number downstream of the density jump is expressed

as a function of the known Froude and Reynolds numbers of the upstream

flow and the slope of the channel.

4.52 Boundary Layer Analysis

The boundary layer at the channel bottom and sides remained laminar,

even in the entraining zone, so that the functional dependence of the

boundary shear stress could be calculated. It will be shown in Chapter 7 (Fall in force flow at a density jump) that the wall stress (τ_w) is given by

$$\tau_w = 2\mu \frac{\beta_2}{\beta_1} \cdot \frac{u'}{y'}$$

where β_1 is the ratio of boundary layer thickness to the depth of

        flow

    β_2 relates the mean velocity to the velocity at the edge of the

        laminar boundary layer, and

    μ is the dynamic viscosity of the fluid

The boundary layer thickness is defined as the distance between the boundary and the velocity maxima (see Section 7.2 for details).

It was found in experiments, that the ratio $\dfrac{\beta_2}{\beta_1}$ remained fairly constant in value, and so it is convenient to write

$$\beta = \frac{2\beta_2}{\beta_1} \qquad = \text{a constant}$$

Hence
$$\tau_w = \beta\mu \frac{u'}{y'} \tag{36}$$

The experimentally determined value of β was found to be 14.3.

Consider a uniform flow down an inclined plane, as shown in Figure 31 and examine the equilibrium of a section of length δx. Equating forces in the x direction one obtains

$$\left(2y_2' + w\right)\tau_w\,\delta x = w\,\delta x \int_0^{y'} \Delta\rho g \cdot \sin\theta\,dy$$

$$= \beta\mu \frac{u'}{y'} w\,\delta x$$

where w is the width of a rectangular channel.
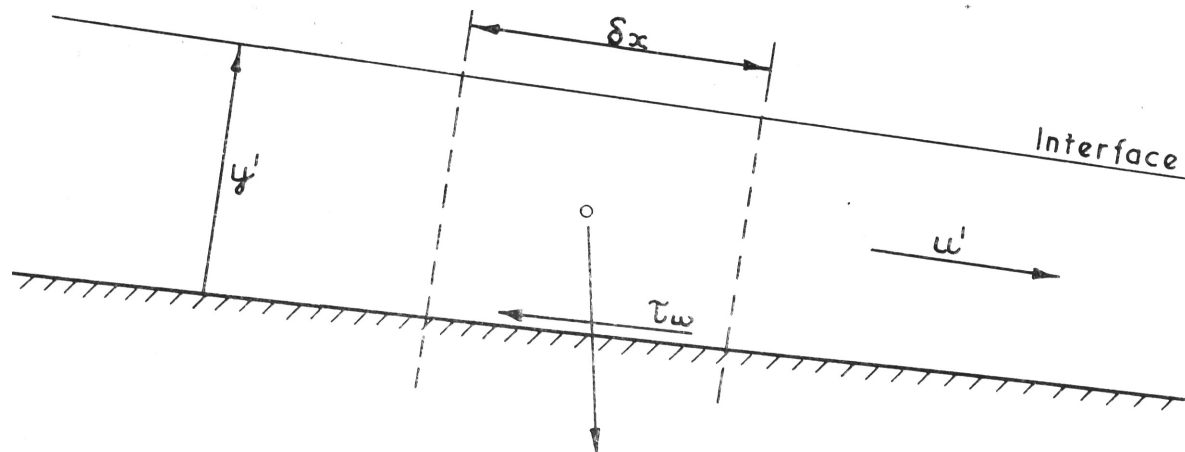
DEFINITION SKETCH — DENSITY FLOW DOWN AN INCLINE

FIGURE 31.

In writing the above equation it has been assumed the shear stress at the sides of the channel and at the bottom are equal, and the shear stress at the interface is zero.

It will be shown in the discussion that follows this analysis, that the above approximations are justifiable for flows downstream of a density jump.

The above expression which equates the forces acting on elemental section of the flow, can be reduced to

$$\beta F_2^2 = R_2 . \sin\theta . w_r \tag{37}$$

by dividing the previous equation by $\rho_0 u_2'^2$. R_2 is the Reynolds number of the flow defined by

$$R_2 = \frac{\rho_0 u_2' y_2'}{\mu} \tag{38}$$

and

$$w_r = \frac{w}{2 y_2' + w} \tag{39}$$

Equation (37) can be rearranged into the form

$$F_2^2 = \frac{K R_1 \sin\theta \; w_r}{\beta}$$

or

$$K = \frac{\beta F_2^2}{R_1 \sin\theta \; w_r} \tag{40}$$

Equation (40) can be related to known conditions upstream of the jump by means of the force flow equation (20) in idealised form

$$\frac{y_{2c}}{y_{1c}} = \frac{2 F_1^2 + 1}{F_1^{4/3}} \cdot \frac{F_2^{4/3}}{2 F_2^2 + 1}$$

The equations of continuity and the defined Froude number give

$$\frac{Q_1^2}{\Delta \rho_1 \, y_{1c}^3} = \frac{(K\,Q_1)^2}{\frac{\Delta \rho_1}{K} \, y_{2c}^3} = 1$$

so that $\dfrac{y_{2c}}{y_{1c}} = K$ \hfill (41)

The friction equation (40), the force flow equation (20) and the above equality (41) may be solved to give

$$\frac{R_1 \sin\Theta}{\beta \, f} = \frac{\left(2 F_2^2 + 1\right) F_2^{2/3}}{2} \hspace{2cm} (42)$$

where f is as defined in Equation (29).

The left hand side of the above equation will be referred to as the friction function. In equation (42) the downstream Froude number is given as a function of the bed slope and upstream conditions which are assumed predetermined.

4.53 Experimental Results

The friction function is graphed against downstream Froude number in Fig. 32. Experimental data are also plotted in the figure and agreement between the theory and experiment is reasonable. Some scatter exists but this is believed to be largely caused by difficulty in establishing a truly uniform flow. A short crested weir at the downstream end of the channel was adjusted until uniform depths were established along the length of the channel. The jump is then effectively friction controlled. This may be verified by making appreciable adjustment to the weir height

$$\frac{R_1 \sin \theta \omega_r}{\beta f} = \frac{\left(2 F_2^2 + 1\right) F_2^{2/3}}{2}$$
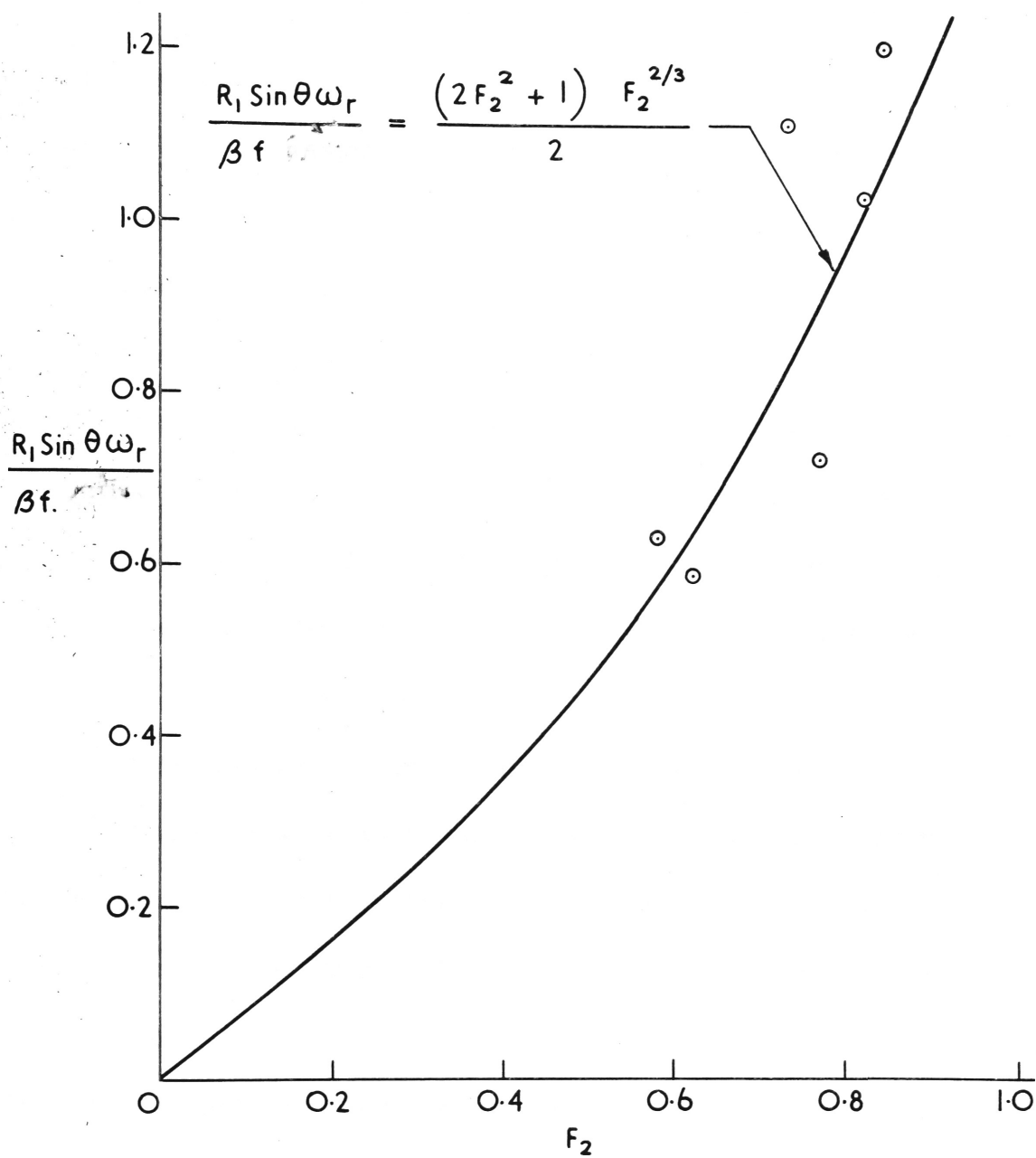
FRICTION FUNCTION VERSUS DOWNSTREAM FROUDE No.

FIGURE 32.

and observing only slight changes immediately downstream of the jump.

4.54 Discussion

In this section the assumptions made in the previous analysis are investigated.

Firstly in deriving equation (37), it was assumed that -

(a) shear at the interface was negligible and

(b) the shear at the sides of the channel was equal to that at the bottom.

Inspection of a typical velocity distribution, taken at the centre line of the channel (Fig. 33) indicates that the shear at the interface (τ_i) is small compared with that at the channel bed. In the example given

$$\frac{\tau_i}{\tau_w} = 0.08$$

so that as a first approximation the interfacial shear will be neglected.

The ratio of interfacial to bottom shear is considerably less than that quoted in the literature. The ratio is given ranging from 0.43 for turbulent density flows (Bata 1959) to 0.64 for wholly laminar flows (Keulegan 1944).

The density currents observed in experiments, were turbulent with laminar boundary layers and therefore the value of shear ratio obtained might have been expected to lie somewhere between the two extremes quoted.

However, the velocity distribution downstream of the jump is determined by the jump itself, and is markedly non-uniform.

Once established, the velocity distribution showed no noticeable change over the channel length, which was generally about forty times the depth of flow. The density gradient within the moving layer inhibited turbulent diffusion in the y direction. Therefore, velocity distributions, once established at the jump, tended to be self preserving or to change only very slowly.

The reason then for the low interfacial shear observed in flow downstream of a density jump, was the low velocity gradient which exists near the interface, under these conditions. The interfacial shear measured by other experimenters had been determined from density flows in which the initial velocity distribution was nearly uniform in the case of turbulent flows or had well developed boundary layers in the case of laminar flows.

Figure 33 also indicates that the second approximation (b) is probably not strictly correct either. Velocities near the bottom of the channel are greater than those near the interface, so it might be expected that side shear forces will be less than those at the channel bottom. However, assumptions (a) and (b) do compensate one another to some extent.

Equation (37)
$$\beta F_2^2 = R_2 \sin \theta \, \omega_r$$

is simply the equation of motion for the downstream flow. It was stated that β, a function of the dimensionless velocity distribution, remained fairly constant in value. This can be checked by plotting the right hand side of Equation (37) against F^2. This has been done in Figure 34 and
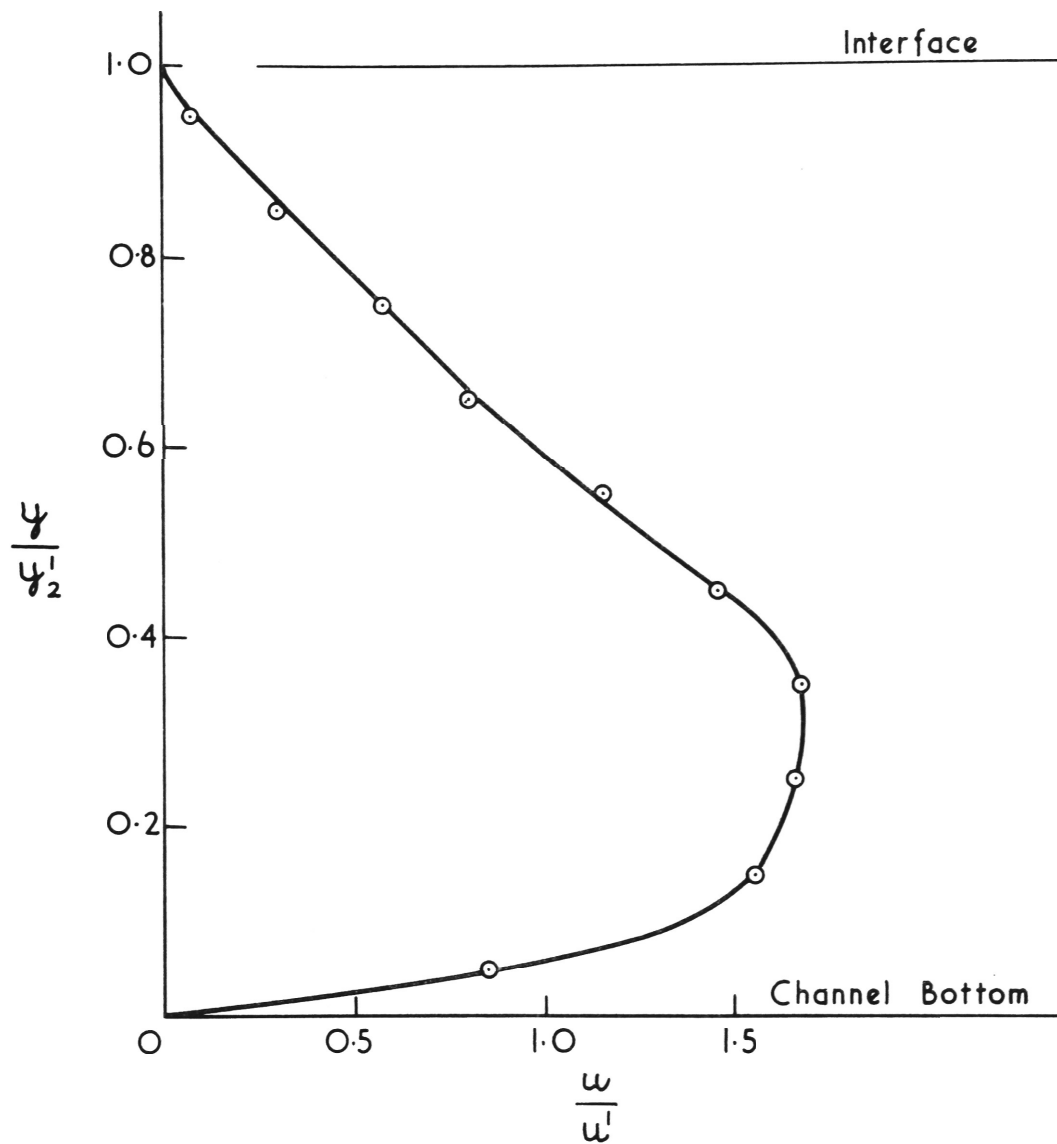
TYPICAL MEAN VELOCITY DISTRIBUTION

DOWNSTREAM OF A FRICTION CONTROLLED DENSITY JUMP

FIGURE 33.

it can be seen a straight line passing through the origin fits the experimental data satisfactorily. Although some scatter is apparent, the data tends to justify the assumptions made in deriving equation (37).

The value of β obtained from the slope of the line of best fit is 14. 3.

β can also be determined from the typical velocity distribution shown in Figure 33.

β is defined as equal to $\dfrac{2\beta_2}{\beta_1}$

β_1 is equal to the ratio of laminar boundary layer thickness to the depth of flow y'. For the example shown $\beta_1 = 0.20$.

β_2 is equal to the ratio of velocity at the edge of the boundary layer to the mean flow velocity and for Figure 33, $\beta_2 = 1.50$.

The value of β calculated from these values is 15, very close to that calculated from the mean data in Figure 34.

4.55 Rough Turbulent Flow

Analysis and Discussion

The case just examined was for a smooth turbulent flow and it was shown the Froude number of a density current flowing down a slope, was related to the Reynolds number of that flow. When the flow is rough turbulent, the downstream Froude number is dependent on the boundary properties, roughness and slope and to a far lesser extent on the viscosity of the fluids.

The boundary shear stress is given by

$$\tau_\omega = \frac{f^*}{4} \rho \frac{u'^2}{2}$$
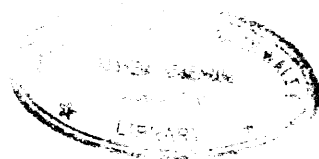
where f is a friction factor (Streeter, 1961) which for the case in question is a function of the boundary roughness only, since interfacial shear, downstream of a density jump, is small by comparison.

Consider the equilibrium of a section of the flow. One has for a two dimensional flow

$$\frac{f^*}{4} \rho \frac{u'^2_2}{2} = \Delta . y'_2 \sin \theta$$

and on dividing both sides by $\Delta . y'_2$ the above reduces to

$$\frac{f^*}{8} F_2^2 = \sin \theta$$

or

$$F_2^2 = \frac{8 \sin \theta}{f^*}$$

The above equation is particularly interesting. The Froude number downstream of a density jump is determined by the boundary properties only. It is quite independent of the density jump itself.

This Froude number, unlike the previous case, is analagous to the normal depth of open channel flow. Normal depth is not a useful concept when dealing with density flows since entrainment can cause variation in the flow rate.

This result is particularly interesting since most naturally occurring density currents are rough turbulent flows. It has been shown above that the Froude number at which any subcritical rough turbulent flow will move down an incline is a function of only the roughness and slope of that incline. Downstream conditions are quite independent of upstream

$$R_2 \sin \theta \omega_r$$

$$\beta = 14 \cdot 2$$
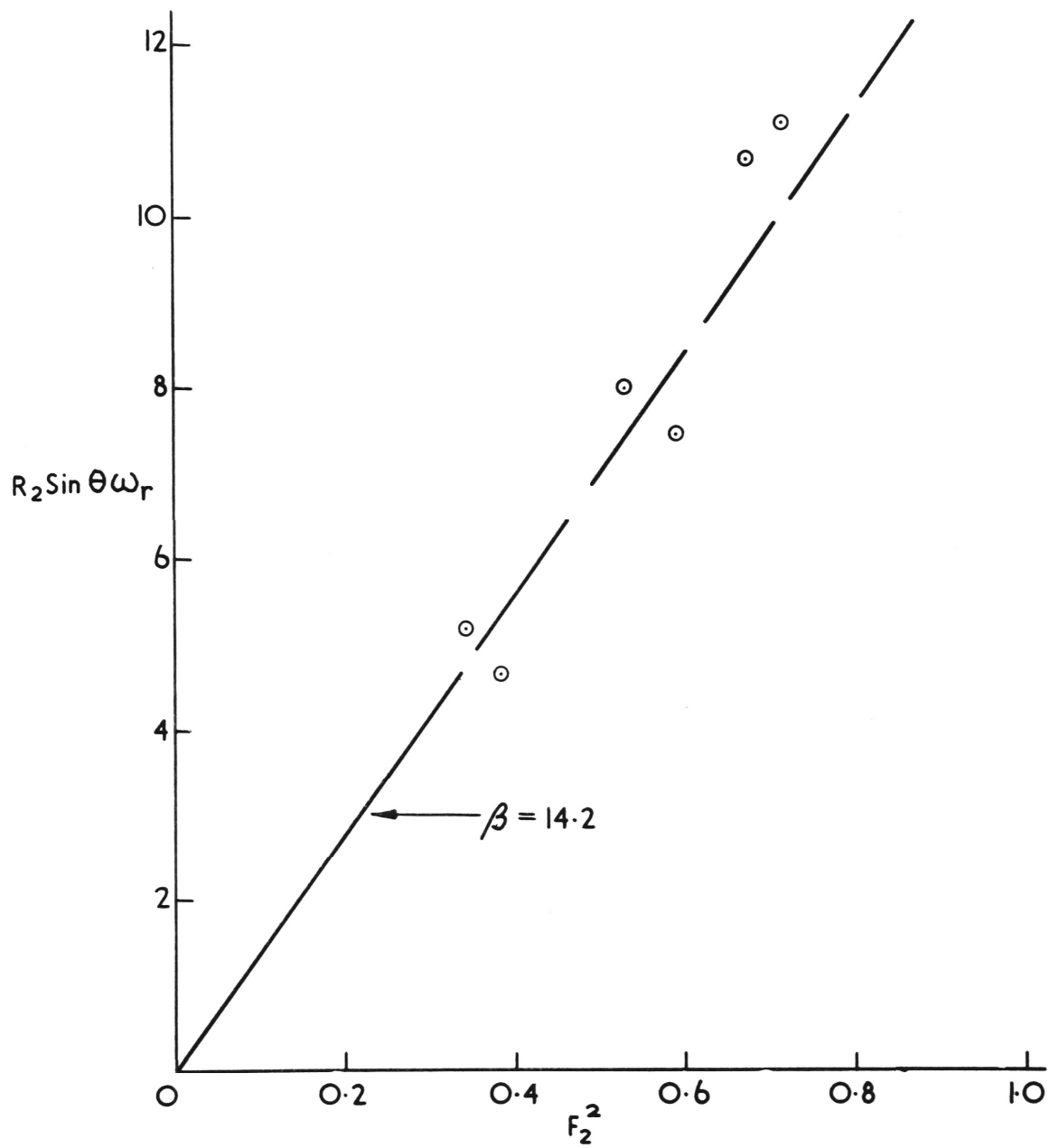
DOWNSTREAM REYNOLDS No. VERSUS F_2^2

FIGURE 34.

parameters.

4.56 The Effect of Bed Slope on the Density Jump

Bed slopes of up to two or three per cent have negligible effect on a density jump. This can be shown by examining orders of magnitude of the respective force components acting on such a jump. The body weight component of the force flow is approximately

$$\Delta L\, y'_2 \sin\theta/2 \quad \approx \quad 5 \Delta\, y'^2_2 \sin\theta/2$$

where L is the length of the density jump and is of the order of $5y'_2$.

The downstream force flow is of the order $\dfrac{\Delta\, y'^2_2}{2}$ so that the body force component on slight slopes is negligible by comparison.

4.6 Steady Density Flows - Concluding Remarks

So far, only steady density flows have been considered; these being the density jump controlled by a broadcrested weir and the density jump controlled by downstream friction. In Appendix C density jumps controlled by sharp crested and undershot weirs are examined both theoretically and experimentally. Theory for a density jump controlled by a channel contraction is also presented. The examples given in Appendix C are not included in the present text, as the line of analysis is similar to that used earlier in this chapter.

It has been shown that, at a transition from supercritical to subcritical flow in a density current, a change in the density and rate of flow can occur downstream of the transition. This change results from entrainment in the transition region. This region has been called

a density jump. It has been shown that the form of the jump and the degree of entrainment which can occur are determined by a control downstream of the jump. It was found definite limits exist to the entrainment and conjugate states of the density jump.

Chapter 5 - Unsteady Density Flows

5.1 Introduction

In this chapter the unsteady nose or front of a density flow is examined. The control of a density jump by an unsteady layer down-stream is also investigated.

It is interesting to examine the development of a starting density flow. The formation of the starting vortex and its subsequent motion is shown in the sequence of photographs in Figure 35.

Immediately the density current begins flowing from the slot, a characterising starting vortex forms (Fig. 35a). This grows to a stable size and moves away from the slot (Figs. 35b and 35c). Behind the starting vortex, or nose, is a layer of depth approximately half that of the nose. This layer moves with a velocity equal to that of the nose (Wood, 1965) so that the depth of this layer is uniform. A density jump is found at the upstream end of the layer as can be seen in Figure 35c.

5.2 Behaviour of the Nose

The motion of the nose is now examined in some detail. Consider the diagrammatic sketch of an unsteady density flow shown in Figure 36.

If one makes the Boussinesq assumption, dimensional analysis yields

$$V_n = \text{function}\left(\frac{\Delta\rho}{\rho_o} g, \; q, \; \mu, \; \ell, \; \rho_o, \; \theta \right)$$

or
$$V_n = \left(q \, \frac{\Delta\rho}{\rho_o} g \right)^{1/3} f_n \left[\frac{\rho_o q^2}{\mu \, V_N x}, \; \frac{\ell \, V_N}{q}, \; \theta \right]$$

where V_n is the nose velocity,

    ℓ is distance travelled by the nose and

    θ is bottom slope.

It will be shown the first term $\dfrac{V_N}{\left(q \, \frac{\Delta\rho}{\rho_o} g \right)^{1/3}}$ is a form of Froude

number. The second term is a Reynolds number and the third term is

the interfacial slope of the layer behind the nose.

Just after flow commences and provided the bottom slope is slight

(< 1 pc.), the last three parameters have little influence on the initial

motion of the density flow. Frictional forces are small compared with

inertial and pressure forces (the Reynolds number is large) and the

interfacial slope has no effect on the motion. Therefore it follows that

initially, the term

$$\frac{V_N}{\left(q \, \frac{\Delta\rho}{\rho_o} g \right)^{1/3}} = \mathscr{f} \qquad \text{equals a constant.}$$

This has been verified experimentally by the writer who from the

results of ten experiments found $\mathscr{f} = 1.045 \pm 0.047$. This figure

agrees closely with values of $\mathscr{f}$ obtained by other experimenters;

Wood (1965) $\mathscr{f} = 1.06 \pm 0.10$, Keulegan (1957) $\mathscr{f} = 1.05$, Ellison and

Turner (1959) and Middleton (1966).

The initial nose velocity is plotted against the flux of density
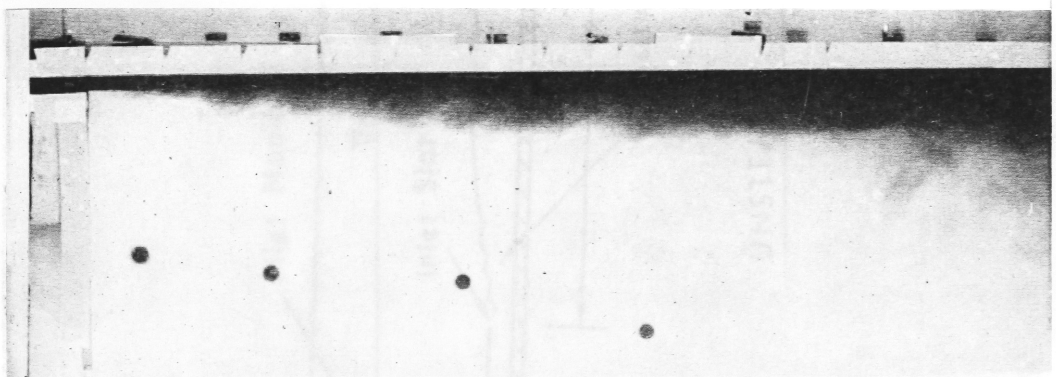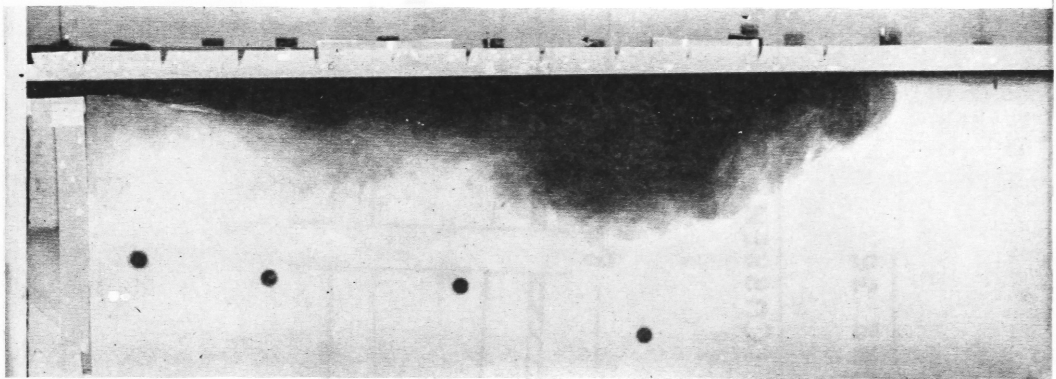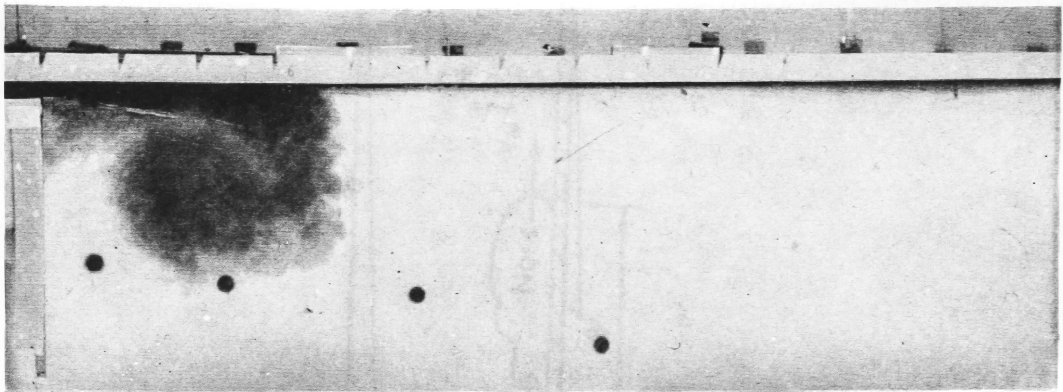
Fig. 35

The starting phenomena.
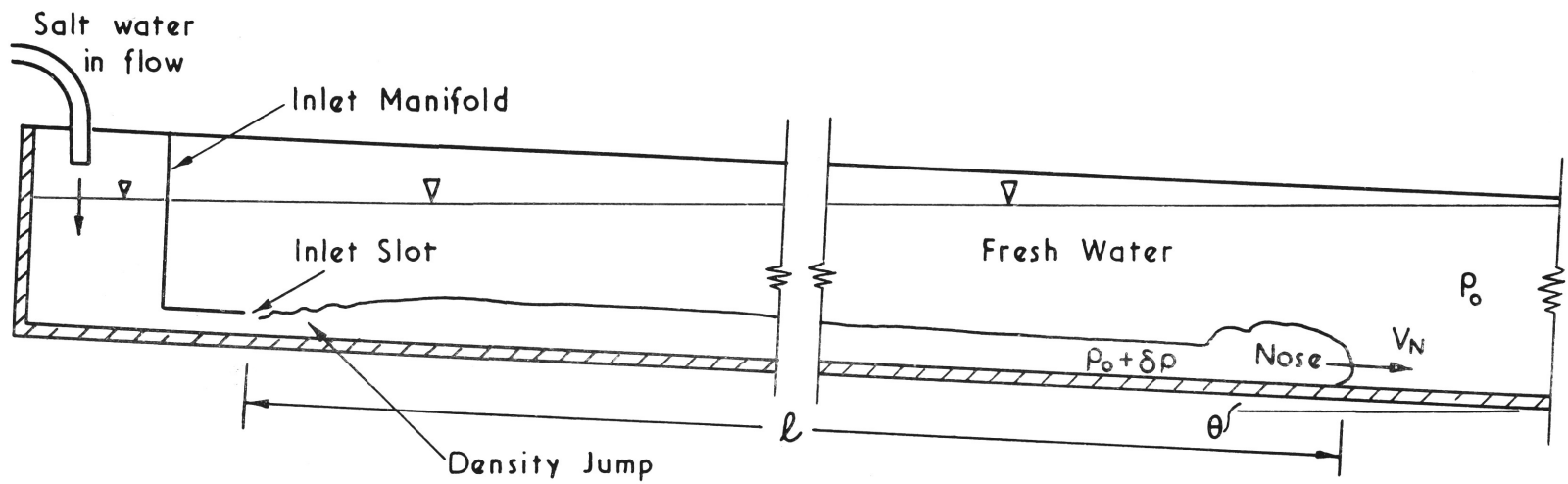
UNSTEADY DENSITY CURRENT EXPERIMENTS

FIGURE 36.

difference to the power one third, for the writer's experiments, in Figure 37.

The nose velocity does not generally remain constant, as can be seen in Figure 38. As the nose moves downstream, frictional forces begin to retard its motion. The nose whose velocity is plotted in Figure 38 moved along a bed of zero slope and the nose velocity is seen to continually decrease. In Figures 39a and 39b nose velocity is plotted against distance travelled for an unsteady density current flowing down a slope. After travelling some distance the flow approaches an equilibrium and the velocity asymptotically approaches a constant value. Raw data for a single experiment are plotted in Figure 40. Figures 37 and 38 were reduced from diagrams such as this.

5.3 The Unsteady Layer

It can be seen in Figure 35 (b and c) that a layer of fluid is left behing a moving nose. Experiments show that this layer moves with a velocity equal to that of the nose. This is not altogether surprising since it is the layer behind the nose which provides the driving force. If the nose were to move faster than the layer its depth would decrease. The nose would lose its driving force and slow down, allowing the layer to catch up. Therefore, the nose is attached to the flowing layer and the nose and the layer cannot move independently of each other. As the layer velocity is friction controlled then so is the nose. The asymptotic

nose velocity will therefore be equal to the uniform flow velocity of the density current. The conditions for uniform flow of a density current were examined in the previous chapter (4.5).

A density jump forms at the upstream end of the moving layer (Fig. 35c). Initially this density jump is of the maximum entraining type. This can be shown from the relationship which exists between and the Froude number of the moving layer.

The Froude number has already been defined as $F = \dfrac{Q^2}{\Delta\, y^{13}}^{\frac{1}{2}}$

The above can be written in terms of the characteristic velocity as

$$F_2 \;-\; \frac{u_2}{\left(\Delta_2\, y_2'\right)^{1/2}}$$

$$= \left[\frac{u'}{\left(\Delta_2\, q_2\right)^{1/3}}\right]^{3/2}$$

where $\Delta_2 q_2$ is the flux of density difference. However, the mean or characteristic velocity (u') equals the nose velocity. Therefore

$$F_2 = \mathscr{f}^{\,3/2}$$

Therefore if the ratio of nose velocity to the third power of the flux of density difference is unity, then the Froude number of the layer is also unity. The density jump upstream of this layer must be of the maximum entraining type.

The velocity of the nose decrease as friction slows the following layer. The Froude number of the layer falls and a roller region forms at the density jump. The roller region continues to migrate upstream

$$\frac{V_n}{\phi^{1/3}} = \beta = 1.05$$

$$\phi = \left[q\,\frac{\Delta\rho}{\rho}g \right]^{1/3}$$

V (ft/sec)

INITIAL NOSE VELOCITY VERSUS (FLUX OF DENSITY DIFFERENCE)$^{1/3}$

FIGURE 37.

$\zeta = 1.06$

V_N
(ft/sec.)

0.10
0.08
0.06
0.04
0.02

0 20 40 60 80 100

x (ft.)

$S_o = 0.00$

$$\phi = \left[q \frac{\Delta \rho}{\rho_o} g \right]$$

$$= 0.88 \times 10^{-3} \ (ft/sec)^3$$
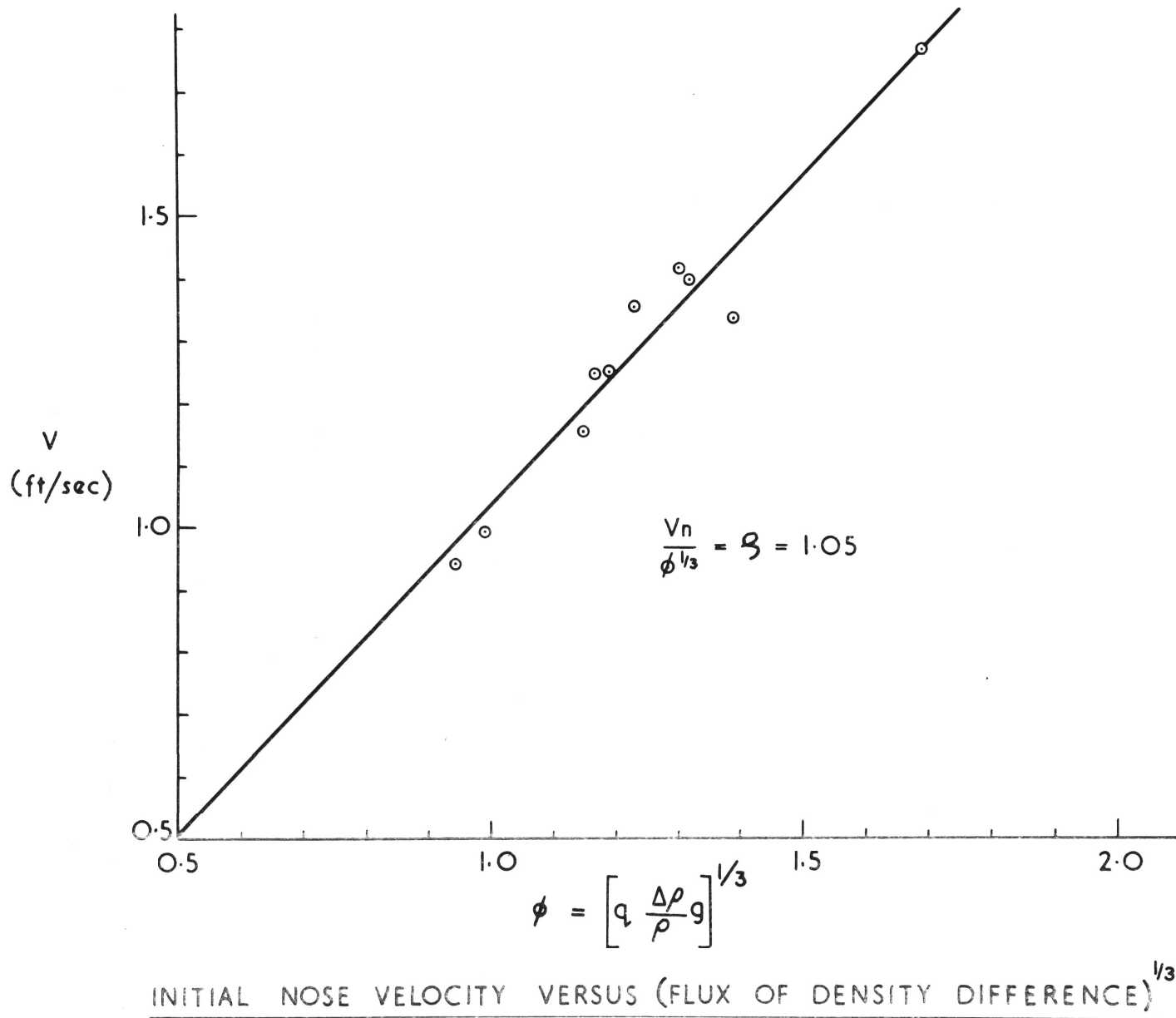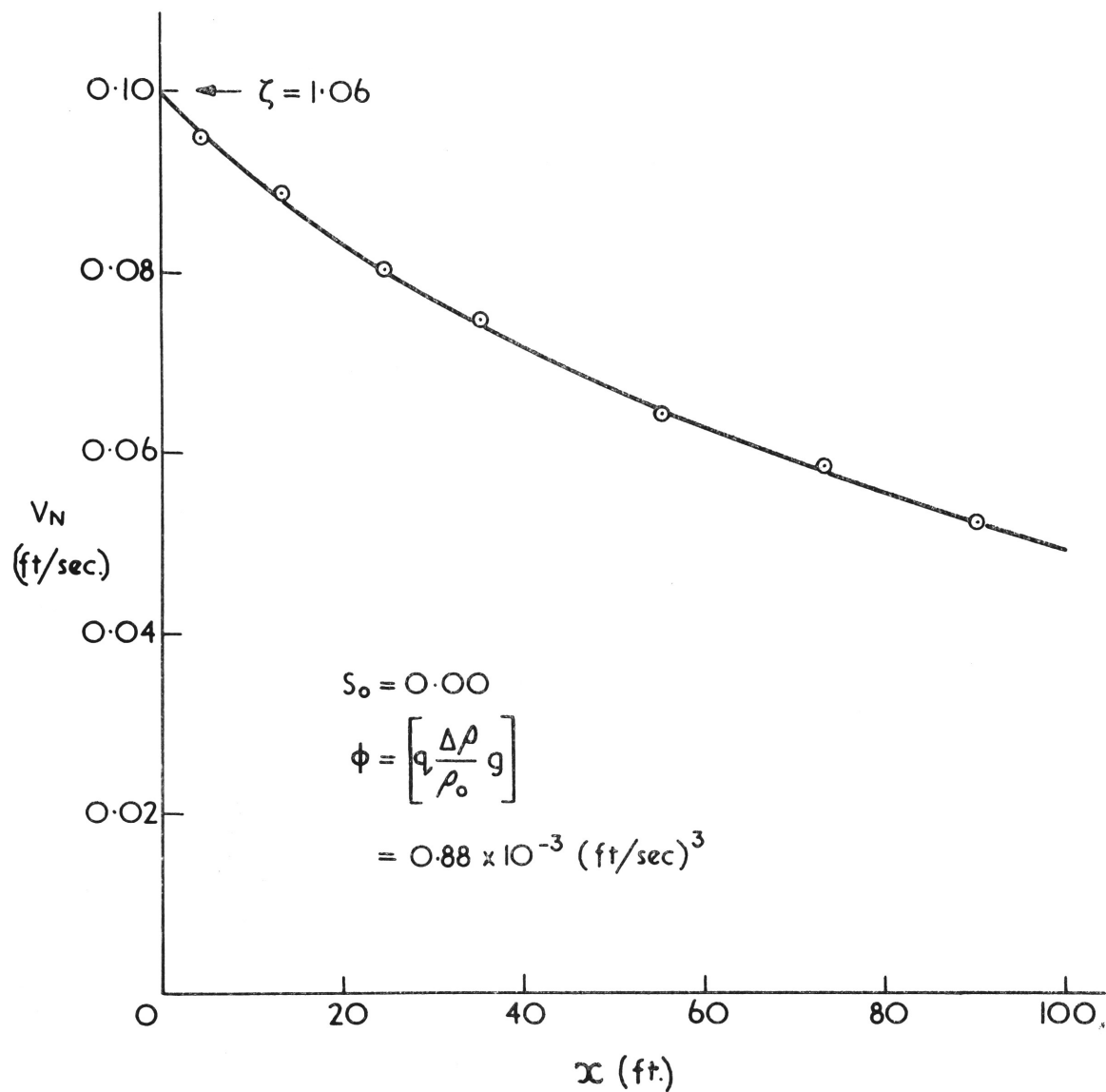
NOSE VELOCITY VERSUS DISTANCE TRAVELLED
TEST No. 4.

FIGURE 38.
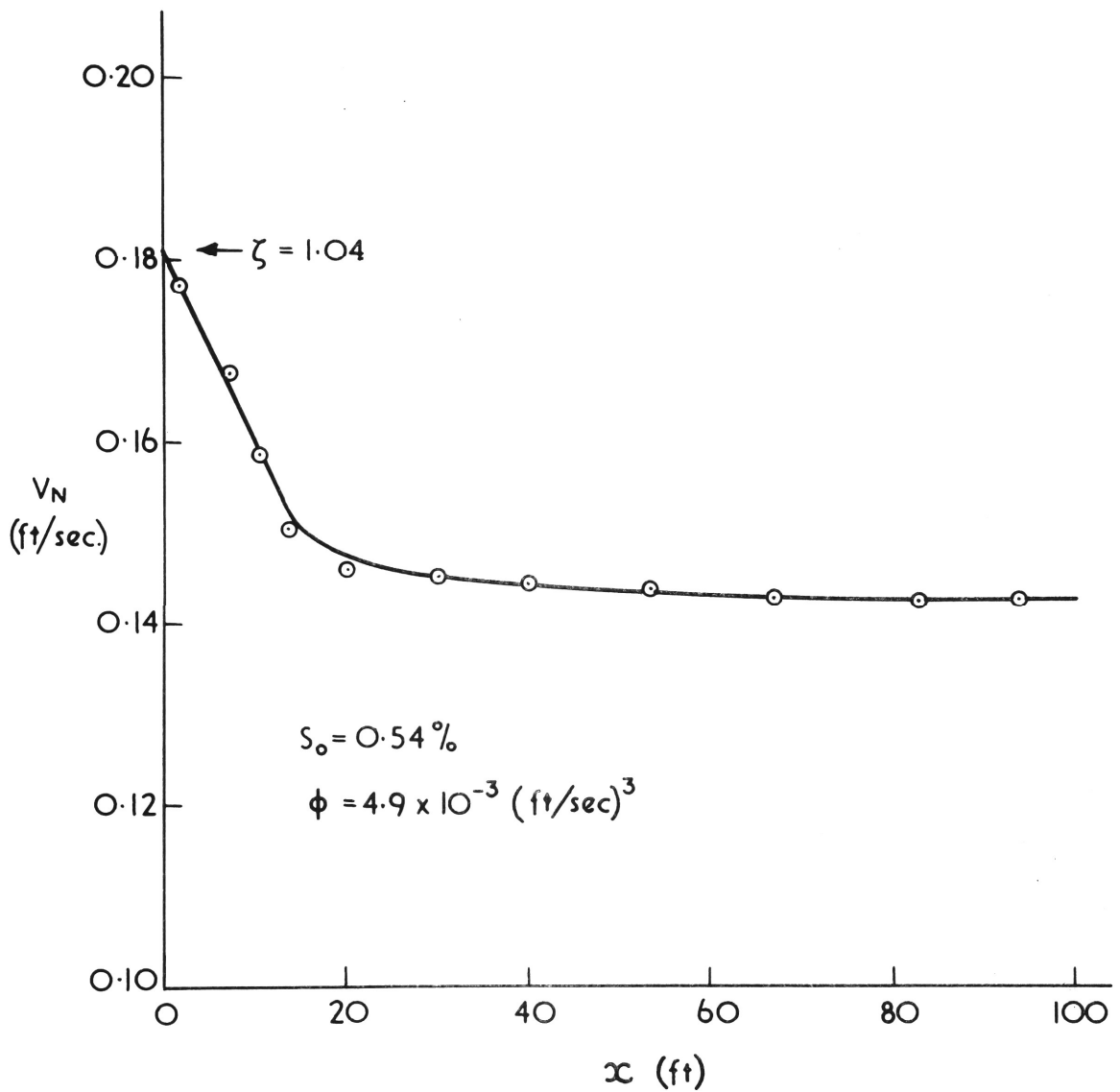
NOSE VELOCITY VERSUS DISTANCE TRAVELLED

TEST No. 9

FIGURE 39a.
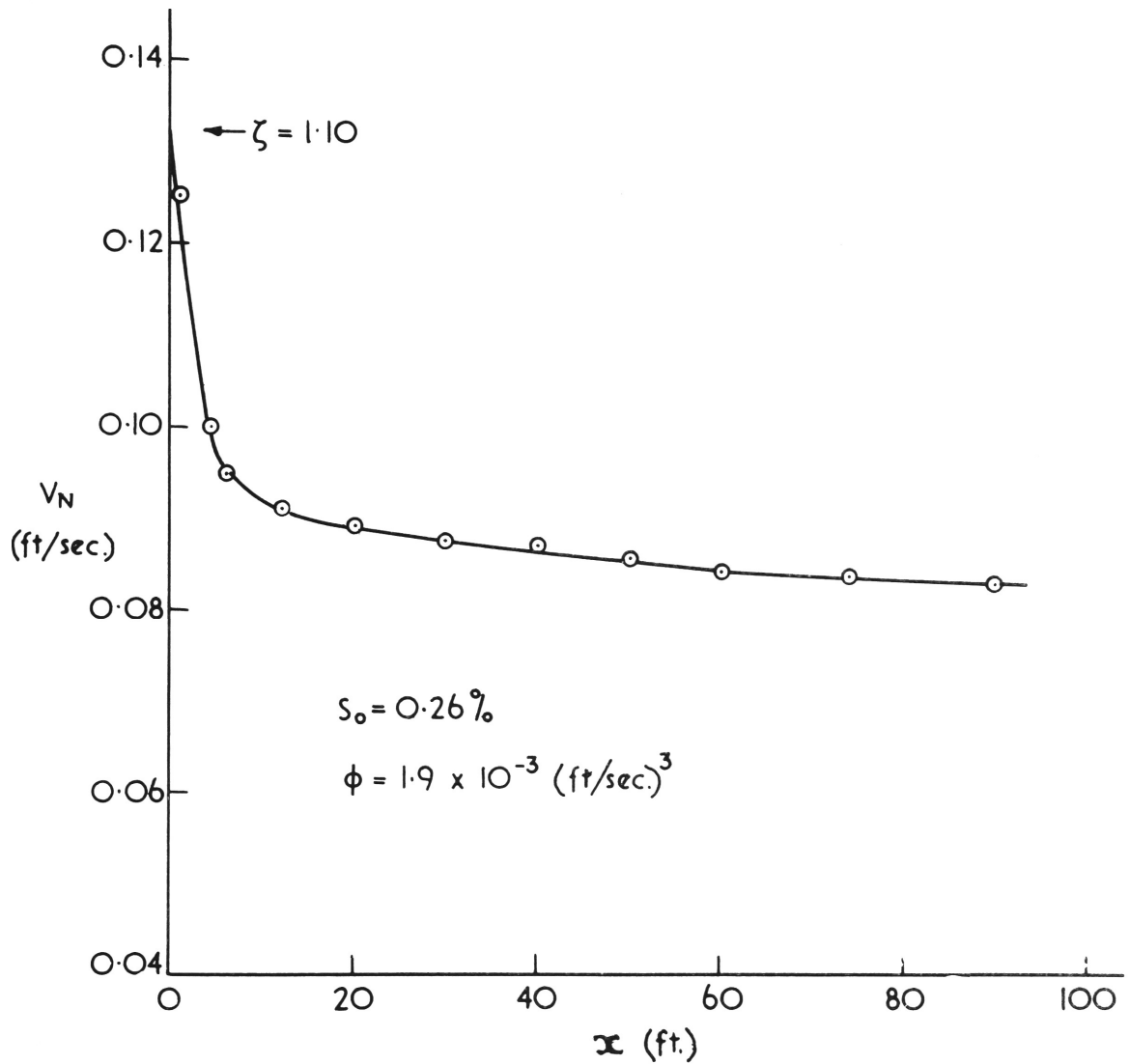
NOSE VELOCITY VERSUS DISTANCE TRAVELLED

TEST No. 10

FIGURE 39 b.

until an equilibrium is attained in the downstream flow. If the bottom slope is zero, as in Figure 38, no equilibrium condition exists and the velocity of the flow will continue to fall, eventually causing the density jump to flood as in experiment 6, (Figure 40).

Preliminary experiments indicated that any instant, the velocity of flow is constant along the length of an unsteady density flow. This was deduced by observing the nose velocity at the instant of flooding of the density jump for density currents moving on a horizontal bottom. This nose velocity was found to be very nearly equal to the calculated layer velocity immediately downstream of the jump at the instant of flooding. It was also noted that the layer depth was constant along the length of the layer. Hence it follows the layer velocity must also be constant over the same length.

It should be noted these conclusions result from only five experiments and are therefore based on limited data.

It was shown in the previous chapter that the Froude number for uniform flow of a density layer is related to the downstream Froude number by the equation

$$\beta F^2 = R_2 \sin \theta \, \omega_r$$

where β was found to equal 14.3.

It has been shown that $F^2 = f^3$. Hence the above equation reduces to

$$f^3 = \frac{1}{\beta} R_2 \sin \theta \, \omega_r$$

The parameter β is dependent on the velocity distribution in the moving layer. The value of β obtained for the present series of experiments was 15.3. It can be seen in Figure 41 that β is fairly constant in value and shows no dependence on the Reynolds number of the flow.

There is, however, one important difference between the friction controlled flow examined in the previous chapter and that examined here. In the earlier experiments downstream density and velocity distributions were measured only a relatively short distance (2-3 feet) downstream of the density jump. It was noted previously, in these experiments the interfacial shear, as obtained from measured velocity profiles, was low. It was put forward that the form of velocity distribution was determined by the density jump and not solely by friction as in the case with uniform open channel flows. The length of the channel in these earlier tests was seven feet.

It can be seen that in the present series of tests, which were conducted in a tilting flume, 120 feet long and 2 feet wide, that uniform velocities were not attained until the nose had travelled 40 feet or so (Figs. 39a and 39b).

The tilting flume was only available for a limited period. Therefore, detailed analyses of the unsteady density flows were not made. Density and velocity distributions in the layer behind the nose were not
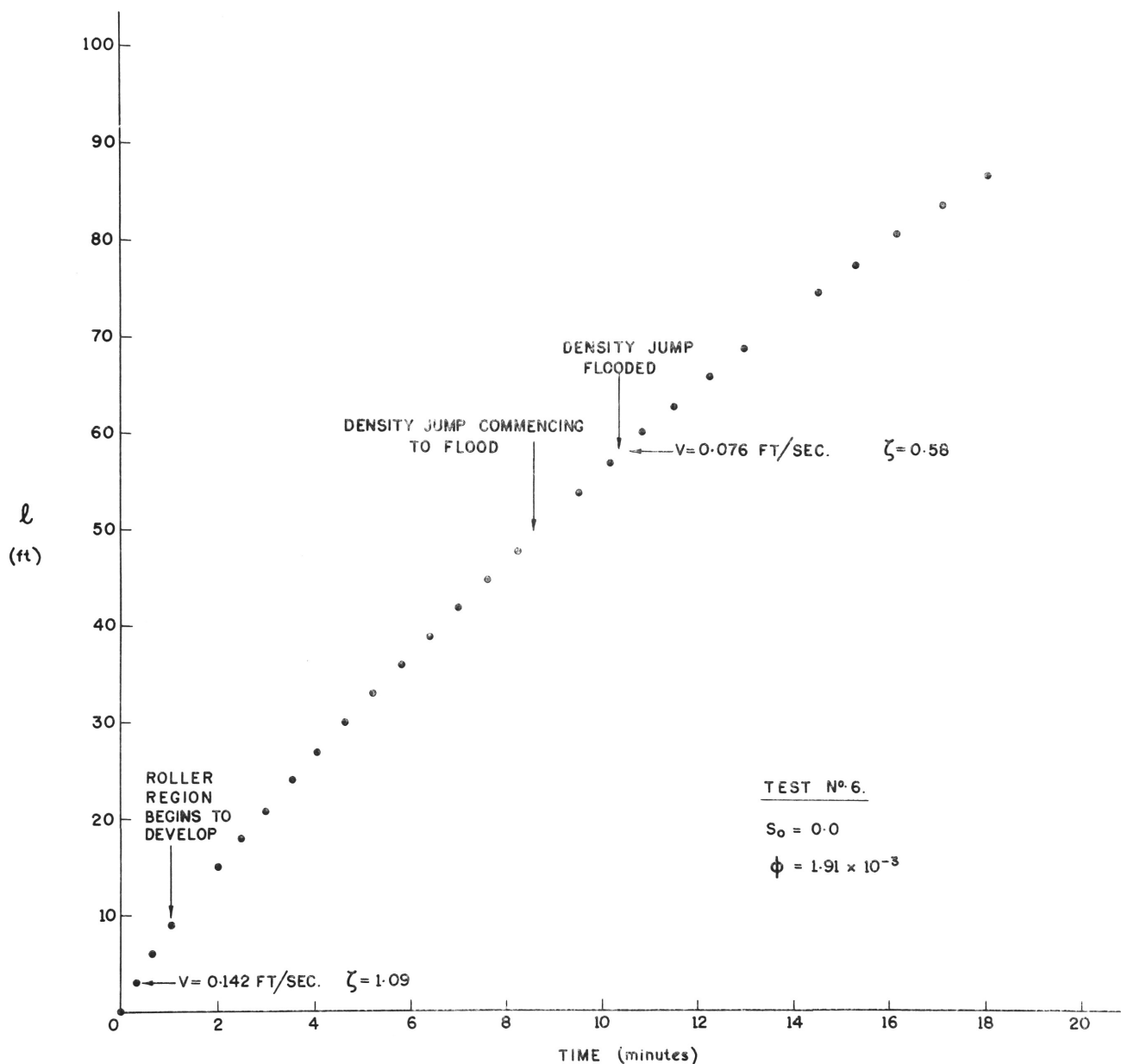
DISTANCE TRAVELLED VERSUS TIME PLOT FOR AN UNSTEADY

DENSITY CURRENT

FIGURE 40.

$$\beta = \frac{R_2 \sin \theta \omega_r}{F^2}$$
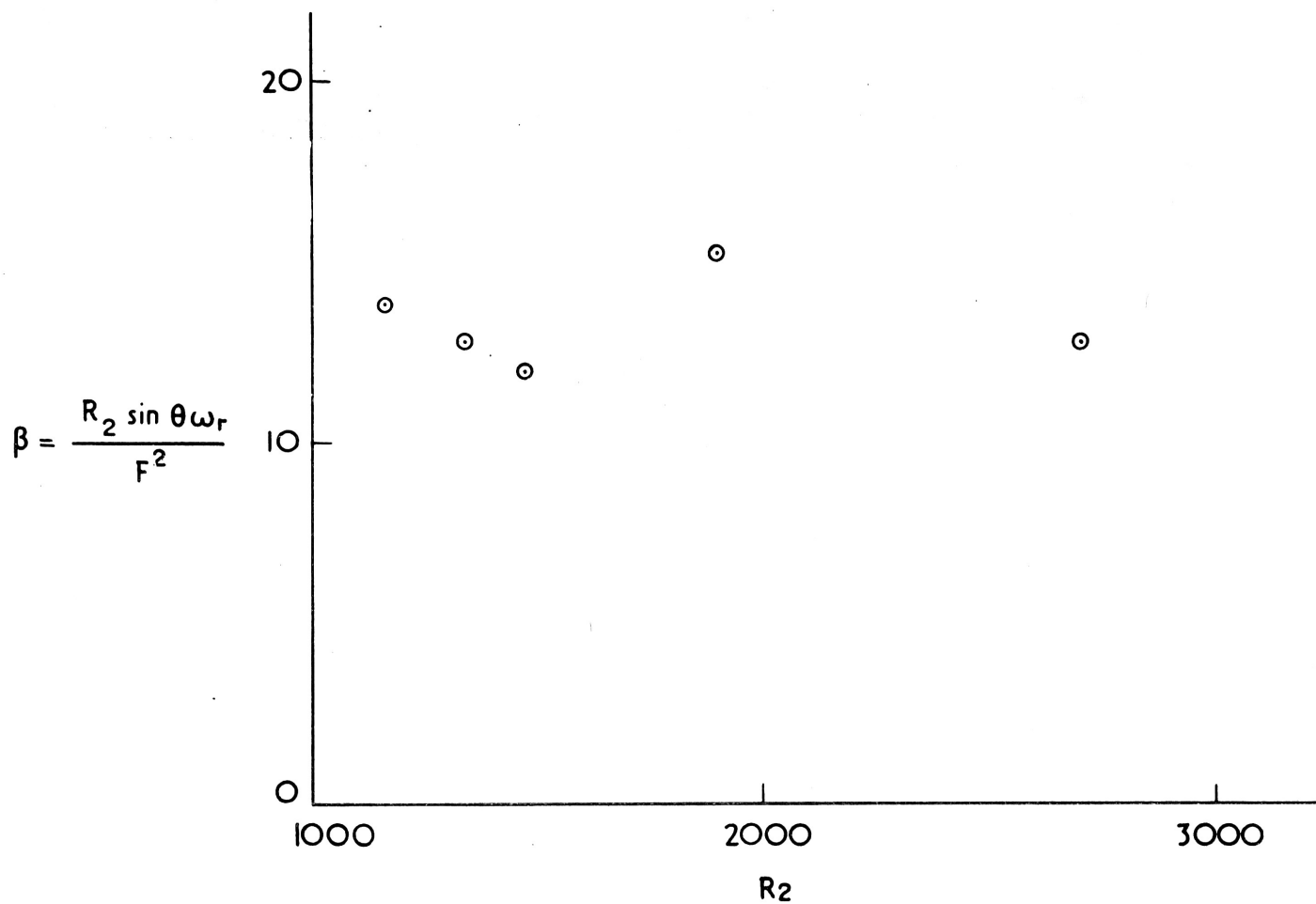
FRICTION FACTOR VERSUS REYNOLDS NUMBER FOR UNSTEADY DENSITY FLOWS

FIGURE 41.

obtained. However, the similarity in the values obtained for β (14.3 and 15.3) suggests the velocity distribution formed immediately downstream of the jump remains stable further downstream. It was noted in the previous chapter, that the frictional forces acting on the density flows downstream of a density jump are less than those obtained by other experimenters working with density currents of uniform density. This difference appears to result from the velocity distribution within the flowing layer being controlled by the non-uniform density distribution rather than boundary friction. Interfacial shear is considerably less than that measured for uniform density flows.

It is important to note that the bottom and interfacial boundary layers were laminar for all experiments involving unsteady flows.

6. The Entrainment Function

6.1 Introduction

In this chapter it is proposed to analyse the entrainment region of a density jump, particularly the effect of gravity on entrainment.

The entraining zone of a density jump has been compared to the spread of a neutral jet. The neutral jet can be considered as the limiting case of a density jump, as the upstream Froude number approaches infinity. This can be seen from the definition of the Froude number as the ratio of fluid momentum to hydrostatic pressure force at a section across the flow. The hydrostatic pressure force of a neutral jet is zero. Therefore the Froude number of such a jet would approach infinity. Arithmetically, the above may be expressed by:-

$$F = \left(\frac{Q^2}{\Delta y^3} \right)^{\frac{1}{2}}$$

Therefore as Δ, the density excess approaches zero, the Froude number must approach infinity.

It is important to note also, for a given density current, with a specified density excess, the Froude number will approach infinity as the depth of flow is reduced to zero.

It follows, therefore, that the characteristics of the upstream end of a density jump, for large values of the upstream Froude number, will approach those of a neutral jet.

6.2 Analysis

Consider the force flow equation (12)

$$\frac{S_m Q^2}{y'} + \frac{S_H y'^2}{2Q}\phi = M = M_1 - \int_{x_1}^{x_2} \frac{\tau_w}{\rho_0} dx$$

The assumption is now made that the velocity and density distributions are self preserving in the entraining zone. Experiments showed this to be a good assumption for the range of F_1 and R_1 used as can be seen in Figure 42.

Equation 12 assumes that the pressure distribution is hydrostatic. The angle of spread of the entraining zone was less than $\tan^{-1} 0.16$ so that accelerations in the y direction are of an order less than those in the x direction and their effect on the pressure distribution is negligible. Measurements along the bottom boundary of submerged hydraulic jump have shown the pressure distribution to be very nearly hydrostatic (Rajaratnam, 1964). The flow geometry in Rajaratnam's experiments is very similar to that for density jumps and they therefore provide supporting evidence for the hydrostatic assumption. Boundary friction is ignored in the following analysis. The effect of this assumption as regards entrainment is discussed later in this chapter.

An interesting point arises when equation (12) is differentiated with respect to y'. One finds

$$\frac{1}{2}\frac{dQ}{dy'}\left[\frac{4 S_m Q}{y'} - \frac{S_H \phi y'^2}{Q^2}\right] + \left[-\frac{S_m Q}{y'^2} + \frac{S_H y'\phi}{Q}\right] = 0$$

and substituting for $\dfrac{Q^3}{\phi y'^3}$ using

$$F^2 = \frac{Q^2}{\Delta y'^3} = \frac{Q^3}{\phi y'^3}$$

the above expression reduces to

$$\frac{dQ}{dy'} = \frac{2Q}{y'} \cdot \frac{S_m F^2 - S_H}{4 S_m F^2 - S_H} \tag{43}$$

The significant feature of the above equation is that as the Froude number approaches the value $F = (\frac{S_H}{S_m})^{\frac{1}{2}}$, entrainment ceases. Hence Q approaches a constant value. Simultaneously the depth of flow y' must approach a constant value. This results from Equation 12 where Q and y' are the only variables. If F were to go below the value $F = (\frac{S_H}{S_m})^{\frac{1}{2}}$ then $\frac{dQ}{dy}$, would be negative.

This is clearly impossible since it would involve a negative diffusion process: salt water becoming fresh or heat concentration and temperature rise without additional energy. Both violate the second law of thermodynamics and will not occur. The minimum Froude number attainable in the entraining zone of a density jump is therefore equal to S_H/S_m to the power one half. $(S_H/S_m)^{\frac{1}{2}}$ is equal to one if the velocities and densities are uniform. Generally $(S_H/S_m)^{\frac{1}{2}}$ will be less than one. $(\frac{S_H}{S_m})^{\frac{1}{2}}$ values together with values of F_2 are plotted against F_1 in Figure 25 for maximum entraining density jumps.

The Entrainment Parameter

The entrainment parameter is a useful concept in that it expresses local entrainment at a section, in terms of local flow characteristics. Ellison and Turner (1959) defined an entrainment parameter (E) as the
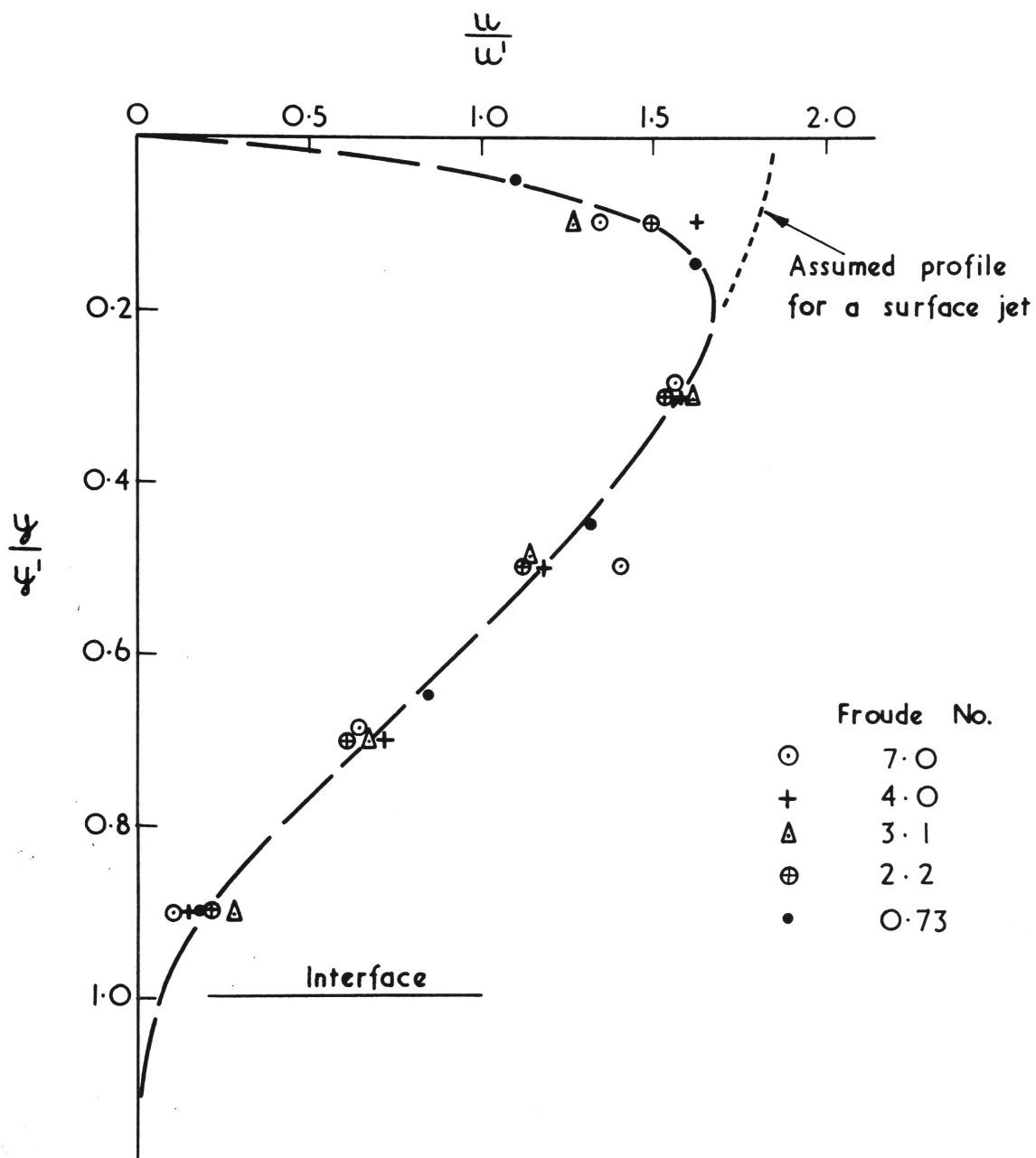
VELOCITY DISTRIBUTIONS IN THE ENTRAINMENT ZONE
OF A DENSITY JUMP

FIGURE 42.

ratio of an entraining velocity, normal to the direction of flow of the density current, to the mean velocity at the section of interest. In mathematical terms the entrainment parameter is defined as -

$$E = \frac{1}{u'} \frac{d}{dx} (y'u') \tag{44}$$

Ellison and Turner defined the depth of their density currents as the mean of the depth to the greatest velocity gradient and the depth of maximum density gradient. Since the velocity and density distributions are self preserving, the depth as defined by Ellison and Turner can be directly related to the interfacial depth. The writer's experiments showed the two depths were equal.

Equation (44) can also be written as

$$E = \frac{y'}{Q} \cdot \frac{dQ}{dx} \tag{45}$$

From Equation (43) one has

$$\frac{dQ}{dx} = \frac{2Q}{y'} \cdot \frac{S_m F^2 - S_H}{4 S_m F^2 - S_H} \cdot \frac{dy'}{dx}$$

and from equation (45)

$$\frac{dQ}{dx} = \frac{E Q}{y}$$

so that equating the above two expressions one has

$$E = \frac{2(S_m F^2 - S_H)}{4 S_m F^2 - S_H} \cdot \frac{dy'}{dx} \tag{46}$$

The above expression is a function which relates the entrainment parameter to the local Froude number and the interfacial slope. The

latter factor, however, is an unknown quantity. Although a theoretical expression could not be derived for the interfacial slope as a function of x, an expression which satisfied the four necessary boundary conditions was found. The boundary conditions will now be examined.

(i) At the Origin

If one considers a density jump originating with a finite Q and Δ from a virtual origin, the Froude number at the origin will be infinite. This fact has been discussed previously where it was shown that as the Froude number approaches infinity, the behaviour of the entraining density current approaches that of a neutral jet. It can be shown that the spread of a self-preserving neutral jet is linear with distance (Streeter, 1961).

Considerable experimental data are available on the entraining characteristics of a neutral jet. Townsend (1956) measured the spread of a neutral two dimensional jet and found $\frac{y'}{x}$ = 0.15.

Measurements of a two dimensional wall jet by Bakke (1957) gave $\frac{dy'}{dx}$ = 0.144. The measured velocity distributions resemble those of a semi - two dimensional jet, except for a thin boundary layer next to the wall. The boundary stress acted to reduce entrainment but by only a small amount. Conditions at the virtual origin are listed below.

(a) $y' = 0$

(b) $F \rightarrow \infty$

(c) $\frac{dy'}{dx} = \alpha = 0.150$

(ii) Conditions far downstream

It has been shown that uniform conditions are attained when

$F = (S_H / S_m)^{\frac{1}{2}}$ provided $\dfrac{dQ}{dy'}$ is to be a continuous function. The case

where $\dfrac{dQ}{dy'}$ is not continuous will be discussed at the end of this chapter.

If a critical depth y_c, is defined as the uniform flow depth when

$F = (\dfrac{S_H}{S_m})^{\frac{1}{2}}$ then from equations (17) and (10)

$$y_c^{\,3} = (\dfrac{S_m}{S_H})^{\frac{1}{2}} \cdot \dfrac{Q^2}{\emptyset}$$

Then at the far downstream end of the entraining zone, the following

conditions apply.

(a) $y' = y_c$

(b) $F = (\dfrac{S_H}{S_m})^{1/2}$

(c) $\dfrac{dy'}{dx} = 0$

A depth profile which satisfies all the boundary conditions and is in

fair agreement with measured depth profiles is given by

$$\dfrac{y'}{y_c} = 1 - e^{-\alpha \frac{x}{y_c}} \tag{47}$$

This assumed profile is plotted together with measured profiles in

Fig. 43. It will be seen that the above expression is a convenient

function as it enables $\dfrac{dy'}{dx}$ to be expressed in terms of a local Froude

number. Therefore, the entrainment function can be expressed solely

as a function of the local Froude number, by substituting for $\dfrac{dy'}{dx}$ in

Equation (46).

If equation (47) is differentiated with respect to x, one finds -

$$\frac{dy'}{dx} = \alpha(1 - \frac{y'}{y_c})$$

(48)

$\frac{y'}{y_c}$ can be eliminated from the above equation by means of the force

flow equation.

The force flow as expressed in Equation 19 may be used to calculate

$\frac{y'}{y_c}$. Hence

$$\frac{M y_{ic}}{\rho_o Q_1^2} = \frac{S_H}{2} \cdot \frac{(2 \frac{S_m}{S_H} F^2 + 1)}{F^{2/3}} Y$$

(19)

and when $y' = y_c$, $F = \left(\frac{S_m}{S_H}\right)^{-1/2}$

so that

$$\frac{M y_{ic}}{\rho_o Q_1^2} = \frac{S_H}{2} \cdot \frac{3}{(S_H/S_m)^{1/3}} \cdot \frac{y_c}{y_{ic}}$$

(49)

If one equates Equation (19) and (49) one obtains

$$\frac{y'}{y_c} = \frac{3 \left(S_m/S_H F^2\right)^{1/3}}{\left(2 S_m/S_H F^2 + 1\right)}$$

(50)

The depth ratio $\frac{y'}{y_c}$ can be eliminated from the interfacial slope

equations to give

$$\frac{dy'}{dx} = \alpha \left[1 - \frac{3\left(S_m/S_H F^2\right)^{1/3}}{\left(2 S_m/S_H F^2 + 1\right)}\right]$$

The expression for the entrainment function can now be written in

terms of the local Froude number

$$E = \frac{(2 \frac{S_m}{S_H} F^2 - 1)}{(4 \frac{S_m}{S_H} F^2 - 1)} \cdot \left[1 - \frac{3 \frac{S_m}{S_H} F^2}{2 \frac{S_m}{S_H} F^2 + 1}\right]^{1/3} \alpha$$

(51)

The above equation is graphed in Figure 44.

6.3 Experimental Verification

Experimental data taken directly from Ellison and Turner's 1959

paper is also plotted in Figure 44 and shows close agreement with the

$$\frac{\psi'}{\psi_c} = 1 - e^{-\alpha \frac{x}{\psi_c}}$$

⊙ Measured Profiles
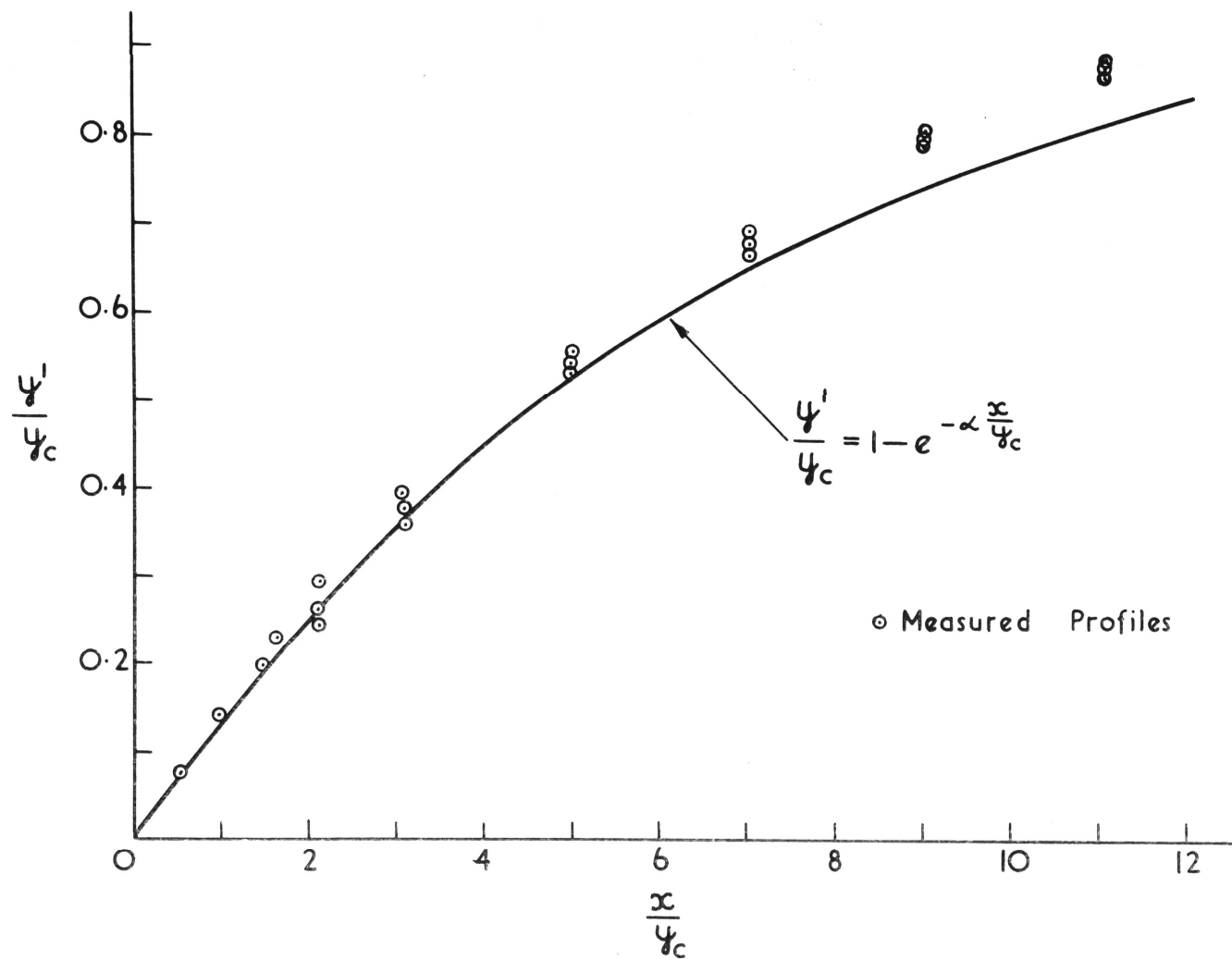
DEPTH PROFILES ENTRAINING REGION OF A DENSITY JUMP

FIGURE 43.
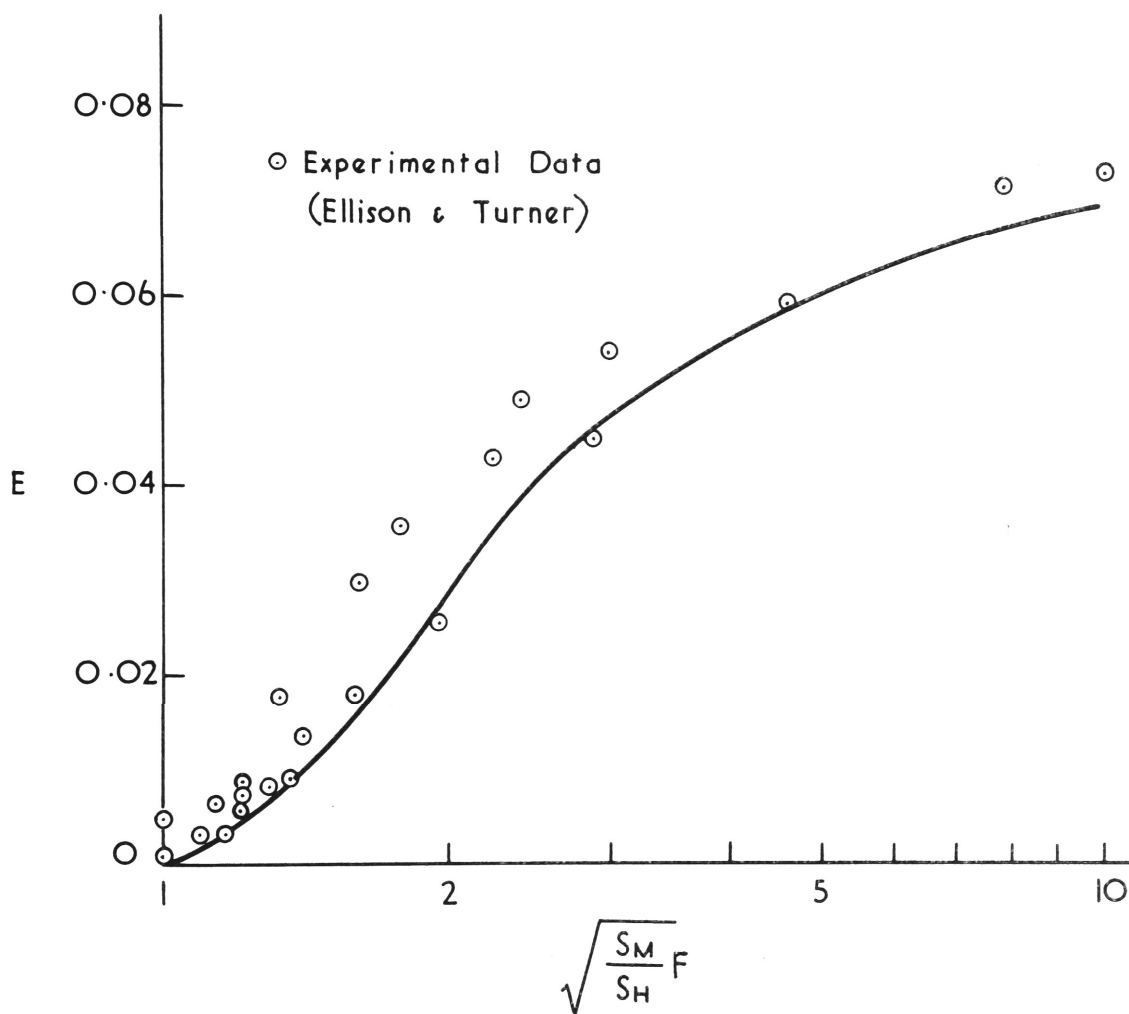
ENTRAINMENT PARAMETER VERSUS LOCAL
FROUDE No.

FIGURE 44.

theoretical curve. The data were obtained from Figure 2 of the above paper where the entrainment parameter is plotted against the Richardson number of the flow. The Richardson number is equivalent to inverse square of the Froude number.

Ellison and Turner's experimental results were for a surface, fresh water current flowing over an ambient layer of salt water. Therefore the zero boundary shear assumption made in the analysis is a reasonable approximation for this case. Ellison and Turner's flow parameters were defined slightly differently to those of the author so that it was necessary to convert the former's data before it could be compared with the derived expression for entrainment. It might be mentioned that Ellison and Turner's data fits the theoretical curve more closely if it is not adjusted. A small discrepancy in theory and experiment does exist, however, and is caused by the choice of depth profile.

6.4 Velocity and Density Distributions in the Entrainment Zone

The velocity used in calculating the Richardson number was the surface velocity since it could be easily measured. It is reasonable to suppose the velocity distribution of Ellison and Turner's density currents was similar to that obtained by the writer because of the similarity of experimental set up. The only significant difference would be the absence of the boundary layer caused by the false bottom in the writer's

experiments. If one extrapolates a surface velocity from the velocity distribution in Figure 42 one finds u_{max} = 1.85 u'.

Ellison and Turner's characteristic depth, taken as the mean depth to maximum velocity and density gradients, was found to occur at the interface so that depth measurements required no correction.

The density gradient near the interface steepens slightly as the Froude number decreases. This results from the fall in the rate of energy dissipation and therefore the turbulences level as uniform conditions are approached.

Turbulent exchange across the interface is reduced and the interface becomes more distinct at the downstream end of the entraining zone.

A further point arising from the forms of the velocity and density distributions (Figs. 42, 45) is that there appears to be a layer containing stagnant fluid of different density to the ambient fluid from $\frac{y}{y_i}$ = 1.0 to 1.3. This layer does not really exist but results from intermittency of the fluctuating interface affecting mean density readings in this range. The density measuring device takes a temporal mean reading at a given depth and therefore readings close to a turbulent interface, such as exists in the entraining zone, can easily lead to an erroneous impression of the actual density distribution. The writer believes the true density gradient close to the interface at any instant is far steeper than that indicated in Figure 45.

FIGURE 45.

DENSITY ~~VELOCITY~~ DISTRIBUTIONS IN THE ENTRAINMENT ZONE OF A DENSITY JUMP
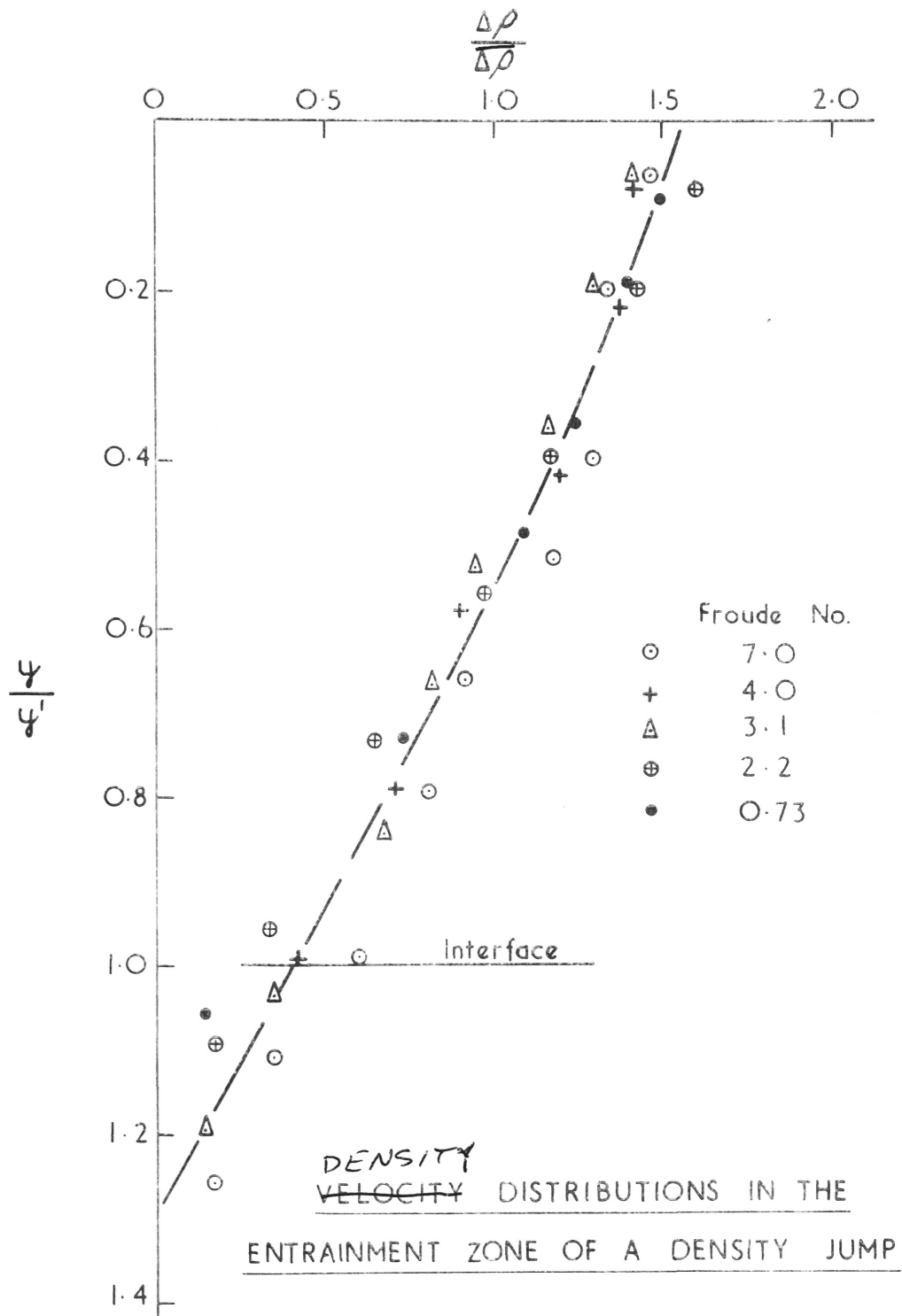
Self preservation of velocity and density distributions was assumed when deriving the entrainment function. This approximation was quite reasonable as can be seen from Figures 42 and 45. The velocity distribution showed no detectable change along the length of the entrainment zone. Values of 1.36 and 0.60 were reduced from the above figures for S_m and S_H respectively for the surface jet.

Conversion of Ellison and Turner's data was effected as given below

$$\left(\frac{S_m}{S_H}\right)^{1/2} F = \left(\frac{1.36}{0.60}\right)^{1/2} \cdot \frac{1}{1.85 \, R_i^{1/2}} = \frac{0.82}{R_i^{1/2}}$$

and was plotted against the entrainment parameter.

6.5 Sources of Error

Experimental data lies slightly above the derived curve. It is believed this error is largely attributable to the selected depth profile which lies below the experimental profile. Under estimation of y' causes $\frac{dy'}{dx}$ to be underestimated in the form of equations selected. The entrainment parameter is directly proportional to the interfacial slope. Therefore, values of E calculated from Equation 51 will be less than experimental values. This error is only apparent at lower Froude numbers in the range one point four to three.

As already discussed, S_H also changes slightly at lower Froude numbers due to the reduction in interfacial turbulence. This is another source of error.

6.6 Effect of Boundary Friction on Entrainment

The presence of boundary friction at a density jump results in a decrease in entrainment.

Boundary friction was not included in the earlier analysis for two reasons; firstly its neglect is a good approximation for density jumps at a free surface, for which experimental data were available, and secondly the differential entrainment equation could not be solved exactly if friction was included.

The entrainment equation containing a friction term can be solved numerically. However, this was not attempted, as the writer's interest was centred more on the analysis of the entrainment function rather than the secondary effects of friction.

The influence of friction on entrainment can be seen from the force flow diagram shown in Figure 46. Consider a density jump with its upstream state given by the point A. If there is no boundary shear, the force flow $\dfrac{M y_{ic}}{\rho_o Q_1^2}$ will remain constant along the length of the entrainment zone. Therefore the value of the flow ratio (K) at any depth Y is given by a point lying on the line of constant $\dfrac{M y_{ic}}{\rho_o Q_1^2}$ passing through A i.e. AB. The point B represents the downstream condition of the entrainment region where, in the ideal case, the Froude number is unity. If boundary shear is present, it can be seen from Equation (12) that $\dfrac{dM}{dx}$ is negative. Since $\dfrac{dy}{dx}$ is everywhere positive it follows $\dfrac{dM}{dy}$ will
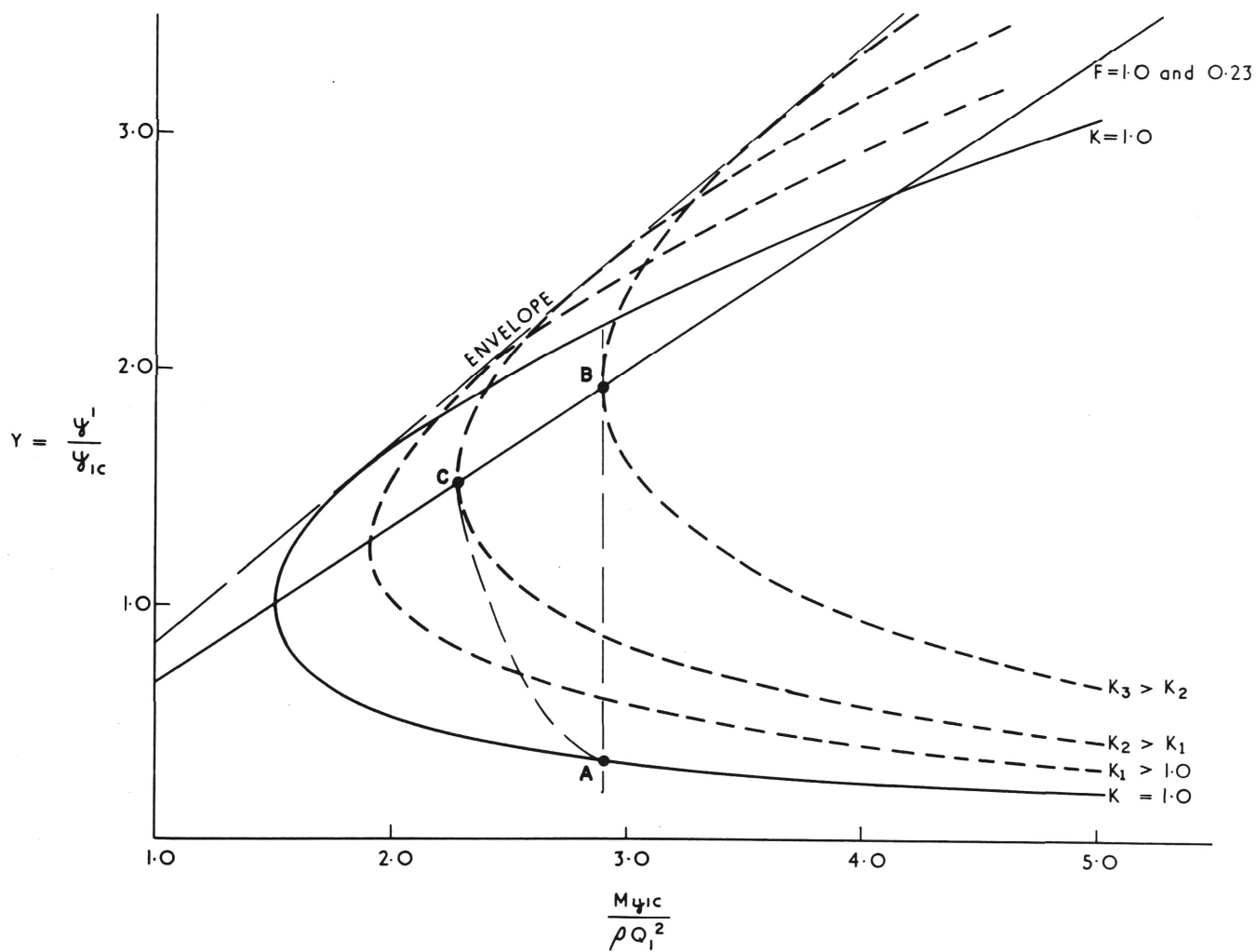
THE FORCE FLOW DIAGRAM

FIGURE 46.

always be negative.   Therefore a plot of flow ratio against depth, for

an entraining zone subject to boundary friction, is given by a line sim-

ilar to AC in Figure 46.   It can be seen entrainment in this case is less

than it was when there was no friction along AB.   Values of K are less

at corresponding depths along AC, than along AB.

The downstream state of the jump is friction controlled provided no

other control acts.   Therefore, unless the slope is critical, the point C

is not reached and a discontinuity in $\frac{dQ}{dy'}$ occurs, in the form of a

roller region.   This possibility is examined in the section following.

6.7 Discontinuities in dQ/dy'

It has been shown that the minimum Froude number attainable in the

entraining zone of a density jump is $\left(\frac{S_H}{S_m}\right)^{1/2}$.   Furthermore uniform flow

conditions are not reached until this value of Froude number is attained.

It follows, therefore, the maximum Froude number possible downstream

of a density jump, occurs when the entrainment zone extends the whole

length of the jump.   Under these conditions entrainment is a maximum.

Experiments have shown that Froude numbers less than $\left(\frac{S_H}{S_m}\right)^{1/2}$ are

possible.   The mechanism of the roller region associated with these

jumps has been discussed previously.   Mathematically, the roller region

represents a discontinuity in $\frac{dQ}{dy'}$.   As there is very little entrainment

in the roller region, $\frac{dQ}{dy'}$, ceases to be continuous once the local Froude

number is conjugate to the non-entraining Froude number of the down-

stream flow. The roller region is directly analagous to the open channel hydraulic jump and responds to a downstream control in a similar fashion. The entrainment zone presents a continuous range of possible states to which a similar range of downstream flows can be coupled. The limits of this range occur when,

(a) the entraining region occupies entire length of the jump and the downstream Froude number is equal to $\left(\dfrac{S_H}{S_m}\right)^{1/2}$,

(b) the roller region is forced back so as to cover the entrainment zone. The jump is then of the non-entraining type. Under certain conditions, for example, when a weir controls the downstream flow, the jump will reach an instability before the non-entraining state can be established.

7. The Fall in Force Flow at a Density Jump

7.1 Introduction

Experiments indicated that the loss in force flow across a density jump was as much as 30 per cent. significantly greater than that experienced in open channel jumps. In this chapter an attempt is made at estimating the probable loss in force flow across a density jump.

It will be shown that for density jumps with high upstream Froude numbers, the major proportion of force flow is lost in overcoming boundary shear at the upstream end of the jump. Most force flow is lost in the upstream half of the density jump, the region where velocities and shears are highest. Two other important observations concerning the upstream end of a density jump were made. These were as follows:-

(i) The velocity distribution was found to be self preserving and consisted of a laminar region between the solid boundary and the velocity maximum, and a turbulent region extending from the velocity maximum to the interface.

(ii) Therefore if the boundary layer is defined as being the region between the solid boundary and the velocity maximum, then the boundary layer is laminar.

(iii) The spread of the density jump in the upstream region was found to be linear and it follows from observation (i) that the spread of the boundary layer in this region of jump is also linear.

A simplifying assumption is made in the following analysis, this being that the pressure gradient in the x direction is neglected. The problem is treated as a neutrally buoyant wall jet. The previous analysis shows that gravitational influence in the entrainment zone of a density jump is small for local Froude numbers greater than four or five. Therefore, it is a reasonably good approximation to treat the upstream end of the density jump as a wall jet.

7.2 Analysis

The analysis takes the following form:-

(a) The boundary shear is expressed as a function of the known self-preserving velocity distribution.

(b) The expression for boundary shear is substituted into a differential form of the force flow equation for a neutral jet.

(c) A solution is found for the differential equation giving the fall in force flow at a section as a function of its distance from the origin and the upstream Reynolds number.

The Boundary Shear

The boundary shear can be determined from the velocity distribution at any section. The total shear force exerted by the boundary on the flow will equal the change in force flow of the density current. The total shear force is found by integrating the boundary shear between sections of interest.

Consider the velocity distribution shown in Figure 47 where δ denotes a distance in the y direction within the laminar boundary layer. The boundary layer thickness (δ'), is defined as the distance from the boundary to the velocity maxima. Since the velocity distribution for a wall jet is self-preserving (Swartz and Cosart, 1961) the two constants β_1 and β_2 can be defined by:-

$$\beta_1 = \frac{\delta'}{y'}$$

$$\text{and } \beta_2 = \frac{u_{max}}{u'}$$

where y' and u' are as previously defined. As the boundary layer is laminar the velocity distribution within the boundary layer is parabolic so that a dimensionless equation relating velocities and depths can be written:

$$\frac{u}{u_{max}} = \frac{\delta}{\delta'} \left(2 - \frac{\delta}{\delta'} \right) \text{ so that } \frac{du}{d\delta} = 2 \left(1 - \frac{\delta}{\delta'} \right) \frac{u_{max}}{\delta'}$$

At the boundary the velocity gradient is given by: $\left(\dfrac{du}{d\delta} \right)_{\delta=0} = 2\mu \dfrac{u_{max}}{\delta'}$ and the shear is given by

$$\tau_w = \mu \left(\frac{du}{d\delta} \right)_{\delta=0}$$

Hence
$$\tau_w = \frac{2\mu \beta_2 u'}{\beta_1 y'} \tag{52}$$

The loss in force flow can be determined by integrating the above shear stress along the boundary, in the direction of flow. The force flow equation for a neutrally buoyant jet is given by:-

$$M_1 = \frac{S_m \rho_0 Q^2}{y'} + \int_{x_1}^{x_2} \frac{2\mu \beta_2}{\beta_1} \cdot \frac{u'}{y'} \, dx \tag{53}$$

where M_1 is a reference force flow at $x = x_1$.

Self preservation implies that the spread of the jet is linear with distance from some virtual origin then $y' = \alpha x$ where α is an experimentally determined constant.

The above equation when differentiated with respect to x yields:-

$$\frac{dy'}{dx} = \alpha \qquad (54)$$

and a relationship between Q and x can be determined by eliminating y' from the force flow equation expressed in differential form.

If equation (53) is differentiated with respect to x one finds:-

$$\frac{dM_1}{dx} = 2 S_m \rho_o \frac{dQ}{dx} - \frac{S_m \rho_o Q^2}{y'^2} \frac{dy'}{dx} + \frac{2 \mu \beta_2 Q}{\beta_1 y'^2} = 0$$

Substituting for $\frac{dy'}{dx}$ and y' in the above, and after some algebra one obtains:-

$$\frac{dQ}{dx} = \frac{\left(Q - \frac{2 \mu \beta_2 S_m^{-1}}{\alpha \rho_o \beta_1} \right)}{2x} \qquad (55)$$

It is convenient to non-dimensionalise the foregoing relationships. Hence reference values are defined as

$$Q = Q_1 \text{ when } x = x_1$$

and when equation (55) is divided by $\frac{Q_1}{x_1}$ one has

$$\frac{dK}{dX} = \frac{\left(K - \frac{2 \beta_2 S_m^{-1}}{\alpha \beta_1 R_1} \right)}{2 X} \qquad (56)$$

$$\text{where } K = \frac{Q}{Q_1}$$

$$X = \frac{X}{X_1}$$

$$\text{and } R_1 = \frac{\rho_o Q_1}{\mu}$$
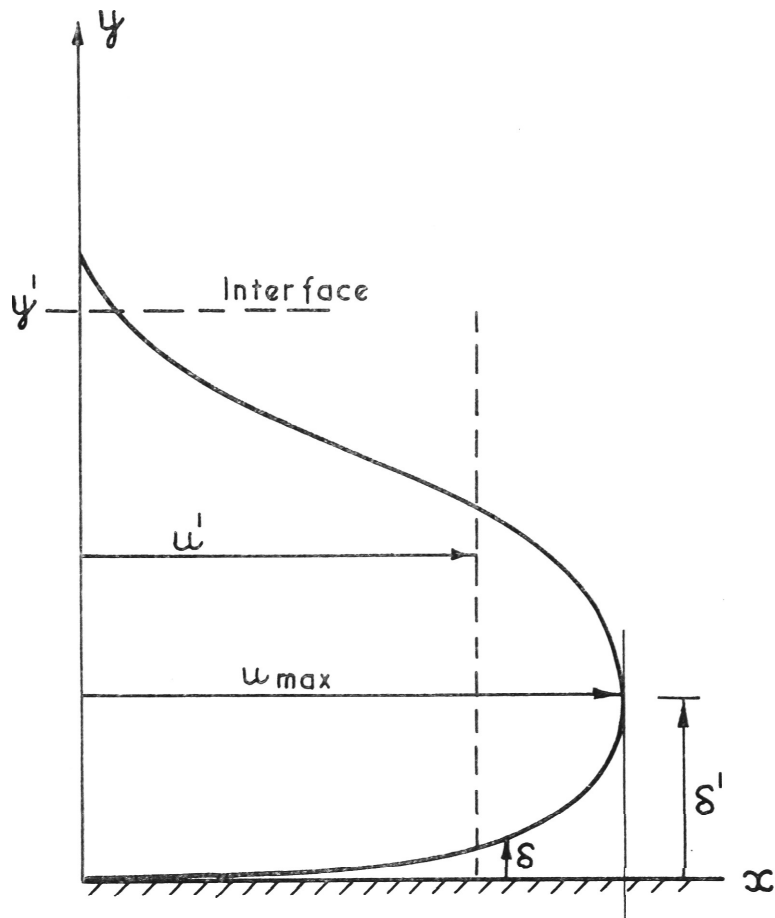
BOUNDARY LAYER DEFINITION SKETCH

FIGURE 47.

The differential equation (56) has a general solution given by

$$\left(K - \frac{2\beta_2 S_m^{-1}}{\alpha \beta_1 R_1} \right) = A \cdot X^{1/2}$$

where A is a constant which can be determined from the boundary conditions at $x = x_1$. x_1 is the distance between the virtual origin and the point at which the velocity distribution first becomes self-preserving. This is sufficiently close to the upstream end/the jump to be taken as that point. At this section, by definition, X = 1 and K = 1 so that the complete solution to the differential equation is therefore

$$K = \left(1 - \frac{2\beta_2 S_m^{-1}}{\alpha \beta_1 R_1} \right) X^{1/2} + \frac{2\beta_2 S_m^{-1}}{\alpha \beta_1 R_1} \tag{57}$$

The force flow equation may be non-dimensionalised by dividing by

$M_1 = \dfrac{S_m \rho_0 Q_1^2}{y_1'}$ so that equation (53) reduces to:-

$$1 - \frac{\alpha K^2}{Y_x} - \frac{\int_x^1 \tau_w \, dX}{M_1} \tag{58}$$

where $Y_x = \dfrac{y'}{x_1} = \dfrac{\alpha y'}{y_1'}$

The non-dimensional force flow ratio (θ) is given by

$$\theta = 1 - \left(\int_x^1 \tau_w \, dX \right) \Big/ M_1$$

Employing equation (58) this can be written:-

$$\theta = \frac{\alpha K^2}{Y_x} = \frac{K^2}{X}$$

K can be eliminated using equation (57) to give

$$\theta = \left[\left(1 - \frac{2\beta_2 S_m^{-1}}{\alpha \beta_1 R_1} \right) + \frac{2\beta_2 S_m^{-1}}{\alpha \beta_1 R_1} \cdot \frac{1}{X^{1/2}} \right]^2 \tag{59}$$

7.3 Discussion

Equation (59) expresses the fall in force flow of a neutral wall jet,

as a function of the distance in the direction of flow and a reference

Reynolds number. As the results of this analysis are to be applied to a

density jump the parameters β_1, β_2, α and S_m were obtained from

measured velocity distributions and angles of spread at the upstream end

of a density jump. Their values were found to be 0.12, 1.60, 0.15 and

1.30 respectively. The ratio of force flows at an upstream section and

at a section downstream are plotted against distance between the sections,

for a range of upstream Reynolds numbers in Figure 48.

It can be seen that the initial fall in force flow is sharp but lessens

further downstream as the boundary shear decreases. It is illustrative

to examine a particular jump, say with an upstream Froude number of five

and a Reynolds number of one thousand. The conjugate depth ratio for

this jump is approximately seven and experiments showed the region of

linear spread extends some three times this figure downstream from the

toe of the jump. Hence $\dfrac{x}{y_1'}$ is approximately twenty. It can be seen

from Figure 48 that no matter what the spread downstream of $\dfrac{x}{y_1'} = 20$

further loss in force flow is small compared with that which has already

taken place. It is to be expected then, that the foregoing theory for fall

in force flow in a neutral jet applies reasonably well to density jump

provided the upstream Froude number is large. Jumps with a Froude

number less than three cannot be satisfactorily approximated by a neutral

jet and so the foregoing theory will not give a good estimate of the fall in

force flow.
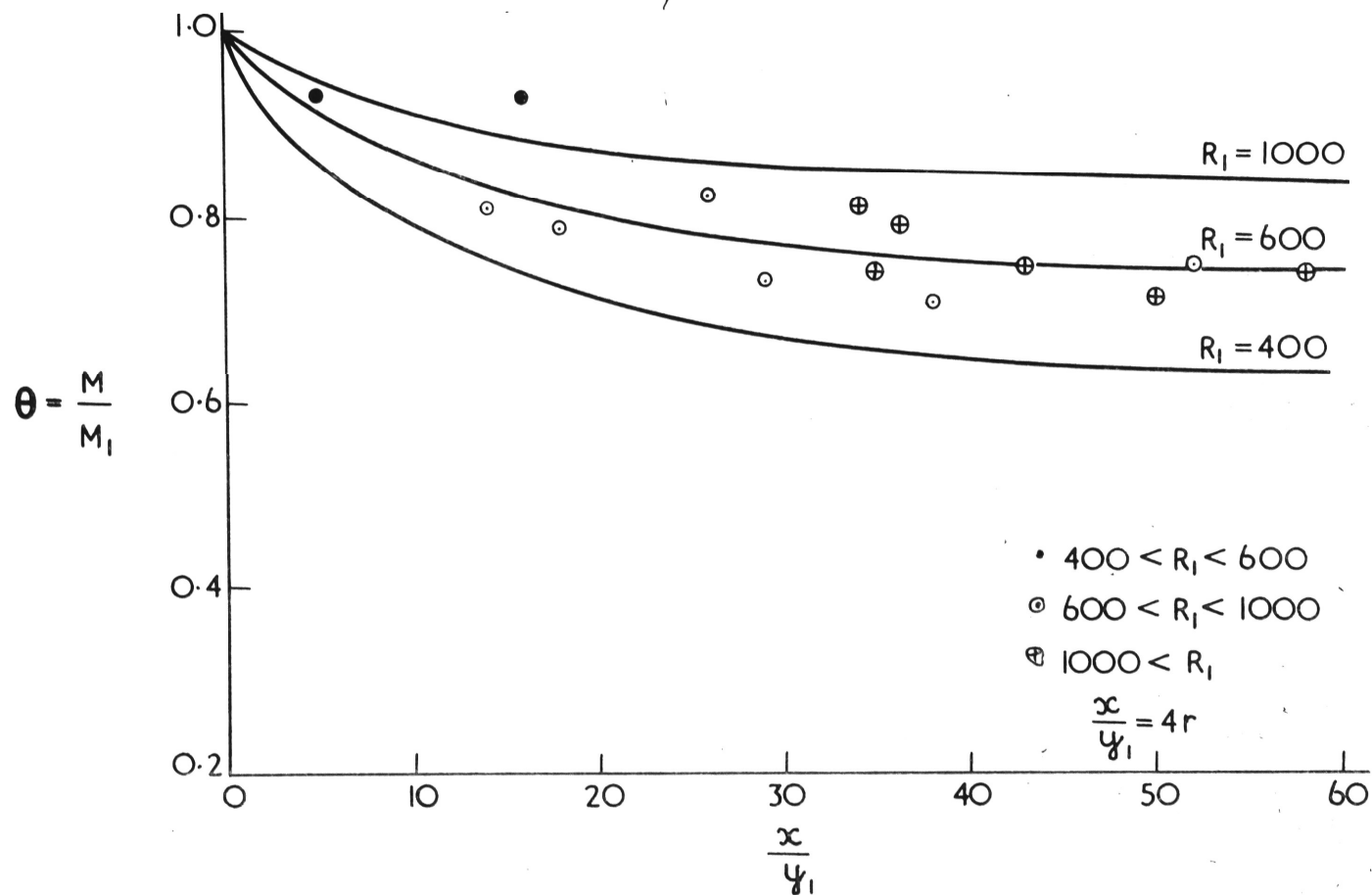
MOMENTUM FALL VERSUS DISTANCE FOR A NEUTRAL JET

FIGURE 48.

Some experimentally determined force flow ratios are shown in Figure 48 and it can be seen that shear forces acting on density jumps are greater than those on a neutral jet of the same upstream Reynolds number. This is not altogether surprising, since the density jump ceases to entrain at some point downstream and the flow becomes uniform. The rate of fall in force flow would remain constant in this region leading to a higher overall loss in force flow, as compared with a neutral jet.

The two points plotted for $400 < R_1 < 600$ were for jumps with upstream Froude numbers less than three, and it can be seen they do not conform to the foregoing analysis. Agreement was satisfactory for jumps with upstream Froude numbers greater than three.

The force flow ratios were calculated from measured entrainments and depth ratios for a number of density jumps. Accuracy in calculating the force flow downstream of the jump was $\pm$ 5 pc. so that the actual loss in force flow could only be estimated with accuracy of approximately $\pm$ 25 pc.

8.   Experimental Equipment

  8.1 Steady State Tests

        All steady state experiments described in this report were made

in the test tank shown schematically in Figure 49.   The tank consisted of

a plywood box 14 feet square by 4 feet deep.   The front of the tank was

made from 3/4 inch perspex sheeting.   A false side was placed approx-

imately 6 inches behind the perspex, and false bottom compartments as

shown in Figure 49 were placed in position.   Wedges were used to force

the false side hard against the false bottom compartments which in turn

pressed against the perspex viewing face of the tank.   The false bottom

compartments were very satisfactory as they permitted easy insertion

of velocity and temperature probes through the bottom of the compartment

into the density current.   Holes of $\frac{1}{2}$ inch diameter were drilled at 3 inch

and 6 inch spacings in the two compartments.   The holes were plugged

with rubber bungs which were inserted until flush with the false bottom.

The probes were lowered through holes drilled through the bungs.   This

prevented the compartments filling with water.

     The compartments could be tilted for experiments on friction con-

trolled density jumps, although this required unwedging of the false

side and rewedging after the adjustment had been made.   Similarly, the

depth of the inlet slot could be adjusted by raising or lowering the inflow

compartment shown in Figure 49.
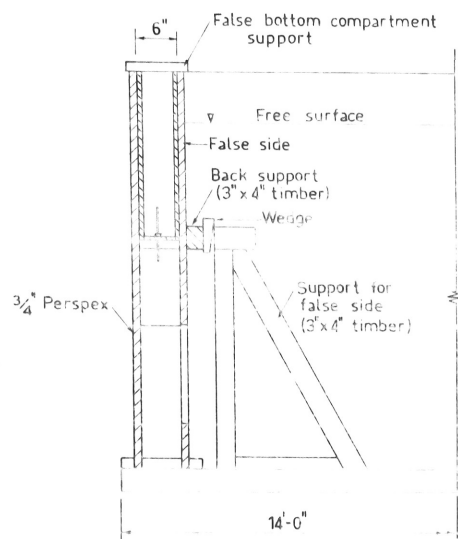
SECTION B-B
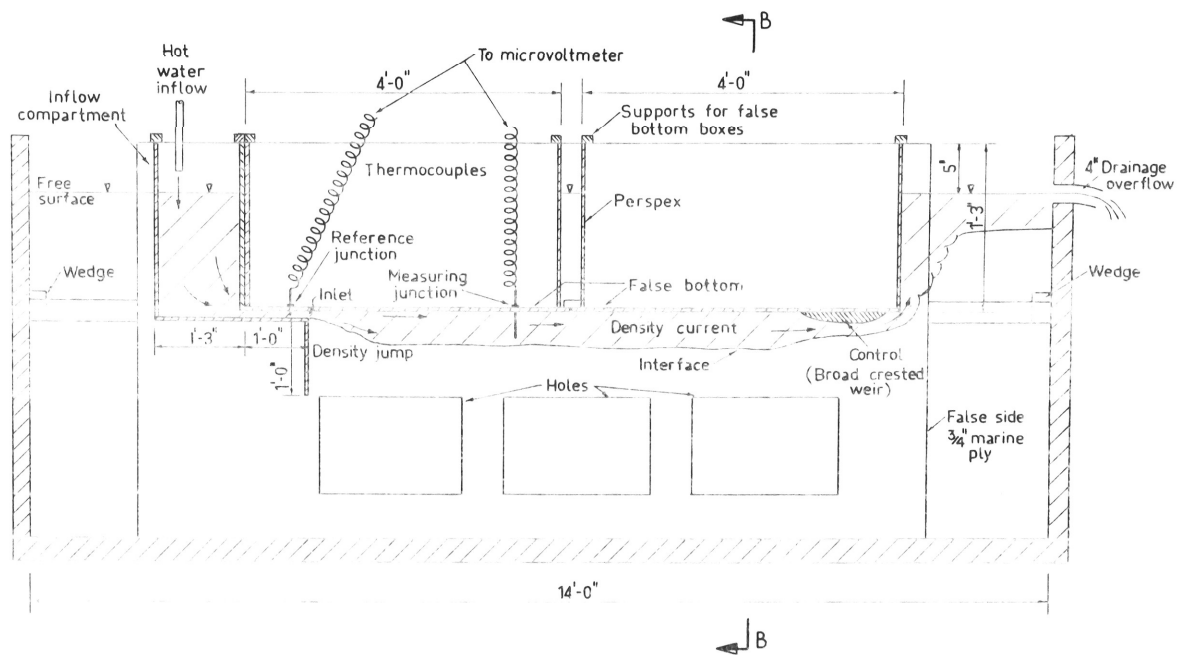
SECTIONAL ELEVATION A-A
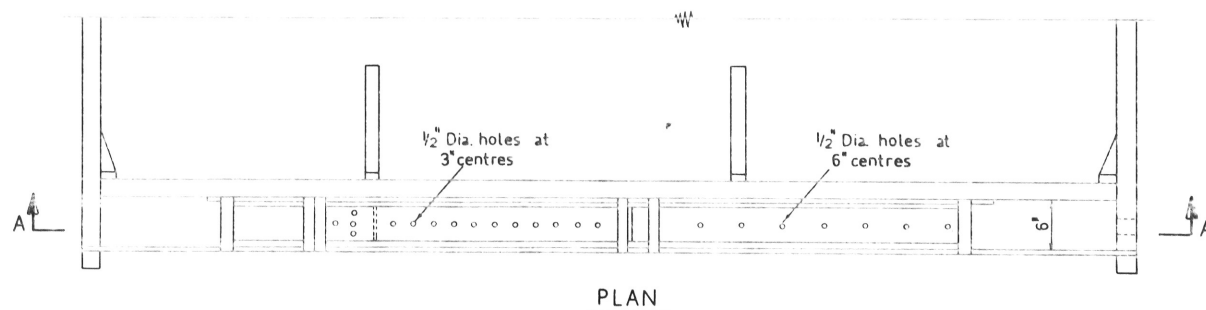
PLAN

NOT TO SCALE

SCHEMATIC LAYOUT OF STEADY STATE TEST TANK

FIGURE 49

The inflowing water was heated by an instantaneous three phase heater (415V) having a maximum capacity of approximately 2.5 kilowatts. The flow was then metered through a rotameter of capacity 0-3 gallons/minute. The rotameter was calibrated for a range of water temperatures and accuracy of measurement of the metered flow was always better than 2 pc.

It was necessary to wait at least ten minutes to one quarter of an hour before taking any readings, after adjusting the flow state in any experiment. This ensured a steady state had been established.

Heat transfer through the boundaries of the tank was found to be quite negligible compared with the total heat flux. Heat loss was not a source of error in experiments. The temperature of the inflowing water was measured by a thermocouple in the inlet, and downstream temperatures were measured relative to this reference.

The outflow from the tank drained into a 4 inch diameter overflow. It was necessary to have a continuous supply of cold water to the tank to make up for ambient fluid entrained into the density jump. Large holes were cut into the false side below the level of the density current as shown in Figure 49.

These holes permitted makeup flow to travel vertically into the density jump and minimised horizontal flows in the ambient fluid.

8.2 Unsteady Flow Experiments

The unsteady flow experiments described in Chapter 5 were made

in a tilting flume 120 feet long, 23 inches internal width and 24 inches deep. The flume was made of marine plywood with one side made of $\frac{1}{2}$ inch perspex. It was supported in a suspended steel frame which was attached via adjustable tie rods to an overhead arch. This permitted the flume to be adjusted to any slope up to a maximum of nearly 3 pc. over its length. However, the maximum slope used in the experiments was 0.54 pc.

As the tests were of limited duration, salt water was used for the density current and the flume was filled with fresh water. The salt water was pumped via an orifice flow meter from a 300 gallon storage tank into the inlet manifold of the flume. The depth of fresh water at the inlet was never less than 12 inches so that circulations induced in the fresh water by the density current were small. The thickness of the density current was never greater than 2 inches.

The accuracy of the orifice meter was approximately 5 pc. over the range of experimental flows. The nose velocity was measured by timing its travel between markers three feet apart along the length of the flume.

The specific gravity of the salt water was measured using a calibrated hydrometer.

9. Velocity Distributions

9.1 Introduction

It has been shown that the values of flow parameters downstream of a density jump are markedly dependent on the velocity distribution of the flow.

Generally, the velocity distribution is non-uniform and is controlled by two factors;

(i) the Reynolds number of the flow, and

(ii) the form of the jump.

The Reynolds number influence is the less important of the two even for the low Reynold's numbers associated with the experimental flows.

Density jumps represent discontinuity of flow energy. Energy is dissipated by turbulent shear forces at the jump and it is these turbulent eddies which determine the form of the downstream velocity distribution. The bottom boundary layer within this flow transition has little effect on the final velocity distribution.

If the jump is friction controlled the downstream velocity distribution must be affected by boundary friction. However, in experiments, the velocity distribution downstream of a friction controlled density jump did not undergo any significant change for large distances downstream of the jump. The experimental flows observed downstream of the density jumps consisted of a turbulent region sandwiched between two laminar boundary layers. One boundary layer originated from the bottom of the

channel and the other from the interface.

The case where the laminar boundary layers spread right across the moving layer has been analysed theoretically by Keulegan (1944). This analytic solution has since been verified experimentally by Ippen and Harleman (1952) Bata and Bogich (1953) and others, who have shown Keulegan's equations hold up to Reynolds numbers of approximately 1000. Although in some experiments, Reynolds numbers downstream of the density jump were as low as 800, the turbulence generated at the jump did not dissipate in the test length of the channel.

9.2 Classification of Velocity Distributions

Typical velocity distributions for a range of downstream Froude numbers are shown in Fig. 50. It can be seen that the distribution becomes more uniform as the downstream Froude number decreases in value.

The velocity distribution shown in the top left of Fig. 50 had an upstream Froude number of 4.1 and a downstream Froude number of 0.80. This same velocity distribution for the same density jump is plotted in Figure 23. In Figure 24 the density distribution for this same jump is plotted. It can be seen the density distribution is quite non-uniform, and this indicates that the entrainment zone extends the length of the density jump. Compare the velocity distribution for $F_2 = 0.80$ and $F_2 = 0.33$. In the latter case the upstream Froude number was 5.2 and the density
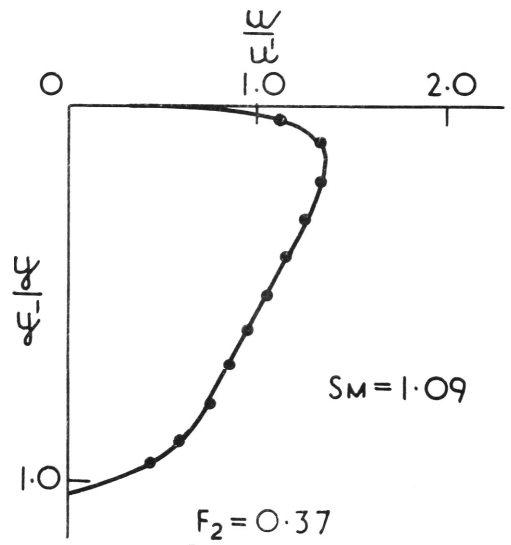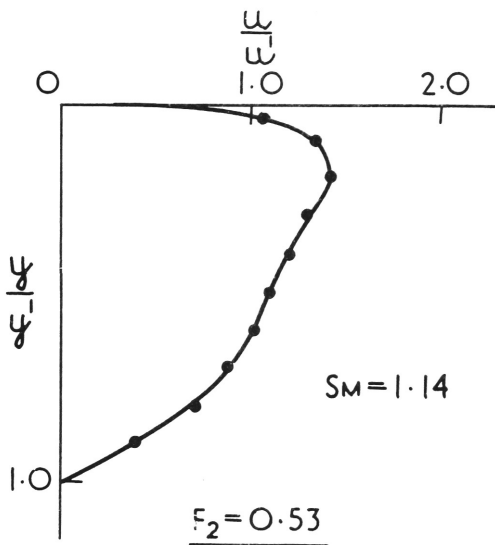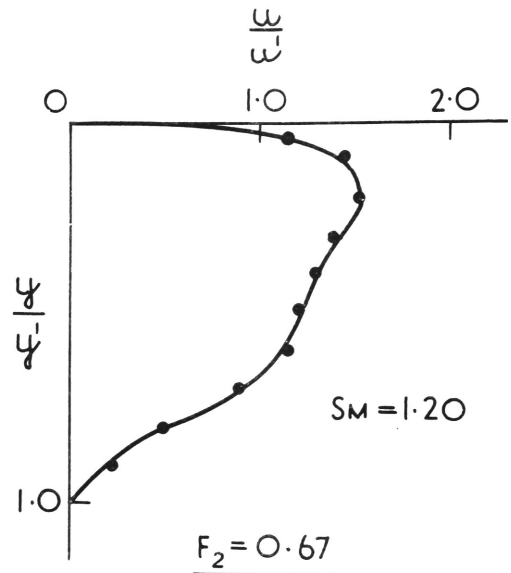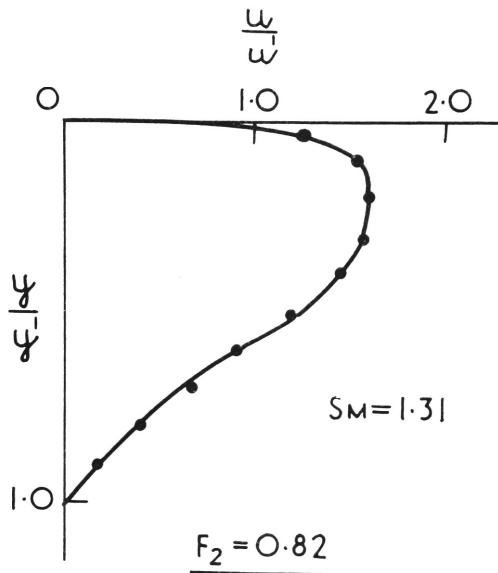
TYPICAL MEAN VELOCITY DISTRIBUTIONS

FIGURE 50.

jump was nearly non-entraining. The density distribution was therefore nearly uniform and the entrainment zone occupied only a short section of the jump. The velocity distribution, too, is more uniform than previously.

It follows, therefore, that the form of the jump is a dominant parameter in determining the downstream velocity distribution. The form of the jump is dependent on two variables, the upstream and downstream Froude numbers.

Density jump forms can be divided into approximately three classes:-

(i) Those with low upstream Froude numbers (less than two)

(ii) Those with upstream Froude numbers greater than two and downstream Froude numbers a maximum.

(iii) Those with downstream Froude numbers less than the maximum.

(i) The first type of jump has a high downstream Froude number but there is little entrainment at the jump. The form of the jump is shown in Fig. 51. The velocity distribution tends to be similar to the upstream velocity distribution.

The inlet Reynolds number varied from about 700 to 1200 in experiments and the velocity distribution in the slot would have approached parabolic form with a velocity correction factor of 1.20. However, the toe of the jump was generally three or four times the upstream depth, downstream of the inlet slot and velocity distribution measured in this

short region of uniform flow gave a constant value of S_m of 1.14 ± 0.04.

(ii)   The second type of jump with upstream Froude number greater than two and a maximum downstream Froude number was found to have a velocity distribution correction factor which was independent of the upstream Froude number.   This result is not surprising as the conjugate state for this type of jump is very nearly the same for all upstream Froude numbers.   When the upstream Froude number is greater than 2 the downstream end of the jump is sufficiently far from the upstream end, so as not to be influenced by upstream conditions.   The velocity correction factor for this type of jump, where the entrainment zone extends the whole length of the jump, was found to be 1.32 ± 0.05.

This type of jump was examined in detail in Section 4. 4.   A typical maximum entraining jump profile is shown in Fig. 43.

(iii)   When the downstream Froude number is small the velocity distribution downstream is influenced by the non-entraining roller region of the jump.

At the transition from the entraining zone to the roller region, the velocity distribution in the jump was the same as that for a maximum entraining jump.   This is to be expected.   The change in form of the velocity distribution is dependent on the roller region.   Since there is virtually no entrainment in the roller region it may be regraded mathematically, as a normal hydraulic jump.   Therefore the characteristics of the roller region are fully defined by either its upstream or downstream
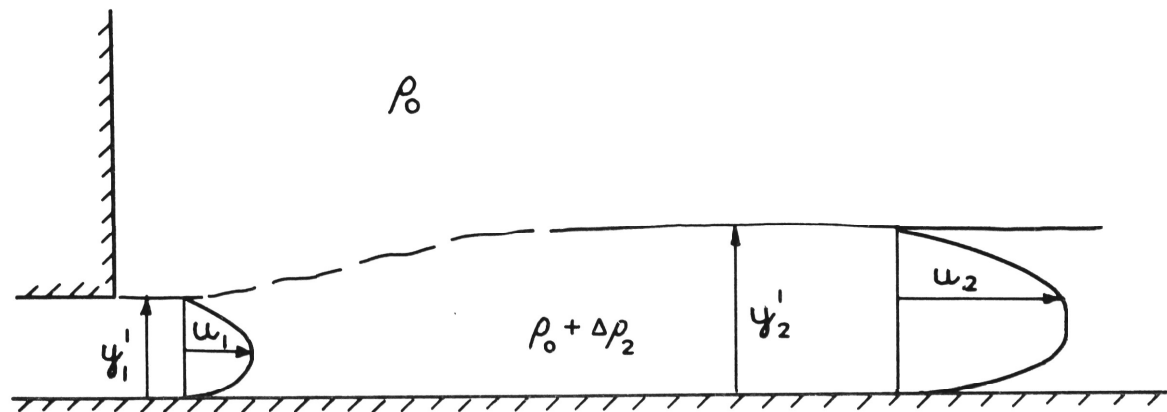
FORM OF A DENSITY JUMP FOR $F_1 < 2$

FIGURE 51.

Froude number. The velocity distribution of a partially entraining jump would be expected to be a function of the downstream Froude number only, as a result of the mechanism described above. A typical partially entraining density jump is shown in Figure 15.

9.3 Force Flow Correction Factors

Force flow correction factors calculated from these velocity distributions are plotted against downstream Froude number in Fig. 52.

An immense amount of reduction was required to obtain this diagram. Details of experimental techniques and tabulation of experimental results are given in Appendix D.

Velocity distributions were taken three or four times the downstream depth from the end of the jump. This position was arbitrarily chosen but it was found the velocity distribution was fully established at the end of the jump. Further changes downstream were caused by either boundary friction (whose effect on the velocity distribution was found to be small) or a control.

It can be seen that the values of S_m given in Fig. 52 do not completely agree with the values published by the writer in a paper describing the earlier part of the program (Wilkinson and Wood 1968). A copy of this paper is included at the end of the appendices. When this paper was written the control mechanism of a density jump was not understood and for the particular experimental set-up, downstream Froude numbers

of one half were constantly obtained. The control in this case was difficult to define as the discharge was controlled outside the test tank, so that analysis of the coupling between the control and the jump was not possible. The test tank was horizontal so that the jump was also partially friction controlled.

The fact that the downstream Froude number was always found to be equal to one half was an interesting coincidence, as maximum depth also occurs at this value of Froude number. It was thought at the time of writing the paper that the maximum downstream depth concept might have been significant. Subsequent analysis, both theoretical and experimental showed this was not so.

Reference to the plot S_m against F_1 shown as Figure 8 in the above paper, for which $F_2 = \frac{1}{2}$ shows a significant trend. Although the mean value of S_m (1.14) agrees well with the results presented here, S_m appears to increase for higher values of F_1 and decrease for lower values. This behaviour is contrary to that found in later experiments in a newly designed test tank. The trend is believed to be caused by (i) Reynolds number effect, (ii) positioning of the velocity probe. The Reynolds numbers of the flows in the early tests were very low (250-500), due to the small size of the experimental apparatus. Positioning of the probe was not as flexible as in later apparatus. Increase in the velocity of flow at the inlet, to achieve higher upstream Froude numbers
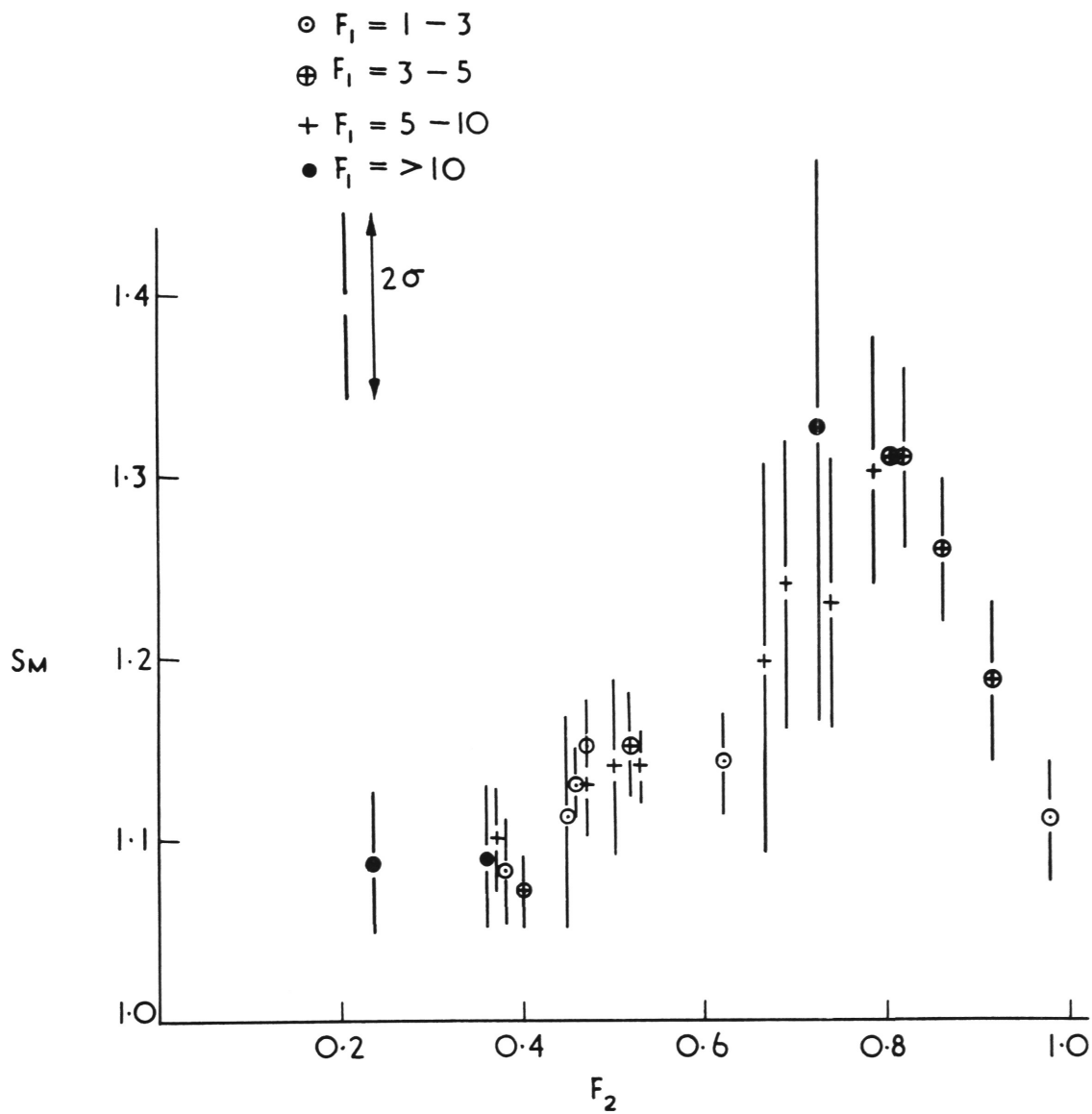
FORCE FLOW CORRECTION FACTOR

VERSUS DOWNSTREAM FROUDE No.

FIGURE 52.

resulted in an increase in non-uniformity of the velocity distribution at the probe. It is worth noting also, that only the extreme values of Froude number were significantly affected.

10. Density Distributions

10.1 Introduction

The density distribution in a density current, downstream of a density jump, is seldom uniform. This non-uniformity results from incomplete mixing of the density flow and the ambient fluid. Uniformity is dependent on the extent of turbulent mixing in the jump after entrainment has occurred. If the roller region occupies most of the density jump, entrained ambient fluid is thoroughly mixed with the inflowing fluid in the roller region of the jump. The resulting density distribution approaches uniformity.

It follows, therefore, that density jumps with high upstream Froude numbers and downstream Froude numbers close to the non-entraining minimum, will have uniform downstream densities.

The other extreme occurs when the jump is of the maximum entraining type. Ambient fluid is entrained along the length of the jump. There is no roller region to mix the fluids and the resulting density distribution downstream is markedly non-uniform. The density distribution is dependent on both the upstream and downstream Froude numbers.

10.2 The Characteristic Density Difference

It was necessary in all experiments to determine the characteristic density difference (Δ) as defined in Equation (7)

$$\Delta = \frac{\phi}{u'y'}$$

$$\text{where} \quad \phi = \int_{0}^{D} u \, \frac{\Delta \rho}{\rho_{\circ}} \, g \, dy$$

It was shown that the flux of density difference ($\emptyset$) is conserved.
It follows, therefore, that $\triangle$ is generally a function of both the density
and the velocity distributions. However, as either the density or the
velocity distributions approaches uniformity, the characteristic density
difference ($\triangle$) approaches the mean density difference $\left(\overline{\frac{\Delta\rho}{\rho_o}}g\right)$ in value.
Since higher velocities are generally associated with regions of higher
density difference, the characteristic density is found to be greater than
the mean density over the depth of flow. For the limiting case of a max-
imum entraining jump of high upstream Froude number, it was found

$$\triangle \; = 1.32 \; \overline{\frac{\Delta\rho}{\rho_o}} \; g.$$

10.3. The Hydrostatic Pressure Correction Factor

The second parameter which was measured was the hydrostatic
pressure correction factor S_H where $S_H = \frac{2}{\Delta y'^2}\int_0^D\int_y^D\frac{\Delta\rho}{\rho_o}g\,dy\,dy$

Dimensional analysis shows that a density jump is fully defined by
two parameters F_1 and F_2. It follows that S_H can be expressed as a
function of these two variables. A plot of experimentally determined
S_H values is shown in Figure 53. Several features of this diagram are
worthy of comment. Firstly S_H is highly dependent on the upstream
Froude number for maximum entraining jumps, if F_1 is less than six.
When F_1 is greater than six, S_m appears to remain constant in value at
approximately 0.6. S_H is highly dependent on the downstream velocity
distribution but approaches unity as entrainment reduces to zero. It

was found that the hydrostatic pressure correction factor could be expressed as a function of a single variable. This variable is equal to the ratio of fluid entrained to maximum possible entrainment assuming uniform velocity and density distributions. S_H is plotted against this variable $\dfrac{K - 1}{K_{max} - 1}$ as the dependent parameter of S_H is now explained. It was stated earlier that the form of the downstream density distribution was determined by the relative lengths of the entraining zone and the roller region of a density jump. The value of K-1 is a measure of the entrained flow at the jump, and therefore is a function of the upstream Froude number and the length of the entraining zone. The value of $(K_{max} - 1)$ is a measure of the entraining potential of the jump, and is therefore a measure of the potential maximum length of the entraining zone. The ratio of these two quantities is a measure of the relative lengths of the entraining and roller zones of a density jump, and is therefore an indicator of uniformity of the downstream density distribution.

The numerical value of the flow ratio K, is not highly dependent on S_H since K varies as S_H to the power one third. The depth ratio varies as the two-thirds power of S_H and is therefore more sensitive to it. Low values of S_H lead to a greater depth ratio than would exist if the density distribution were uniform.

The non-uniformity in density is largely counteracted by the non-uniformity of velocity. Both S_H and S_m tend to vary in inverse
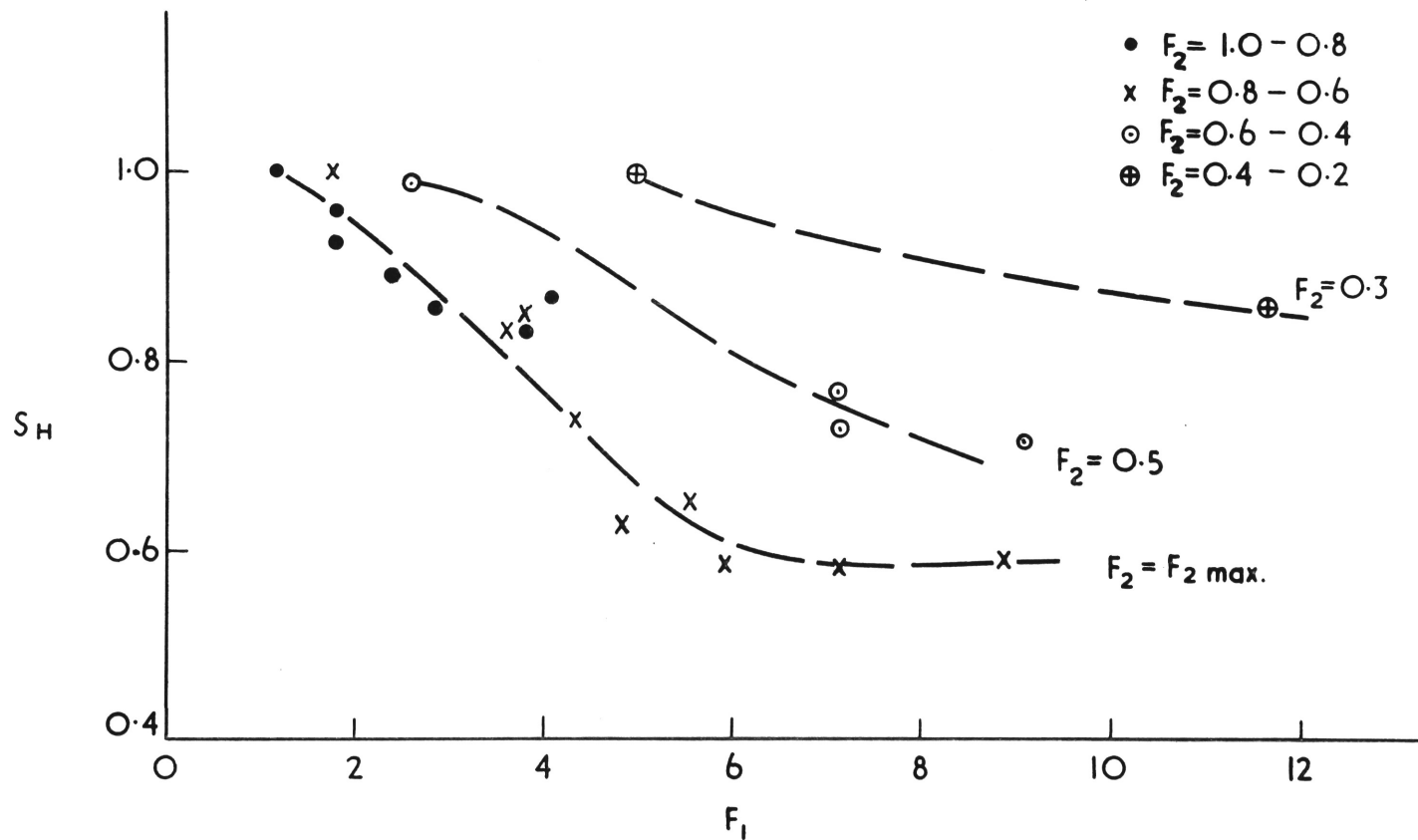
DENSITY DISTRIBUTION AS A FUNCTION OF UPSTREAM

AND DOWNSTREM FROUDE Nos.

FIGURE 53.

$$K_{max} = \frac{2 F_1^2 + 1}{3 F_1^{4/3}}$$
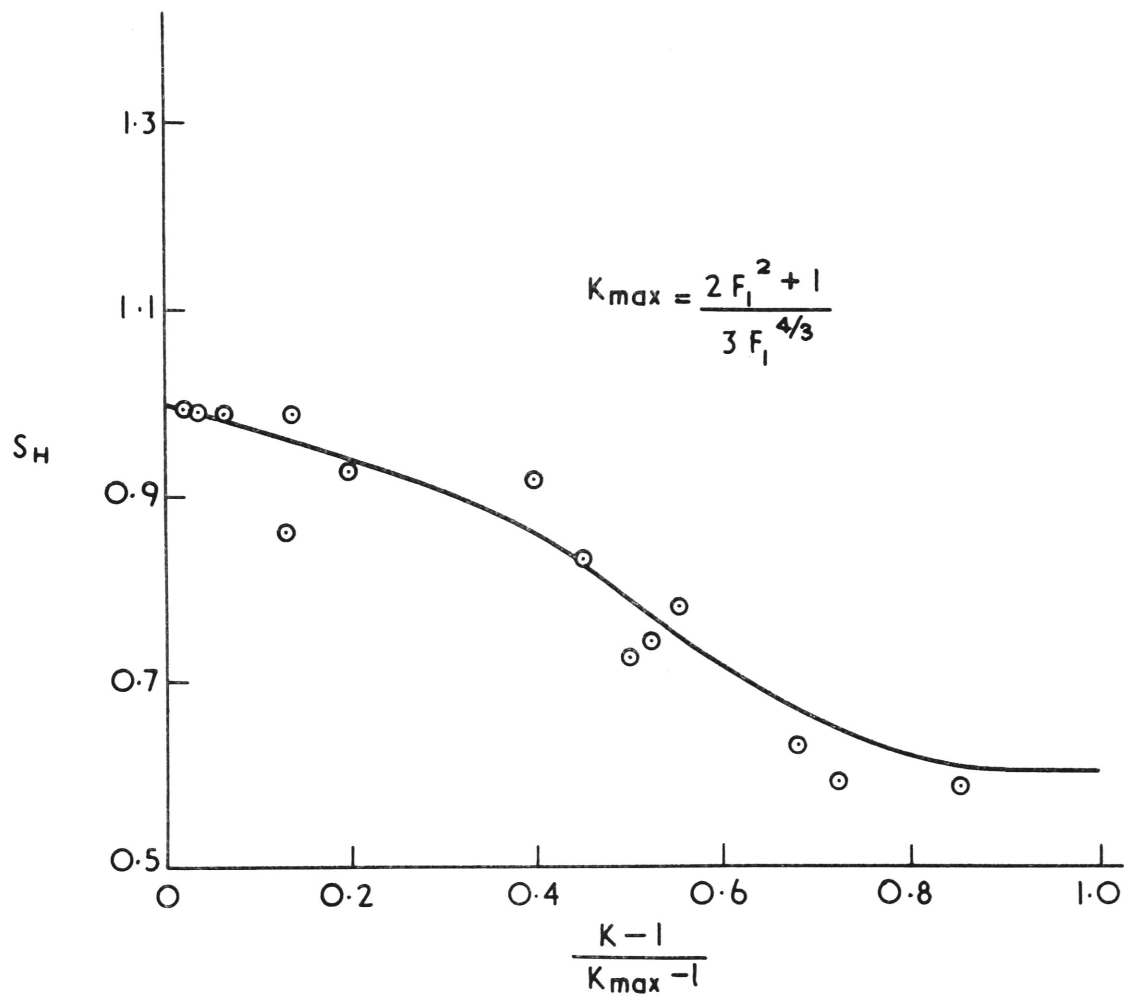
S_H VERSUS $\dfrac{K-1}{K_{max}-1}$

FIGURE 54.

proportions so that estimations of depth and entrainment downstream of a density jump can be calculated with reasonable accuracy ($\pm$ 10 pc.) by assuming that the densities and velocities are uniform.

The force flow ratio is potentially a greater source of error than non-uniform density and velocity distribution. This results from the compensatory nature of the latter variables.

Appendix A.

11. The Flooded Density Jump

The flooded density jump controlled by a broad-crested weir

(Figure 16) may be analysed using Equation 25. This equation relates

conditions downstream of the jump and conditions at the point of control.

It is independent of the state of the jump.

$$\frac{y_2'}{y_{2c}} = \frac{3 + 2\frac{h}{y_{2c}}}{F_2^2 + 2} \tag{60}$$

As there is negligible entrainment at a flooded jump it follows that

$$y_{2c} = y_{1c}$$

and from continuity

$$\frac{y_2'}{y_{2c}} = \frac{1}{F_2^{2/3}}$$

Hence equation (25) can be reduced to the following:-

$$\frac{h}{y_{1c}} f = \frac{1}{2}\left(\frac{F_2 + 2}{F_2^{2/3}} - 3\right) f \tag{61}$$

The above equation is plotted in Figure 19 as the line PCD for the

case where $F_1 = 50$. and hence from equation (19), f = 0.073.

The lower limit of validity of equation (61) occurs at the intersection

of the above curve with equation (28) at the point D. At D the flooded

jump becomes a non-entraining density jump.

The parameter f was introduced into equation (61) so that this equation

could be plotted simultaneously with equation (28).

Appendix   B.

12. Brink Depth at a Free Overflow in a Density Stratified Flow

The apparently simple physical features of the free overflow have long attracted the attentions of applied mathematicians, striving for an analytical solution to this free streamline problem. Several approximate analyses have yielded results in close agreement with experimental profiles (Rouse 1936). In fact, simple one dimensional energy and momentum analyses, which assume zero pressure at the brink section, give $\frac{\partial t}{\partial c}$ = 0.66 and 0.67 respectively, surprisingly close to the experimental value of 0.715. More elaborate iterative, analogue and transformation methods employed by Jaeger, Roy and Southwell and Vaisey are reviewed by Henderson (1966). All give depth profiles which agree closely with those observed in experiments.

It is not intended here to attempt an additional solution, but rather to look at the effect of non-uniform velocity and density distributions on the brink flow. The force flow equation is applied to the upstream flow, and again at the brink, where a zero pressure profile is assumed to exist. Curvelinear effects at the brink are ignored. If the velocity distribution is assumed to be self preserving between the upstream section and the brink (not an altogether justifiable assumption but one that is often made in open channel hydraulics), then from equation 19 one can write:-

$$Y_2 \frac{2 S_{m2} F_2^2 + S_H}{2F_2^{2/3}} = Y_b S_{m2} F_b^{4/3}$$

where F_b is the Froude number of the brink flow.

The Froude number of the flow upstream of the overfall is given by:

$$F_2 = \frac{S_H}{S_m}^{\frac{1}{2}}$$

and from continuity one has

$$F_b = F_c \frac{Y_2}{Y_b}^{3/2}$$

If the above equalities are substituted into the force flow equation one finds

$$\frac{3Y_2}{2} \left(\frac{S_m}{S_H}\right)^{1/3} = Y_b \frac{S_m}{S_H} \left(\frac{S_H}{S_m}\right)^{2/3} \frac{Y_2^2}{Y_b}$$

which reduces to the interesting results

$$\frac{Y_b}{Y_2} = \frac{y_b'}{y_2'} = \frac{2}{3} \tag{62}$$

This result indicates the brink depth is independent of upstream velocity and density distributions, provided the above assumpsions are valid.

Experiments by Rouse and others on open channel flows over a free overfall give

$$\frac{y_b}{y_2} = 0.712$$

which agrees surprisingly well with the approximate one dimensional

theory above.

Density current experiments enable a check to be made on the effect of non-uniform density and velocity distributions on the brink depth.

Eight measurements of the brink depth ratio, with Froude numbers upstream of the jump varying from 1.8 to 10.7 gave

$$\frac{y_b'}{y_2'} = 0.685 \pm 0.039$$

The brink depth ratio showed no dependence on the jump Froude number. Hence it follows it will also be independent of the velocity and density distributions.

A plot of brink depth ratio against jump Froude number is shown in Figure 55.

Appendix C.

13. Other Control Mechanisms of a Density Jump

13.1 The Sharp Crested Weir

The characteristics of a density jump controlled by a sharp crested weir are very similar to those when the control is a broad crested weir. Both exhibit the same hysteresis effect during a cycle of weir raising and lowering. Numerous attempts have been made to solve the free stream-line problem of flow over a sharp crested weir. Generally, however, a simpler semi-empiric equation is used to determine the discharge characteristics, as given below

$$q = \frac{2}{3} C_d \sqrt{2g} \left(y_2' - h \right)^{3/2} \tag{63}$$

where q is the flow per unit width,

C_d is the discharge coefficient

and h is the weir height.

An experimental equation is available (Rouse 1945) giving C_d as a function of boundary geometry and is applicable for $(\frac{y_2'}{h} - 1) < 0.8$

$$C_d = 0.611 + 0.075 \left(\frac{y_2'}{h} - 1 \right) \tag{64}$$

Equation (63) may be rearranged into the form

$$F_2^2 = \frac{8}{9} C_d^2 \left(1 - \frac{h}{y_2'} \right)^3 \tag{65}$$

or

$$\frac{h}{y_2'} = 1 - \left(\frac{q F_2^2}{8 C_d^2} \right)^{1/3} \tag{66}$$
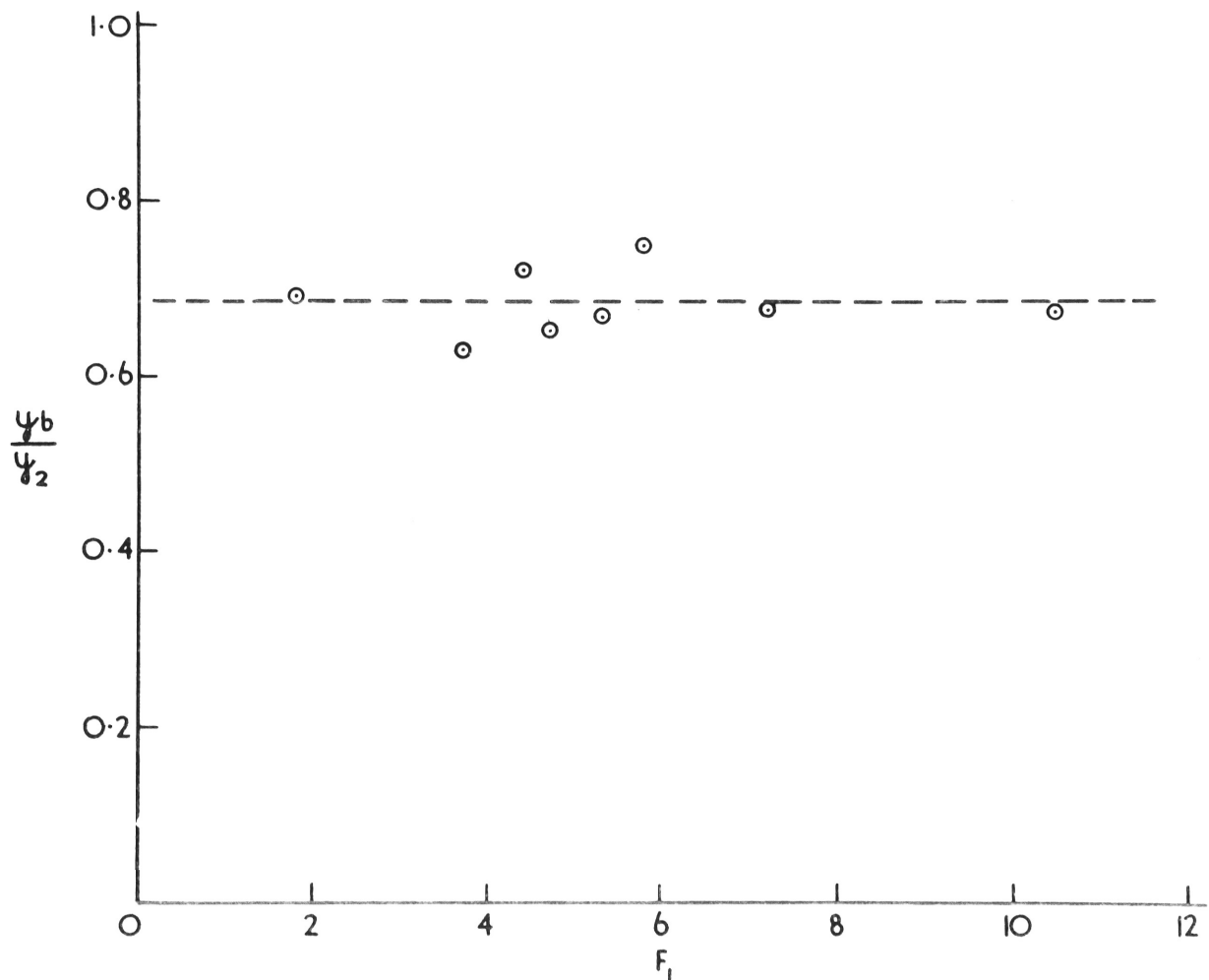
BRINK DEPTH RATIO VERSUS UPSTREAM FROUDE No. OF A MAXIMUM ENTRAINING JUMP

FIGURE 55.

The downstream depth can be eliminated in the above, by means of equation (19). Using the same technique as previously, one finds

$$\frac{h}{y_{1c}} f = 2 \left[1 - \left(\frac{9 F_2^2}{8 C_d^2}\right)^{1/3} \right] \frac{F_2^{2/3}}{2 F_2^2 + 1} \tag{67}$$

The above equation is of prime importance since it relates weir height to the downstream Froude number. C_d may be expressed an implicit function of the downstream Froude number by substituting equation (66) for $\frac{h}{y_2'}$ in Equation (64). Solutions may be obtained for the downstream Froude number and weir height, by selecting values of $\frac{h}{y_2'}$ and calculating F_2, C_d and $\frac{h}{y_{1c}} f$ using equations 65, 64 and 67 respectively.

Equation (67) is plotted in Figure 56 and it can be seen a limit of stability occurs when $F_2 = 0.19$. This is therefore the minimum Froude number attainable downstream of a jump controlled by a sharp crested weir. The non-entraining Froude No. conjugate to this value, is 10.6, which is the maximum upstream Froude No. for which the minimum downstream Froude number is attainable by a non-entraining jump.

The dashed curve in Figure 56 is for a broadcrested weir and it can be seen it lies below the curve for the sharp crested weir. This result was expected, since the vena contracta associated with a sharp crested weir effectively "increases" the weir height relative to a broad crested weir of the same height. Experimental data are again in close agreement with the predicted curve. A photograph of density flow over a sharp crested weir is given in Figure 57.

Experimental data are again in close agreement with the predicted curve. A photograph of density flow over a sharp crested weir is given in Figure 57.

13.2 Undershot Gates and Contractions as Controls

Undershot gates and contractions are examined together as controls for a density jump. The control characteristics are similar in either case and the full range of downstream Froude numbers are attainable for all values of upstream Froude number. There are no unstable regions, so that the minimum Froude number attainable downstream is always the non-entraining value, and the maximum is unity for the ideal case.

The undershot gate will be examined first, and a definition sketch is given in Figure 58.

13.21 The Undershot Gate

Analysis

If the energy equation is applied upstream and downstream of the gate, and as there is no entrainment between these sections, one has:

$$\frac{S_{E2} \, Q^2}{2g \, y_2'^2} + y_2' = \frac{S_{E3} \, Q^2}{2g \, (C_c \, h)^2} + C_c \, h \tag{68}$$

where $C_c h$ is the depth of flow immediately downstream of the gate. The contraction coefficient (C_c) remains constant to within ± 5 pc. of 0.61 for values of $\frac{h}{y_2}$ less than 0.70, in open channel flows. Unfortunately this is not true of density currents. The change in C_c is believed to be caused by boundary layer effects at the interface of the density current

$$\frac{h}{y_{1c}} f = 2 \left(1 - \left[\frac{9 F_2^2}{8 Cd^2} \right]^{1/3} \right) \frac{F_2^{2/3}}{2 F^2 + 1} \theta$$

for $\theta = 1.0$
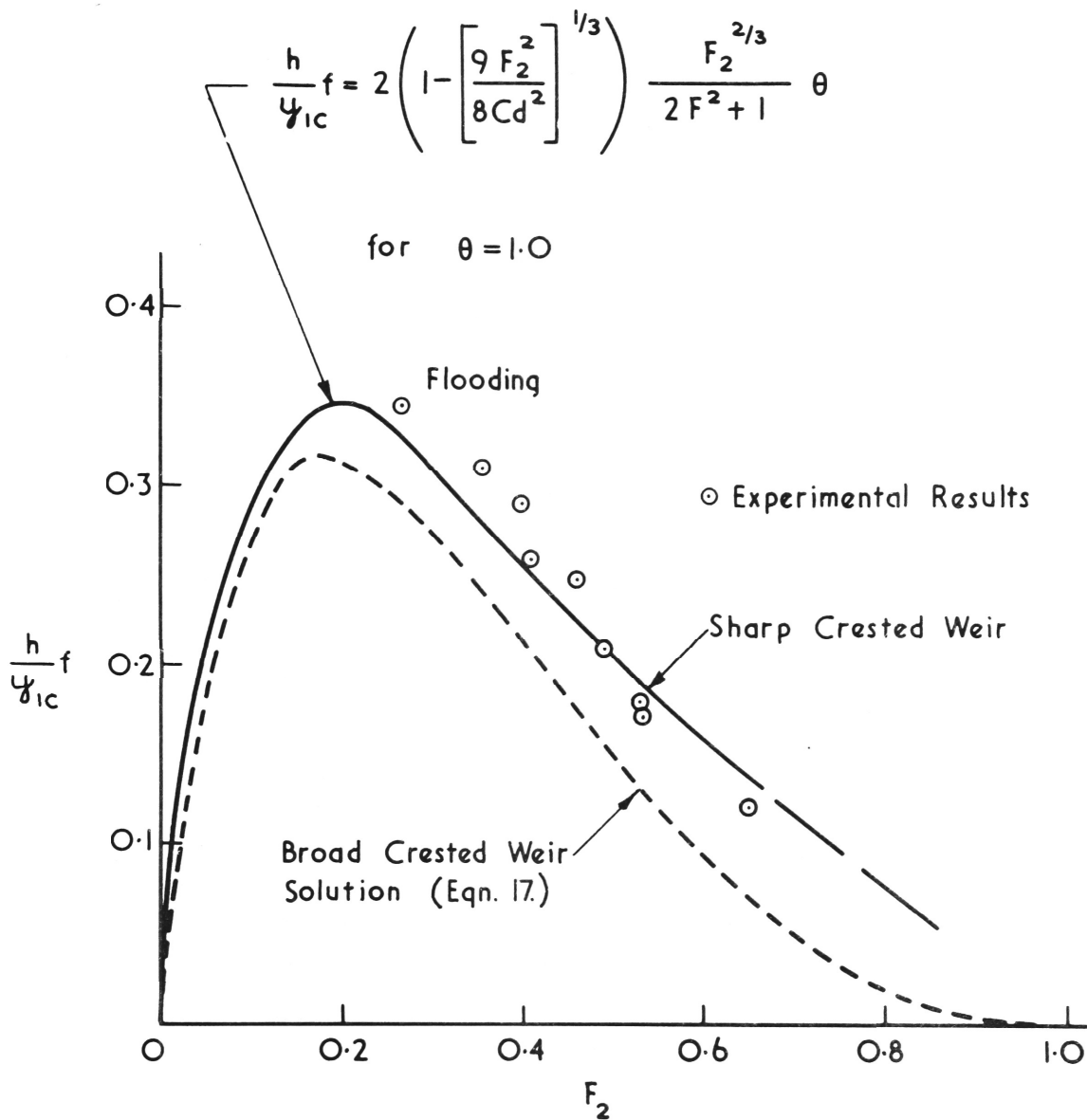
WEIR HEIGHT (SHARP CRESTED WEIR) VERSUS

DOWNSTREAM FROUDE No.

FIGURE 56.

Fig. 57: Flow over a sharp crested weir.

Interface

y_2^1

Undershot Weir

$C_c h$

h
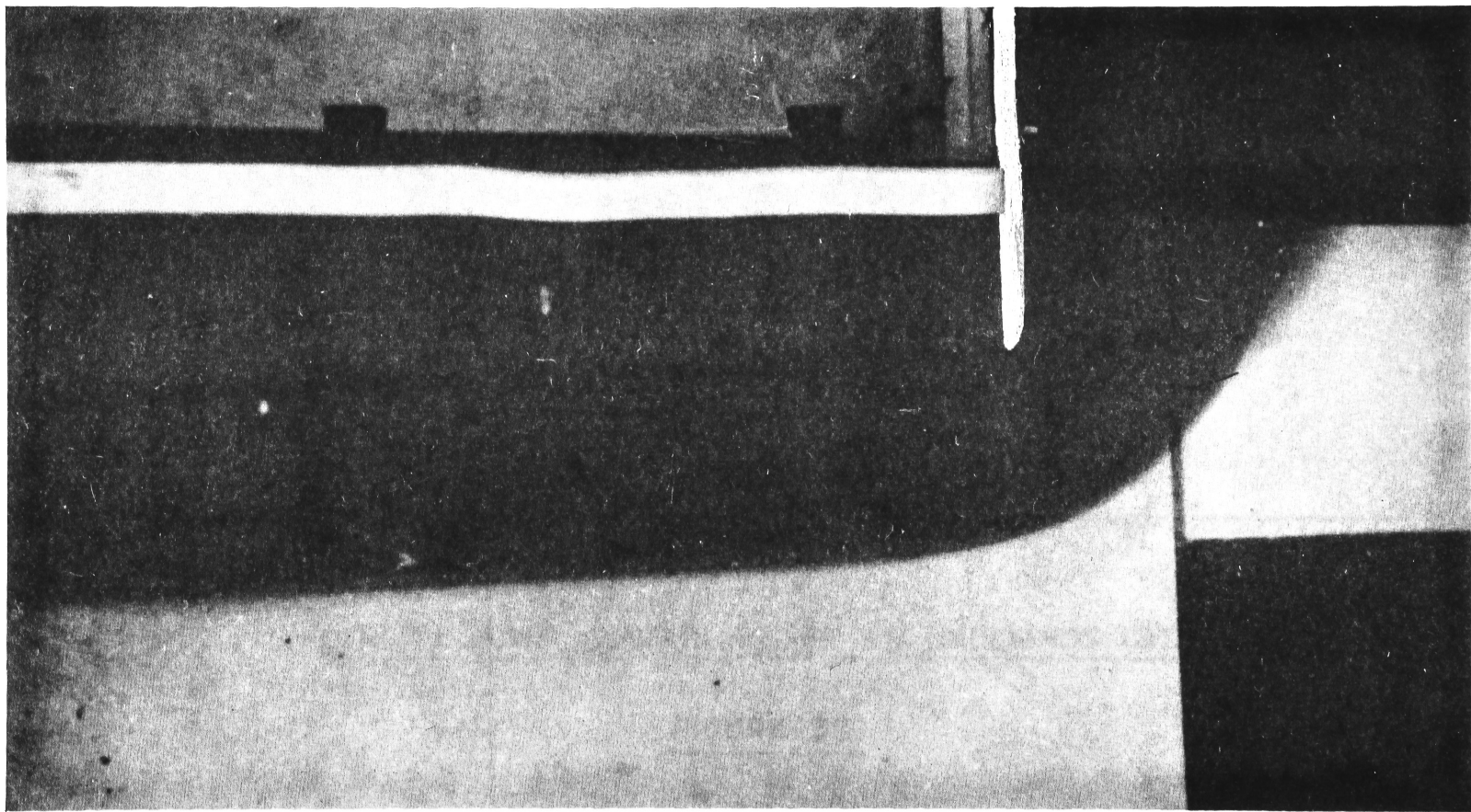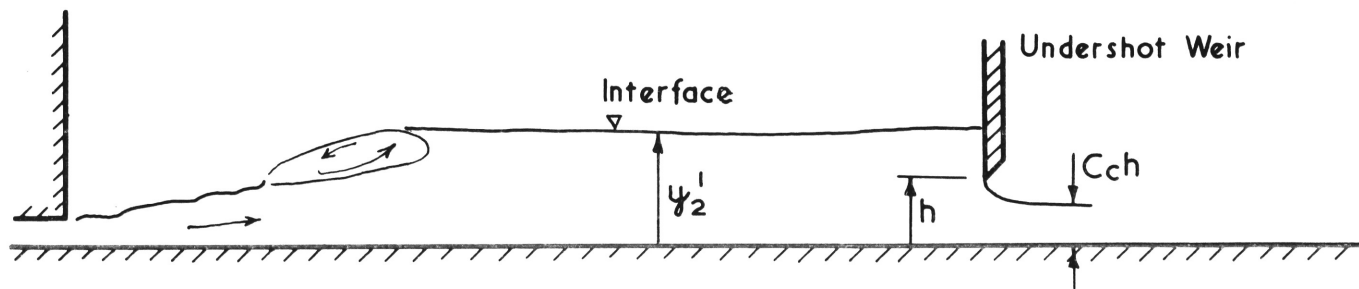
DENSITY JUMP CONTROLLED BY AN UNDERSHOT GATE

FIGURE 58.

and the ambient fluid. Therefore, in the present analysis, C_c shall be treated as a variable, and its dependence of $\dfrac{h}{y_2}$ will be discussed later.

Equation (68) may be rearranged into the form

$$y_2' \left(S_{E2} F_2^2 + 2 \right) = C_c h \left[S_{E3} F_2^2 \left(\frac{y_2'}{C_c h} \right)^3 + 2 \right]$$

so that

$$F_2^2 = \frac{2 \left(1 - \dfrac{C_c h}{y_2'} \right)}{\left[S_{E3} \left(\dfrac{y_2'}{C_c h} \right)^2 - S_{E2} \right]} \tag{69}$$

Equation (69) relates the downstream Froude number to the ratio of gate height to upstream depth and is graphed in Figure 59. The force flow equation as written in Equation (31) may now be employed to express F_2 as a function of gate height only.

An explicit solution cannot be obtained for either variable so a graphical solution is plotted in Figure 60.

Experimental Results

Agreement between experiment and theory was satisfactory for downstream Froude numbers less than approximately 0.65. Within this range momentum fall within the jump again compensated for the non-uniformity of velocity and density distributions downstream of the jump, to give experimental results in close agreement with the idealised theory.

More exact solutions for particular cases may be calculated by substituting appropriate velocity and density distribution factors into equations (20) and (69). However, in practice, it is doubtful if the accuracy would be further increased.

Depression of the Interface by an Undershot Weir

At downstream Froude numbers greater than 0.65, agreement between the above theory and experiment is poor. This is caused by a change in the flow geometry such that the picture in Figure 58 no longer represents the actual flow.

As the gate is lowered ("lowered" as defined previously is "up" in the picture). The interface is seen to be depressed as in Figure 61b and c. Experiments indicate the interface can be depressed by as much as one quarter of its initial depth before the gate breaks the interface as shown in Figure 61c. The degree of depression at the interface depends on the Froude number and Reynolds number of the flow, and the boundary layer development length between the jump and the gate. The curve shown in Figure 62 is therefore only a typical example of depression, and is not to be interpreted as a general result. The dominant controlling parameter is believed to be the boundary layer thickness in the ambient layer. This, of course, is dependent on the development length only, provided the boundary layer is laminar.

Boundary layer development in stratified flows has been investigated

$$F_2^2 = \frac{2\left(1 - \dfrac{C_c h}{y_2'}\right)}{S_{E3}\left(\dfrac{y_2'}{C_c h}\right)^2 - S_{E2}}$$

for
$$S_{E1\,\&\,2} = 1$$

⊙ Experimental points
Series Y & Z
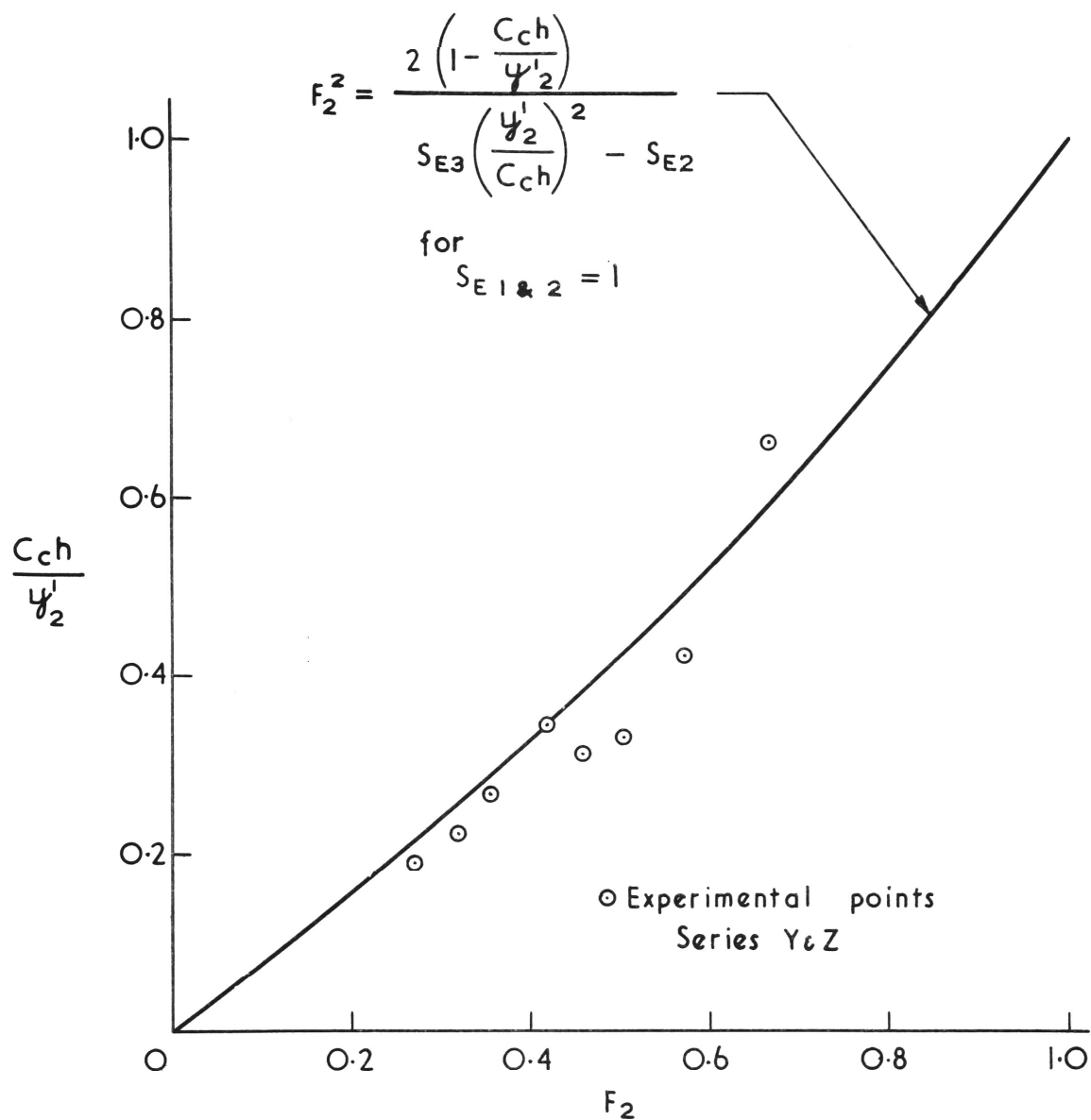
GATE-HEIGHT RATIO VERSUS DOWNSTREAM FROUDE No.

FIGURE 59.

The y-axis is labeled $\dfrac{C_c h}{y_{1c}} f$ and the x-axis is labeled F_2.

Obtained from
simultaneous solution
of Equations 31 & 69.
See text
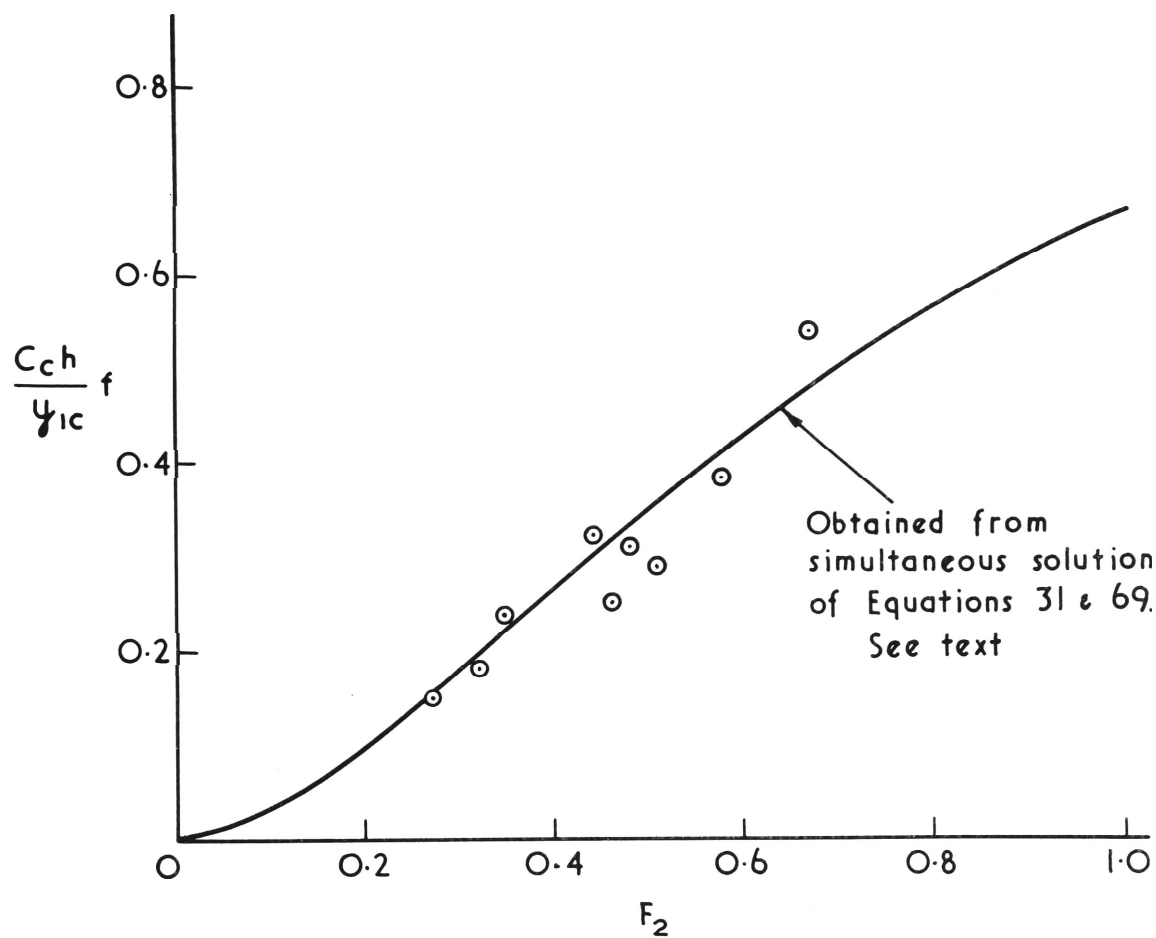
GATE-HEIGHT FUNCTION VERSUS

DOWNSTREAM FROUDE No.

FIGURE 60.
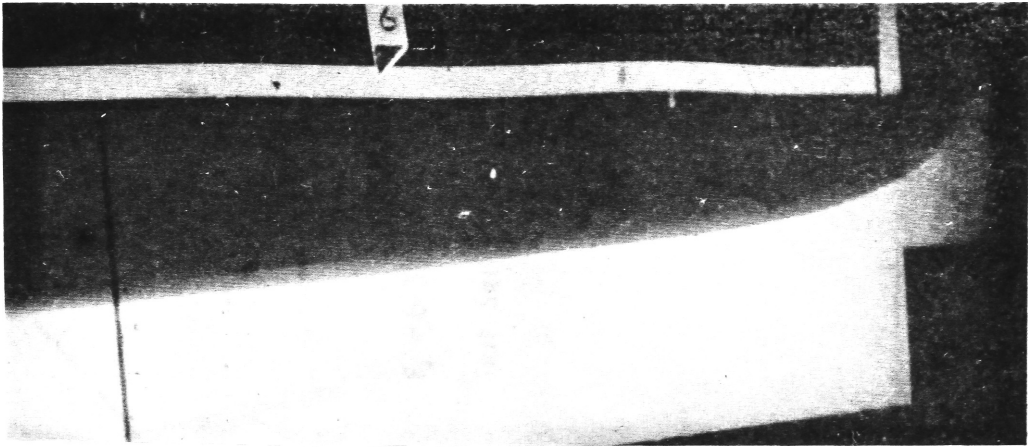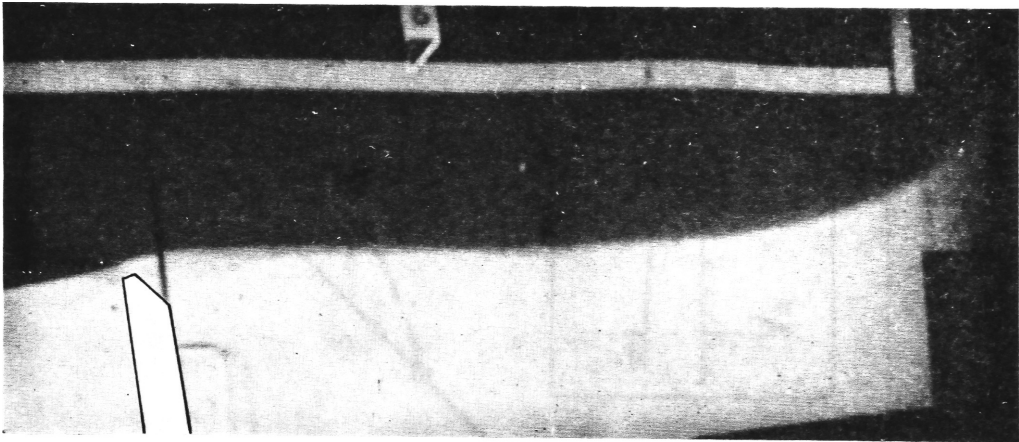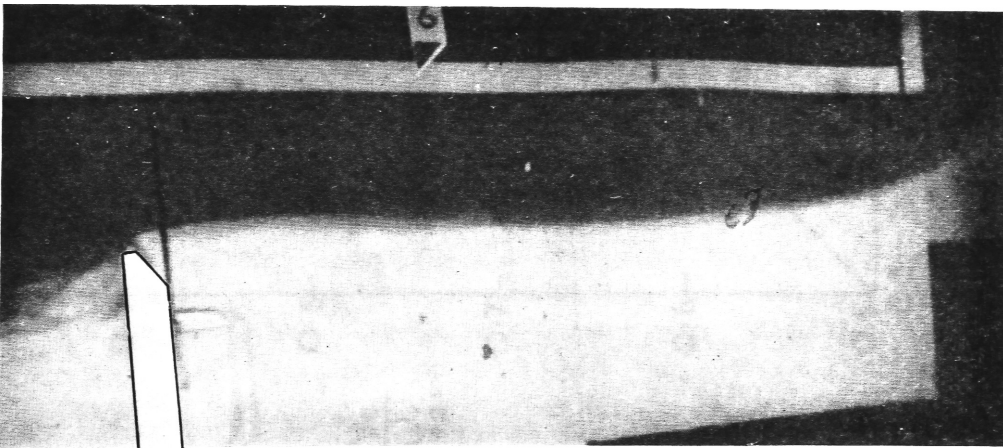
Fig. 61: Interfacial depression at an undershot gate.
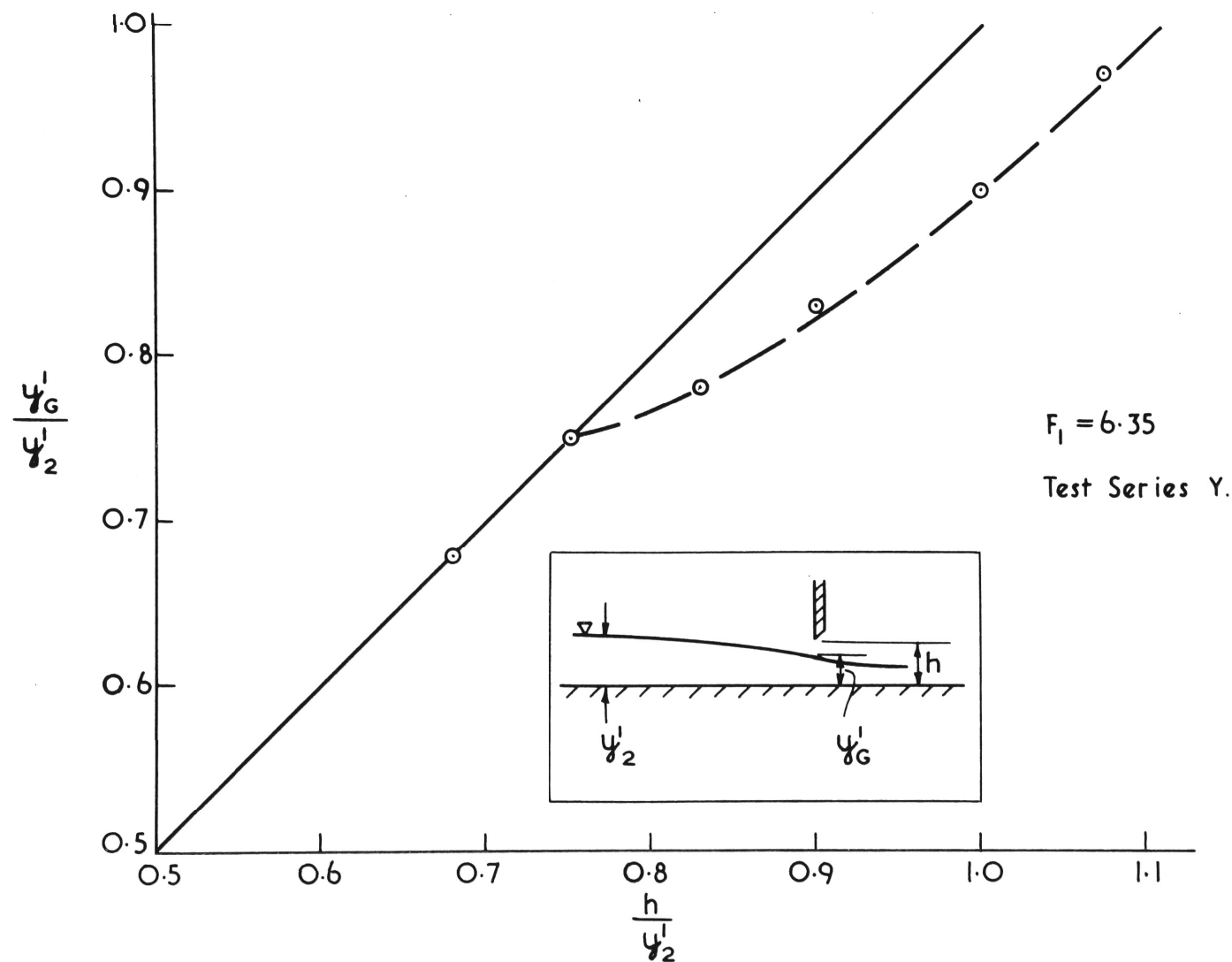
INTERFACIAL DEPTH VERSUS GATE HEIGHT
SUPPRESSION OF THE INTERFACE BY AN UNDERSHOT GATE

FIGURE 62.

by Ippen and Harleman (1952), Keulegan (1944) and Bata (1959). However, in this case, no quantitative theory was derived for the depression phenomenon. Various stages of depression are shown in Figures 61a, b and c.

The Contraction as a Control

A contraction as a form of control of a density jump is shown in Figure 63. The energy equation may be applied upstream and at the contraction to give

$$\frac{S_{E2} \, Q^2}{2g \, y_2'^2 \, B^2} + y_2' = \frac{S_{E3} \, Q^2}{2g \, y_3'^2 \, b^2} + y_3'$$

where B and b are the channel widths upstream and at the contraction respectively.

At the control the depth of flow is critical depth. Therefore

$$\frac{S_{E3} \, Q^2}{g \, y_3'^3 \, b^2} = 1 \tag{70}$$

and substituting the above into the energy equation

$$y_2' \left(S_{E2} \, F_2^2 + 2 \right) = 3 \, y_3' \tag{71}$$

From Equation (70) and continuity one can write

$$S_{E3} \, F_2^2 \left(\frac{y_3'}{y_2'} \right)^3 \left(\frac{b}{B} \right)^2 = 1$$

So eliminating y_3' in Equation (71) one finds

$$\frac{b}{B} = \frac{3^{3/2} \, S_{E3}^{1/3} \, F_2}{\left(S_{E2} \, F_2^2 + 2 \right)^{2/3}} \tag{72}$$

A graph of the above equation is given in Figure 64 for the case where the velocity distributions upstream and downstream of the jump are uniform. No experiments were performed to verify the contraction equation (72), but in the light of previous experimental results there is no reason to suspect its validity.

It can be seen no instabilities occur over the full range of the contraction ratio, from zero to one. Therefore all downstream Froude numbers between the usual limits are attainable by any density jump, depending on the contraction ratio.
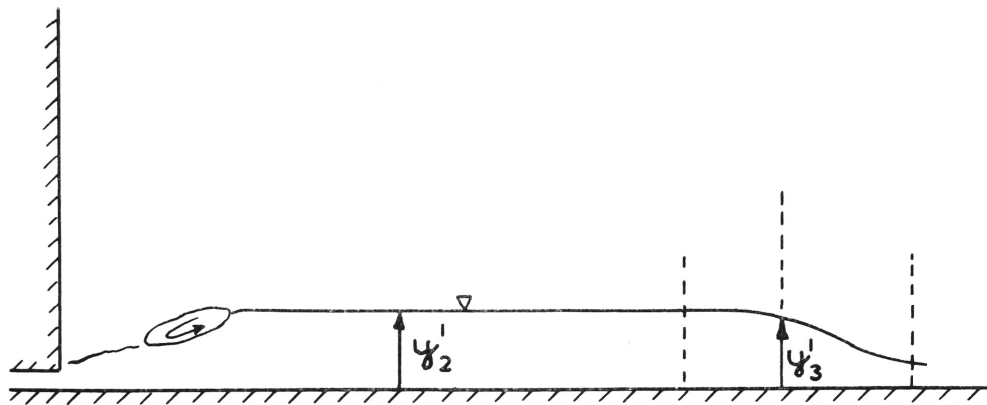
Elevation
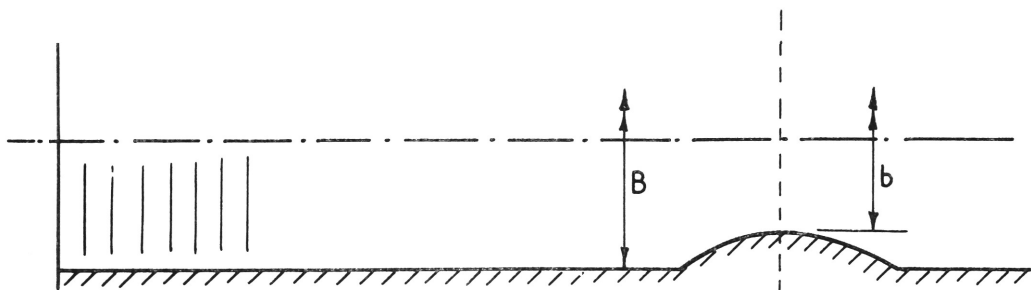
Plan

DENSITY JUMP CONTROLLED BY A CONTRACTION

FIGURE 63.

$$\frac{b}{B} = \left(\frac{3}{S_{E2} F_2^2 + 2}\right)^{3/2} \cdot S_{E3}^{1/3} F_2$$

for

$$S_E = 1.0$$
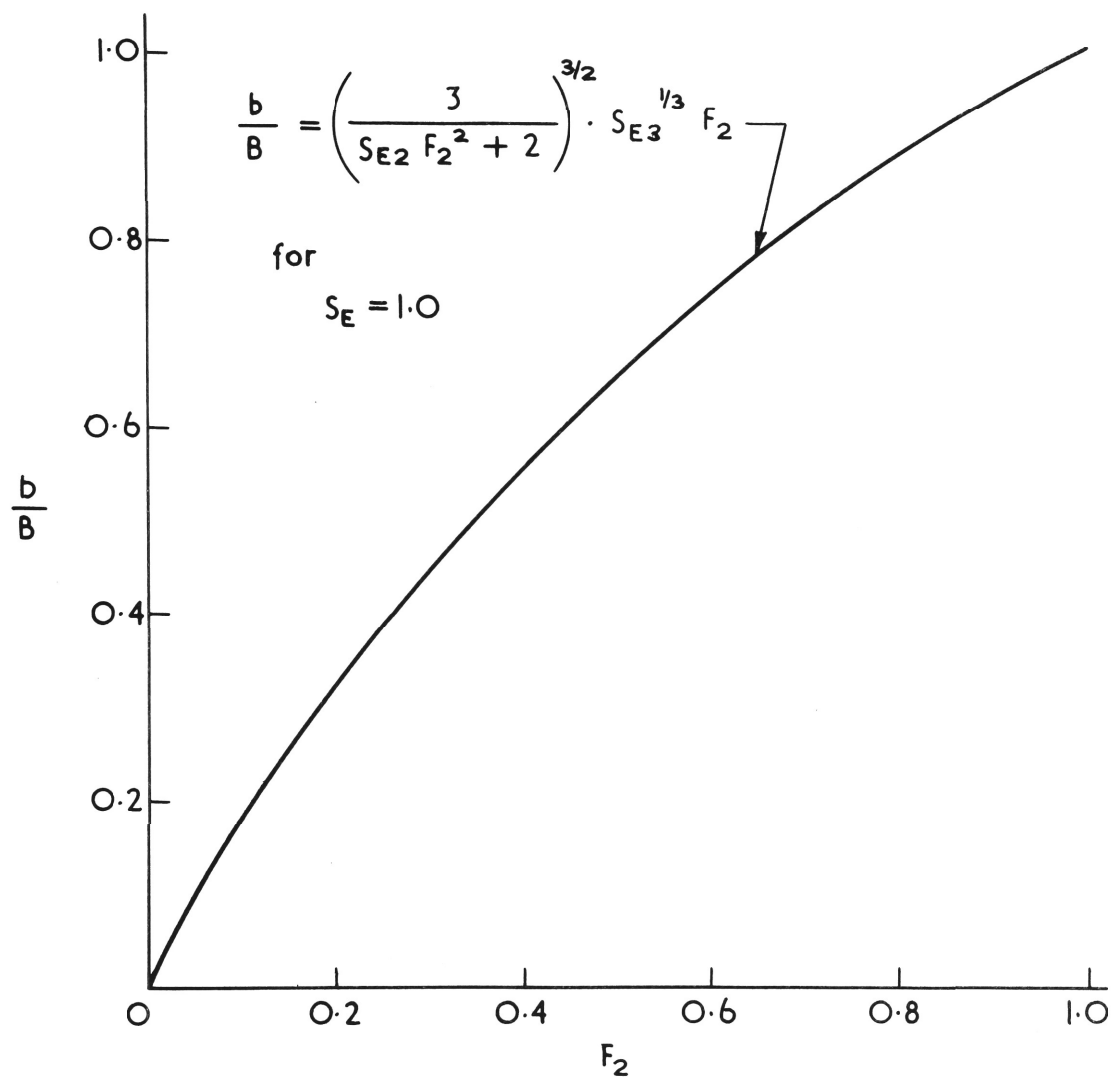
CONTRACTION RATIO VERSUS DOWNSTREAM FROUDE No.

FIGURE 64.

Appendix   D.

14. Velocity Measurement

Introduction

Velocity measurement in density currents is always a problem; firstly because of the very low velocities involved and secondly because of the general small scale associated with laboratory density currents. Typical density currents examined by the writer ranged in depth from one to four inches, and in velocity from 0.02 ft/ sec. to 0.15 ft. / sec.

Several methods of velocity measurement were examined. An excellent review of techniques of velocity measurement in density currents is given by T. R. Fietz (1966).

The basic requirements of the velocity meter for the present study were as follows:-

(i) Size: It must conform to certain dimensional restrictions so as not to interfere with the flow pattern, particularly in the region of the interface.

(ii) Shape: It must be of such a shape that velocity profiles may readily be taken, and also that it may be removed from the test tank without damage.

(iii) Availability and/or Simplicity

The meter must be either readily commercially available or be of very simple design and construction.

(iv) Calibration

It is desirable that the meter maintain a constant calibration and is unaffected by temperature variation or salt water.

Review of some velocity measuring devices

Pitot tube devices do not have a good low velocity response and are therefore unsuitable. Although the sensitivity of U tube manometers can be increased by using two immiscible fluids of similar densities, experience showed this technique was fraught with experimental difficulties.

Drag type Meters rely on the dynamic drag on an immersed body. The drag is measured via a strain gauge or some other electronic device. Drag meters are particularly suceptible to calibration drift and the devices suitable for use at the velocities to be measured, are necessarily delicate and easily damaged.

Current Meters rely on an impeller whose speed of rotation is measured electronically, and is proportional to the fluid velocity. They were unsuitable for the present work due to their size and high threshold velocity.

Dynamically Balanced Meters

The stagnation pressure of a fluid flow can be balanced by an opposing fluid jet in a suitably designed nozzle. This principle was first discussed by Bagnold (1951) and subsequently a modified meter was constructed by Fietz (1966). This instrument is shown schematically in Figure 65. The meter is designed to operate in salt water although with slight

Saltwater-Freshwater interface

METER "OVERBALANCED"

Saltwater-Freshwater interface

METER "UNDERBALANCED"

Fresh-water head tank

Scale measuring ΔH

Head loss ΔH

Length L

Head loss tube.

Salt-water-Fresh-water interface

Space s

L_E

electrode

Bypass holes,

Opposing flow tube.

Salt-water:

Nozzle,

Balancing chamber

To waste

Gap

Body diameter D

METER "BALANCED"

Conductivity   Measuring
Electronics

FIGURE 65: SCHEMATIC SKETCH OF BAGNOLD VELOCITY METER

modification it could be used in either fresh or salt water.

The meter generates a physical balance between the stagnated salt water flow and an opposing metered flow of fresh water. The opposing flow is fed through a fine bore head-loss tube which magnifies the stagnation pressure. The balancing flow is adjusted until the interface between the fresh and salt water is stationary at a conductivity detecting point in the nozzle.

The meter was found to measure velocities in the range of 0.03 to 0.5 ft/sec. with an accuracy of five per cent. The response of the meter is linear.

The meter does have several disadvantages. These are:-

(1) Sensitivity to the temperature of opposing fresh water flow. This effect can be accounted for by calibrating over a range of temperatures.

It was found the change in response could be predicted by the known change in viscosity of the fresh water with temperature.

(2) The slow response after adjusting the fresh water flow. The time required to take a velocity measurement was at least ten minutes. Fietz suggests several modifications to the meter to improve its accuracy and ease of use.

It was decided the Bagnold meter was unsuitable for use with this project for the following reasons:-

(1) The meter available would require extensive modifications if it were to be used in the test tank.

(2) The time required for each reading and the number of measurements required would make steady state difficult to maintain for the duration of a test.

A further modified Bagnold meter in which the balance point was detected visually rather than electronically, was constructed by the writer. Balancing of the stagnation pressure was far more rapid with this meter and also the physical size was considerably reduced. The small size of the meter can be gauged from the photograph of one of the meters in Figure 66. The accuracy of this meter was 7 pc. slightly less than that of Fietz. The meter was calibrated over the range 0.03 ft./sec. to 0.5ft/sec.

Details of the meter are given in a technical note published in the "British Journal of Scientific Instruments". A copy of the note is included at the end of the appendices.

The meter was found suitable for use in either salt or fresh water density currents. Soon after the meter had been developed new larger, experimental tanks became available and it was necessary to change to thermal density currents, as salt water was not available in sufficient quantities. It was found with thermal density currents, that insertion of the probe through a thermal gradient caused air to come out of solution and form tiny bubbles in the glass nozzle of the probe. These bubbles altered the probe geometry and therefore changed its calibration. No way of preventing this effect could be found so that use of the probe was
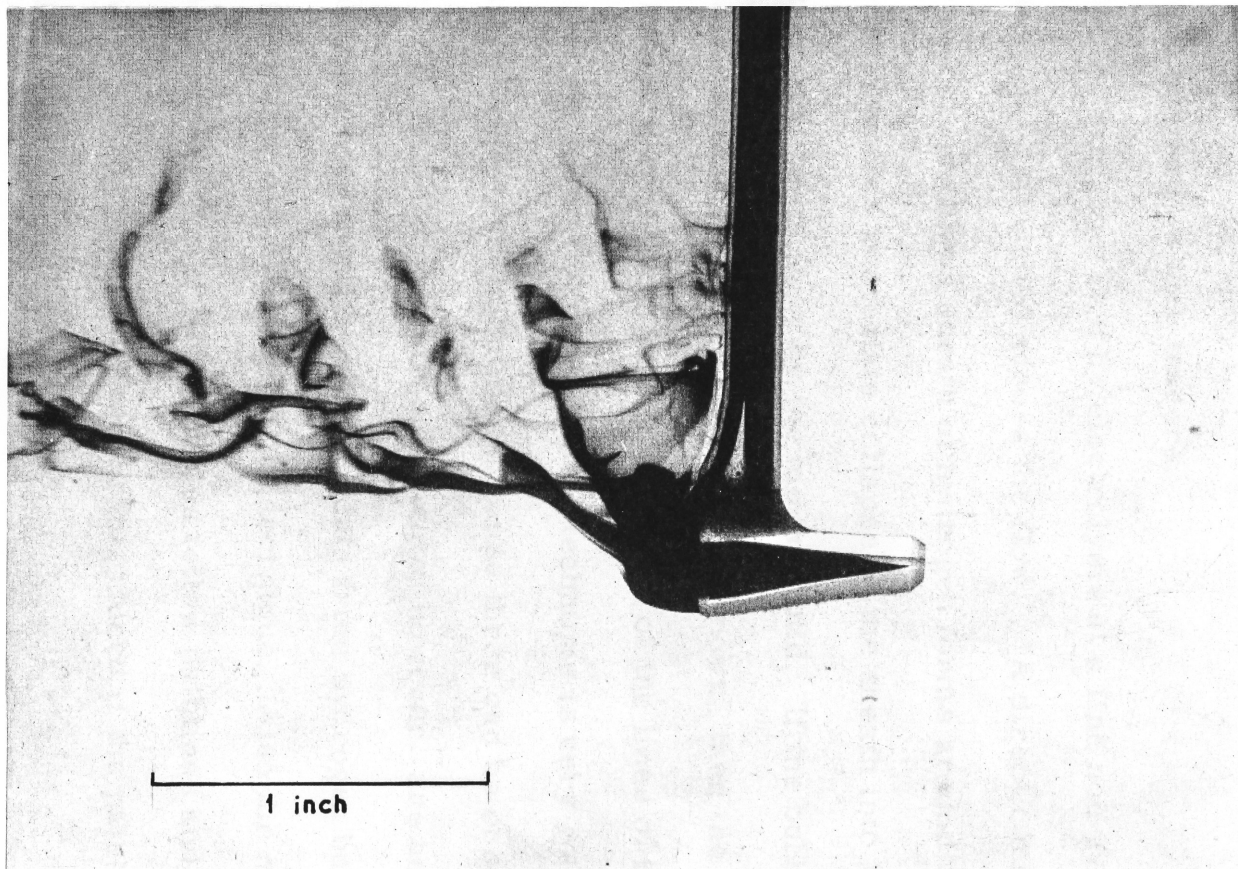
Fig. 66: Modified low velocity meter.

abandoned in thermally induced density currents.

Hydrogen Bubble Technique

The hydrogen bubble technique of flow visualisation makes use of tiny hydrogen bubbles as flow tracers.

The bubbles are generated by electrolysis at a fine non-reactive wire (usually platinum) stretched across the flow. A direct current is pulsed onto the wire cathode and a sheath of hydrogen forms around the wire. Surface tension causes immediate collapse of the sheath into tiny hydrogen bubbles which are swept away by the moving fluid. If the bubbles are suitably illuminated, and the period of pulsing is known, then the velocity profiles may be calculated from still photographs of the lines of bubbles, after they have left the wire. Hydrogen bubble technique is very good for obtaining qualitative velocity distributions because these can be observed directly (see Figure 67). Quantitative measurements, however, are another matter. The time required to obtain meaningful data from hydrogen bubble photographs is the major disadvantage of the technique. Also the method is not suitable for unsteady flows. The bubbles follow pathlines and unless the flow is steady significant errors can be introduced if the pathlines are interpreted as streamlines (Hama 1962).

The equipment used by the writer was deliberately kept as simple as possible. A schematic diagram of the set-up is given in Figure 68.

A D. C. voltage from a battery supply was bridged via a commutator,

across a 1K ohm potentiometer. The commutator consisted of a 10
inch diameter perspex disc with six aluminium foil, segmented contacts
glued to its surface (see Fig. 69). A switching arm with two wire brushes
attached to its end lay on the disc in a similar fashion to a turntable arm.
As the commutator disc rotated the circuit was made and broken as the
conductive aluminium sectors passed beneath the brushes. The switching
of this apparatus was very clean and no transients could be observed when
an oscilloscope was placed in the circuit. The speed of /the turntable was
measured to be constant to within 0.5 pc. over several revolutions and
wow and flutter were negligible for the heavy weight turntable used.

The duration of, and the interval between pulses, could be varied by
simply changing the width and spacing of the conductive sectors of the
commutator.

The positive terminal was attached to a matt black strip of galvanised
steel which was placed behind the generating wire against the back of test
tank as shown in Figure 70. The steel strip served two functions; firstly
it provided a non-reflective high contrast background for the hydrogen
bubbles and secondly, it made a convenient anode as it was only three
inches away from the cathode.

The negative tapping of the potentiometer was connected to the gen-
erating wire. The potentiometer was adjusted until the bubbles were of
optimum size. The generating wire was platinum and 0.002 inch diameter.
A diagram showing the wire suspension apparatus is shown in Figure 70.
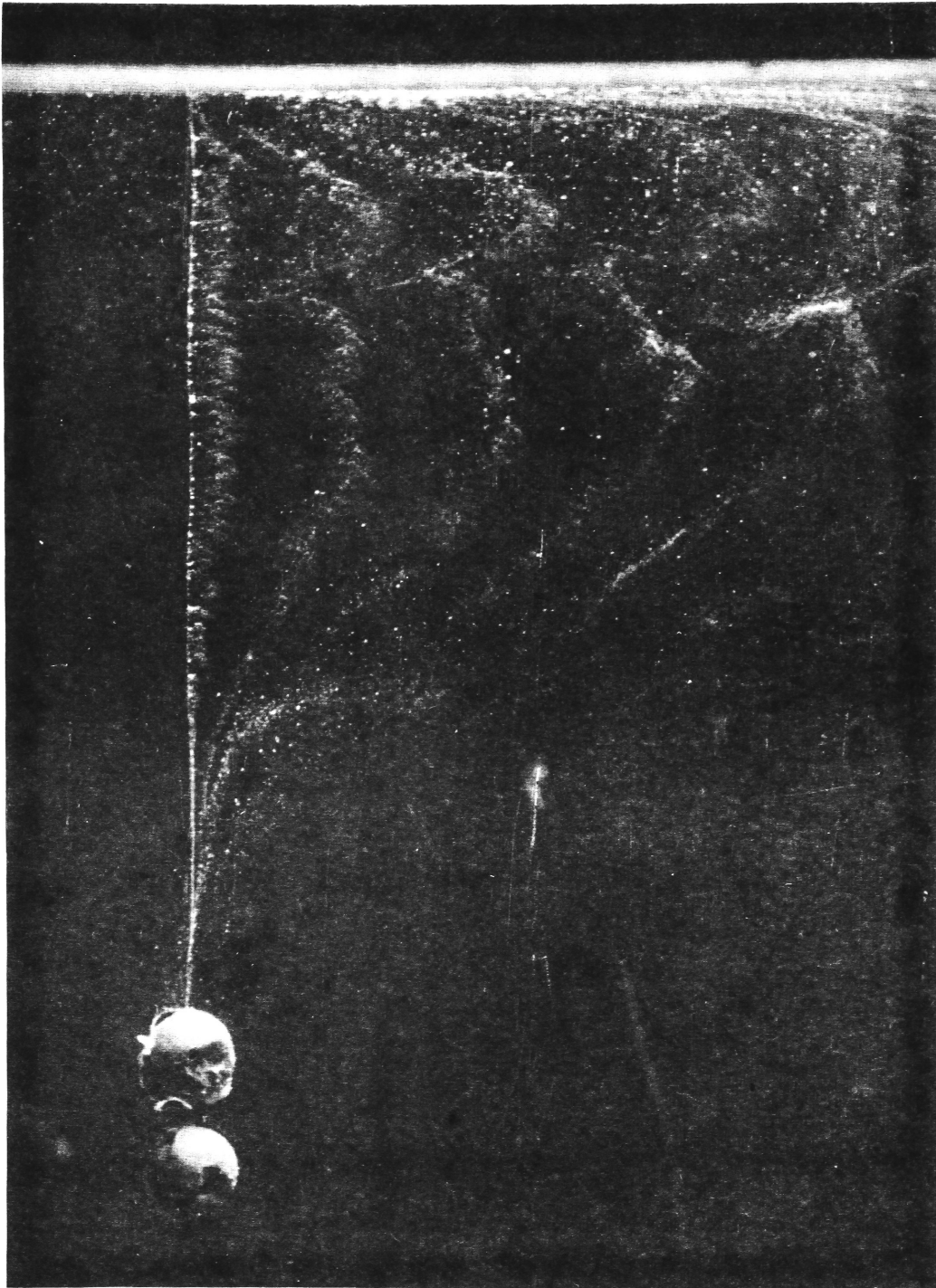
Fig. 67: A typical photograph of hydrogen
bubble traces.
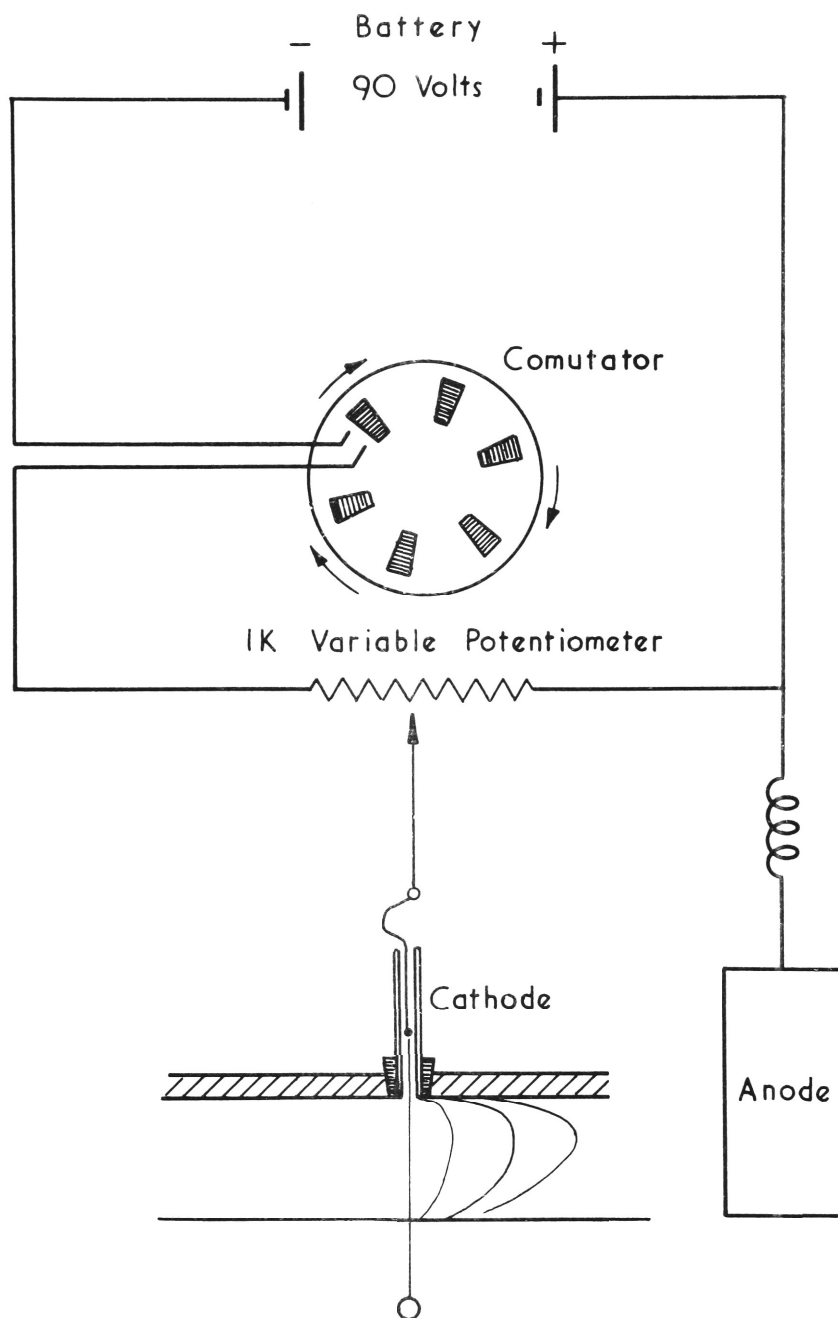
DIAGRAMMATIC SKETCH OF HYDROGEN
BUBBLE GENERATOR

FIGURE 68.

The platinum wire was attached to an insulated copper wire, which was supported by friction inside a 3/8" glass tube. This enabled the platinum wire to be manipulated or removed without upsetting the density current below. The glass tube fed through a rubber bung, which fitted into $\frac{1}{2}$ inch diameter holes that had to be drilled at convenient spacings, along the length of the test tank.

A lead sinker of 1/4 inch diameter was attached to the end of the platinum wire. The sinker could be withdrawn, with the wire, through the glass tube. It served to keep the wire taut during experiments. The sinker was insulated by painting with cellulose acetate (nail polish) so that bubbles were generated only on the exposed wire.

The bubble lines were illuminated by electronic flash synchronised with the camera shutter. The flash unit was positioned in the bottom of the false "bottom" compartment, so that bubbles were illuminated from above. This avoided reflections which might have caused glare spots in the photographs. Illumination was found to be adequate using a small portable electronic flash unit (Canon). A typical aperture was f8 with 125 ASA black and white film. A tele-extension was fitted to the single lens reflex camera, so that it could be positioned some distance back from the side of the tank (approximately two to four feet) and the area of interest (three to four inches square) still occupied the whole of the photograph.

The spacing of the subject and the camera minimised parallax errors which otherwise would have had to have been corrected.

Sources of Error in using Hydrogen Bubbles for Velocity Measurement

An obvious source of error in velocity measurement using hydrogen bubble technique is caused by the rising of the bubbles. It is desirable, therefore, to have bubbles of the minimum possible size. The bubble diameter was found to be dependent on two factors:

(i) The surface current density (amps/ cm^2).

(ii) The age of the wire.

(i) The optimum surface current density was found to be approximately 0.1 amperes/ sq. cm. but this varied by as much as $\pm$ 50 pc. depending on the temperature, conductivity of the water and "age" of the wire. Therefore it was always necessary to adjust the potentiometer until satisfactory bubbles were obtained. Fortunately the smaller bubbles left the wire very evenly, so that bubble traces were uniform.

The change in conductivity of water over the temperature differences used in experiments ($10^{o}C$) was slight. The warmer water was more conductive than the cooler water so that bubble density was greater in the former. Since the hot water generally had higher velocities than the cool water this effect was advantageous.

Hydrogen bubble technique is not suitable for use near an interface of salt and fresh water if the fresh water forms the density current.

This was the case in some of the experiments described in a paper by Wilkinson and Wood (1968). The hydrogen bubble probe could only be placed
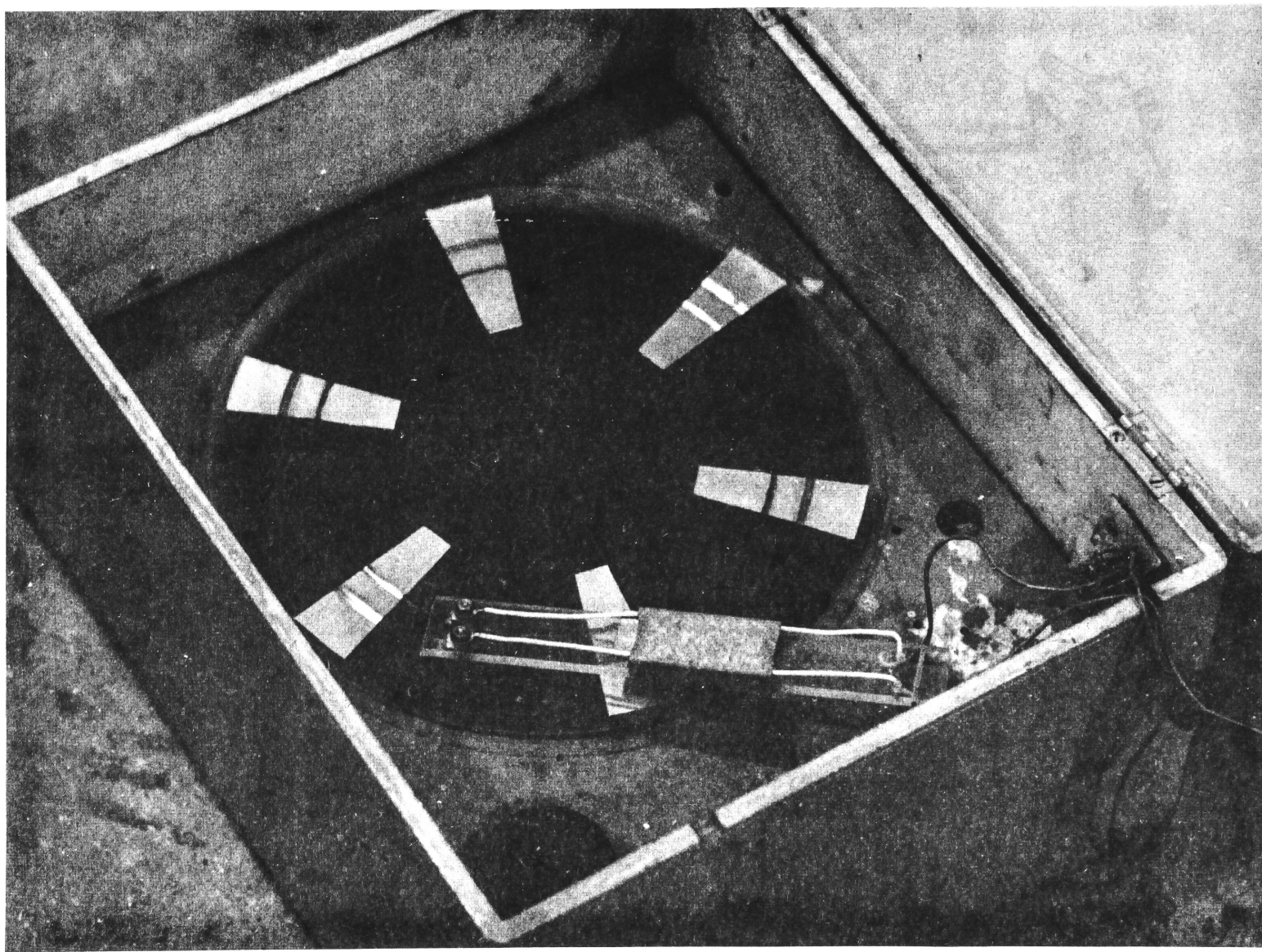
Fig. No. 69: The hydrogen bubble commutator.
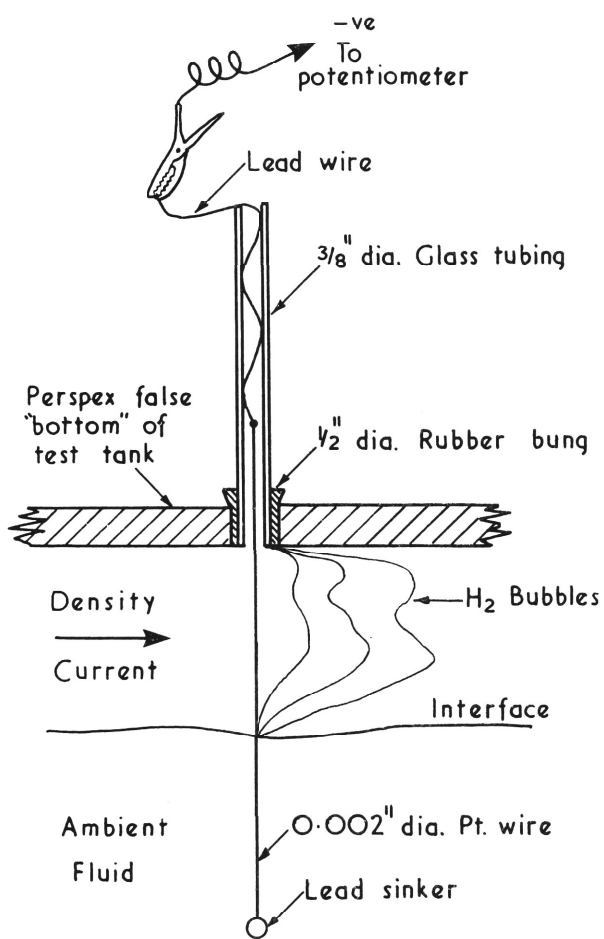
SIDE ELEVATION

Not to Scale
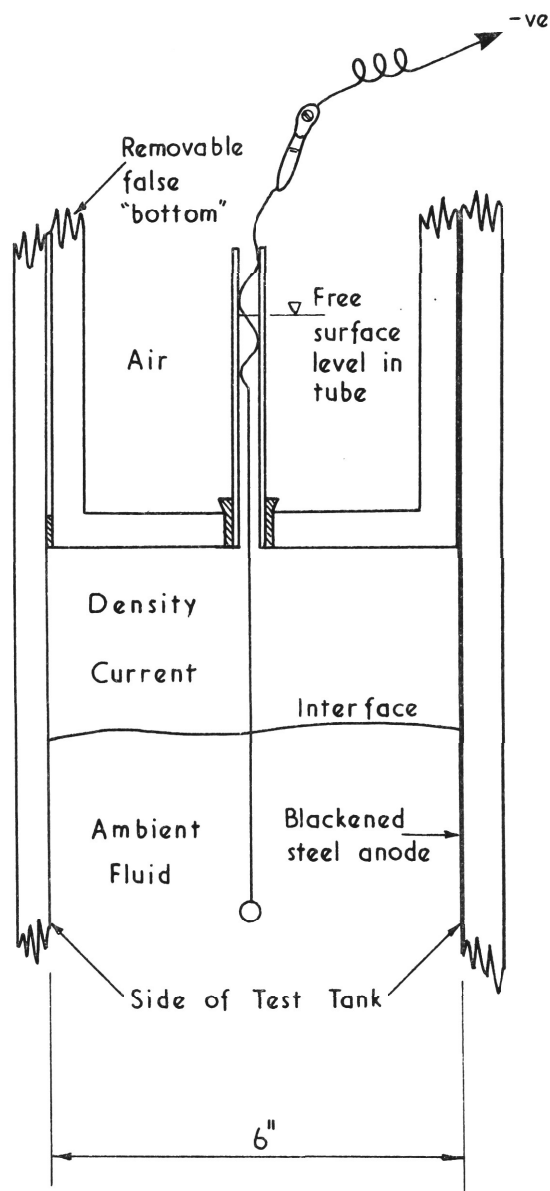
END ELEVATION

HYDROGEN BUBBLE APPARATUS

FIGURE 70.

to within several millimetres of the interface if one was to obtain uniform bubbles. Although this did not affect calculation of velocity distribution correction factors to any extent, interfacial velocities and shears could not be measured. The technique is therefore unsuitable if high conductivity gradients exist across the area in which velocity measurements are required.

(ii) "Ageing" of a wire is a surface chemistry effect and causes a deterioration of bubble uniformity and size with time. Some days the effect was worse than others but the usual "ageing" time was two to three minutes. The wires had to be removed for several seconds to restore them to their former state. The phenomenon is thought to be caused by deposition of impurities on the wire. These are washed away when the wire is removed. Sometimes agitation of the wire would counteract the ageing effect.

An excellent uncertainty analysis is given in a paper on the use of hydrogen bubbles for quantitative measurement by Schraub et al (1964). Six sources of error are listed and discussed in this paper. It is now proposed to look at the relevance of these errors to the present work.

(1) Measurement Uncertainty - Errors caused by optical distortion, film resolution etc. are of second order and may be neglected.

(2) Averaging Uncertainty. These errors arise in attempting to predict Eulerian velocities from Lagrargian time average velocities of marker bubbles. Errors of this type arise if the flow is (i) unsteady (not applicable); (ii) turbulent. Turbulence causes variation from one bubble line

to the next and this is the major source of error in the present series of tests. The turbulence caused a scatter about a mean velocity. It is necessary, therefore, to give an error estimate, the standard deviation, with any velocity measurements presented. Accuracy can only be increased by increasing the number of readings. Six or seven photographs were generally required, to obtain a velocity with the desired accuracy, $\pm$ 5 pc. with 95 pc. confidence.

(3) Displacement uncertainty can arise when bubbles move out of the x, y generation plane. Errors of this type will only occur if there are severe velocity gradients in the direction normal to this plane. Lateral gradients near the centre of the test tank were negligible so that errors of this type did not present a problem.

(4) Response uncertainties caused by the virtual inertia of the bubble are negligible. This point was discussed in detail by Schraub et al (1964).

(5) Resolution uncertainties are caused by (a) the finite size of a bubble making it unable to respond to turbulence of a scale of the same order as the bubble diameter, (b) the time interval between bubble pulses places an upper limit on the frequency of turbulent fluctuations which can be measured. This latter restriction outweighs the former completely and the maximum turbulent frequency that could be measured with a bubble pulse rate of approximately 5/ sec. was 2 hertz.

Turbulence spectra were not required in these series of experiments.

(5) Bubble Rise rate uncertainty. Errors due to bubbles rising will be greatest when a velocity gradient exists in the direction of rise. The error caused by bubble rise will be calculated for a particular example in order to estimate the probable magnitude of this error source.

Consider a bubble rising in a fluid of constant shear in the direction of rise. Let the velocity at some point (x_o, y_o) be u_o (see Fig. 71). The equation of the velocity field is given by

$$u = \frac{u_o}{y_o} \, y = ey$$

$$\text{where} \quad e = \text{constant}$$

Let the rise velocity of the bubble be constant and equal to v. The x coordinate of a bubble at any time t after leaving x_o, y_o at t = 0 is given by

$$x = \int_o^{\delta t} u \, dt + x_o$$

and the y co-ordinate is given by

$$y = y_o - v \, t$$

The component of velocity is given by

$$u = \frac{u_o}{y_o} (y_o - vt)$$

The distance the bubble will move in the x direction is given by

$$\delta x = \frac{u_o}{y_o} (y_o \, \delta t - \frac{v \, \delta t^2}{2})$$

in a time δt.

The distance ($\delta x'$) a bubble with no rise velocity would have moved if released at time t_0 from $x = x_0$

$$y = y_0 - v\,\delta t \quad \text{is given by}$$

$$x' = \frac{u_0}{y_0}(y_0 - v\,\delta t)\,\delta t$$

The error in length (ϵ) of the bubble trace is therefore

$$\epsilon = \delta x - \delta x' = \frac{u_0}{y_0}\;\frac{v\,\delta t^2}{2}$$

The relative error in velocity ϵv is given by

$$\varepsilon_v = \frac{u_0}{y_0}\cdot\frac{v\,\delta t}{2} \Big/ \frac{u_0}{y_0}(y_0 - v\,\delta t)$$

$$= e\frac{v}{u_0}\,\delta t \Big/ 2\left(1 - e\frac{v}{u_0}\,\delta t\right) \times 100\%$$

$$\approx \frac{e v\,\delta t}{2 u_0} \times 100\%$$

Typical values of the variables in the above error equations are

ϵ = 4 ft. / sec. / ft. maximum shear encountered near the false "bottom".

$\dfrac{v}{u_0}$ = 0.03 the maximum rise rate was approximately 0.003 ft/ sec. Generally the rise rate was less than this figure.

δt = 0.219 sec. interval between pulses.

It follows the maximum probable error due to bubble rise is

$$\epsilon_v = 3 \text{ pc.}$$

and hence errors arising from this source are small.

(6) Velocity defect caused by wire wake.

Hydrogen bubbles always lie in the wake of the generating wire and therefore do not move with the velocity of the mean flow. Although the Reynold's numbers of the flow past the wire, based on the wire diameter,

Line of Bubble Generation

$$\delta x' = \frac{u_o}{y_o}(y_o - v\delta t)\,\delta t$$

ε_x

Position of bubble at $t = \delta t$

$$\delta x = \int_0^{\delta t} u\,dt$$

$v\delta t$

u_o

A

Path of bubble released from A at $t=0$

x

y

$$u = \frac{u_o}{y_o}\,y$$
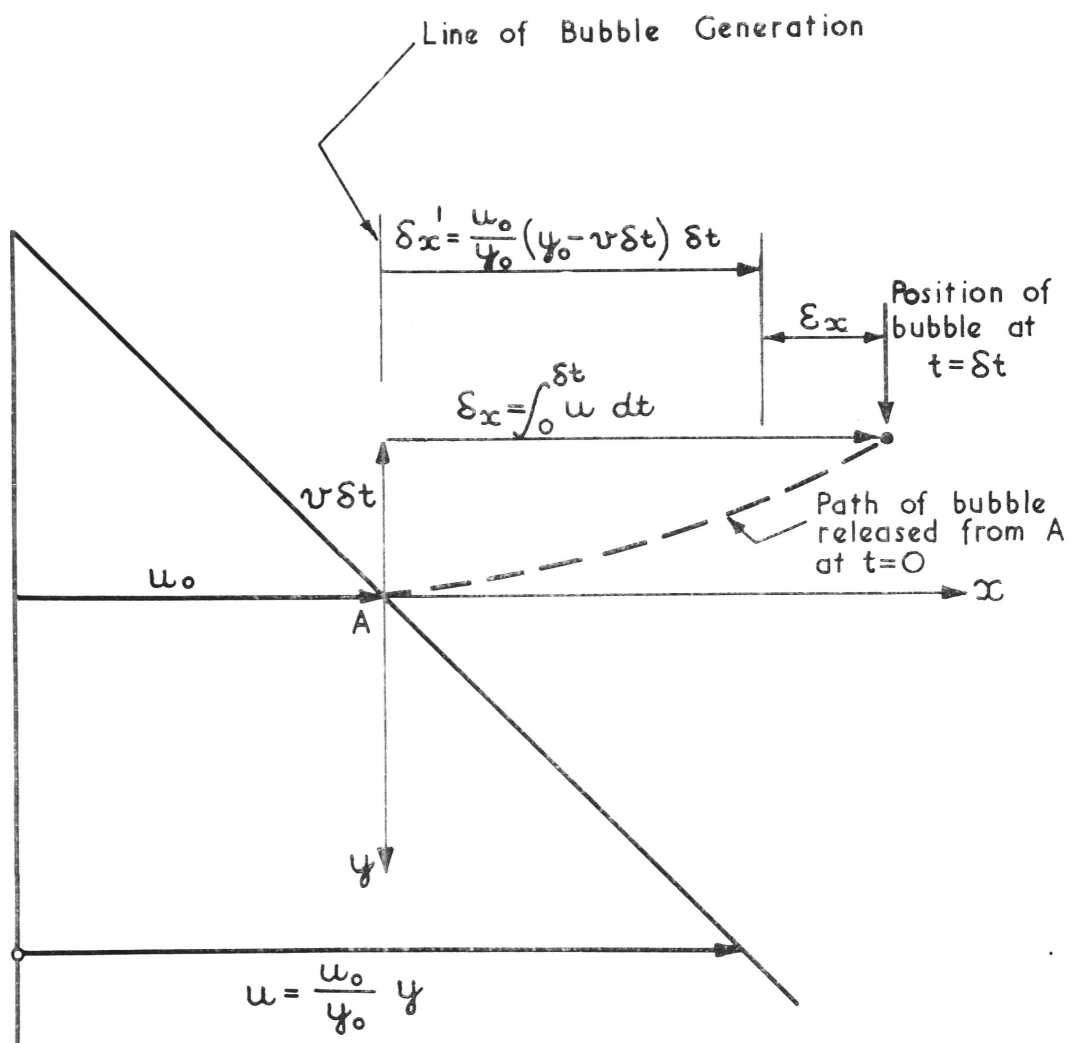
ERROR DUE TO BUBBLE RISE

FIGURE 71.

are generally less than four, viscous flow theory over estimates the velocity defect in the wire wake. The sheath of hydrogen bubbles around the wire causes a marked reduction in the local shear and so reduces the drag on the wire. Schraub et al (1964) state the bubbles reach mean flow velocities at less than seventy wire diameters downstream. This figure was obtained by analysis of high speed motion picture film of bubbles leaving a generating wire.

Hence for a wire of 0.002 inches diameter the bubbles reach mean flow velocities 0.14 inches from the wire. Bubble lines closer than this to the wire were not used in reductions.

Conclusions

Experiments have indicated the major source of error in deducing velocities and momentum correction factors was caused by turbulent fluctuations in the velocity. Reduction of velocity data was very time consuming and it was found six or seven instantaneous velocity profiles was about the limit which could be profitably analysed. Accuracy of the final velocity data was of the order $\pm$ 6 to 8 pc.

Reduction of Velocity Data

The photographs of bubble traces were processed and the negative was projected onto a paper screen. The projection distance was adjusted until the interfacial depth was five inches. The depth of the interface was measured during the experiment and the photograph always had a

length scale (the distance of the interface from the bottom) associated with it.

The bubble lines were traced onto the projected image and the distance between suitable consecutive traces was measured. The momentum correction factors were then calculated by numerical integration of these velocity distances, for each instantaneous profile. The mean value of Sm was taken for all profiles for those particular flow conditions and finally a plot was obtained of S_m versus F_2 as shown in Figure 52.

Appendix E.

Experimental Determination of Densities

The results presented in this report were obtained from thermally induced density currents. Density currents driven by salinity gradients were used in earlier experiments as reported by Wilkinson and Wood (1968) but it is not proposed to discuss these again.

The theory presented in this report is only strictly valid for density currents in which the density difference is caused by a difference in dissolved salt concentrations. For density currents of this type, the equation of continuity of density excess is exactly true. However, this equation is not exactly true for thermal density currents, because of the non-linearity of temperature and density for water. A plot of this relationship, obtained from standard tables (The Handbook of Physics and Chemistry, 1961), is given in Figure 72. Experimentally determined checked points are also plotted in this figure. The reason for checking the standard curve was to test for possible discrepancies caused by dissolved gases in the water. The errors introduced by assuming a linear temperature-density relationship for water can be estimated from the above figure. Maximum error in density for a range of possible temperatures is tabulated below.

Temperature of Ambient Fluid $T_o{}^o C$	Temperature of Density current at inlet $T_1{}^o C$	Maximum error in Density
10	20	7 pc.
15	25	6 pc.
20	30	4 pc.
25	35	1.5 pc.

Most density current experiments lay in the temperature range $15^o C$ to $25^o C$ and the maximum error in density was 6 pc. The error in calculating the mean density of a layer with this variation in temperature from top to bottom is only 2 pc. The error introduced by the linearity assumption for thermal density currents, over the temperature range used in experiments, was negligible.

Temperatures were measured with a copper-constantan thermocouple which was calibrated over the range of temperatures required. The reference junction was placed in the inlet slot and the temperature of the density current downstream was measured relative to the inlet temperature, using the active junctions. The experimental layout is shown schematically in Figure 73.

The measuring probe consisted of a length of 0.10 diameter inch stainless steel tubing which acted as a junction support and an immersion depth indicator.

The copper and constantan wires were lead through the tube and the ends were joined and lightly soldered. About 0.2 inch of the junction
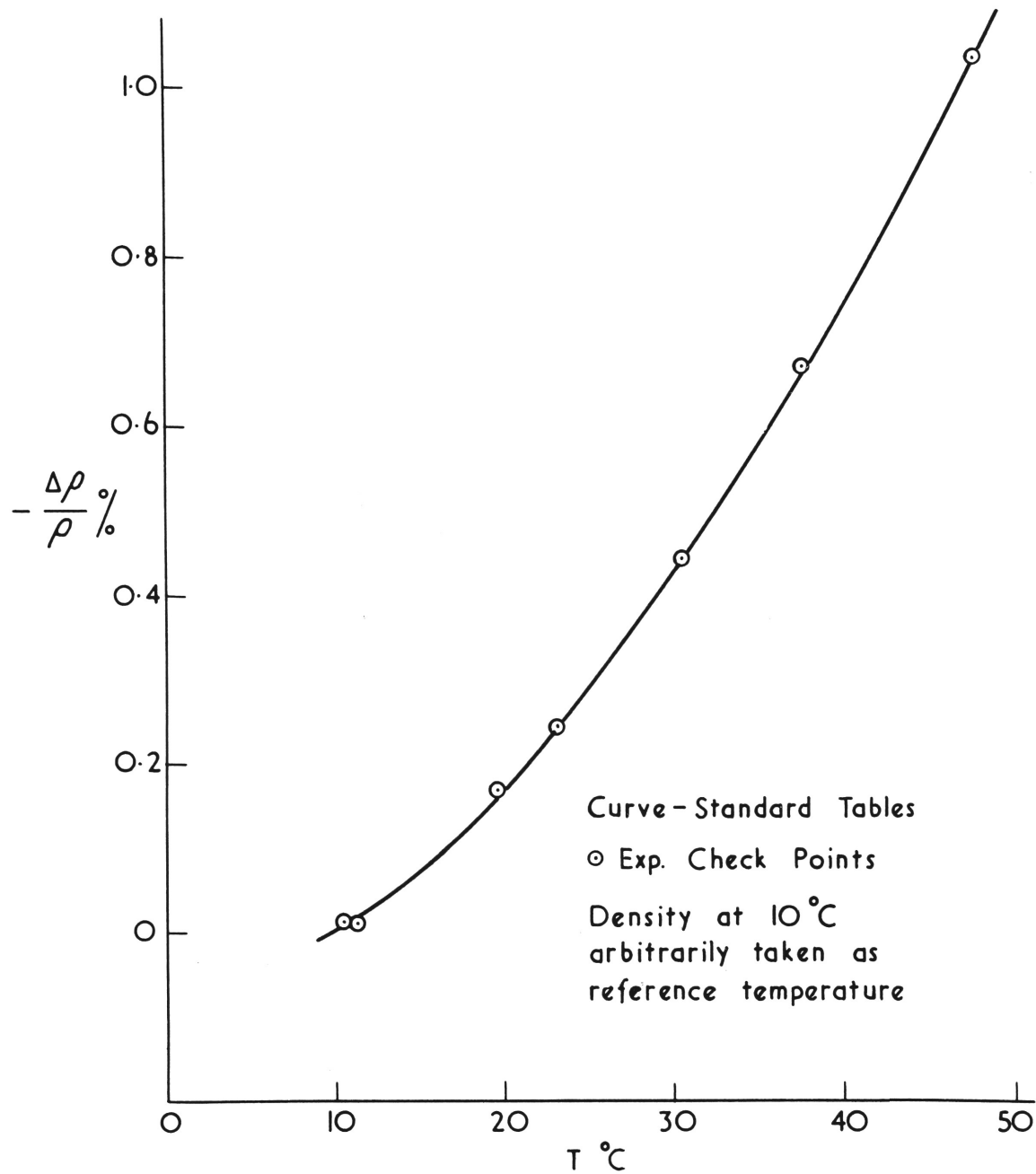
TEMPERATURE VERSUS DENSITY DEFICIT

FOR H₂O

FIGURE 72.

protruded from the end of the stainless steel tube. Epoxy resin was painted over the junction and tube end. This insulated the junction electrically from the surrounding water without upsetting its thermal sensitivity. The transient response of the thermocouple was adequate for the type of measurement required. The thermocouple took 1.8 seconds to reach 95 pc. of its final reading for an instantaneous change in temperature of $10^{\circ}C$. The response would not have been sufficiently rapid to measure thermal turbulence spectra without sophisticated electronic compensation. More delicate thermocouples, with improved transient response could easily be constructed if turbulence spectra were required.

The sensitivity of the thermocouple was found to be 0.04, milli-volts per degree centigrade temperature difference. The response was linear over the range of interest and the calibration was not sensitive to change in the reference temperature.

Thermometers were used to check water temperatures at the inlet and in the cooler ambient fluid. This was necessary for two reasons; firstly to establish an absolute temperature scale from which the densities could be calculated. Secondly the difference in temperature of the two thermometers gave a check for gross errors in the thermocouple readings.

Thermocouples were used in experiments because of their smaller size and higher sensitivity compared with a thermometer.

Appendix F.

Design Example - A power station cooling pond outfall.

In this design data typical of the practice of the Electricity Commission of N. S. W. is used. The design itself is hypothetical.

Design Data

Cooling water is discharged from a power station into a cooling pond via a concrete lined channel, as shown in Figure 74. The discharge is 2,200 cusecs and its temperature is $80^{\circ}F$. The temperature of the pond water below the thermocline is $63^{\circ}F$. The concrete lined channel (AB) has a slope of 1/20 up to the abrupt transition at B where the depth increases abruptly to 80 ft. The purpose of the design is to establish -

(1) the degree of mixing at the outfall (B), between the hot inflow and
  the cooler ambient pond water, and

(2) to determine whether this mixing can be reduced.

Design Comments

When warm water is discharged into a cooling pond it forms a surface layer. Stratification of this type is desirable since it permits maximum heat transfer from the heated water by the processes of radiation and evaporation. As the cooling water is eventually re-used, the greater the heat loss from the cooling pond, the more efficient will be the cooling cycle within the power station. It follows, therefore, that mixing of the pond water and the inflowing water at the outfall should be minimised, so that the temperature of the surface layer is as high as possible.

To
microvolt meter

Cu wire

Cu wire

Constantan wire

Perspex false
"bottom"

T₁ hot reference junction

Density Current

T₂ cold junction

To
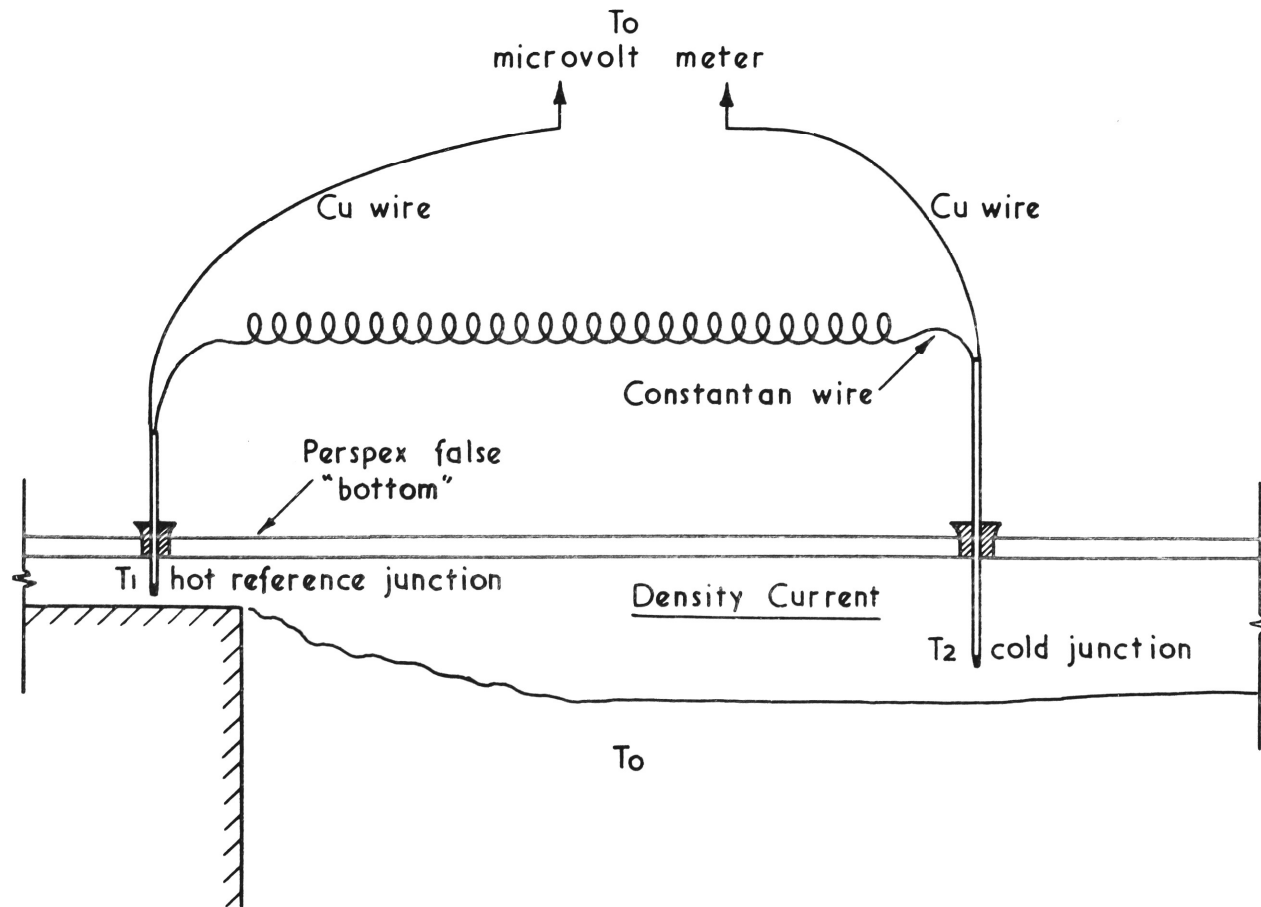
THERMOCOUPLE LAYOUT

FIGURE 73.

A density jump will form at a cooling pond outfall as shown in Figure 75.

It has been shown the amount of fluid which can be entrained into a density

jump increases with the upstream Froude number of the flow (F), defined

previously as

$$F = \frac{u'}{\left(\frac{\Delta \rho}{\rho_o} g y'\right)^{1/2}}$$

The first requirement, therefore, is to have the densimetric Froude

number as low as possible (i.e. the flow depth as great as possible) at

the outfall. This may be accomplished in two ways:-

(1) By artificial roughening in the outfall channel.

(2) By utilising a hydraulic jump as an energy dissipator.

The densimetric Froude number (F) is related to the open channel

Froude number (F_{oc}) (where $F_{oc} = \dfrac{u}{(gy)^{1/2}}$ by the equation

$$F = \left(\frac{\rho_o}{\Delta \rho}\right)^{1/2} F_{oc}.$$

It can be seen that although the channel flow may be subcritical, the

same flow when considered as a density current at the outfall, will al-

most always be supercritical. It is desirable, therefore, that the Froude

number of the channel flow, at the outfall be as low as possible. For

the channel in question, Froude numbers less than 0.8 could not be

achieved, even with artificial roughening. This simplest means of

obtaining low Froude numbers at the outfall is to make use of a hydraulic

jump. This is shown in Figure 75.

The density jump which forms at the outfall is controlled by the

expansion at C. The interfacial depth at this section will be critical

depth provided the interfacial depth in the reservoir is less than the critical depth at C. The layer depth in the cooling pond depends on many factors, the heat balance between the layer and the atmosphere, wind stress and mixing due to wave action. However, field measurements have indicated the thermocline is generally 5 to 10 feet below the surface and it will be shown this is significantly less than critical depth at the point of control.

The density current, being a surface current, is subject to only relatively small frictional forces between the outfall and the expansion at C, so that the interfacial depth downstream of the density jump will be critical depth. The density jump would therefore be of the maximum entraining type.

It has been shown that entrainment at a density jump can be reduced by means of a downstream control. It is proposed, therefore to anchor a floating barrier downstream of the outfall, and so control entrainment into the jump. The barrier depth necessary to cause the density jump to be non-entraining is calculated. This is compared with the earlier case where the density jump is expansion controlled and maximum entraining.

In the following design, subscripts denote the section in Figure 75 to which the variable applies.

(1) Conditions in the Outfall Channel

The Froude number of the flow in the concrete lined channel can be

Power
Station
X

A

B

C

Concrete
Lined
Channel

Cooling Water
Outfall

Cooling Water
Intake

Cooling Water

Reservoir

Dam

0   500   1000 ft.

SCALE
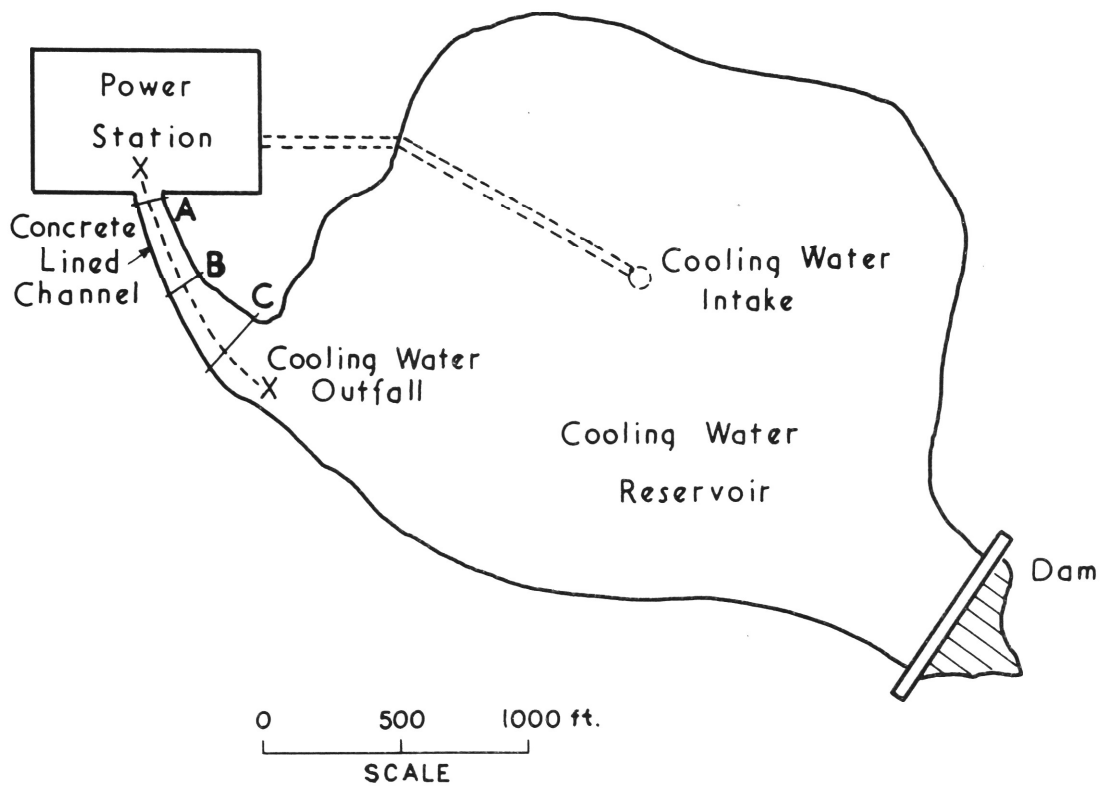
LOCATION   PLAN

FIGURE   74.
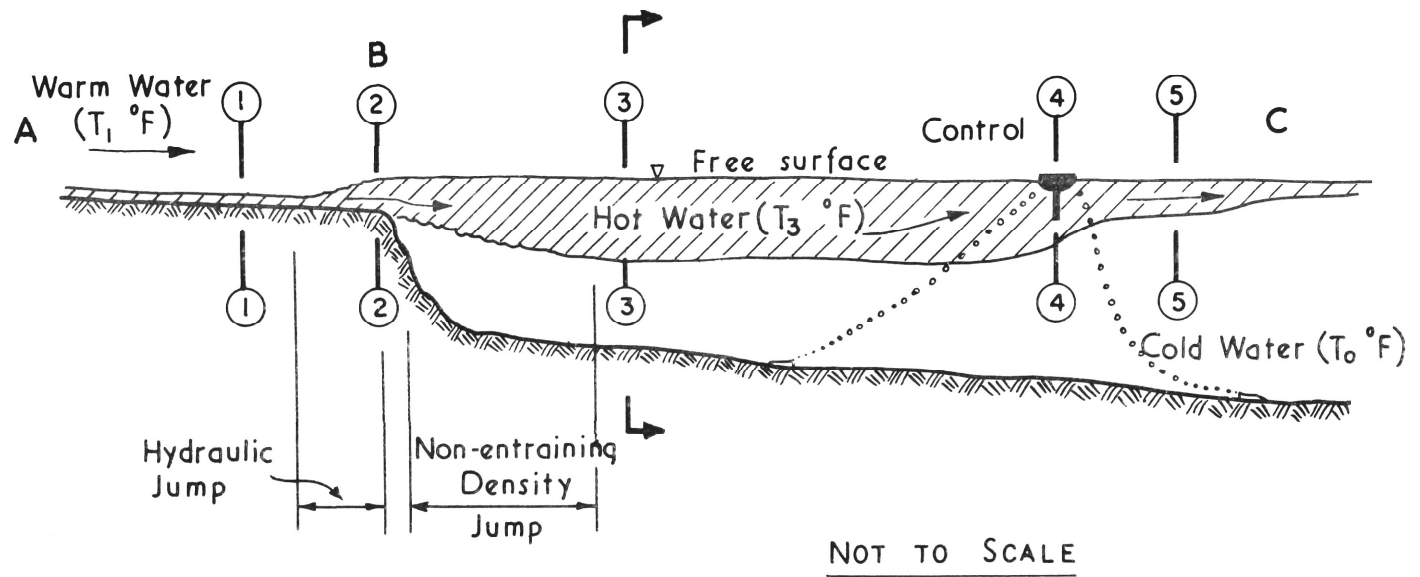
SECTION X-X ALONG THE COOLING WATER OUTFALL
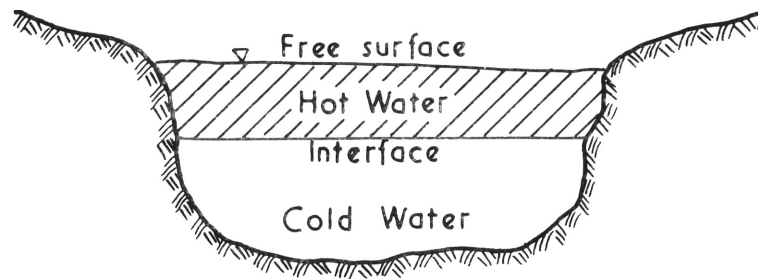
SECTION 3-3

FIGURE 75.

determined from the Manning equation

$$Q = \frac{1.5 \, y \, w \, R^{2/3} \, S^{\frac{1}{2}}}{n}$$

where Q = the total discharge

         y = depth of flow

         w = channel width (rectangular channel = 150 ft.)

         R = hydraulic radius = $\dfrac{wy}{2y+w}$

         n = Manning's n = $0.015 \, (ft)^{1/6}$ for concrete.

The Froude number of the channel flow is given by:-

$$F_{oc1} = \frac{Q}{w_1 y_1^{3/2} g^{\frac{1}{2}}} = \frac{1.5 \, y_1^{1/6} \, S^{\frac{1}{2}}}{ng^{\frac{1}{2}}}$$

Solving the above we get $y_1 = 0.8$ ft., and

$$F_1 = 3.8$$

The flow in the channel is supercritical and a hydraulic jump will

occur when the channel flow meets the reservoir. The depth of flow

downstream of the hydraulic jump is given by $y_2 = \dfrac{y_1}{2} \left(\left[1 + 8F_{oc1}^2 \right]^{1/2} - 1 \right)$

$$= 4.3 \text{ ft.}$$

The densimetric Froude number of the flow, downstream of the hydraulic

jump (Section 2-2 in Figure 75) is given by:-

$$F_2 = \frac{Q}{wy^{3/2} \left(\frac{\Delta\rho}{\rho_o} g \right)^{1/2}}$$

There is a $17^{\circ}F$ difference in temperature between the pond water and

the heated inflow, which gives rise to density difference of 0.22 pc. be-

tween the two. Substituting into the above expression for F_2 we find

$$F_2 = 6.2$$

(2) Conditions at the Outfall
The Density Jump -- Uncontrolled

A density jump will form between sections 2-2 and 3-3 in Figure 75. It has been shown density jumps with this form of flow geometry downstream, are of the maximum entraining type. The entrainment into such a jump is given by equation 35.

$$K = \frac{(2\, S_{m2}\, F_2{}^2 + 1)\ \theta}{3\, S_{m3}{}^{2/3} S_{H3}\, F_2{}^{4/3}}$$

If it is assumed the inflowing velocity distribution is uniform then $S_{m2} = 1.0$. The downstream force flow correction factor can be obtained from Figure 27 so that $S_{m3} = 1.30$.

The hydrostatic pressure correction factor is given in Figure 30 so that

$$S_{H3} = 0.62$$

Boundary friction at the jump for this case is small (air-water interface) and will be neglected so that $\theta = 1.0$

Equation (35) can now be solved to give $K = 2.7$. The temperature of the layer downstream is given by

$$T_3 = T_o + \frac{T_1 - T_o}{K} = 63 + \frac{17}{2.7}$$

$$\therefore \quad T_3 = 69^{\circ}F$$

The thickness of this layer can be calculated from Equation (32)

$$r = \frac{\left(2\, S_{m2}\, F_2{}^2 + 1\right)\ \theta}{3\, S_{m3}{}^{1/3}\, S_{H3}{}^{2/3}\, F_2{}^{2/3}}$$

When the above equation is solved for the particular case under examination

$$r = 9.7$$

hence $\qquad y_3' = ry_2' = 42$ ft.

The eleven degree fall in temperature of the surface layer, caused by mixing at the outfall, would result in a marked drop in the thermal efficiency of the cooling pond. This loss can be avoided if mixing at the outfall is prevented by means of a suitably designed control downstream of the transition region.

Prevention of Mixing at the Outfall

Mixing at a cooling pond outfall can be prevented in two ways.

(1) The tailwater can be controlled so as to force the density jump into a non-entraining or flooded regime.

(2) Experiments by the writer (Foster and Wilkinson, 1969) have shown if the bottom slope at the outfall is less than approximately 15°, entrainment at the density jump is negligible. This results from a blanketing effect of the bottom and ambient fluid is prevented access to the entraining region of the jump.

A sloping cooling pond outfall of this type has been used at Liddell power station in New South Wales. In the case being examined bottom slopes of less than 15° could not be practically achieved, so that the first method must be used. A tailwater control in the form of a floating

barrier, can be used downstream of the density jump, to control entrainment. The barrier acts as an overshot weir.

If the density jump is to be non-entraining, the depth downstream of the jump can be calculated by equating force flows upstream and downstream of the jump. So that

$$\frac{\rho_0 Q^2}{y_2'} + \frac{\Delta\rho\, g\, y_2'^2}{2} = \frac{S_{m3}\,\rho_0\, Q^2}{y_3'} + \frac{\Delta\rho\, g\, y_3'^2}{2}$$

and if we divide throughout by $\dfrac{\Delta\rho\, g\, y_2'^2}{2}$ and put $\dfrac{y_3'}{y_2'} = r$

we get

$$2\,F_2^2 + 1 = \frac{2\,S_{m3}\,F_2^2}{r} + r^2$$

Note: If $S_{m3} = 1.0$ the above equation reduces to the familiar form

$$r = \tfrac{1}{2}\left(\left[1 + 8F^2\right]^{1/2} - 1\right) \text{ or } 1$$

For the example considered, S_{m3} can be obtained from Figure 52 by estimating F_3 to lie between 0.2 and 0.3. Hence $S_{m3} = 1.06$ and trial and error solution of the force flow equations gives

$$r = 8.3 \text{ so that } y_3' = 36 \text{ ft.}$$

The downstream densimetric Froude number is given by

$$F_3 = r^{-3/2}\, F_2$$

$$= 0.26$$

The estimate for S_{m3} was satisfactory.

4. Design of the Control

The barrier depth necessary to obtain this non-entraining condition may be calculated by equating flow energies at sections immediately downstream of the density jump, and at the barrier. Hence

$$\frac{\rho_0\, Q_3^2}{2g\, w_3^2\, y_3'^2} + \Delta\rho\, y_2' = \frac{\rho_0\, Q_4^2}{2g\, w_4^2\, y_4'^2} + \Delta\rho\left(y_4' + h\right)$$

but at the barrier which is now the point of control

$$\frac{\rho_o Q_4^2}{\Delta \rho \, w_4^2 \, y_4'^3} = 1$$

There is negligible entrainment between Sections (3) and (4) and

as the density jump is non-entraining

$$Q_1 = Q_2 = Q_3 = Q_4$$

Experiments have shown that if the barrier is placed six times the

downstream depth ($\sim$ 250 ft.) downstream of the outfall, it will be clear

of the density jump. The channel width at this point (w_4) is 180 ft. The

three previous equations can be solved to give

$$y_4' = 12.0 \text{ ft.}$$

and $h = 16$ ft.

The layer depth immediately downstream of the control will be close

to critical as this region is still controlled by the expansion, so that

$y_5' \approx y_4' \approx 12.0$ ft. There will be some mixing in this region but ex-

periments have shown this is small and certainly far less than that

which would have occurred at the outfall if the barrier were not present.

Thus the surface temperature of the cooling in the vicinity of the out-

fall would be 80°F.

Conclusions

It has been shown that unless prevented, mixing at the outfall will

cause a reduction in the temperature difference between the inflowing

cooling water and the ambient pond water. In the design example considered, which is typical of Electricity Commission of New South Wales practice, the initial temperature difference of 17^OF, would be reduced by 65 per cent by mixing immediately downstream of the outfall. Such mixing would significantly lower the thermal efficiency of the cooling pond by lowering the surface temperature of the pond and so reducing the heat exchange to the atmosphere. The depth of the thermocline would also be increased.

The floating barrier, if lowered to the calculated depth of 16 ft., some 250 ft. downstream of the outfall, will effectively prevent mixing in the transition region.

It has been noted that mixing is also inhibited when the bottom slope in the transition region is less than approximately 15°.

Appendix   G

A   Summary   of   Experimental
Data.

(i)   Typical reduction of test **data for a** single experiment.

(ii)   Test data for maximum entraining density jumps.

(iii)   Density jump controlled by a broad crested weir.

(iv)   Density jump controlled by sharp crested weirs.

(v)   Density jumps controlled by an undershot gate.

(vi)   Density jumps controlled by friction.

(vii)   Unsteady flow experiments.

(viii)   Fall in force flow.

(ix)   Force flow correction factors.

(x)   Some typical mean velocity distributions.

(xi)   Hydrostatic pressure force correction factors.

(xii)   Some typical mean density distributions.

(i) <u>Typical Reduction of Test Data for a Single Experiment</u>

It is impractical to include all the experimental data in full detail in this report. Therefore only the basic parameters are tabulated for each experiment. However, one complete reduction is given in the following pages.

<u>Test No. P3</u>
<u>Upstream Conditions</u>

Q_1 = 2.35 gal/min. Flow upstream of density jump.

y_1' = 0.40 inches   Depth of flow upstream (determined by height of the inlet slot).

w = 6.1 inches   Channel width.

T_1 = 31.4 $^{\circ}$C   Upstream temperature of density flow.

T_0 = 22.0 $^{\circ}$C   Temperature of the ambient fluid.

$\triangle_1$ = 0.25 pc. The characteristic density deficit of the upstream flow is equal to the mean density since the density distribution is uniform.

F_1 = 7.2   The upstream Froude number = $\dfrac{Q_1}{\triangle_1^{\frac{1}{2}} y_1^{3/2}}$ ✓

R_1 = 1,320   Upstream Reynold's number

$$= \dfrac{Q_1}{w r_1}$$

where r_1 is the kinematic viscosity of the upstream flow.

<u>Downstream Conditions</u>

The control — A free overfall situated 36 inches from the up-stream end of the density jump.

$y_2' = 4.25$ inches   Interfacial depth

$r = 10.6 = \dfrac{y_2'}{y_1'}$ Conjugate depth ratio

Calculation of the characteristic density difference   (Δ_2)

$$\Delta_2 = \frac{1}{u_2' y_2'} \int_0^D \frac{u \Delta \rho \, g \, dy}{\rho_0}$$
obtained by numerical integration of measured velocity and density distributions.

The mean velocity distribution was obtained from 6 separate sets of hydrogen bubble traces.

y/y_2'	u/u_2'
0.1	1.40
0.3	1.60
0.5	1.40
0.7	0.65
0.9	0.07

The force flow correction factor - determined from these data was found to be

$$S_{m2} = \frac{1}{u_2'^2 y_2'} \int_0^D u^2 \, dy \; = 1.32$$

The mean density distribution was obtained from the temperature distribution tabulated below:-

y (in)	T ($^\circ$C)
0.5	27.9
1.0	27.1
1.5	26.2
1.95	25.8
2.55	25.2
3.0	24.6
3.4	23.8
3.9	23.5

Temperature Distribution

y/y_2'	$\dfrac{\Delta \rho}{\rho_0}$ pc.
0.11	0.159
0.23	0.136
0.36	0.107
0.46	0.099
0.60	0.084
0.71	0.065
0.80	0.048
0.91	0.040

Distribution of Density Difference

$$\overline{\Delta\rho_2} = \frac{1}{y_2'} \int_0^D \Delta\rho \, dy \qquad = 0.92 \text{ pc.}$$

Numerical integration gave

$$\Delta_2 = 1.18 \, \frac{\overline{\Delta\rho_2}}{\rho_0'} \qquad = 0.109 \text{ pc.}$$

The hydrostatic pressure correction factor was obtained by

numerical integration

$$S_{H2} = \frac{2}{\Delta_2 \, y_2^2} \int_0^D \int_y^D \Delta\rho \, y \, dy \, dy$$

$$= 0.58$$

The flow ratio K was found to equal

$$K = \frac{\Delta_1}{\Delta_2} \qquad = 2.28$$

and the downstream Froude number was obtained from continuity

$$F_2 = \left(\frac{K}{r}\right)^{3/2} \, . \quad F_1 \quad = \quad 0.72$$

(ii) Maximum Entraining Jump Test Data

Comments

The density jumps in the following series of tests were controlled by a free overfall in close proximity to the end of the jump. Generally the overfall was at a distance equal to the jump length from the end of the density jump. Frictional effects downstream of the density jump were negligible over this distance. The following data are plotted in Figures 26 and 27.

Test No	Q_1 $\frac{gal}{min}$	y_1' in.	y_2' in	T_0 °C	T_1 °C	$\frac{\Delta\rho_1}{\rho_0}$ %	F_1 —	r —	K —	F_2 —	Δ_2 %	y_b in
P1	1·58	0·40	2·40	21·9	30·8	0·25	4·85	6·0	1·65	0·72	0·148	1·7
P2	1·93	0·40	3·1	22·0	31·2	0·25	5·9	7·7	1·87	0·70	0·134	2·0
P3	2·35	0·40	4·25	22·0	31·4	0·25	7·2	10·6	2·28	0·72	0·109	2·9
P4	1·45	0·40	1·95	21·8	30·9	0·25	4·4	4·9	1·43	0·69	0·175	1·4
P5	1·23	0·40	1·45	21·9	31·0	0·25	3·8	3·6	1·30	0·85	0·192	1·05
P6	0·87	0·40	0·65	21·9	31·1	0·25	1·80	1·6	1·03	0·96	0·243	0·45
Z2	3·90	0·43	6·6	13·4	26·9	0·30	9·7	15·6	2·73	0·71	0·110	—
Z6	3·77	0·54	4·5	12·9	30·0	0·37	6·0	8·3	2·03	0·72	0·18	0·28
Z7	3·96	0·54	4·9	12·8	28·0	0·34	6·6	9·1	2·10	0·73	0·16	—
S1	1·48	0·25	4·2	20·2	27·3	0·189	10·7	16·8	2·80	0·73	0·067	—
F1	2·74	0·40	5·6	22·2	31·2	0·25	8·8	14·0	2·55	0·66	0·10	—
F3	1·05	0·40	1·05	22·3	21·3	0·25	2·8	2·6	1·13	0·82	0·22	—

(iii) Summary of results for density jumps controlled by a broad-crested weir.

F_1	K	r	F_2	$\dfrac{h}{y_1'}$	$\dfrac{h}{y_{1c}}f$	$\dfrac{h}{y_2'}$
10.5	2.60	14.0	0.83	0.0	0.0	0.00
10.7	2.44	14.4	0.73	1.58	0.063	0.11
10.5	2.09	14.7	0.58	2.38	0.105	0.16
9.7	2.00	14.8	0.48	3.70	0.175	0.25
9.7	1.70	15.1	0.37	4.40	0.220	0.29
9.7	1.59	15.1	0.32	5.60	0.265	0.37
9.7	1.19	14.5	0.23	6.40	0.290	0.44
16.5	3.05	24.5	0.73	0.0	0.000	0.00
16.5	2.90	25.4	0.65	2.7	0.065	0.105
16.5	2.50	26.2	0.48	6.0	0.145	0.23
16.3	2.00	26.4	0.35	8.8	0.210	0.35
16.3	1.50	26.0	0.26	10.8	0.260	0.42
16.3	1.10	25.3	0.19	12.5	0.300	0.49
16.2	1.15	25.5	0.20	12.5	0.300	0.49
16.4	1.55	26.0	0.27	10.8	0.260	0.41
16.5	2.05	26.2	0.36	8.8	0.210	0.35

(iv)   Summary of results for density jumps controlled by a sharp
       crested weir.

Test №	F_1	K	r	F_2	$\frac{h}{y_{1c}}$ f
T7	7.45	1.88	9.7	0.65	0.120
T3	5.5	1.66	7.9	0.53	0.180
T4	5.5	1.44	7.6	0.46	0.245
T6	6.9	1.39	9.3	0.40	0.290
T8	7.45	1.06	9.3	0.26	0.340
T2	3.1	1.10	3.6	0.53	0.170
T9	7.45	1.67	10.3	0.49	0.210
T5	5.5	1.28	7.6	0.41	0.260
T10	7.45	1.25	9.5	0.36	0.310

(v) Summary of results for density jump controlled by an undershot gate.

Test №	F_1	K	r	F_2	$\dfrac{C_c h}{y_2'}$	$\dfrac{C_c h}{y_{1c}} f$
Y9	6.45	1.16	9.7	0.26	0.19	0.15
Y8	6.5	1.37	9.7	0.31	0.22	0.18
Y7	6.5	1.42	9.8	0.36	0.26	0.24
Z8	6.4	1.46	9.5	0.41	0.34	0.32
Y6	6.5	1.70	10.0	0.45	0.31	0.25
Z10	6.6	1.80	10.0	0.50	0.33	0.31
Y2	6.35	1.90	9.9	0.53	0.42	0.38
Y1	6.35	2.15	9.8	0.67	0.66	0.54

(vi)   A summary of test data for density jumps controlled by friction.

Test №	Q_1	y_1'	y_2'	T_0	T_0	$\Delta\rho/\rho_0$	Δ	ω_r	$\sin\theta$	F_1	r	K
units	gal/min	in.	in.	°C	°C	%	%		%			
V1	2·00	0·37	4·6	12·4	26·7	0·28	0·10	0·40	0·63	7·0	12·4	2·8
V2	2·10	0·57	2·9	12·8	26·8	0·28	0·185	0·52	0·63	3·6	5·1	1·51
V3	1·65	0·55	1·8	10·4	29·0	0·35	0·275	0·62	0·63	2·6	3·3	1·27
V4	2·30	0·55	3·6	10·6	24·9	0·26	0·120	0·46	0·98	4·3	6·6	2·16
V5	2·18	0·37	3·8	12·2	26·2	0·29	0·115	0·45	0·98	6·9	10·3	2·52
T5	1·77	0·37	3·5	16·1	23·7	0·17	0·074	0·47	0·98	7·5	9·5	2·10

$$f_1 \quad R_2 \sin\theta \, \omega_r$$

$$f_2 = \frac{R_1 \sin\theta \, \omega_r}{\beta}$$

Basic Parameters

Test №	F_1	F_2	R_1	R_2	$\sin\theta$ %	f_1	f_2
V1	7·0	0·77	1060	3000	0·63	7·5	0·72
V2	3·6	0·58	1060	1600	0·63	5·2	0·63
V3	2·6	0·62	940	1200	0·63	4·7	0·59
V4	4·3	0·82	1130	2400	0·98	10·7	1·02
V5	6·9	0·84	1000	2500	0·98	11·1	1·20
T5	7·5	0·73	860	1750	0·98	8·0	1·11

Density distributions for the friction controlled density jump.

Test №	y/y_2'	$T\,°c$	$\Delta P/P_o\ \%$	Test №	y/y_2'	$T\,°c$	$\Delta P/P_o\ \%$
V1	0.07	22.1	0.17	V4	0.07	21.9	0.205
	0.20	22.1	0.17		0.28	21.2	0.19
	0.39	18.9	0.12		0.47	18.4	0.12
	0.33	19.6	0.14		0.61	17.2	0.10
	0.50	17.9	0.10		0.72	16.4	0.045
	0.63	16.6	0.075		0.89	12.9	0.020
	0.78	14.9	0.045		1.00	12.2	0.015
	0.87	14.0	0.030		1.17	11.2	0.005
	0.96	13.5	0.020				
	1.22	12.4	0.000	V5	0.06	22.1	0.190
					0.16	21.8	0.185
V2	0.10	24.3	0.25		0.24	21.0	0.170
	0.30	23.8	0.23		0.34	19.8	0.140
	0.45	22.6	0.21		0.45	18.8	0.120
	0.69	20.0	0.15		0.58	18.0	0.100
	0.59	21.6	0.18		0.66	17.0	0.080
	0.79	19.8	0.14		0.76	16.8	0.075
	0.93	18.0	0.10		0.87	15.8	0.060
	0.97	15.8	0.06		0.92	15.3	0.050
					0.97	14.8	0.045
V3	0.11	26.7	0.33	T5	0.11	21.0	0.101
	0.31	27.2	0.35		0.23	20.9	0.099
	0.47	26.2	0.32		0.34	20.5	0.090
	0.70	23.3	0.25		0.48	19.9	0.075
	0.83	21.7	0.20		0.63	19.5	0.069
	0.95	19.7	0.16		0.77	19.0	0.057
					0.86	18.9	0.053
					0.94	18.5	0.046

(vii)   Unsteady Flow Experiments

Reference Figure 32.

All unsteady flow experiments were made in a tilting flume 120 ft. long, 23 inches internal width and 2 ft. deep.

Starting Characteristics

Test No	Q_i	$\Delta \rho/\rho_o$	ϕ	V_N (initial)	$\zeta = V_N/\phi^{1/3}$	$\sin \theta$
Units	$cfs \times 10^2$	%	$(ft/sec)^3 \times 10^3$	ft/sec		%
2	2.28	0.45	3.3	0.125	1.04	0.0
3	2.34	0.56	2.3	0.140	1.06	0.0
4	1.84	0.23	0.81	0.095	1.06	0.0
5	1.92	0.30	0.91	0.099	1.01	0.0
6	2.18	0.61	2.2	0.142	1.09	0.0
7	2.28	0.50	2.7	0.134	0.97	0.54
8	1.53	0.58	1.5	0.115	1.01	0.54
9	2.36	1.20	4.8	0.177	1.04	0.54
10	2.22	0.26	1.85	0.136	1.10	0.26
11	1.62	0.31	1.6	0.125	1.07	0.26

Unsteady density flows on a slope

$$\zeta_o = \frac{V_o}{\phi^{1/3}}$$ where V_O is the uniform velocity of the nose attained after travelling distance ℓ.

F_2 is the Froude number of the layer behind the nose, calculated from the equality discussed in Chapter 4. $F_2 = \zeta_o^{3/2}$

Test Nᵒ	ζ_o	F_2	R_2	$\sin\theta$	$\ell\ (ft)$
7	0.78	0.69	1350	0.54 pc.	62
8	0.75	0.65	1180	0.54 pc.	30
9	0.83	0.76	1450	0.54 pc.	54
10	0.65	0.53	1900	0.26 pc.	60
11	0.76	0.66	2700	0.26 pc.	39

Comparison of β for nose and $F_2^{2/3}$ at the instant of flooding of the jump. Equality of these two variables indicates the nose is travelling at the same speed as the flow immediately downstream of the jump. At the instant of flooding F_2 is calculated from the known value of F_1 assuming a non-entraining density jump.

Test Nº	β	$F_2^{2/3}$	ℓ (ft)	F_1
2	0.48	0.54	54	3.15
4	0..54	0.45	77	5.9
5	0.59	0.64	39	2.1
6	0.58	0.54	50	3.2

Complete Reduction of Unsteady Flow Experiment

Test No. 6 - Density difference due to dissolved salt (N_aC1)

$Q_1 = 2.18 \times 10^{-2}$ cusecs

$\quad = 0.61$ pc. $\qquad y_1 = 0.48$ in.

$\qquad\qquad\qquad\qquad$ w $= 23$ in.

$T_o = 21.5^{\circ}C$

$T_1 = 23.8^{\circ}C$

$\ell (ft)$	$t \; \genfrac{}{}{0pt}{}{min}{sec}$
3	0.20
6	0.38
9	1.03
15	2.01
18	2.31
21	3.00
24	3.32
27	4.04
30	4.37
33	5.15
36	5.49
39	6.24
42	6.59

Comments.

Roller region starting to develop at jump. $y_2' = 1.2$ in.

Low amplitude wave downstream of jump

Roller region extends half length of jump $y_2 = 1.3$ in.

Roller region extended early the length of the jump intermittent flooding

$\ell(ft)$	t min & sec
45	7.34
48	8.13
54	9.29
57	10.09
60	10.49
63	11.28
63	12.12
69	12.56
75	14.29
78	15.17
81	16.09
84	17.06
87	18.03
90	19.00

Comments

Density jump flooded $y_2' = 1.4''$

entrainment ceased

Inlet flooded to a depth of 1''

$y_2' = 1.5''$.

$$\phi = \frac{Q_1}{\omega} \cdot \frac{\Delta\rho}{\rho_o} = 2.2 \times 10^{-3} \ (ft/sec)^3$$

$F_1 = 3.2$

Initially $t < 1$ minute $\quad \zeta = 1.09$

At flooding $t = 9$ min $- 11$ min. $\quad \zeta = 0.58$

$F_2 = 0.40$

$F_2^{2/3} = 0.54$

(viii)   <u>Fall in Force Flow</u>

Force flow ratios downstream of density jumps are calculated from

both equations 32 and 35 for maximum entraining density jumps.   The

mean value of the force flow ratio is plotted against upstream Reynolds

number in Figure 48.   The dimensionless jump length is taken as 4r .

Test No	θ (Eqn 32)	θ (Eqn. 35)	$\bar{\theta}$	R.	$\frac{x}{Y_.}$
P1	0. 87	0. 76	0. 82	880	26
P2	0. 73	0. 73	0. 73	990	28
P3	0. 72	0. 76	0. 74	1320	35
P4	0. 83	0. 75	0. 79	820	18
P5	0. 81	0. 81	0. 81	660	14
P6	0. 97	0. 97	0. 93	480	6
22	0. 70	0. 74	0. 72	2100	50
26	0. 85	0. 77	0. 81	1900	34
27	0. 83	0. 75	0. 79	2300	36
V5	0. 73	0. 76	0. 79	1150	43
Γ5	0. 75	0. 67	0. 74	960	38
S1	0. 78	0. 71	0. 71	850	52
F1	0. 76	0. 74	0. 75	1450	58
F3	0. 95	0. 92	0. 93	540	16

(ix) Force Flow Correction Factors

Tabulated below are force flow correction factors deduced from hydrogen bubble velocity distributions measured downstream of the density jump. The factors quoted are the mean of n values of S_{m2} calculated from n photographs,

where
$$S_{m2} = \frac{1}{u'^2_2 \, y'} \cdot \int_{o}^{D} u_2^2 \; dy$$

for each bubble trace.

Sigma (σ) is the standard deviation (adjusted for small sample range) of S_{m2} for the n readings.

Test №	S_{m2}	σ	n	F_1	F_2
A	1.10	.03	5	3.6	0.37
B	1.14	.05	5	4.4	0.62
C	1.13	.02	4	4.8	0.46
D	1.13	.05	9	8.8	0.47
E	1.20	.11	6	6.0	0.67
F	1.30	.06	2	6.5	0.79
G	1.09	.04	8	11.8	0.38
H	1.08	.03	7	7.1	0.39
I	1.09	.03	6	16.5	0.23
J	1.14	.02	6	3.5	0.50
K	1.07	.02	10	4.4	0.40
L	1.09	.05	6	3.6	0.37
M	1.15	.03	7	6.0	0.47
N	1.31	.05	11	4.1	0.82
01	1.26	.04	11	4.1	0.86
02	1.14	.05	10	2.6	0.50
03	1.31	.05	10	4.4	0.81
04	1.15	.03	8	7.1	0.52
05	1.14	.03	7	7.1	0.53
R	1.33	.16	2	12.5	0.71
S	1.11	.03	6	1.05	0.98
T	1.19	.05	7	1.9	0.92
U	1.23	.07	5	2.1	0.76

(x)   Typical Mean Velocity Distributions

The following velocity distributions are the mean of n velocity distributions obtained from n photographs.   Values of n are tabulated on the previous page.

y/y_2'	Velocity u/u_2'						
Test Nº	01	F	05	G	D	02	I
F_2	0.82	0.79	0.53	0.38	0.47	0.50	0.23
0.05	1.19	1.09	1.19	1.14	0.92	0.82	1.08
0.15	1.53	1.6	1.42	1.37	1.23	1.05	1.35
0.25	1.43	1.54	1.40	1.30	1.32	1.27	1.35
0.35	1.31	1.43	1.23	1.19	1.29	1.28	1.21
0.45	1.28	1.33	1.18	1.14	1.27	1.20	1.15
0.55	1.26	1.64	1.10	0.98	1.20	1.10	0.98
0.65	1.03	0.85	0.92	0.90	1.09	1.07	0.91
0.75	0.78	0.67	0.82	0.79	0.85	0.92	0.82
0.85	0.19	0.46	0.59	0.73	0.62	0.74	0.75
0.95	0.02	0.03	0.25	0.45	0.25	0.62	0.29
S_{m2}	1.26	1.30	1.14	1.09	1.13	1.14	1.09

(xi) Hydrostatic Pressure Force Correction Factors

Test №	S_{H2}	F_1	F_2	$\frac{K-1}{K_{max}-1}$
S	1.00	1.1	0.98	0.01
06	0.93	1.8	0.96	0.20
F3	0.89	2.8	0.92	0.40
05	0.83	3.9	0.85	0.45
04	0.63	4.8	0.73	0.68
26	0.59	6.0	0.70	0.72
P3	0.58	7.1	0.72	0.83
F1	0.59	8.8	0.68	
P2	0.99	2.6	0.99	0.13
P4	0.78	7.1	0.78	0.55
P5	0.73	7.1	0.73	0.52
D	0.72	8.8	0.72	0.50
06	1.00	4.8	1.00	0.03
S	1.00	1.05	0.98	0.04

(xii)   Typical Mean Density Distributions

Test №	S	06	F3	05	P5	04	P3
$k-1/k_{max-1}$	0.01	0.20	0.40	0.45	0.52	0.68	0.83
S_{H2}	1.00	0.93	0.89	0.83	0.73	0.63	0.58
y/y_2'			$\Delta\rho_2/\overline{\Delta\rho_2}$				
0.05	1.00	1.03	1.36	1.40	1.57	1.65	1.76
0.15	1.00	1.03	1.32	1.33	1.48	1.52	1.74
0.25	1.00	1.03	1.28	1.27	1.35	1.30	1.55
0.35	1.00	1.03	1.23	1.21	1.22	1.08	1.32
0.45	1.00	1.02	1.10	1.16	1.07	0.98	1.10
0.55	1.00	1.02	1.12	1.00	0.96	0.87	0.90
0.65	1.00	0.98	0.92	0.97	0.85	0.75	0.74
0.75	1.00	0.94	0.82	0.80	0.74	0.62	0.55
0.85	1.00	0.84	0.72	0.69	0.60	0.46	0.34
0.95	0.96	0.84	0.47	0.17	0.37	0.25	0.11

Appendix H

List of Main Symbols.

b = width of channel contraction

B = channel width

C_c = contraction coefficient

C_d = discharge coefficient

D = distance between channel bottom and free surface

E = entrainment parameter

$$f \; = \; \frac{2\,F_1^{\,4/3}}{2\,S_{m_1}\,F_1^{\,2}\,+\,1}$$

f' = friction factor

F = Froude number

g = 32.2 ft/sec (gravitational acceleration)

h = weir height (overshot weir)

h = weir opening (undershot weir)

K = $\dfrac{Q_2}{Q_1}$ flow ratio

M = sum of fluid momentum and hydrostatic pressure per unit span

p = pressure

q = flow per unit width

Q = flow per unit width

r = conjugate depth ratio

R = $\dfrac{u'y'}{\nu}$ Reynold's number

R_i = Richardson number

S_E = Kinetic energy correction factor

S_H = hydrostatic pressure correction factor

S_m = momentum correction factor

u = local x component of velocity

u' = characteristic x component of velocity

v = local y component of velocity

v' = characteristic y component of velocity

V_n = nose velocity

w = channel width

w_r = w/ $(2 y_2' + w)$

x = length scale along the boundary parallel to the direction of mean flow

X = x/ y_{2c} = dimensionless x scale

y = length scale perpendicular to the x direction

y' = characteristic depth defined as the distance between the visual interface and the channel bottom

y_b = brink depth at a free overfall

y_{ic} = critical depth at Section i)

Y = y'/ y_{1c} = dimensionless y scale

α = angle of spread of a jet

β_1 = ratio of boundary layer thickness to the depth of flow

β_2 = ratio of velocity at the defined edge of the boundary layer to mean velocity of the flowing layer

$$\beta = \frac{2\beta_2}{\beta_1}$$

δ = y scale in the boundary layer

δ' = boundary layer thickness

Δ = characteristic density difference

$\Delta\rho$ = local density difference

$\mathcal{E}$ = total energy flux

θ = inclination of bottom boundary to the horizontal

Θ = ratio of force flow at two different sections

μ = dynamic viscosity

γ = kinematic viscosity

ρ = local density

ρ_0 = density of the ambient fluid

ϕ = flux of density difference/unit width

τ = local shear stress

τ_i = interfacial shear stress

τ_w = boundary shear stress

$$\varsigma = V_n / (q \frac{\Delta\rho}{\rho_0} g)^{1/3}$$

Appendix I

List of References

1. Bagnold, R. A., "Measurement of very low velocities of water flow". Nature, N.4260, June 23, 1951, pp. 1025-1027.

2. Bakke, P. "An experimental investigation of a wall jet", Jour. Fluid Mech. 2, 1957, pp. 467-472.

3. Bakhmettef, B. A. "Hydraulics of open channels", McGraw-Hill, New York, 1932.

4. Ball, F. K., Aust. Jour. of Physics, Vol. 9, 1956, pp. 373-386.

5. Ball, F. K. Tellus, Vol. 9, No. 2, May 1957, pp. 201-208.

6. Ball, F. K. Antarctic Meteorology, Pergamon Press, London, 1959, pp. 9-16.

7. Bata, G. L., and Bogich, K., "Some observations on density currents in the laboratory and in the field", Proc. Min. Intern. Hyd. Conv., September, 1953, pp. 387-400.

8. Bata, G. L. "Frictional Resistance at the interface of density currents". Intern. Assoc. Hydr. Research, 8th Congr., August 1959.

9. Batchelor, G. K., "The conditions for dynamical similarity of motions of a frictionless perfect-gas atmosphere". Quart. Jour. Res. Met. Soc. 79, 1953, pp. 224-235.

10. Benjamin, T. B., "Theory of the vortex breakdown phenomenon" Jour. Fluid Mechanics, Vol. 14, Part 4, Dec. 1962, pp. 593-629.

11. Ellison T. H. and Turner, J. S., "Turbulent entrainment in stratified flows" Jour. Fluid Mechanics, Vol. 6, Part 3, Oct. 1959, pp. 423-448.

12. Fietz, T. R., Water Research Laboratory Report No. 85, 1966.

13. Fietz, T. R., Jour. Sci. Instruments Vol. 44, 1967, pp. 37-42.

14. Foster, D. N. and Wilkinson, D. L. "Hydraulic studies for Liddell Power Station" Vol. IV Water Research Lab. Report No. 11, May 1969.
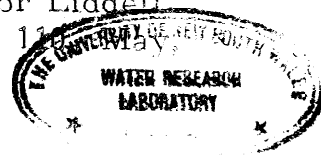
15. Hama, F. R., "Physics of Fluids", 5, p. 644, 1962.

16. "Handbook of Chemistry and Physics" (Chemical Rubber Co.)
    Annual, Ohio.

17. Henderson, F. M., "Open channel flow", New York, Macmillan, 1966.

18. Ippen, A. T., and Harleman, D. R. F., "Steady-state characteristics
    of subsurface flow", Nat. Bur. Standards (U. S.) Cir. 521, pp. 79-93,
    1952.

19. Keulegan, G. H., "Laminar flow at the interface of two liquids,"
    Nat. Bur. Standards (U. S.) Circular 32, 1944.

20. Keulegan, G. H., "Form characteristics of arrested saline wedge",
    Nat. Bur. Standards (U. S.) Rep. 5482, October, 1957.

21. Koh, R. C. Y. "Viscous stratified flow towards a line sink", Cal.
    Inst. of Tech. Report No. K. H. -R-6, Jan. 1964.

22. Lied, N. T. "Stationary hydraulic jumps in a Katabatic Flow near
    Davis, Antartica, 1961" Aust. Met. Magazine, No. 47, Dec. 1964.

23. Lofquist, K. "Flow and stress near an interface between stratified
    fluids", The Physics of Fluids", Vol. 3, No. 2, Mar. -April 1960,
    pp. 158-175.

24. Middleton, G. V. "Experiments on density and turbidity currents",
    Canadian Jour. of Earth Sci. Vol. 4, 1967, pp. 475-505.

25. Rajaratnam, N., "Submerged sluice gate flow as a wall jet problem"
    Proc. 2nd Australasian Conf. on Hyd. and Fluid Mech., Auckland,
    New Zealand, 1965.

26. Rouse, H. "Discharge characteristics of a free overfall", Civil
    Engineering Vol. 6, No. 4, April, 1936. pp. 257-260.

27. Rouse, H., Yih, C. S., and Humphreys, H. W., "Gravitational
    convection from a boundary source", Tellus, Vol. 4, No. 3, Aug.
    1952, pp. 201-210.

28. Schraub, F. A., Kline, S. J., Henry, J., Runstadler, P. W.,
    Littell, A., "Use of hydrogen bubbles for quantitative determination
    of time dependent velocity fields in low speed water flows". Report
    MD-10, Thermosciences Div., Dept. Mech. Eng., Stanford Uni.
    Feb. 1964.

29. Schweitzer, H. "Attempts to explain the Fohn" Archiv. fur Meteorologie, Geophysich, und Hisclimatologie, Series A, 1953, Vol. 5 No. 3 p. 350.

30. Streeter, V. L. "Handbook of Fluid Dynamics", McGraw-Hill, 1961.

31. Swartz, W. H. and Cosart, W. P. "The two dimensional turbulent wall jet". Jour. Fluid Mech. Vol. 10, Pt. 4, June 1961, pp. 481-495.

32. Townsend, A. A. "The structure of turbulent shear flow", Cambridge University Press, 1956.

33. Wilkinson, D. L., Wood, I. R., "The entraining hydraulic jump", Proc. 3rd Australasian Conf. on Hyd. and Fluid Mech. 1968.

34. Wilkinson, D. L., "A simple meter for measurement of low velocities in water flow", Jour. of Sci. Inst. 1968, Series 2, Vol. 1.

35. Wood, I. R., "Studies in Unsteady self preserving turbulent flows" Uni. of N. S. W., Water Research Laboratory Report No. 81, Nov. 1965.

36. Wood, I. R., "Horizontal two-dimensional density current". Proc. A. S. C. E., Jour. Hyd. Div., Vol. 93, No. HY2, Mar. 1967, pp. 35-42.

37. Wood, I. R., "Selective withdrawal from a stably stratified fluid". Jour. Fluid Mech. (1968), Vol. 32, Pt. 2 pp. 209-223.